

**Effect of water on the electrochromic properties of
CeO₂-TiO₂, WO₃ and Nb₂O₅:Mo sol-gel layers and
devices prepared with them**

Dissertation

zur Erlangung des Grades

Doktor der Ingenieurwissenschaften

an der Naturwissenschaftlich-Technischen Fakultät III

Chemie, Pharmazie, Bio- und Werkstoffwissenschaften

der Universität des Saarlandes

vorgelegt von

Donglan Sun

Saarbrücken

2005

Tag des Kolloquiums: 14.12.2005

Dekan: Prof. Dr. Kaspar Hegetschweiler

Berichterstatter: Prof. Dr. Michel A. Aegerter

Berichterstatter: Prof. Dr. rer. nat. Wulff Possart

Vorsitzender: Prof. Dr. Michael Veith

Beisitzer: Dr. Andreas Rammo

Acknowledgment

First of all, I would like to express my appreciation to my supervisor Professor Dr. M.A. Aegerter giving me the chance to study under his direction within a talented team of researchers. As my supervisor, he has constantly forced me to remain focused on achieving my goal. His observations and comments helped me to establish the overall direction of the research and to move forward with investigation in depth. He also gave a good proof reading of my thesis.

I am grateful to Dr. S. Heusing for generously sharing her time and knowledge in my work and translating the abstract into German. I also want to thank all the colleagues in INM, especially those in our group for their selfless support and encouragement. I am also appreciative of Mrs. M. Bonnard help during this period.

I would like to express my sincere gratitude to Dr. I. Grobelsek, Dr. T. Krajewski, Dr. M. Koch, Dr. H. Shen, Ms. A. Haettich, and Mr. T. Rügamer who made interesting characterizations.

My thanks will also be given to the colleges working in computer department, electronic workshop and chemical order department.

Last, but not least, I am indebted very much to my family, especially my parents, my husband and my son. Without support from them, it would have been impossible to finish this thesis.

List of abbreviations:

AES	Auger Electron Spectroscopy
AFM	Atomic Force Microscopy
CA	Chronoamperometry
CE	Counter electrode
C.E.	Coloration efficiency
CP	Chronopotentiometry
CRT	Cathode ray tube
CV	Cyclic voltammetry
CVD	Chemical vapor deposition
EC	electrochromic
ED	Electron diffraction
EDX	Energy Dispersive X-ray
ESCA	Electron Spectroscopy for Chemical Analysis
EXAFS	Extended X-ray Absorption Fine Structure
FTIR	Fourier Transform Infrared
FTO	Fluorine doped tin oxide
GIXR	Grazing Incidence X-ray Reflectivity
HR-TEM	High-resolution Transmission Electron Microscopy
INM	Leibniz-Institut für Neue Materialien
i_{pc}	Peak of cathodic current density
IS layer	Ion-storage layer
ITO	Indium tin oxide
LC	Laser calorimetry
LCD	Liquid crystal display
M	Molar/Liter
NRA	Nuclear Reaction Analysis

PC	Propylene carbonate
PEG	Polyethylene glycol
PTD	Photothermal Deflection technique
PVD	Physical vapor deposition
Q	Charge
RBS	Rutherford Back Scattering
SAXS	Small Angle X-ray Scattering
SEM	Scanning Electron Microscopy
SIMS	Secondary Ion Mass Spectroscopy
SNMS	Secondary Neutral Mass Spectroscopy
t	Thickness
T_b	Transmittance at the bleached state
T_c	Transmittance at the colored state
T_s	Sintering temperature
TCE	Transparent conductive electrode
TCO	Transparent conducting oxide
UV	Ultra violet
UV-VIS-NIR	Ultra violet-visible-near infrared
WDX	Wavelength Dispersive X-ray
WE	Working electrode
WLI	White Light Interferometer
XPS	X-ray Photoelectron Spectroscopy
XRD	X-Ray Diffraction
XRF	X-Ray Fluorescence
Δm	Mass change
ΔOD	Optical density change

Abstract

Electrochromic (EC) materials change their optical properties (transmittance or reflection) in a reversible manner when a current flows through them. Large EC glazings can be used for architectural and automotive applications in order to control the solar radiation entrance. The typical configuration of EC devices made with the sol-gel process (and used in our lab) is glass/ fluorine doped tin oxide (FTO)/ EC layer/ inorganic-organic composite electrolyte/ ion-storage (IS) layer/ FTO/ glass. The ion storage capacity of the IS layer plays an important role in the transmittance change of EC devices. WO_3 layers are the best studied EC layers and their Li^+ intercalation ability is larger than 30 mC/cm^2 . The charge capacity of the IS layer should be similar to obtain a high coloration change.

My work was dedicated to improve the ion storage capacity of $(\text{CeO}_2)_x(\text{TiO}_2)_1$ as IS layer. First the composition of the sol and the dip coating and annealing parameters have been optimized. Then the influence of water added to the electrolyte on the properties of the EC and IS layers and the EC devices has been studied. The ion storage capacity was improved from 7 mC/cm^2 to 14.5 mC/cm^2 by improving the sintering temperature to $550 \text{ }^\circ\text{C}$. It can be even increased to 26 mC/cm^2 by increasing the thickness of the layer and with 3 wt.% water added into the liquid electrolyte. When a small amount of water is added to the liquid electrolyte, 1 M LiClO_4 in propylene carbonate (PC), the ion storage capacity of the $(\text{CeO}_2)_x(\text{TiO}_2)_1$ layer is greatly increased by a factor up to 3 and the ion intercalation kinetics is faster than that in the dry electrolyte. The ion intercalation reversibility is also improved.

The nature of the intercalated ion was studied using an Electrochemical Quartz Crystal Microbalance (EQCM). It was found that the charge balance of the $(\text{CeO}_2)_{0.81}(\text{TiO}_2)_1$ layer during reduction and oxidation is not only due to Li^+ intercalation and deintercalation, but also to ClO_4^- desorption and adsorption.

Finally large size EC devices using WO_3 or $\text{Nb}_2\text{O}_5\cdot\text{Mo}$ ($\text{Mo}:\text{Nb} = 0.3$) as EC layer, $(\text{CeO}_2)_{0.81}(\text{TiO}_2)_1$ as ion storage layer and an inorganic-organic composite electrolyte have been fabricated. The change of the optical density ΔOD reaches 0.45 for WO_3 and 0.43 for $\text{Nb}_2\text{O}_5\cdot\text{Mo}$ ($\text{Mo}:\text{Nb} = 0.3$). The response time for optical switching of the EC devices becomes shorter and the lifetime increases from about 10000 cycles to more than 50000 cycles when the water content of the electrolyte is increased to 3 wt.%. Contrary to the devices made with dry electrolyte, less switch-in behavior during the initial cycles is observed with the devices made with wet electrolyte. The colored state memory effect of the devices with wet electrolyte is shorter than that made with dry electrolyte, but the behavior is nevertheless still adequate for architected windows as only a 40% relative variation of the transmittance change is observed after about 17 h. In a word, the optical properties and the long term stability of EC devices made with $(\text{CeO}_2)_{0.81}(\text{TiO}_2)_1$ as ion storage layer can be drastically improved when the electrolyte contains a low amount of water (2 to 3 wt.%).

Abstract (Deutsch)

Elektrochrome (EC) Materialien ändern ihre optischen Eigenschaften (Transmission oder Reflektion) reversibel bei Anlegen einer Spannung und einem dadurch bedingten Stromfluß. Große EC Verglasungen können im Architektur- und Automobilbereich angewendet werden um die Sonneneinstrahlung zu kontrollieren. Ein typischer Aufbau von EC-Fenstern, hergestellt mit der Sol-Gel-Technik (und in unseren Labors verwendet), ist Glas/ transparente elektrisch leitfähige Schicht (z.B. Fluor dotiertes Zinnoxid, FTO)/ EC-Schicht/ anorganisch-organischer Komposit-elektrolyt/ Ionenspeicher (IS) -Schicht/ FTO/ Glas. Die Ionenspeicherkapazität der IS-Schicht spielt eine wichtige Rolle bei der Transmissionsänderung der EC-Fenster. WO_3 Schichten sind die am besten untersuchten EC-Schichten und die von ihnen interkalierte Ladungsmenge an Li^+ Ionen ist größer als 30 mC/cm^2 . Die Ladungskapazität der IS-Schicht sollte ähnlich groß sein um eine hohe Transmissionsänderung zu erzielen.

Meine Arbeit hatte das Ziel, die Ionenspeicherkapazität von $(\text{CeO}_2)_x(\text{TiO}_2)_1$ als IS-Schicht zu verbessern. Zuerst wurden die Zusammensetzung des Sols und die Parameter der Tauchbeschichtung und des Sinterns optimiert. Dann wurde der Einfluß des zum Elektrolyten zugesetzten Wassers auf die Eigenschaften der EC- und IS-Schichten und der EC-Fenster untersucht. Die Ionenspeicherkapazität konnte durch Erhöhen der Sinter Temperatur auf 550°C von 7 mC/cm^2 auf $14,5 \text{ mC/cm}^2$ verbessert werden. Durch Erhöhen der Schichtdicke und durch Zugabe von 3 Gew% Wasser zum flüssigen Elektrolyten konnte sie sogar auf 26 mC/cm^2 erhöht werden. Bei Zugabe einer geringen Menge Wasser zum flüssigen Elektrolyt, 1 M LiClO_4 in Propylencarbonat (PC), wird die Ionenspeicherkapazität der $(\text{CeO}_2)_x(\text{TiO}_2)_1$ Schicht bis um einen Faktor 3 deutlich erhöht, und die Kinetik der Ionen-Interkalation ist schneller als in trockenem Elektrolyt. Die Reversibilität des Ionen-Interkalationsprozesses wird ebenfalls verbessert.

Die Art der interkalierten Ionen wurde mit einer Elektrochemischen Quarz-Mikrowaage (EQCM) untersucht. Hierbei wurde entdeckt, dass der Ladungsausgleich in der $(\text{CeO}_2)_x(\text{TiO}_2)_1$ Schicht bei Reduktion und Oxidation nicht allein auf der Interkalation und Deinterkalation von Li^+ -Ionen beruht sondern gleichzeitig eine Desorption bzw. Adsorption von ClO_4^- -Ionen erfolgt.

Schließlich wurden auch großflächige EC-Fenster mit WO_3 bzw. $\text{Nb}_2\text{O}_5:\text{Mo}$ ($\text{Mo}:\text{Nb}=0,3$) als EC-Schicht, $(\text{CeO}_2)_{0,81}(\text{TiO}_2)_1$ als Ionenspeicherschicht und einem anorganisch-organischen Komposit-elektrolyten hergestellt. Die Änderung der optischen Dichte ΔOD betrug 0,45 für WO_3 und 0,43 für $\text{Nb}_2\text{O}_5:\text{Mo}$ ($\text{Mo}:\text{Nb}=0,3$). Durch das Erhöhen des Wassergehaltes des Elektrolyten auf 3 Gew% wurden die Schaltzeiten für das optische Schalten der EC-Fenster verkürzt und die Langzeitstabilität nahm von 10.000 Schaltzyklen auf mehr als 50.000 Schaltzyklen zu. Im Gegensatz zu den EC-Fenstern, die mit trockenem Elektrolyt hergestellt waren, wurde mit feuchtem Elektrolyt ein geringeres Einschwingverhalten während der ersten Schaltzyklen beobachtet. Der Memory-Effekt der EC-Fenster im gefärbten Zustand ist zwar mit feuchtem Elektrolyten kürzer als mit trockenem Elektrolyten, aber das Verhalten ist gleichwohl ausreichend

für Architekturverglasung, da nach 17 h nur eine relative Änderung der Transmissionsänderung um 40 % beobachtet wird. Zusammenfassend kann gesagt werden, dass die optischen Eigenschaften und die Langzeitstabilität der EC-Fenster mit $(\text{CeO}_2)_{0,81}(\text{TiO}_2)_1$ als Ionenspeicherschicht drastisch verbessert werden können, wenn der Elektrolyt eine geringe Menge an Wasser enthält (2 bis 3 Gew%).

Table of Contents

Acknowledgement.....	I
List of abbreviations.....	II
Abstract.....	IV
Abstract (in German).....	V
1. Introduction and objective.....	1
2. Fundamental.....	3
2.1 Thin film technology.....	3
2.1.1 Properties of thin films.....	3
2.1.2 Substrate cleaning.....	5
2.2 Sol-gel processing.....	6
2.2.1 Sol-gel chemistry.....	7
2.2.2 Wet coating deposition technology.....	9
2.2.3 Advantage and disadvantage of sol-gel technology.....	12
2.3 Electrochromism.....	13
2.4 Electrochromic devices.....	14
2.5 Electrical conductors and electrolyte.....	17
2.5.1 Electrical conductors.....	17
2.5.2 Electrolyte.....	18
3. Background.....	20
3.1 Materials for electrochromic devices.....	20
3.1.1 Overview.....	20
3.1.2 Tungsten trioxide.....	21
3.1.3 Doped and undoped niobium pentoxide.....	23
3.1.4 Cerium and cerium-titanium oxides.....	26
3.1.5 Nickel oxide.....	29
3.2 Smart windows.....	31
3.3 Water effect on the properties of EC layers.....	35
3.4 Development of EC layers and devices at the Leibniz-Institute of New Materials (INM).....	36
4. Experimental.....	38
4.1 Preparation of the sols and corresponding films.....	38

4.1.1	Cleaning of the substrate.....	38
4.1.2	Tungsten trioxide	38
4.1.3	Molybdenum doped Niobium oxide	38
4.1.4	Cerium-titanium oxide.....	39
4.1.5	Nickel oxide.....	39
4.1.6	Electrolyte.....	40
4.1.7	Mounting of EC-devices.....	40
4.2	Structure and composition analysis.....	40
4.2.1	Thermal analysis.....	40
4.2.2	Profilometry.....	40
4.2.3	X-ray diffraction.....	41
4.2.4	High Resolution -Transmission Electron Microscopy.....	41
4.2.5	X ray Photoelectron Spectroscopy.....	41
4.3	Electrochemical and optical measurements.....	41
4.3.1	Electrochemical characterization of the layers.....	41
4.3.2	Optical characterization.....	43
4.4	Microbalance.....	43
5.	Results and discussion.....	46
5.1	Cerium-titanium sols and layers.....	46
5.1.1	Influence of the sol composition on coating thickness and Li ⁺ charge exchanged.....	46
5.1.2	Influence of the water content of the electrolyte on Li ⁺ storage ability.....	51
5.1.3	Influence of the sintering temperature.....	60
5.2	Li ⁺ insertion and deinsertion mechanisms studied in dry and wet liquid electrolyte by EQCM.....	71
5.2.1	Overview of the mass changes during 100 CV cycles.....	72
5.2.2	Mass change analysis during cycling.....	75
5.3	Water effect on the electrochromic properties of WO ₃ and Nb ₂ O ₅ :Mo (Mo:Nb = 0.3) sol-gel double layers.....	83
5.3.1	WO ₃ sol-gel layer.....	83
5.3.2	Nb ₂ O ₅ :Mo (Mo:Nb = 0.3) sol-gel double layer.....	87
5.4	Conclusion for the sol-gel EC layers in liquid electrolyte.....	91

5.5	EC-devices.....	93
5.5.1	EC-devices made with WO ₃ sol-gel EC layers.....	93
5.5.2	EC devices made with Nb ₂ O ₅ :Mo (Mo:Nb = 0.3) EC layer.....	101
5.5.3	Memory effect of the EC devices.....	114
5.5.4	Optical microscopy analysis of WO ₃ or Nb ₂ O ₅ :Mo (Mo:Nb = 0.3) based EC devices	116
5.5.5	Devices made with NiO _x -TiO ₂ as ion storage layer.....	119
6.	Summary.....	120
	Annex.....	125
A.	Calibration of the microbalance (EQCM).....	126
B.	TEM results of the (CeO ₂) _{0.81} (TiO ₂) ₁ sol-gel layers.....	128
C.	CV profile of (CeO ₂) _{0.81} (TiO ₂) ₁ sol-gel layer with different scan rate.....	130
D.	XPS spectrum.....	131
E.	Results about EC devices with single and double (CeO ₂) _{0.81} (TiO ₂) ₁ sol-gel layers as counter electrode.....	134
F.	Devices made with NiO _x -TiO ₂ as ion storage layer.....	137
G.	List of chemicals used in this work.....	146
H.	List of equipments used in this work.....	147
	References.....	148
	List of Publications.....	160

1 Introduction and objective

International interest in solar energy research has strongly fluctuated during the last thirty years. It was high during the latter half of the 1970s as a consequence of the oil crisis but faded somewhat in the 1980s. Today it is recognized worldwide that the technologies involved in energy efficiency and solar energy could alleviate the environmental crisis manifested by global heating through the greenhouse effect. The hazardous increases of UV radiation through the holes in the ozone layer also contribute to the pressure to limit the use of fossil and nuclear fuels because of their environmental impacts. However this revival is also due to the increasing interest of other specialized markets such as automotive, aerospace, defense, toys etc., which look very promising at short term, with sales impact exceeding several billion dollars [1].

A wide class of materials, called chromogenic materials, is known to change in a persistent but reversible manner their optical properties such as optical transmission, absorption, reflectance and/or emittance in response to changes in ambient conditions.

For instance Cd or Ag doped glasses and organic dye doped polymers or organic dyes incorporated in inorganic porous matrices change their color when exposed to UV or visible light. This property, called photochromism, is widely used today in commercial products such as spectacle lenses. A few materials, such as VO_2 , are known to exhibit an analogous effect when heated at a defined temperature and are known as thermochromic materials. Others, called barochromic materials, change their color when exposed to a change in ambient pressure; this is exhibited for instance by samarium sulphide. Other devices used liquid crystals or polymer dispersed materials incorporated in a liquid; the application of an electric field changes the orientation of these molecules altering the optical absorption or scattering of the layer.

Technologically, however, the most promising chromogenic effect is called electrochromism and is defined as the persistent but reversible optical change produced electrochemically. A wide range of materials are known today to exhibit a reversible coloration by the application of an electric field or more precisely by the passage of an electric current and ions through them. These materials are required to exhibit a mixed electronic and ionic conductivity and consequently are often amorphous and porous to provide an open network for rapid ionic diffusion. The changes of their optical properties (transmittance or reflectance) is usually due to a reduction or oxidation of the material. A common feature of such materials, unlike the liquid crystals used in displays, is that once the material is colored, the applied voltage can be switched off and the color retained, making the electrochromic (EC) devices more energy efficient [1,2,3].

Solid-state electrochromic devices are therefore of considerable technological and commercial interest for e.g. smart window, displays and automotive rearview mirrors [4-6]. Large

electrochromic glazing can be used for architectural and automotive applications in order to control the solar radiation entrance into buildings and automobiles for saving air-conditioning costs in summer and heating costs in winter [7].

EC materials can be organic or inorganic chemicals. Inorganic EC materials are essentially transition metal oxides like tungsten oxide (WO_3), niobium oxide (Nb_2O_5), molybdenum oxide (MoO_3), nickel oxide (NiO) etc. Coatings of these compositions have been fabricated by different techniques as e.g. electron beam deposition, electrochemical deposition, chemical vapor deposition, physical vapor deposition and sol-gel-technique. Other materials are inorganic complexes (e.g. $\text{Fe}[\text{Fe}(\text{CN})_6]$, Prussian blue), organic polymers (e.g. polyaniline) and organic molecules (e.g. viologens).

In the last ten years a wide range of EC coatings and also devices were prepared by the sol-gel process. The advantages of this technique are the possibility to easily fabricate coatings of mixed and doped oxides by mixing the different salts in a sol and to use this sol for dip-coating, spray coating or other coating techniques. The process also offers advantages in controlling the microstructure of the deposited coatings. These parameters influence the kinetics, durability, coloring efficiency and charge storage ability of the EC electrodes. Another advantage is the lower cost of the deposition process for large areas compared to conventional vacuum method, which offers therefore the possibility to reduce the cost of the devices. However by comparing the layer's properties made by sputtering and other methods with the layers made by sol-gel method, fluctuation of the data reported for sol-gel method is noticed.

The objective of this work was to find out the cause of this fluctuation in the sol-gel results obtained at Leibniz-Institute of New Materials (INM) Germany and to eventually propose a remedy to improve the properties of some of the known EC layers and devices made with them. Among many parameters tested in a preliminary study, it was found that the water content of the electrolyte have a great influence on the CeO_2 - TiO_2 ion-storage capacity of the layer used at INM. This was proved by mounting and determining the properties of large EC devices built with WO_3 , Nb_2O_5 :Mo and CeO_2 - TiO_2 sol-gel layers.

The manuscript is organized in the following way: Chapter 2 describes the "fundamental" used in this work including thin film techniques, coating methods and an introduction about electrochromism. Chapter 3 gives the background for this work by describing the constituent materials that have been used and EC devices. Chapter 4 is devoted to the experimental procedures, including sample preparation and characterization. Chapter 5 presents and discusses the experimental results. Finally a summary and conclusion are given in chapter 6.

2 Fundamental

2.1 Thin film technology

In recent years the thin film technology has grown world-wide into a major research area. The importance of coatings and the synthesis of new materials for the industry have also resulted in a tremendous increase of innovative thin film processing technologies. Coatings today serve important roles in many applications, including microelectronics [8], catalysis [9], corrosion protection [10], and chemical sensors [11], displays [8], etc.

Thin films consist of two dimensional materials created by the process of condensation and growth of atoms, molecules or ions [12]. Their properties are usually different from the corresponding bulk materials due to their physical dimension, geometry and microstructure. They are largely affected by their high surface-to-volume ratio and influence many phenomena such as gas adsorption, diffusion, and catalytic activity, etc.

The substrate materials have also a significant effect and many factors should be taken into consideration [13]. For example, the cleaning, the surface energy and the roughness of the substrate affect decisively the adhesion of the film on the substrate. Also the stability of the substrate with the temperature variations as well as the different aging processes affects their properties. The crystalline structure, strength and the internal tension of the substrate material should be taken into account before the deposition process.

Independent of the film material, the mechanical characteristics, the optical properties, the film thickness etc. of coatings are strongly influenced by the deposition parameters and conditions and are therefore strongly related to the coating technologies. To produce efficient coatings for a certain application, it is necessary to know all the parameters that influence a desired film property during the deposition process. For example, for the films produced by the sol-gel process (dip coating technique), some of the relevant parameters which must be taken into consideration are the composition of the sol, the dipping time, the withdrawal speed, the heat treatment, the interaction with the surrounding atmosphere during the withdrawal of the substrate and the reaction with the substrate during densification.

2.1.1 Properties of thin films

The properties of thin films can be divided into macroscopic and microscopic ones. Among the macroscopic properties are e.g. the refractive index, the optical absorption and reflection, the film thickness, the adhesion, the stress, the density, the scattering of the light and the hardness. The microscopic quantities are e.g. the chemical composition, the chemical bonding between the elements, stoichiometry, topography, roughness of the surface, state and formation of interfaces, crystalline or amorphous state and also the crystalline structure.

There are various analytical tools available to characterize these properties and some of them are summarized in table 2.1 (the list of abbreviation is given at page II). These characterization techniques use different probes such as photons, electrons, ions and also forces as in Atomic Force Microscopy (AFM). These probes interact with the sample which then emits electrons, photons, ions etc., which are then collected by a detector to give information to describe the film properties [14].

Table 2.1. Techniques used to characterize thin films (adapted from [14])

Film properties	Characterization method
	Macroscopic
Density	GIXR, RBS
Stress	Bending
Adhesion	Tape test, Cutting
Optical quantities	UV-VIS-NIR Spectroscopy
Hardness	Pencil test, nano indentation
Thickness	TEM, SEM, Stylus, white light
Thermal conductivity	PTD, LC
	Microscopic
Composition	
-surface composition	ESCA, AES, XPS
-film composition	EDX, WDX, RBS, NRA, XRF, SNMS, ESCA
-interface composition	TEM/EDX
State of oxidation	ESCA, AES, SIMS, Raman, EXAFS
Structure and texture	XRD, ED, FTIR, SAXS
Roughness of surface	AFM, GIXR, WLI
Formation of interface	TEM, GIXR
Grain and crystalline size	XRD, TEM
Surface topography	AFM, SEM, WLI, GIXR

The structural properties of the deposited films are very important. The arrangement of atoms in a material is determined by the strength and the directionally of the interatomic bonds. The arrangement of the atoms may be regular (crystalline) or irregular (polymeric or glassy). The degree of crystallinity of films can be determined precisely by X-ray and electron diffraction techniques. With electrons, one can investigate very thin layers. Electron diffraction method gives a better determination of hydrogen atoms or ions, which is not possible by X-ray diffraction [15].

The surface properties of thin films affect their quality. Szanyi [16] have studied the origin of haze in CVD tin oxide thin films, where the surface quality of these films are of great importance in the production of solar control architectural glazing. The haze was correlated with the surface roughness and the concentration of internal voids. The surface chemical composition, impurities concentration, roughness and defects can be determined using many techniques such as SEM, AFM, XPS, AES, SIMS etc.

The mechanical properties of films are affected by the growth process, structure, chemical composition and incorporated impurities. They are also influenced by the state of cleaning of the substrate. The state of stress of the films is also very important and is related to the structure and microstructure properties as well as to the substrate and the heat treatment. It can be measured adequately using the bending-beam method. The obtaining of crack-free layer depends on the thermal expansion of the film and substrate and is characterized by a critical thickness, i.e. the maximum achievable thickness without crack formation for single step deposition. Additives incorporated to the sols help to increase the critical thickness of sol-gel coatings [17].

The adhesion and hardness of films are also important properties to be tested. The film density influences the hardness of the film. It is also important to test the influence of weathering (temperature, humidity) on the coatings. Humidity and salt water are of special importance in tropical areas and at sea level. All of these factors and tests should be taken into consideration.

The optical properties of thin films may drastically change the reflection, transmission and absorption of the substrate. They are determined by measuring their optical constants, i.e. the extinction coefficient and the refractive index and they depend strongly on the film thickness and the substrate surface conditions. The most common applications related with the optical properties are the antireflective coatings, reflection coatings, interference filters, beam splitters and wave guides [12].

2.1.2 Substrate cleaning

Surfaces exposed to the atmosphere are generally contaminated. Any unwanted material and/or energy on a surface is regarded as a contaminant. Most scientific and technical investigations and applications, however, require clean surface. So, the cleaning of the surface of the substrate before being coated is a very important issue in thin film deposition technology as otherwise the film may not adhere well or may not adhere at all. In the case of coatings, clean often means absence of detrimental impurities. In optical coating applications, even very minute contaminations of special materials can interfere with the functioning of sensitive devices whereas other materials may have practically no influence.

Cleaned surfaces can be classified into two categories: atomically clean surfaces and technologically clean surfaces [15]. With the exception of very sophisticated products, practical

coating applications require only technologically clean surfaces. The most common cleaning methods for getting a technologically cleaned surface are:

- i. **Cleaning with solvents:** Cleaning with solvents is a widespread procedure that is always included whenever cleaning of glass surfaces is discussed. Various cleaning solvents are used, such as distilled water to which detergents, diluted acids or bases as well as non-aqueous solvents such as alcohols and ketones can be added. The type of the solvents to be used depends on the nature of the contaminants.
- ii. **Rubbing and immersion cleaning:** This method perhaps is the simplest method of removing superficial dirt glass and is considered as a precleaning operation. It is done by rubbing the surface with cotton or a brush dipped in a mixture of precipitated chalk or fine powder of CeO_2 or Al_2O_3 and alcohol or ammonia.
- iii. **Ultrasonic cleaning:** Ultrasonic cleaning provides a valuable method of removing stronger adherent contaminants. It is effective for breaking loose contaminants by ultrasonic waves propagating in a cleaning fluid. The cavitation is the prime mechanism of cleaning of this method.
- iv. **Cleaning by heating:** Heating the glass surfaces causes a more or less strong desorption of adsorbed water and various hydrocarbon molecules. It is essential that this procedure be done not more than six hours before the coating procedure when its aim is to remove the adsorbed water.

A combination of several methods is usually used to achieve an optimum cleanliness of the substrate surface.

2.2 Sol-gel processing

The sol-gel process is a versatile solution process for making ceramic and glass materials. In general, the sol-gel process involves the transition of a system from a liquid "sol" (mostly colloidal) into a solid "gel" phase [19]. Applying this process, it is possible to fabricate ceramic or glass materials in a wide variety of forms: ultra-fine or spherical shaped powders, thin film coatings, ceramic fibers, micro porous inorganic membranes, monolithic ceramics and glasses, or extremely porous aerogel materials. An overview of the sol-gel process is presented in a simple graphic work below. (Fig. 2.1).

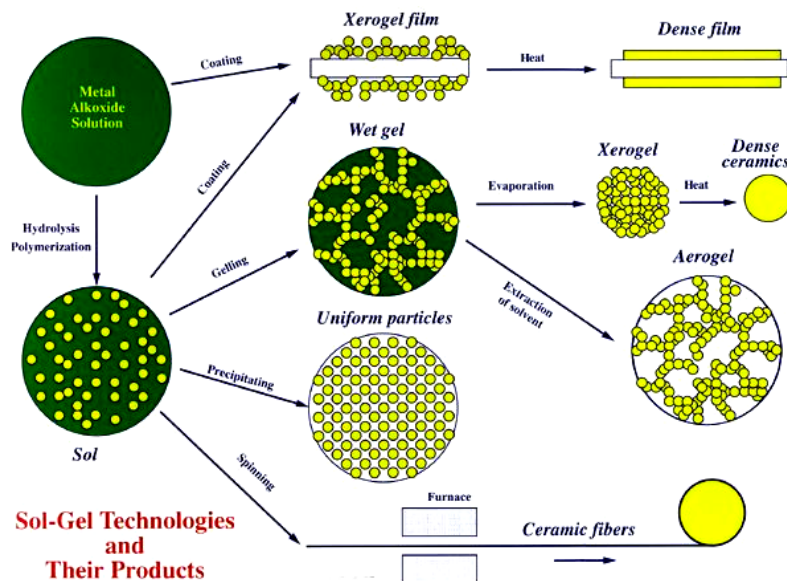


Fig. 2.1. An overview of the sol-gel process [19]

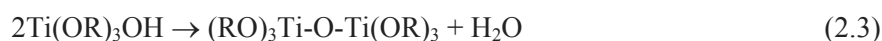
In a typical sol-gel process, the precursor is subjected to a series of hydrolysis and polymerization reactions to form a colloidal suspension called a "sol". The starting materials used in the preparation of a "sol" are usually inorganic metal salts or metal organic compounds such as metal alkoxides. Further processing of the "sol" enables one to make ceramic materials in different forms. Thin films can be produced on a substrate by spin coating or dip coating. When the "sol" is cast into a mold, a wet "gel" will form. With further drying and heat-treatment, the "gel" is converted into dense ceramic or glass articles. If the liquid in a wet "gel" is removed under a supercritical condition, a highly porous and extremely low density material called "aerogel" is obtained. If the viscosity of a "sol" is adjusted into a proper viscosity range, even ceramic fibers can be drawn from the "sol". Ultra-fine and uniform ceramic powders can be formed by precipitation, spray pyrolysis, or emulsion techniques.

2.2.1 Sol-gel chemistry

The sol-gel process uses inorganic or metal organic precursors. The most commonly used organic precursors for sol-gel film formation are metal alkoxides ($M(OR)_z$), where R stands for an alkyl group (C_xH_{2x+1}). Normally, the alkoxide is dissolved in an alcohol and hydrolyzed by the addition of water under acidic, neutral or basic conditions, although film formation is also possible by the deposition of alkoxides followed by exposure to moisture. Hydrolysis replaces an alkoxide ligand with a hydroxyl ligand, as shown in the equation:

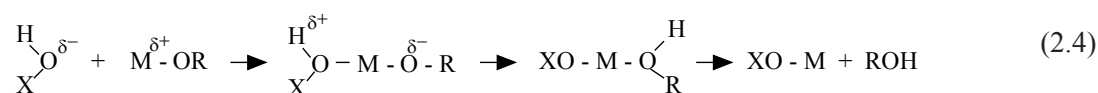


Condensation reactions involving the hydroxyl ligands produce polymers composed of M-O-M bonds. In most cases, these reactions also produce water or alcohol as byproducts, as shown in following equations, for titanium condensation:



Further reactions lead to the formation of titanium oxides.

The above hydrolysis and condensation reactions can be described by the so called associative $\text{S}_{\text{N}}2$ mechanism:



The reaction starts with the nucleophilic addition of negatively charged $\text{HO}^{\delta-}$ groups onto the positively charged metal $\text{M}^{\delta+}$, leading to an increase of the coordination number of the metal atom in the transition state. The positively charged proton is then transferred toward an alkoxy group and the protonated ROH ligand is finally removed [20].

The chemical reactivity of metal alkoxides toward hydrolysis and condensation mainly depends on the electronegativity of the metal atom and its ability to increase its coordination number “N”, i.e. on its size (Table 2.2) [20]. Silicon alkoxides are rather stable while titanium alkoxides are very sensitive to moisture. The hydrolysis rate of Ti(OEt)_4 ($k_h = 10^{-3} \text{ M}^{-1}\text{s}^{-1}$) is about five orders of magnitude greater than that of Si(OEt)_4 ($k_h = 5 \cdot 10^{-9} \text{ M}^{-1}\text{s}^{-1}$). Gelation times of silicon alkoxides are of the order of hours whereas titanium alkoxides have gel times of the order of seconds or minutes. Most alkoxides are very sensitive to moisture and must be handled with care under a dry atmosphere otherwise precipitation occurs as soon as water is present. Alkoxides of highly electronegative elements such as PO(OEt)_3 cannot be hydrolyzed under ambient conditions, whereas the corresponding vanadium derivatives VO(OEt)_3 are readily hydrolyzed into vanadium pentoxide gels.

Table 2.2. Hydrolysis rate of metal alkoxides as a function of the electronegativity "c", ionic radius "r" and maximum coordination number "N" of the metal.[20]

alkoxide	c	r(Å)	N	hydrolysis rate
Si(OPri) ₄	1.74	0.40	4	slow
Ti(OPri) ₄	1.32	0.64	6	fast
Sn(OPri) ₄	1.89	0.69	6	fast
PO(OEt) ₃	2.11	0.34	4	no hydrolysis
VO(OEt) ₃	1.56	0.59	6	fast

The chemical reactivity of metal alkoxides is also related to the alkyl group R; the larger the R, the slower is the hydrolysis because of steric hindrance.

Chemical precursors play a key role in the sol-gel coating and affect directly the porosity, refractive index, hardness and other performance characteristics of the resultant coatings and thin films. In addition, the type of precursor is frequently a decisive factor for production in terms of cost and usability.

2.2.2 Wet coating deposition techniques

Nowadays there are two main categories of deposition: vapor deposition and wet coating techniques. Vapor deposition techniques can be classified into two main classes: physical vapor deposition (PVD) and chemical vapor deposition (CVD). Vapor deposition is widely used in industry, but it is more expensive compare to wet coating technique.

Another advantage of wet coating techniques is that molecular structures developed by chemical synthesis can be used to develop new properties either when preserving these structures on the surface, or to develop new desired molecular structures by heat-treatment and subsequent chemical reaction on the surface. So, there are several basic processing routes after wet chemical deposition: the first route comprises a high temperature treatment after the coating step in order to get "glass-like" or "ceramic-like" materials on the glass surface and the second type of technique would include a low-temperature UV- or infrared type of curing, where the functional chemical structures developed in the liquid coating material are more or less maintained during this post-treatment.

Several methods can be used to make sol-gel coatings. Dip coating and spin coating are two of the most used basic techniques. Spin coating produces usually a one-sided coating, while dip coating yields a double-sided coating. Both techniques are used in manufacturing to make different coatings and thin films.

i. Dip coating technique

Dip coating is a process where the substrate to be coated is immersed in a liquid and then withdrawn with a well-defined withdrawal speed under controlled temperature and atmospheric conditions. An accurate and uniform coating thickness depends on a precise speed control and minimal vibration of the substrate and fluid surface so that vibration-free mountings and very smooth movement of the substrate are essential. The coating thickness is mainly defined by the withdrawal speed, the solid content and the viscosity of the liquid. If the withdrawal speed is chosen such that the shear rate keeps the system in the Newtonian regime, the coating thickness can be calculated by the Landau-Levich equation (2.5) [21].

$$h = 0.94 \cdot \frac{(\eta \cdot v)^{2/3}}{\gamma_{LV}^{1/6} (\rho \cdot g)^{1/2}} \quad (2.5)$$

where: h = coating thickness

η = sol viscosity

v = withdrawal speed

γ_{LV} = liquid-vapor surface tension

ρ = density

g = gravity.

The schematics of a dip coating process are shown in Fig. 2.2.

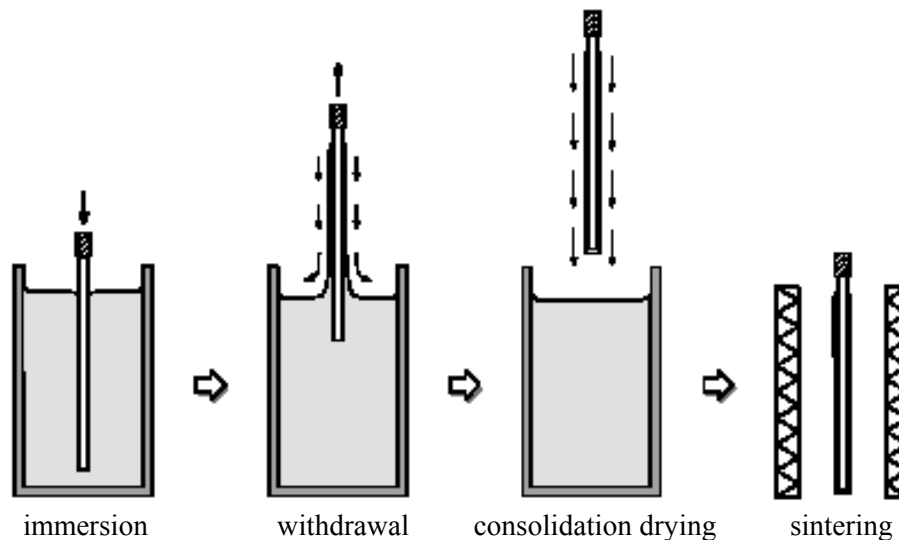


Figure 2.2. Stages of the dip coating process: dipping of the substrate into the coating solution, wet layer formation by withdrawing the substrate, gelation of the layer by solvent evaporation and sintering at high temperature [22].

If reactive systems are chosen for coatings, as it is the case in the sol-gel process using alkoxides or prehydrolyzed systems, the control of the atmosphere is indispensable in order to control the evaporation of the solvent. The subsequent destabilization of the sols by solvent evaporation leads to a gelation process and the formation of a transparent film due to the small particle size in the sols (nm range) [23]. This is schematically shown in Fig. 2.3.

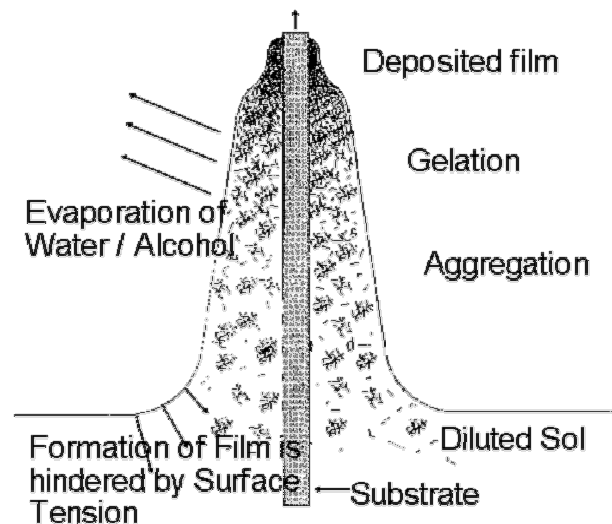
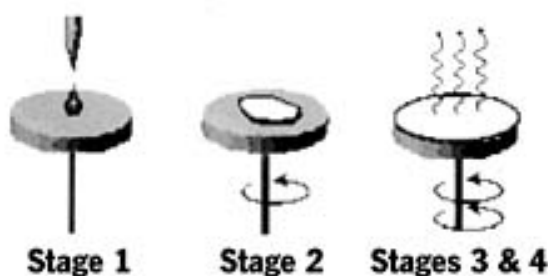


Fig. 2. 3. Gelation process during dip coating process, obtained by evaporation of the solvent and subsequent destabilization of the sol [23]

In general, sol particles are stabilized by surface charges, and the stabilization condition follows the Stern's potential consideration [24]. According to Stern's theory the gelation process can be explained by the approach of the charged particle to distances below the repulsion potential. Then the repulsion is changed to an attraction leading to a very fast gelation. This takes place at the gelation stage as indicated in Fig. 2.3. The resulting gel then has to be densified by thermal treatment, and the densification temperature is depending on the composition. But due to the fact that the gel particles are extremely small, the system shows a large excess energy and in most cases a remarkable reduced densification temperature is observed compared to bulk system.

ii. Spin coating technique

Spin coating is used for many applications where flat small substrates or objects need to be coated with thin layers of material. For example, several cathode ray tube (CRT) manufacturers use this method to make anti-glare or anti-reflection coatings. In spin coating, the material to be coated is first dissolved or dispersed into a solvent, then deposited onto the surface and then spun off to leave a uniform layer for subsequent processing stages and ultimate use. Fig. 2.4 shows the principle of a spin coater for general applications.



- Stage 1: Deposition of the coating fluid onto the substrate
- Stage 2: Aggressive fluid expulsion from the substrate surface by the rotational motion
- Stage 3: Gradual fluid thinning
- Stage 4: Coating thinning by solvent evaporation

Fig. 2.4. The four stages of spin coating [25]

The final film thickness is little affected by the deposition and spin-up stages, but is essentially determined by the spin-off stage in which the thickness becomes uniform. The thickness of an initially uniform film during spin-off is described by [25]

$$h(t) = \frac{h_0}{(1 + 4\rho\omega^2 h_0^2 t / 3\eta)^{1/2}} \quad (2.6)$$

where: $h(t)$ - thickness with spinning time h_0 - initial thickness

ρ - density of the liquid η - viscosity of the liquid

ω - angular velocity t - time

iii. Drying and curing techniques

Drying and curing techniques are important for obtaining the appropriate coating properties. Depending on the type of the coating material high and low temperature curing can be distinguished. If a high chemical durability is required, the coating temperature is usually chosen just below the transformation temperature of the glass T_g in order to maintain the shape of the substrate. Glass frits or sol-gel systems are then converted into ceramic- or glass-like coatings. If special functions have to be obtained, the control of the atmosphere may be of importance as e.g. in the case of electronically conductive coatings where the oxidation state is important for the electrical performance. Organic polymer or organic-inorganic hybrid coating materials can be cured by a low temperature treatment or UV-curing.

2.2.3 Advantage and disadvantage of sol-gel technology

From the above introduction, a number of reasons for the particular value of and interest in sol-gel synthesized materials become apparent [26]:

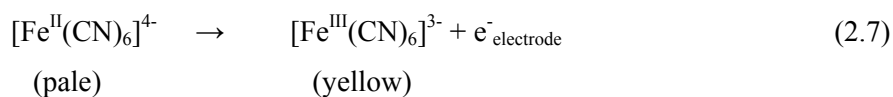
1. The temperatures required for all stages apart from densification are low, frequently close to room temperature. Thus thermal degradation of both the material itself and any entrapped species is minimised and high purity and stoichiometry can be achieved.
2. Since organometallic precursors involving different metals are frequently miscible, homogeneous controlled doping is easy to achieve.
3. The chemical conditions are mild. Hydrolysis and condensation are catalysed by acids and bases, but extreme pH conditions may be easily avoided, especially by the use of "two step" methods in which acid catalysed hydrolysis is followed by rapid neutralisation or buffering.
4. Highly porous materials and nanocrystalline materials may be prepared in this way.

5. By appropriate chemical modification of the precursors, control may be achieved over the rates of hydrolysis and condensation, and over the colloid particle size and the pore size, porosity and pore wall chemistry of the final material.
6. By controlling the aging and drying conditions, further pore size and mechanical strength control may be achieved.
7. The low temperature range of sol-gel processes is generally below the crystallisation temperature of oxide materials, and this allows the production of unusual amorphous materials.
8. Sol-gel processing requires less capital investment to deposit coatings over large areas than conventional vacuum methods, and hence offers a possible solution for lowering the costs.

Despite of all these advantages, the processing of sol-gel materials is not without limitations. The precursors are often expensive and sensitive to moisture and limit the large-scale production plants to specialised applications such as optical coatings. The process is also time-consuming, particularly when a careful aging and drying are required. Although this need is not a limiting factor when long continuous production runs are envisaged, it does mean that the total volume of material in the processing line is inevitably significantly higher than in faster processes. Finally the problems of dimensional change on densification and of shrinkage and stress cracking on drying, although not insuperable, do require careful attention.

2.3 Electrochromism

Electroactive species often exhibit new optical absorption bands (i.e. shows a color) when an electron-transfer or 'redox' reaction occurs in which they either gain or lose an electron; that is to say, it undergoes a reduction or an oxidation process. This property is found among many organic and inorganic compounds [2,3]. For example, the ferrocyanide ion in aqueous solution shows pale yellow color, but during an electrochemical oxidation (loss of electron to an electrode):



a brilliant yellow pool forms around the electrode that then diffuses into the bulk. The change in color is directly attributed to the oxidation of iron(II) to iron(III) in the complex.

There are also many organic systems which can change their color by electricity such as bipyridiliums (also known as viologens or paraquats). They become highly colored on reduction, owing to intense optically-affected intramolecular charge transfer in the product.

This work focuses only on transition metal oxides which have this property. Several inorganic transition metal oxides exhibit electrochromism and can be quite easily deposited as thin films,

which is appropriate for device manufacturing. The transition metals are primarily found in the groups IIIB to VIII in the periodic table, with partly filled d-bands, and the origin of electrochromism is found in the electron configuration. The Fermi level of these compounds is either in the band gap for certain elements or in a band for others. In the former case, if the band gap is larger than the energy of incoming radiation the oxide is transparent. The metal ion of such a material can be reduced by the insertion of electrons (together with positive ions), and the Fermi level will shift into the next higher band, so that the material will start to interact with the incoming radiation and become absorbing. For crystalline materials a free-electron condition can arise, and the material may also reflect the incoming radiation. This behavior is most pronounced in the infrared range.

The formation of an absorbing state upon reduction is called cathodic electrochromism, while the formation upon oxidation is called anodic electrochromism. The insertion and extraction of ions is called intercalation and deintercalation. Due to the well established works done on electrochromism for optical applications, the terms “bleached” and “colored” are often seen.

2.4 Electrochromic devices

Turn a switch to darken a window without curtains, shutters or screens: how simple, how neat! This is already achieved automatically in electrochromic rearview mirrors now available in cars. Extension of such controlled coloration to windows and displays is under widespread examination, and several firms have now demonstrator models of windows.

Thin films of EC materials need mechanical support, and to be modulated they have to be supplied with ions and electrons. Therefore a single thin film has to be deposited on an electronically conducting substrate. It is a glass or a plastic substrate coated with a thin transparent conductive electrode (TCE), usually a doped form of tin oxide e.g. fluorine doped tin oxide (FTO: $\text{SnO}_2:\text{F}$) or a tin doped indium oxide (ITO: $\text{In}_2\text{O}_3:\text{Sn}$). The electrochemical measurements of such layers can be performed using an ion containing liquid electrolyte, counter and reference electrodes (see section 4.3.1).

To describe a more practical process it is however illustrative to look at a free-standing EC-device. Four main applications of EC devices are illustrated in Fig. 2.5:

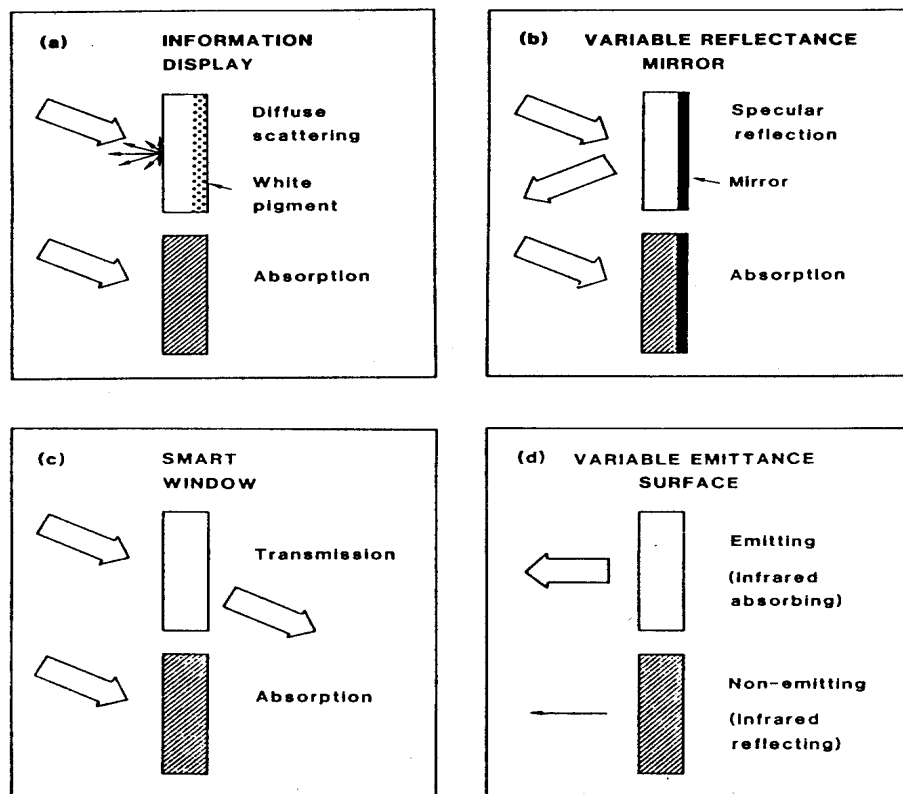


Fig. 2.5. The four major applications of EC devices. Arrows indicate incoming and outgoing electromagnetic radiation; the width of the arrow indicates the radiation intensity (from Granqvist) [2].

Fig. 2.5(a) refers to information display. The device embodies an EC film in front of a diffuse scattering pigmented surface. The EC film can be patterned and, for example, be part of a seven-segment numeric display unit. It is possible to achieve excellent viewing properties with better contrast--particularly at off-normal angle than in the conventional LCDs.

Fig. 2.5(b) shows how an EC film can be used to produce a mirror with variable specular reflectance. This application is the most mature one, and antidazzling rear-view mirrors built on EC oxide films are available for cars and trucks.

EC windows are illustrated in Fig. 2.5(c). The basic idea is to make an architectural or automotive window with variable transmittance so that only a desired amount of visible light and/or solar energy is let through. It will be discussed in detail below.

Variable emittance surfaces, outlined in Fig. 2.5(d) are based on a special device design with a crystalline tungsten oxide (WO_3) film at the exposed surface of an EC device. Intercalation/deintercalation of ions makes this surface infrared reflecting/absorbing, i.e., the thermal emittance is low/high. Variable emittance surfaces can be employed for temperature control under conditions when radiative heat exchange dominates over conduction and convection, such as for space vehicles.

The configuration of an EC window is now discussed in detail. There are three major window configurations: battery-like, solution phase and hybrid structures [27]. A typical configuration of the battery-like structure EC-devices is shown in Fig. 2.6. It is mainly used in this work.

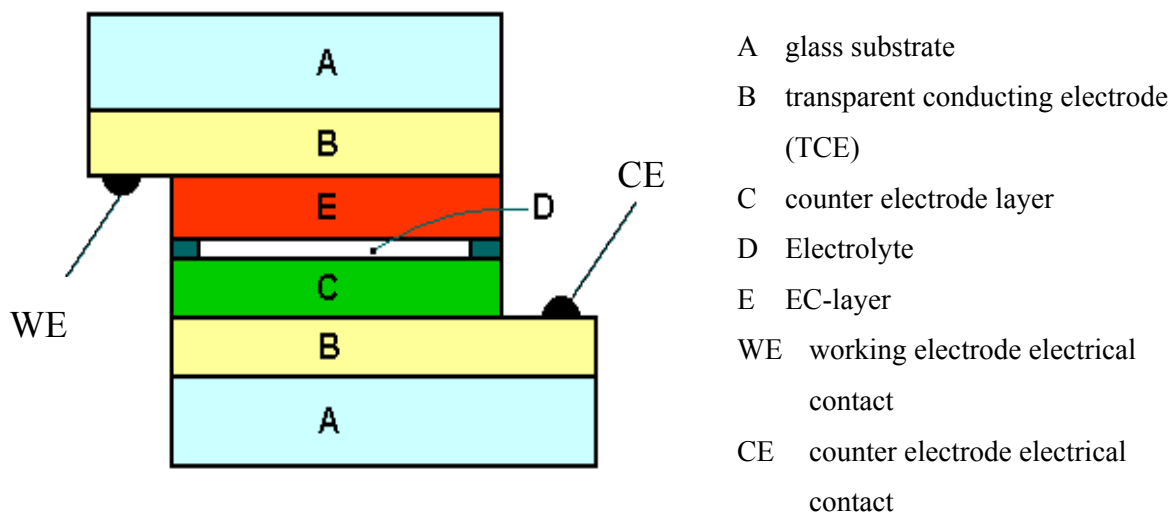
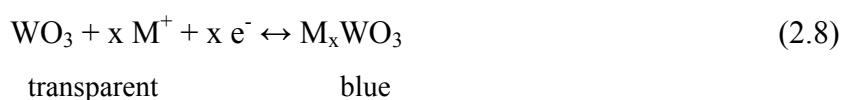


Fig. 2. 6. Scheme of an EC-device

The system consists of 3 functional layers, which are located between two glass or plastic substrates coated with TCE. One of the TCE is coated with an EC coating (EC-layer), the other with a counter electrode (CE layer, also called ion storage layer). Both layer systems are separated by an ionic conductive electrolyte with very low electronic conductivity. In order to have high diffusion coefficients and fast kinetics, the ions should be small, therefore proton (H^+) or lithium (Li^+) are preferred. The electrical contacts are attached at the TCE coatings.

The operating mode is explained here with an EC window of the configuration glass/ TCE/ WO_3 / electrolyte/ CeO_2 - TiO_2 / TCE/ glass, one of the configuration used in this work. Initially the system is transparent. After applying a voltage with negative polarization at the WO_3 side, WO_3 is reduced and simultaneously the M^+ ions (M^+ : H^+ , Li^+) stored in the ion-storage layer diffuse through the electrolyte into the WO_3 layer to form a deep blue colored intercalation compound M_xWO_3 . The following reversible coloration and bleaching reactions occur:



WO_3 colors blue in the reduced form and is therefore a cathodic EC material. After reversing the polarization, M_xWO_3 is oxidized and simultaneously the M^+ -ions diffuse back to the counter electrode. The counter electrode, which was oxidized during the coloration step, will be reduced and the EC-device is bleached. The counter electrode layer can be either an ion storage layer (IS-layer) which do not change its color during intercalation/deintercalation of the M^+ -ions (e.g. cerium

oxide-titanium oxide, $\text{CeO}_2\text{-TiO}_2$), or a complementary, anodic EC layer, which colors in the oxidized form (e.g. nickel oxide, NiO) so that the coloration of the EC-window can be intensified.

The electrolyte may be a liquid, a polymer, a gel or a thin film electrolyte. Polymer and gel electrolytes lead to laminated sandwich structures whereby thin film electrolytes (e.g. Ta_2O_5) lead to an all-thin film EC-devices. In this case, EC-devices with only one glass or plastic substrate can be fabricated [28]. Liquid electrolytes are not useful for large area applications, because of the buckling of the glass and the risk of leakage. Therefore polymer, gel or solid electrolytes are preferred for large area EC-devices.

Two other configurations, the “solution phase structure” and the “hybrid structure”, have been proposed [27]. In the hybrid EC windows the counter electrode coating is missing and instead a redox material is dissolved in the liquid or gel electrolyte. This configuration glass/ electrode/ EC-layer (WO_3)/ electrolyte with redox system/ electrode/ glass/ mirror layer is used for EC mirrors for automotives by Donnelly [29]. The WO_3 layer is colored or bleached by intercalation or deintercalation of cations (Li^+) respectively. The back reaction (bleaching) without applying a voltage is due to a redox system in the electrolyte (ferrocene).

In the “solution EC window” both EC materials are dissolved in the liquid or gel electrolyte, where they can freely diffuse. This configuration glass/ electrode/ electrolyte with two EC-redox system/ electrode/ glass/ mirror layer are used for EC-mirrors by Gentex [30-33]. After applying a voltage, one of the EC dyes (bipyridine derivative) is reduced and colored. The other anodic coloring EC-dye is oxidized at the positive electrode and therefore also colored. The back reaction of the two dyes to the bleached state happens without applying a voltage.

These last two EC-devices are of the so-called “self-erasing type”. They are used in EC mirrors but they have also been applied for EC windows. A continuous current is required to maintain the self-erasing device in the colored state, while “battery-like EC devices” have extended open circuit memory, so that these systems need only energy for the change of the coloration, but not for maintaining it. Therefore they are advantageous for large EC-glazing and for EC-displays which should show the same information during a long time (e.g. price label, display panel).

2.5 Electrical conductors and electrolyte

The EC material needs to be incorporated with supportive components, such as transparent electrical contacts and an ion conducting electrolyte, to provide electric currents.

2.5.1 Electrical conductors

The transparent conductive electrode (TCE) is a critical component in an EC device; it should enable a rapid charge transport and hence its sheet resistance should be in the order of 1 to $100 \Omega_{\square}$.

The sheet resistance is defined as

$$R_{\square} = \rho/t \quad (2.9)$$

where ρ is the specific resistivity and t is the thickness of the layer.

There are three kinds of transparent conductive coatings: metallic thin films, conducting polymers, and transparent conducting oxide (TCO).

TCOs are the most common used materials to produce transparent conducting films. They are essentially based on In_2O_3 , SnO_2 , ZnO , CdO , etc. These materials are usually insulators and have a wide band gap ($E_g > 3 \text{ eV}$), so that they show an excellent transparency in the visible region. To get them conducting nonstoichiometry and/or appropriate dopants, like Sn for In_2O_3 , Sb or F for SnO_2 , Al, Ga for ZnO , etc., should be introduced in order to create an electron degeneracy in the wide band gap [34]. Tin doped In_2O_3 (ITO) and fluorine doped SnO_2 (FTO) are the most used TCO for EC-devices. The disadvantage of ITO coated glass is their high price and the increase of their sheet resistance during a heat treatment at $T > 300 \text{ }^\circ\text{C}$. Therefore, as a certain heat treatment is necessary for the production of EC and ion-storage sol-gel layers, FTO coated float glass was selected as substrate in this work.

The ITO coatings are mainly deposited by sputtering technique and are often used to test small EC-coatings and EC-devices. FTO coated glass is cheaper and easily available in large sizes as K-glass ($R_{\square} = 17 \text{ } \Omega_{\square}$, Pilkington, used in this work), TEC15 ($15 \text{ } \Omega_{\square}$), TEC10 ($10 \text{ } \Omega_{\square}$), TEC8 ($8 \text{ } \Omega_{\square}$) from Libbey Owens Ford are therefore the favorite TCOs for large area EC-devices. The FTO layers are essentially fabricated by spray pyrolysis on float glass at $550 \text{ }^\circ\text{C}$, so that their sheet resistance remains stable up to this temperature, which is important for the required heat treatment of the sol-gel layers [35].

2.5.2 Electrolyte

Another critical component in the EC device shown in Fig. 2.6 is the ionic conducting electrolyte. The ions should move fast from the EC-layer through the electrolyte and for the battery-type EC-devices to the complementary EC-layer or the IS layer.

The requirements for an electrolyte for EC-devices according to Granqvist [36] and Vaivars [37] are

1. high ionic conductivity between $10^{-3} - 10^{-7} \text{ S/cm}$ (depending on the application)
2. low electronic conductivity (small than 10^{-12} S/cm)
3. long cycling durability at operation temperature
4. good adhesion with the adjacent layers (no delamination for several years, even after temperature switching tests and more than 10^4 switching cycles)
5. optical transparency for most EC application (display may be an exception)

6. chemical compatibility with the functional layers
7. electrochemical stability in the voltage range used for switching the EC-device
8. long term stability against UV-light if the UV-light is not filtered by the functional layers for certain application (e.g. EC-devices for architectural or automotive glazing)

The literature on ionic conductors is vast and several reviews on inorganic ion conductors suitable for EC devices and other applications can be found in [1,38-39]. Most of the research in this field was done on H^+ and Li^+ conductive coatings, the last one being used in this work.

Principally there are two classes of materials which can be used as a sol-gel electrolyte: the first one is based on the fabrication of an inorganic oxide material (e.g. Ta_2O_5 , Nb_2O_5) and the other on the preparation of organic-inorganic hybrids which combine the better conductive properties of polymer type material with the better mechanical strength of inorganic material. Such a system was used in this work.

In general, the solid (gel) electrolytes described in the literature contain, as a basic compound, an ionic conductor (most frequently a lithium salt), an organic matrix and organic solvents (anhydrous ones). These solvents must cause ionic dissociation and provide the required ionic mobility, in other words they should provide a suitable conductivity.

3 Background

3.1 Materials for electrochromic devices

3.1.1 Overview

Electrochromism has been known since 1953 when Kraus [40] discovered that a vapor-deposited WO_3 layer on a semitransparent metal layer (Cr, Ag) was intensely blue colored when cathodically polarized in 0.1 N H_2SO_4 . However world wide research on this topic started only after the fundamental work of Deb [41, 42] on the same material two decades later. Today several other materials are known to exhibit such a property. Most of them are inorganic oxides of transition metals, but recently more and more organic materials, mostly doped polymers, have been also discovered [27, 43-46]. Usually simultaneous electrochemical injection of electrons and charge compensation cations produces a colored state so that the coloration and bleaching of these materials is described schematically by



where Me is a metal atom, I^+ is a singly charged ion such as H^+ , Li^+ , Na^+ , K^+ , Ag^+ , e^- is an electron and n depends on the particular type of oxide. Some materials color when they are cathodically polarized, others when anodically polarized and a few of them color in both states, as e.g. V_2O_5 and Rh_2O_3 . An overview of these elements is shown in Fig. 3.1.

ELECTROCHROMIC OXIDES:

H																				He	
Li	Be																				
Na	Mg																				
K	Ca	Sc	Ti	V	Cr	Mn	Fe	Co	Ni	Cu	Zn	Ga	Ge	As	Se	Br	Kr				
Rb	Sr	Y	Zr	Nb	Mo	Tc	Ru	Rh	Pd	Ag	Cd	In	Sn	Sb	Te	I	Xe				
Cs	Ba	La	Hf	Ta	W	Re	Os	Ir	Pt	Au	Hg	Tl	Pb	Bi	Po	At	Rn				
Fr	Ra	Ac																			




Fig. 3.1. Transition metals whose oxides (shaded boxed) lead to well-documented cathodic and anodic electrochromism [2]

The cathodic electrochromic transition metal oxides are based on Ti, Nb, Mo, Ta and W. The most frequent material used in devices is WO_3 , which is also chosen for blue coloring devices in this work. Another cathodic EC material, used in this work for gray color devices, is molybdenum doped Nb_2O_5 [104].

The corresponding anodic oxides are based on Cr, Mn, Fe, Co, Ni, Rh and Ir.

3.1.2 Tungsten trioxide

“Tungsten” is actually the Swedish name for heavy stone. The whitish metal is rare in nature, the average earth supply being 0.0001 % [47]. Though it occurs in nature in various oxide compounds, it is the pure tungsten trioxide which is of interest for EC devices. The material is the most widely studied cathodic EC material, because it has the largest coloration efficiency (C.E.) (30 to 70 cm²/C) [35] (see the definition in section 4.3.2).

The coating changes its color from transparent or slightly yellow to deep blue when protons (H⁺) or lithium ions (Li⁺) are intercalated and a tungsten bronze is formed. The bronze can be also formed when sodium, potassium or silver ions are used, but with increasing size of the ions, their rate of diffusion decreases and therefore the rate of optical modulation decreases.

The ionic diffusion coefficient also depends on the microstructure of the coatings and can vary by three orders of magnitude by changing the density of the coatings [39, 48]. Polycrystalline tungsten oxide, which crystallizes between 300 °C and 400 °C, modulates the optical transmittance by reflection (especially in the near infrared region) whereas amorphous tungsten oxide does it by absorption [39, 49, 50]. Therefore the variation of the transmittance in the visible range, which is important for EC glazing, is usually obtained with amorphous WO₃ coatings.

At least four basic sol-gel routes have been developed for the preparation of the WO₃ sol [1]:

- 1) acidification of sodium tungstate [51-53];
- 2) use of peroxytungstic acid [54-58];
- 3) hydrolysis of alkoxides [54,59-61];
- 4) reaction of tungsten chloride and oxychloride with alcohols [62-66]

The first method is one of the earliest efforts to produce sol-gel WO₃ films and its major advantage is the formation of WO₃ at room temperature with no formation of decomposition products. It is therefore possible to produce thick and unstressed films. However the stability of the solutions (which is an important parameter for industrial production) and the adhesion of the coatings to the substrate were not found adequate [51], although the sol stability could be slightly improved by complexing it with appropriate additives such as dimethylsulfoxide [SO(CH₃)₂] [52].

In the second method, tungsten and tungsten carbide powder are digested by an aqueous solution of hydrogen peroxide. The product, a peroxytungstic acid, is isolated and then dissolved in a polar solvent such as alcohol or water. The acid is decomposed into tungsten oxide during a heat treatment of the film at low temperature (100-200 °C). It is an inexpensive route and therefore promising for industrial use.

A synthesis based on the peroxytungstic route was patented [58]. Metallic W is formed with a mixture of a peroxy acid such as hydrogen peroxide and an organic acid such as acetic or propionic acid at low temperatures (-10 to 12 °C). The resulting product, a W-peroxy acid, is then esterified to produce a peroxyester-W derivative (PTE). The sol is stable if stored below 10 °C and it is claimed that the optical transmittance of the coatings decreases from 85 % to less than 15 % in a matter of seconds. Such a method can be in principle extended to other metals such as Mo, Mn, Cr, Rh, Ir, Ni etc. By the addition of additives to the peroxytungstic sol such as oxalic acid, the coloration efficiency of the WO₃ coatings can be increased and the dependence of the transmittance change on the switching cycle can be eliminated [67, 68].

Based on the same route, Schmidt et al. [69] patented an EC thin-film system and components thereof, whereby an improvement of WO₃ (and MoO₃) sol-gel layers was obtained by addition of alkali metal salts into the sol. Thus some of the oxides were converted into alkali metal tungstate (or molybdate respectively) without any adverse effect on the EC function or on the ability to process the layers. This procedure considerably accelerates the establishment of a stable operating state. Long-term switching experiments show that near cycling-independent coloration times are obtained by the incorporation of lithium ions during the layer formation [70, 71]. This method was already used to produce large area WO₃ coatings on FTO glass for EC-devices up to 50 cm x 80 cm [72]. With a modified sol (addition of solvents with higher boiling point than ethanol and some additives), spray coated WO₃ films of the size 35 cm x 35 cm were fabricated with homogeneous optical properties [73].

The tungsten alkoxide (third method) is the classical sol-gel route for any kind of oxide but is expensive and consequently not useful for industrial application [74]. Crack-free films could only be prepared with small thickness (< 50 nm). It is therefore necessary to repeat the deposition process to obtain thicker films to get a sufficient optical contrast.

According to Livage [66] the reaction of tungsten oxy-chloride (WOCl₄) with isopropanol is also a good method of preparation as it is cheap and leads to a sol that is stable for several months because of the formation of molecular oligomers (WOCl_{4-x}(OⁱPr)_x)_n [62]. In this method, tungsten chloride is reacted with an anhydrous alcohol and the resulting material is diluted with more alcohol to obtain the precursor sol. The films have a high uniformity, better than those prepared via a colloidal route. The same precursor has also been used to deposit WO₃ by spray pyrolysis [75]. Micrometer-thick hydrated films of composition WO₃·nH₂O are easily obtained, with the control of the amount of water and adequate heat treatments controlling the film morphology, essential for these applications. The EC properties were found to depend upon the values of n. It was also found that the switching time and the long term memory decrease when the amount of water increases due to faster ion diffusion through the gel network [63]. When Li⁺ ions are used, the best

electrochemical stability was encountered for $n = 0.5$ as higher amount of water leads to a gradual decrease of the current, an indication of the occurrence of an irreversible process [74].

Large area WO_3 sol-gel films ($20 \times 20 \text{ cm}^2$) were also fabricated on K-glass (FTO) [74] using the alkoxide route by mixing 2-propanol, acetic acid and tungsten pentaethoxide.

Mesoporous tungsten oxide films were fabricated via different block copolymer templates and an ethanolic WCl_6 solution [76-78] showed improved kinetic performance over its sol-gel counterpart in protonic or lithium conducting electrolyte. The block copolymers were removed by calcination at $300 \text{ }^\circ\text{C}$ or $400 \text{ }^\circ\text{C}$ [76, 77] or by room temperature ultraviolet (UV) illumination /ozone treatment method [77,78]. The mesoporous tungsten oxide layers show a faster coloration and bleaching kinetics, due to the faster diffusion of Li^+ or H^+ ions, but the transmittance change and the coloration efficiency were found smaller than those of standard sol-gel films.

EC tungsten oxide film was also fabricated by an original soft chemistry route, in which the transparent conducting glass substrate was successively dip-coated with poly(acrylic acid) (PAA) and ammonium tungstate solutions [79]. The as-coated composite layer of $\text{PAA}/(\text{NH}_4)_2\text{WO}_4 \cdot n\text{H}_2\text{O}$ was dried at a low temperature ($100 \text{ }^\circ\text{C}$), and the ammonium tungstate component was polycondensed by acid treatment in 1 N HCl to form an EC PAA/ WO_3 film. Transmission electron microscopy showed that the PAA/ WO_3 film contains regularly dispersed WO_3 grains with an average size of $\sim 5 \text{ nm}$. According to the Auger depth profile analysis, the relative content of W, O, and C was quite homogeneous across the thickness of film. Depending on the concentration of PAA in the coating solution (1.0-3.0 wt.%), the thickness and the tungsten oxide content of the film were found to vary; therefore, the electrode property of the PAA/ WO_3 layer could be easily controlled. By using a 2.5 wt.% PAA solution, an optimum EC function was achieved with a coloration efficiency of $\sim 38 \text{ cm}^2/\text{C}$ and a cycle life longer than 11000 when a charge of $Q = 12.5 \text{ mC}/\text{cm}^2$ was exchanged.

3.1.3 Doped and undoped niobium pentoxide

Another cathodic electrochromic material used in this work is molybdenum doped niobium pentoxide ($\text{Nb}_2\text{O}_5:\text{Mo}$). Niobium oxide is a promising material as EC electrode for EC-devices. A detailed summary on the properties of sol-gel niobium pentoxide were given by Aegerter [80].

Stoichiometric niobium oxides mainly exist in the form of NbO , Nb_2O_3 , NbO_2 and α , β Nb_2O_5 [81]. The first two compounds have been obtained by melting the richest niobium oxide, Nb_2O_5 , with Nb at high temperature. Non-stoichiometric suboxide phases have also been observed. Niobium pentoxide, also known as niobia or niobic acid anhydride, is however the most studied material. It has been prepared by different methods such as oxidation of metallic niobium in air, by hydrolyzing alkali-metal niobates, niobium alkoxides and niobium pentachloride or by precipitation from solution in hydrofluoric acid with alkali-metal hydroxide or ammonia [82].

Traditionally, niobium pentoxide is used in metallurgy for the production of hard materials or in optics as additive to prevent the devitrification and to control the refractive index of special glasses. In electronics it is used for the preparation of electroacoustic or electrooptical components such as LiNbO_3 and KNbO_3 or relaxor ferroelectric ceramics such as $\text{Pb}(\text{Mg}_{1/3}\text{Nb}_{2/3})\text{O}_3$ [82]. However, in the last 15 years, its interesting semiconducting properties and the advent of more sophisticated methods of preparation allowed to obtain in a controlled way of innovative systems such as highly porous materials, very fine powders and coatings. These new materials have found further important applications in the fields of electrochromism, batteries, solar cells and catalysis [80].

The sol-gel method was recognized as a promising route for the preparation of niobium oxide gels, powders and coatings only in 1986 by Alquier et al. [83] who presented four different routes for the synthesis of sols and gels: the dissolution of NbCl_5 in water with or without addition of hydrogen peroxide, the “classical” but expensive way using alkoxides (e.g. $\text{Nb}(\text{OEt})_5$) and a cheaper synthesis using chloroalkoxides. Griesmar et al. [84] from the same laboratory showed later the possibility to obtain Nb_2O_5 xerogels by reactively modifying $\text{Nb}(\text{n-PentO})_5$ with acetic acid, previously synthesized by reacting $\text{Nb}(\text{OEt})_5$ with n-pentanol. These authors only mentioned that such chemical routes could be also useful to prepare coatings but only amorphous phases (gels) and, upon heating in air at 500°C , pure tetragonal niobium pentoxide powders have been obtained. A characterization concerning the above applications has not been presented. Hence, the use of sol-gel derived niobium oxide for EC coatings and devices, solar cells, batteries and catalysis is quite recent.

The first mention of the EC properties of Nb_2O_5 coatings was published by Reichman and Bard in 1980 [85]. Such an effect was observed with a $15\ \mu\text{m}$ thick coating produced on the surface of a niobium metallic disk oxidized at approximately 500°C for 10 min. A blue coloring effect, seen in reflection under H^+ and later also under Li^+ insertion [86], was chemically stable and showed fast kinetics (1-2 s).

Since then, several more adequate deposition techniques have been used to obtain niobium oxide EC films among which CVD [87], DC magnetron sputtering [88], electrochemical method [89] and the dip or spin coating process via the sol-gel route. In the following, we only concentrate on niobium pentoxide coatings made via the sol-gel method.

The first attempt to fabricate sol-gel Nb_2O_5 for electrochemical purpose was reported by Lee et al. [90] who spin-coated an ITO coated glass electrode with a mixture of NbCl_5 dissolved in ethanol. However the durability of the EC response was only a few cycles although the quality of the films could be improved by adding trialkoxysilane in the solution. Faria and Bulhoes prepared thick Nb_2O_5 films ($2.8\ \mu\text{m}$) on ITO glass from a 40 wt.% citric acid /60 wt.% ethylene glycol solution to which a niobium oxalate complex $\text{NH}_4\text{H}_2[\text{NbO}(\text{C}_2\text{O}_4)_3]\cdot 3\text{H}_2\text{O}$ was added [91]. Under Li^+ insertion

the films showed a blue color with a transmittance change of 80 % to 30 % at 631 nm. Much better results have been obtained by Ohtani et al. [92] and Özer et al. [93,94] using sols made from niobium alkoxides such as $\text{Nb}(\text{OEt})_5$ and by Aegerter et al. [95-97] who synthesized $\text{Nb}(\text{OBU}^n)_5$ by reacting NbCl_5 with sodium butoxide in butanol. The improvement in the EC properties of the layers was essentially due to the fact that the layers obtained with these precursors were thin (typically 100-150 nm) and consequently of much better quality even if the deposition procedure had to be repeated 2-4 times in order to get a coating presenting larger change in optical transmittance under H^+ or Li^+ insertion. Aegerter et al. [98-100] also developed a cheaper sol synthesis by dissolving NbCl_5 powder (0.2 M) in butanol (0.28 M) and acetic acid (0.05 M) and submitting the sol for a few minutes to the action of an ultrasonic irradiation. The result was a transparent solution, stable for several months. The films presented reversible and fast insertion/extraction kinetics for Li^+ ions with a coloration efficiency of $22 \text{ cm}^2/\text{C}$ at 600 nm. After insertion, the amorphous films had a brown color while the crystalline ones were dark blue and consequently their optical absorption spectra are different. The method was then extended to other alkoxy groups by Schmitt et al. [101], who dissolved NbCl_5 in ethanol, and Macek et al. [102,103] in propanol, respectively.

From the above reports it clearly appears that till today the best niobium oxide coatings for EC purpose prepared by the sol-gel process are those made from alkoxides- or chloroalkoxides- based sols. The choice of the precursor does not seem to have a large influence on the final EC properties; the dissolution of NbCl_5 in an alcohol under a sonocatalysis process is surely the fastest and cheapest procedure.

An intensive study of the properties of undoped Nb_2O_5 and doped $\text{Nb}_2\text{O}_5:\text{X}$ ($\text{X} = \text{Sn}, \text{Zr}, \text{Li}, \text{Ti}, \text{Mo}$) layers, prepared with the sonocatalytic method, as a function of the sintering temperature, of the doping material and its concentration was recently performed in our group [100, 101, 104-106]. An 0.4 M sol to produce Nb_2O_5 films was prepared by dissolving NbCl_5 powder in ethanol and acetic acid leading to a niobium chloroalkoxide solution of the type $\text{NbCl}_{5-x}(\text{OEt})_x$. The doping at different concentration was realized by dissolving in ethanol SnCl_4 for tin, ammonium zirconate $[(\text{NH}_3)_2\text{ZrO}_3]$ for zirconium, LiCF_3SO_3 for lithium, titanisopropoxide $[\text{Ti}(\text{i-PrO})_4]$ for titanium and phosphormolybdenum acid $\text{H}_3[\text{P}(\text{Mo}_3\text{O}_{10})_4]\cdot\text{H}_2\text{O}$ for molybdenum. The solutions were mixed with the niobium chloroalkoxide solution and then submitted to an ultrasonic irradiation treatment for a few minutes resulting in a transparent sol. The coatings were deposited on ITO or FTO coated glass substrates by dip coating technique and heat treated at a given temperature. This procedure was repeated one time and the samples were then sintered for 30 min at different temperatures ranging from $400 \text{ }^\circ\text{C}$ to $600 \text{ }^\circ\text{C}$, resulting in transparent layers with thickness between 60 to 90 nm. The doping of the Nb_2O_5 layers with Li, Ti and Mo has two interesting effects: a deeper coloring with the same amount of niobium atoms [increase of the change of the optical density ΔOD from 0.3

(undoped) to 0.63 by doping with Mo (Mo:Nb=0.2)] and the possibility to have a gray color in the intercalated state (e.g. with Mo doped coatings). These results showed that molybdenum doped niobium is more promising than others because of its high transmittance change and its gray color which is different from that of WO_3 . In this work, we also investigated the EC layer and EC-devices made with it.

3.1.4 Cerium and cerium-titanium oxides

Cerium is the most abundant member of the series of elements known as lanthanides or rare earths, the elements in the Periodic Table in which the inner 4f electron shell is being filled. Despite the label “rare” applied to the 4f element series, Ce is not especially rare. Cerium ranks 25th in the listing by abundance of all the nature occurring elements in the crust of the earth. It is used in metallurgy, glass and ceramics, catalysis and as luminescent phosphor.

Cerium made its first major contribution to chemical technology one hundred years ago, in 1891 outside the Opern café in Vienna as a successful installation of gas lights, using the Welsbach gas mantle based on a thorium- and cerium-oxide impregnated fabric. Cerium still contributes to lighting, but today is also found in automobiles, televisions and many more technologies.

Cerium is characterized chemically by having two stable valence states, Ce^{4+} , ceric and Ce^{3+} , cerous, and this property underlies several technological uses. Its ability to easily intercalate or deintercalate electric charge and therefore to change from Ce^{4+} to Ce^{3+} is used in our work.

Ceric salts tend to be orange or red in color due to charge transfer interactions. The simple uncoordinated ceric ion in a glass matrix or the oxide, absorbs in the ultraviolet range but not in the visible. Ce^{3+} has also no absorption bands in the visible range and the ionic salt in general are colorless [107]. This means that a transfer from CeO_2 to Ce_2O_3 is not accompanied by a color change in the visible range, so that a cerium based film is a good candidate to realize an ion-storage layer remaining fully transparent.

The first work about the preparation of pure CeO_2 coatings by sol-gel method was reported by Atkinson et al. [108]. The coatings were prepared from cerium hydroxide, which was peptized with HNO_3 with a nitrate to ceria ratio of 27:100. However the authors only reported on the mechanical stability of the films in relation to crack formation. Later Stangar et al. [109] have prepared pure CeO_2 sols by thermal decomposition of cerium ammonium nitrate $\text{Ce}(\text{NH}_4)_2(\text{NO}_3)_6$. Peroxy complexes were made by adding H_2O_2 to the yellow solution of the starting compound. A brown $\text{Ce}(\text{IV})$ complex decomposed into a yellow gelatinous precipitate which was used after peptization with HNO_3 for making very stable sols and coatings. Sols were stable for a few months and the coatings obtained with fresh or aged sols are homogenous and crack free with a particular texture. The electrochemical properties showed a reasonably good reversibility for Li^+ insertion/deinsertion and the total charge exchanged during cycling was found to depend on the thickness of the coatings

and varied from 1 mC/cm^2 for a 25 nm thick film to 9 mC/cm^2 for a 250 nm thick coating. However the kinetics was slow.

Much better results have been reported one year later by Orel et al. [110] using sols made with the same precursor $\text{Ce}(\text{NH}_4)_2(\text{NO}_3)_6$. In this method precipitates have been obtained by addition of NH_4OH at $\text{pH} = 9$. After washing with bidistilled water in order to remove NH_4^+ , Cl^- , and NO_3^- , peptization was performed by adding an equimolecular quantity of HNO_3 to obtain a colloidal sol. Coatings have been obtained by a dip coating technique followed by heat treatment at $300\text{-}500 \text{ }^\circ\text{C}$. The authors reported that the amount of charge exchanged increased with the cerium oxide concentration in the sol and the thickness of the films (up to 8 dips corresponding to 280 nm). The highest value was about 20 mC/cm^2 .

CeO_2 films prepared using $\text{CeCl}_3 \cdot 7\text{H}_2\text{O}$ as a precursor was reported by Skofic et al. [111]. The films were heat-treated in an air or argon atmosphere. The structure, electrochemical and optical properties of these films depend on the preparation conditions. It was found that the films heat-treated in argon have higher charge capacity.

CeO_2 films have been also obtained using other deposition methods like physical vapor deposition (e-beam) [112], laser-induced ablation [113], spray pyrolysis [114] or sputtering [115].

The diffusion rate of Li^+ ions into pure CeO_2 layers is low and this limits the use of such material for EC devices that have to respond in a fast way to changes in the light environment. When comparing the size of the insertion sites in CeO_2 (1.02 \AA) with that of the lithium ion radius (0.6 \AA), it is not favorable for lithium intercalation. Therefore, it is suitable to substitute cerium atoms by another element of smaller ionic radius in order to modify the structure. Considering that the diffusion rate of lithium in TiO_2 is more than 1000 times higher than in CeO_2 [115,116], Baudry et al. already in 1990 [117] were the first to propose the replacement of about 50 % of the cerium by titanium. They prepared $\text{CeO}_2\text{-TiO}_2$ sols by dissolving $\text{Ce}(\text{NH}_4)_2(\text{NO}_3)_6$ and tetraisopropyl orthotitanate $\text{Ti}(\text{i-PrO})_4$ in ethanol. The sol was stable for at least one week at room temperature. The charge insertion and extraction for dip-coated films measured during cyclic voltammetry (CV) (scan rate 10 mV/s) was 10 mC/cm^2 . A series of papers were then published on the development of this method [118-122].

Avellaneda et al. [123] prepared $(\text{CeO}_2)_x(\text{TiO}_2)_{1-x}$ layers with a molar ratio of $\text{Ce/Ti} = 0.5$ using the same precursor in isopropanol, but the solution mixture was submitted for a few minutes of the action of an ultrasonic irradiation. The coatings were heated at $450 \text{ }^\circ\text{C}$ (15 min) and studied in 1 M LiClO_4 in PC electrolyte by CV (50 mV/s). The intercalated and deintercalated charge of an approx. 100 nm thick layer was 16 mC/cm^2 and remained constant from the 10^{th} CV cycle up to more than 4000 CV cycles.

Equimolar CeO₂-TiO₂ films were fabricated with the same precursors in a mixture of ethanol and water and with addition of a small amount of acetic acid by Ghodsi et al. [124]. The films were prepared by dip coating and heated at 100 °C and showed a porous structure. The intercalation process was however not fully reversible, probably because of the too low sintering temperature of the layer.

By using Ce(NO₃)₆•6H₂O as the precursor for cerium, Munro et al. [69, 71] prepared thick CeO₂-TiO₂ layers by a single dip coating step. The precursors were dissolved in ethanol and the solution was heated under reflux in order to achieve a colloidal sol. The layers were heat treated at 400 °C. 140 nm thick crack free single layers were obtained. 200 nm thick coatings were obtained in a single dip coating step by aging the sol for several days [72]. This facilitates the industrial fabrication of large and thick coatings by a single dip coating step. By using these layers, large area (50 cm x 80 cm) EC devices were fabricated.

Mixing of two alkoxides, Ce(OBu^s)₄ and Ti(OBuⁿ)₄ was also used for preparing the CeO₂-TiO₂ sol [125,126]. In this case the coatings were found amorphous for concentrations of CeO₂ below 50 % and the size of the CeO₂ nano crystallites imbedded in the TiO₂ amorphous matrix increases from ~1 nm for 5 % CeO₂ to 5 nm for pure CeO₂.

CeO₂-TiO₂ coatings have also been prepared by Stangar et al. [109] using the route proposed by Makishima et al. [127] in which CeCl₃ was used in combination with tetraisopropyl orthotitanate Ti(i-PrO)₄ with a Ce/Ti mole ratio of one to one. Their overall properties were similar to those found by Baudry et al. [117-122] but their electrochemical properties were inferior. No comments about the size of the CeO₂ nanoparticles have been reported.

Optical and electrochemical properties of sol-gel spin-coated CeO₂-TiO₂ films (50 % CeO₂) were also studied by Ozer et al. [128] using the precursors Ce(NH₄)₂(NO₃)₆ and titanium ethoxide [Ti(OC₂O₅)₄] dissolved in ethanol and addition of HNO₃. The intercalated charge during CV cycling (scan rate 20 mV/s) in 1 M LiClO₄ in PC of a 250 nm thick layer was 10 mC/cm².

Stangar et al. [109] compared the properties of CeO₂ coatings with (CeO₂)_x(TiO₂)_{1-x} coatings made with sol-gel dip coating method. The solar transmission values of both coatings are in the range 0.6-0.8 and depended on the coating thickness. Cyclic voltammetric measurements in LiOH electrolyte showed that the pure CeO₂ system exhibits higher overall electrochemical reversibility when compared to the CeO₂-TiO₂ system. The CeO₂ system is also less sensitive with regard to the coating thickness. Coulometric measurements show that CeO₂ also exhibits larger charge incorporation, which was determined as a function of the coating thickness.

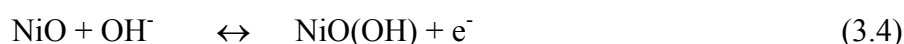
Keomany et al. [125] also compared the properties of CeO₂ coatings with those of (CeO₂)_x(TiO₂)_{1-x} coatings made by the spin-coating method. Films of mixed oxides with composition range from

25 % to 50 % CeO₂ were found to exhibit a higher diffusion coefficient for lithium and with a Li⁺ storage capacity remaining at an acceptable level.

3.1.5 Nickel oxide

Nickel oxide and nickel hydroxide are well known anodic EC materials and may be a promising counter electrode in complementary-type EC-devices where transmission changes are increased due to the simultaneous coloring process of cathodic and anodic films. Nickel oxide changes from a colorless state to a brown colored Ni oxy-hydroxide upon electrochemical oxidation with high coloration efficiency (35-50 cm²/C) [129]. The majority of the works on Ni oxide electrodes discusses proton (and/or hydroxyl ion) intercalation/deintercalation.

Nickel belongs to the group VIII in the periodic table of elements. The most stable oxidation state is Ni(II). Nickel(II) oxide is formed when the hydroxide, carbonate, oxalate, or nitrate of nickel(II) is heated. Nickel(III) is not as stable as Nickel(II), but there are two known crystalline forms of black NiO(OH). The more common one is β-NiO(OH) and is obtained by the oxidation of nickel(II) nitrate solutions with bromine in aqueous potassium hydroxide below 25 °C [130]. Proposed mechanisms for the electrochromic reaction of nickel hydroxide or nickel oxide in aqueous electrolyte are given by the following reactions [131-135]. Without doubt, the EC coloration is related to the redox process Ni(III) (dark)/Ni(II) (bleached):



bleached colored

Until now, four kinds of precursors were used to deposit pure nickel oxide films by the sol-gel method. Nickel alkoxides are polymeric and generally insoluble in alcohols at room temperature [136], making them unsuitable for this purpose. The first successfully deposited nickel oxide films have been obtained from mixture of nickel nitrate [Ni(NO₃)₂(H₂O)₆] in alcohol [137] or ethylene glycol [138,139] solutions. Doubts about the thermal stability of metal nitrates are likely to restrict its use to small-scale applications.

Another precursor is nickel sulphate hexahydrate [NiSO₄·6H₂O] [140]. LiOH solution was added to a solution of nickel sulphate until pH = 9.0 were reached. The green precipitate was washed with water and then peptised with glacial acid to pH = 4.5. Formamide [HCONH₂], glycerol and an aqueous solution of polyvinyl alcohol (PVA) were added to improve the adherence and abrasion resistance of the final films. The films were made by dip-coating technique followed by a heat

treatment at 300 °C for 15 min, leading to 100 nm thick layers per dip. The electrooptical study in LiOH electrolyte showed high transmittance change of about 60 % at 450 nm. The coloration efficiency was rather high, about 30 to 40 cm²/C at 400 nm, but the spectral transmittance of the bleached state decreases continuously after 10 cycles, indicating that the Ni(III) phase is progressively and irreversibly formed during cycling. Further studies of layers prepared with this sol [141-144] showed that the thermal treatment of the layers is very important for the EC activity and the electrochemical stability: a lower temperature and shorter heating time lead to higher EC response but to lower reversibility and stability. A heat treatment at 270 °C for 60 min was found to show acceptable transmittance change and good reversibility [142].

Nickel chloride [NiCl₂·6H₂O] as a precursor was tested by Sharma et al. [145]. They use a solution of nickel chloride in butanol and ethylene glycol for the deposition of NiO_xH_y thin films. The intensity of the anodic/cathodic CV peaks measured in KOH solution enhanced with the increase of the heat treatment temperature up to 300 °C but decreased for higher values. The hydrolysis of the nickel chloride in butanol was controlled by addition of acetic acid [146]. The increase in acetic acid leads to denser films and a decrease of the positive current density in CV cycle. The addition of citric acid to this sol was also studied [147]. A variation of the transmittance from 80 % to 50 % at 500 nm was obtained for layers heated at 350 °C. Films sintered at 450 °C did not show an EC effect.

Nickel oxide films deposited from nickel(II)-acetate tetrahydrate Ni(OCOCH₃)₂·4H₂O precursor dissolved in methanol have been reported by Jimenez-Gonzalez et al. [148]. Williams et al. prepared a sol of nickel(II) acetylacetonate Ni(acac)₂ or Ni(OCOCH₃)₂·4H₂O in N,N-dimethylaminoethanol (dmaeH), yielding new complexes [Ni(ac)₂(dmaeH)] and [Ni(acac)₂(dmaeH)₂] [149]. These compounds are good precursors and have a reasonable solubility in methanol or ethanol and are highly soluble in dmaeH, making them suitable for sol-gel applications. The NiO film changed its color from transparent to brown when it was oxidized. The coloration efficiency increased from the first up to the 50th cycle from 13.5 to 27 cm²/C respectively. Sols prepared with Ni(OCOCH₃)₂·4H₂O in dry dmaeH were successfully used to deposit NiO_x thin films on conductive ITO glass [150]. The films were studied in KOH electrolyte and showed also an activation period, during which the charge capacity and the EC response increased. After this period, a steady state was reached, but the films were not stable after long cycling (~100 cycles depending on the thickness of the layer). Kim et al. [151] also tested NiO films prepared using nickel acetate as precursor. The cyclic voltametric measurement of the layers was conducted between -0.8 V and +1.5 V vs. Ag/AgCl in 0.1 M KOH solution at a scan speed of 20 mV/s. The corresponding transmittance change at 550 nm was 83 % to 25 %.

Different research groups also tried to make doped nickel oxide films for EC devices, for example, nickel-silicon oxide films by Moser et al. [64,139,141,142], lithiated nickel oxide thin films by

Svegl et al. [152] and nickel titanium oxide thin films by Martini et al. [153]. According to their results, higher Ti contents lead to improved adherence and abrasive resistance and higher transparency of the films in their bleached state.

Recently Heusing et al. [154] studied mixed nickel-titanium oxide sol-gel layers, using Ni(II)acetate and tetrapropyl orthotitanate in ethanol as precursors. The dip-coated films were heated at 300 °C and were homogeneous and transparent. They showed a good anodic EC behaviour in 1 M LiClO₄ in propylene carbonate. The transmittance changed in 2 min from 85 % down to 45 % (550 nm) by exchanging 21 mC/cm². These electrodes may be promising as anodic EC electrodes in EC-devices with Li⁺ ion conducting electrolyte.

3.2 Smart windows

As shown in section 2.4, a smart window is an EC device used for regulating the transmittance between a transparent (bleached) and an absorbing (colored) state and finds a variety of applications. For example, it can be used to regulate the incident solar energy and glare for the improvement of energy efficiency of buildings, vehicles, aircraft, spacecraft and ships [3,4,155, 156]. The potential market for smart windows is very large. Flabeg (Germany) has made the largest prototype EC architectural windows installed in buildings. The windows had a transmittance change range of $T_{vis} = 50-15\%$ [157] and took a few minutes to color or to bleach.

The transmittance of an EC device can be expressed by the transmittance at certain wavelength, or by its photopic transmittance T_{vis} determined from the UV/VIS spectra of the devices in both states by

$$T_{vis} = \frac{\sum_{\lambda=380\text{ nm}}^{780\text{ nm}} D_{\lambda} T(\lambda) V(\lambda) \Delta\lambda}{\sum_{\lambda=380\text{ nm}}^{780\text{ nm}} D_{\lambda} V(\lambda) \Delta\lambda} \quad (3.6)$$

whereby λ represents the wave length, $T(\lambda)$ the spectral transmittance of the sample, D_{λ} the spectral energy distribution and $V(\lambda)$ the luminous efficiency of the human eye (DIN EN 410) [158].

For WO₃ and Nb₂O₅ the values of T_{vis} and transmittance measured at 550 nm are quite similar.

An overview summarizing the work from 1998 to 2001 on EC devices for regulating the transmittance was given by Granqvist [159]. However few EC devices have been prepared by the sol-gel technique. Heusing et al. [35] recently reviewed EC devices based on sol-gel technique. The first “all sol-gel” EC device was reported by Livage et al. [160] in 1988, which laminated a device consisting of a SnO₂ counter electrode, a WO₃ layer and a TiO₂-gel ionic conductor. The problem there was the SnO₂ counter electrode that exhibited irreversible coloration.

Most of the sol-gel EC devices reported in the literature have been based on WO_3 or doped WO_3 as EC layer, and a counter electrode made with various transition metal materials. A comparative study of “all sol-gel” EC windows made with various counter electrodes was recently given by Krasovec et al. [158] who tested 24 different layers such as $\text{SnO}_2(\text{Mo, Sb})$, LiCo-oxide, CeVO_4 and V/Ti-oxide with EC device configuration glass/ FTO/ WO_3 / ormolyte- Li^+ / counter electrode layer/ FTO/ glass. The device with Sn/Mo (1:1) oxide counter electrode showed the smallest transmittance in the colored state ($T_{\text{vis}} = 3.5\%$), but had a rather low transmittance in the bleached state ($T_{\text{vis}} = 63\%$). The combination of a WO_3 film with either Ce/V, V/Ti/Ce or Sn/Mo oxides counter electrodes showed a photopic transmittance in the colored state of $25\% < T_{\text{vis}} < 30\%$, whereby the highest transmittance in the bleached state was $T_{\text{vis}} \sim 70\%$ as shown for a Ce/V-oxide film. The experiments with different Ce/V- and Fe/V-oxide counter electrodes showed that EC devices with Ce/V-oxide (Ce/V = 1:1) had the highest transmittance in the bleached state ($T_{\text{vis}} \sim 70\%$), with a transmittance in the colored state remaining above 15%. A deeper coloration was obtained with Fe/V (1:2)-oxide devices ($T_{\text{vis}} = 4\%$), but the transmittance of the bleached state was low ($T_{\text{vis}} = 62\%$).

Svegl et al. [152] reported sol-gel EC-devices with a sol-gel WO_3 film on FTO as electrochromic electrode, a $\text{Li}^+(\text{H}^+)$ ormolyte and a sol-gel counter electrode consisting of either $\text{Li}_{0.99}\text{Co}_{1.01}\text{O}_2$ or $\text{Li}_{0.94}\text{Ni}_{1.06}\text{O}_2$ deposited on FTO glass. After galvanostatic coloration and bleaching process both devices showed a dark blue coloration ($T_{550} \sim 3\%$) in the colored state. The bleached state had a higher transmittance for EC devices with $\text{Li}_{0.94}\text{Ni}_{1.06}\text{O}_2$ ($T_{550} \sim 68\%$) than with $\text{Li}_{0.99}\text{Co}_{1.01}\text{O}_2$ ($T_{550} \sim 46\%$) as counter electrode. The electrochromic efficiency of the EC devices was $\sim 25 \text{ cm}^2/\text{C}$ and $\sim 40 \text{ cm}^2/\text{C}$ for $\text{Li}_{0.94}\text{Ni}_{1.06}\text{O}_2$ and $\text{Li}_{0.99}\text{Co}_{1.01}\text{O}_2$ as counter electrode respectively. The devices showed good reversibility and stability after performing about 1000 galvanostatic cycles. The disadvantage of $\text{Li}_{0.99}\text{Co}_{1.01}\text{O}_2$ films is the slight yellow color of the EC devices in the bleached state.

Ozer et al. [161] reported a sol-gel EC-device of the configuration glass/ FTO/ WO_3 / α -PEO/ NiO_xH_y / FTO/ glass with a lithiated oxymethylene-linked poly(ethylene oxide) (α -PEO) ionic conductor. The devices had a fast optical response (50 s) and a transmittance change from 80% to 50% at 550 nm but a short cycling lifetime.

Recently Orel et al. [162] reported on a hybrid EC-devices with a new sol-gel redox I_3^-/I^- electrolyte. The EC properties and the stability of EC hybrid devices were tested up to 1800 cycles showing high transmittance change from $T_{\text{vis}} = 66 - 69\%$ (bleached state) down to 27 - 31% (colored state) after 10 s (coloration) and 5 s (bleaching) switching time. The cycling stability was improved with redox electrolytes having an embedded co-solvent of high boiling point.

The first “all sol-gel” EC device consisting of a WO_3 layer, a CeO_2 - TiO_2 counter electrode and a TiO_2 gel electrolyte was described by Macêdo and Aegerter [121]. It had an optical transmittance change of 60 % to 20 % during the first cycle and a response time of a few seconds. The transmittance of the colored state was not stable and increased to 35 % after 360 cycles. These results were comparable to EC devices obtained by other techniques, but a delamination of the device was observed during extended cycling due to the degradation of the TiO_2 gel ion-conductor.

INM has also used since many years CeO_2 - TiO_2 as counter electrode for the development of EC devices. An “all sol-gel” EC system, patented by Schmidt et al. [69], consisted of a lithium doped sol-gel WO_3 layer, a sol-gel $(\text{CeO}_2)_x$ - $(\text{TiO}_2)_{1-x}$ counter electrode and an organic-inorganic nanocomposite electrolyte. The systems were described by Munro et al. [71], Heusing et al. [72,163] and Mennig et al. [164]. EC-devices of the configuration glass/ ITO/ WO_3 / nanocomposite electrolyte/ $(\text{CeO}_2)_x$ - $(\text{TiO}_2)_{1-x}$ / ITO/ glass up to a size of 35 x 35 cm^2 showed a reversible transmittance change from 75 % to 22 % (-2.5 V/ +2 V) at 633 nm, fast switching kinetics and a high cycling stability.

EC-devices and EC displays up to 50 x 80 cm^2 using the same configuration but FTO as transparent conductor were also fabricated. They showed homogeneous coloration and bleaching kinetics and high cycling and UV-stability [72,163]. The devices showed a reversible transmittance change from 70 % to 25 % at 550 nm (voltage ± 2.5 V), and a switching time of 3 min when a 1 mm thick electrolyte was used.

Avellaneda et al. [165] reported all sol-gel EC devices (2 x 3 cm^2) of the configuration WO_3 /ormolyte/ CeO_2 - TiO_2 using a silica-polyethyleneglycol ormolyte described by Dahmouche et al. [166]. The devices were assembled at room temperature and heat treated at 50 °C for 2 hours to harden the ormolyte. The best results were obtained with $[\text{O}]/[\text{Li}] = 15$ giving a 48 % transmittance in the colored state and 78 % in the bleached state.

EC windows using niobium oxide or doped niobium oxide were not as intensively developed as the ones using WO_3 , because the coloration efficiency of niobium oxide is smaller than that of WO_3 . Avellaneda [167] realized a cell with the configuration glass/ ITO/ Nb_2O_5 / electrolyte/ CeO_2 - TiO_2 / ITO/ glass. By switching between +1.5 and -2.0 V only a small Li insertion has been observed and no coloration has been observed. Schmitt [104] using the same configuration with a 125 nm thick Nb_2O_5 and a 240 nm thick CeO_2 - TiO_2 counter electrode also measured a very small Li insertion and no color change.

Orel et al. [102,103,168] succeeded to observe a transmission change between 60 % and 33 % with a sol-gel SnO_2 :Sb(7 %):Mo(10 %) layer as counter electrode switching between -4.0 V and +2.0 V during 120s. Due to the very high negative applied potential, the cell had a very poor stability of < 500 cycles.

However, Schmitt [104] fabricated cells with a 180 nm thick $\text{Nb}_2\text{O}_5:0.4 \text{ Mo}$ EC electrode sintered at 500 °C and a $\text{TiO}_2\text{-CeO}_2$ IS electrode with a thickness varying between 240 nm (1 layer) to approx. 950 nm (4 layer). A voltage of + 2.5 V to – 2.5 V was applied during 120s. The highest amount of charge exchanged was 18 mC/cm^2 obtained with 3 IS layers and the maximum change in transmission was $\Delta T_{\text{vis}} = 0.28$. The best cells were stable only up to 15,000 cycles.

Recently, researches involving new methods such as a combination of transition metal oxides and organic materials to make EC devices have been reported. Cummins et al. [169] constructed an ultrafast EC window. One electrode of this window is based on a transparent nanostructured TiO_2 (anatase) film (4.0 μm thick) deposited on conducting glass (FTO, 10 Ω_{\square} , 0.5 μm thick) and modified by chemisorption by a monolayer redox chromophore bis(2-phosphonoethyl)-4,4'-bipyridinium dichloride. The other electrode is based on a transparent nanostructured SnO_2 film (3.0 μm thick) supported on the same conducting glass and chemisorbed with a monolayer of the redox chromophore [β -(10-phenothiazyl)propoxy]phosphonic acid. The electrolyte used was LiClO_4 (0.2 mol l^{-1}) in γ -butyrolactone. The window withstood over 10^4 EC test cycles with switching times (coloring and bleaching) of less than 250 ms. The coloration efficiency was about 270 $\text{cm}^2 \text{ C}^{-1}$ and the memory (time required for the low end transmittance to increase by 5 %) was better than 600 s.

The modulation of the optical properties requires the application of a DC voltage whose magnitude is easily obtained from solar cells. Such cells can be external to the EC device, but if semitransparent, they can be intergrated in a multilayer construction comprising a superimposed solar cell and electrochromic tandem configuration [6]. For example, Deb et al. [170] described a PV-powered EC window in detail. The device employs a wide band gap a-Si $_{1-x}$ C $_x$ /H n-i-p PV cell as a semitransparent power source and a $\text{Li}_y\text{WO}_3/\text{LiAlF}_4/\text{V}_2\text{O}_5$ EC device as an optical-transmittance modulator. The EC device is deposited directly on top of a PV cell deposited on a glass substrate. The PV-EC device modulates the transmittance by more than 60 % over a large portion of the visible spectrum. The coloring and bleaching times of the EC device are approximately 1 min under normal operating conditions (+/-1 V).

A new photoelectrochromic device with excellent coloring and bleaching characteristics was recently developed by Hauch et al. [171]. In contrast to other photoelectrochromic devices, the electrochromic layer (e.g. WO_3) and the photoactive layer (in this case a dye-covered TiO_2) are situated on the same TCO-coated glass substrate. The opposing electrode is a platinized TCO-coated glass. The electrolyte contains Li^+ and a redox couple (I^- and I_3^-) in an organic solvent (e.g. propylene carbonate). Under illumination, the EC layer can reach a transmittance of 23 % in 2 min, and in the dark it bleached to a transmittance of 64 %. The coloration is fast even for large areas, because the TCO layer is not necessary for the coloration process.

3.3 Water effect on the properties of EC layers

It is already known that water plays an important role in the lithium intercalation and coloration behavior of some electrochromic materials [53,172-175]. Judeinstein et al. [53,172] studied amorphous and crystalline sol-gel $\text{WO}_3 \cdot n\text{H}_2\text{O}$ layers ($n = 0$ to 2) in propylene carbonate (PC) with 1 M LiClO_4 and found that the Li^+ diffusion into the oxide layer becomes easier when the water content of the layer increases. For a given crystallinity, the response time for optical switching becomes shorter as the water content increases, but the drawbacks are a shorter memory time and a faster degradation of the layers. The reversibility during the first CV cycles increased with the hydration state of the $\text{WO}_3 \cdot n\text{H}_2\text{O}$ layer. A high reversibility is observed for hydrated oxides such as amorphous $\text{WO}_3 \cdot 1.8\text{H}_2\text{O}$, but the amount of injected charge decreases when the number of cycles increases. In less hydrated samples (amorphous $\text{WO}_3 \cdot 0.6\text{H}_2\text{O}$) the intercalated charge is smaller, but upon cycling it increases and the reversibility improves. Knowles et al. [174] also showed that some water must be incorporated into the WO_3 film to obtain a coloration.

Similar results were obtained by Bohnke et al. [173] in the examination of evaporated WO_3 thin films using an organic electrolyte (1 M LiClO_4 in PC) containing different amounts of water (0.1 % to 10 %). They observed that the higher the water content in the electrolyte is, the faster the electrochromic response is. In other words, the coloration kinetics which is very slow in anhydrous Li^+ electrolyte can be increased considerably by adding water to the electrolyte to become even faster than in H^+ electrolyte. Water in the electrolyte was also found important to obtain a reversible process. Pyper et al. [176] investigated by in situ Raman spectroscopy the electrochemical reduction of sol-gel WO_3 thin films in dry lithium electrolyte (PC with lithium salt, 7 ppm water) and after addition of 500 ppm of water. They did not observe a change of the peak pattern of the lithium bronzes and concluded that no hydrogen intercalation takes place in these mixed electrolytes, but suggested that water may play a catalytic role for the Li^+ intercalation.

In contrast to these results, Janke et al [175] showed that the intercalated charge density of sputtered WO_3 and $\text{CeO}_{2-x}\text{TiO}_2$ thin films decreases with increasing water content in the electrolyte (0.5 % to 9-10 % water in 1 M LiClO_4 in PC) and with increasing cycle number, whereby the degradation of $\text{CeO}_{2-x}\text{TiO}_2$ is similar to that of WO_3 up to 4-5 % water content and slightly smaller with higher water content (up to 8-10 %). The degradation processes of evaporated WO_3 thin films in aqueous media were studied by Arnoldussen [177]. It was suggested that water plays a crucial role in both efficient coloring/ bleaching and in film degradation because the EC films formed by evaporation are amorphous molecular solids consisting of trimeric W_3O_9 molecules bound weakly to each other through water-bridge, hydrogen and van der waal's bonding.

The few published results show that the influence of water on the electrochromic properties of EC layers is very important, particularly for the long-term behavior, but depends strongly on the

preparation of the layers (sputtering or sol-gel techniques) and the heat treatment of the layers. No reports are available yet for the influence of water on the sol-gel $(\text{CeO}_2)_x(\text{TiO}_2)_{1-x}$ ion storage layer and on the electro-optical behavior of the sol-gel Nb_2O_5 , NiO and WO_3 layer developed at INM as well as on the behavior of EC devices built with these layers using a solid inorganic-organic composite electrolyte (see next section).

3.4 Development of EC layers and devices at the Leibniz-Institute of New Materials (INM)

INM develops electrochromic layers and devices since more than 10 years ago. An “all sol-gel” electrochromic system was patented by Schmidt et al. in 1994 [69]. It consisted of a lithium doped sol-gel WO_3 layer, a sol-gel $(\text{CeO}_2)_x-(\text{TiO}_2)_{1-x}$ counter electrode and an organic-inorganic nanocomposite electrolyte and was described in details later by Munro et al. [70,71], Heusing et al. [72,163] and Mennig et al. [73].

The WO_3 sol was made using the peroxopolytungstic route patented by Cronin in 1993 [58]. It was improved by adding of alkali metal salts into the sol. Thus some of the oxides were converted into alkali metal tungstate without any adverse effect on the electrochromic function or on the ability to process the layers. This procedure accelerates considerably the establishment of a stable operating state.

The $(\text{CeO}_2)-(\text{TiO}_2)$ sol was made by dissolving $\text{Ce}(\text{NO}_3)_3 \cdot 6\text{H}_2\text{O}$ and $\text{Ti}(\text{i-PrO})_4$ in ethanol. The best layer was got by heating the layer at 450°C in air after dip-coating. The charge intercalated was about 7 mC/cm^2 during a CA process (-2 V , 2 min) and 3 mC/cm^2 during a CV cycle (50 mV/s , $-2 \text{ V}/+1 \text{ V}$) [69, 71].

The organic-inorganic nano composite electrolyte is based on glycidylxypropyltrimethoxysilane (GPTS), tetraethylene glycol (TEG), LiClO_4 and $\text{Zr}(\text{n-PrO})_4$. The electrolyte was filled as a liquid between the functional layers and then hardened at 105°C for several hours. It has an ionic conductivity of $1.6 \times 10^{-6} \text{ S/cm}$ at 298 K [178, 180].

These layers were used to produce large area EC-devices up to $50 \times 80 \text{ cm}^2$ [72, 73] having the configuration:

glass/ FTO/ WO_3 / inorganic-organic composite electrolyte/ $(\text{CeO}_2)_x(\text{TiO}_2)_{1-x}$ / FTO/ glass.

The device showed a reversible transmittance change from 70 % down to 25 % at 550 nm (voltage $\pm 2.5 \text{ V}$) and a switching time of 3 min with a 1 mm thick composite electrolyte. The life time of the device was 10^4 coloring and bleaching cycles.

Pure or doped niobium oxide sols were developed by Schmitt et al. [100,101,104,105,179]. By dissolving NbCl_5 powder in ethanol and acetic acid, a niobium chloroalcoxide solution of the type $\text{NbCl}_{5-x}(\text{OEt})_x$ was produced. The doping at different concentration was realized by dissolving in

ethanol SnCl_4 for tin, ammonium zirconate for zirconium, LiCF_3SO_3 for lithium, titanium isopropoxide for titanium and phosphomolybdic acid hydrate for molybdenum. The solutions were mixed with the niobium chloroalcoxide solution and then submitted to an ultrasonic irradiation treatment for a few minutes resulting in transparent sols.

The molybdenum doped niobium oxide sol was used to produce a gray coloring electrochromic film. With a doped ratio $\text{Mo:Nb} = 0.2$, ΔT_{vis} (calculated according to DIN EN 410) of the film was 0.6 and the coloration efficiency was $21.5 \text{ cm}^2/\text{C}$. The best EC devices (size $8 \times 4 \text{ cm}^2$) made with this film had the configuration:

glass/ FTO/ $\text{Nb}_2\text{O}_5:\text{Mo}$ ($\text{Mo:Nb} = 0.2$)/ 1 M LiClO_4 in PC/ $(\text{CeO}_2)_x(\text{TiO}_2)_{1-x}$ / FTO/ glass.

The highest amount of charge exchanged was 18 mC/cm^2 but the maximum change in the transmission when a voltage of -2.5 V was applied for 120 s was only $\Delta T_{\text{vis}} = 0.28$. The best cells were only stable up to 1.5×10^4 cycles [179].

The results presented in this dissertation will be compared to those previously obtained at INM. The following tables show typically what has been obtained for WO_3 and $\text{Nb}_2\text{O}_5:\text{Mo}$; $\text{TiO}_2\text{-CeO}_2$ layers and devices made with them.

Table 3.1. Sol-Gel EC devices achieved at INM until 2000: Materials and configurations, device size, variation of transmittance (T) at $\lambda = 550 \text{ nm}$, potential range, number of color/bleach (c/b) cycles and switching time (t_{sw})

Device construction	Size (cm^2)	ΔT (%)	Number of CA cycles	t_{sw} (s)	C.E. (cm^2/C)	Ref.
K-glass/ WO_3 / inorganic-organic composite electrolyte/ $(\text{CeO}_2)_{0.81}(\text{TiO}_2)_1$ / K-glass	4000	45	10000	180		73, 164
K-glass/ $\text{Nb}_2\text{O}_5:\text{Mo}$ / 1 M LiClO_4 in PC/ $(\text{CeO}_2)_{0.81}(\text{TiO}_2)_1$ (480 nm)/ K-glass	6×8	$\Delta T_{\text{vis}} = 0.28$	15000	120	16	104, 179

Table 3.2. Optical and electrochemical properties of sol-gel EC layers achieved at INM until 2000

Sol-gel layer	Heating temperature ($^\circ\text{C}$)	Thickness (nm)	Q_{in} (mC/cm^2)		ΔT (%)	C.E. (cm^2/C)	Ref.
			CA (-2V, 2min)	CV (50mV/s)			
WO_3 (single layer)	240	200	18	8	60	33	70
$(\text{CeO}_2)_{0.81}(\text{TiO}_2)_1$ (single layer)	450	200	7	3			
$\text{Nb}_2\text{O}_5:\text{Mo}$ (double layer)	100, 500	210	45	23	60	21.5	104, 179

4 Experimental

4.1 Preparation of the sols and corresponding films

4.1.1 Cleaning of the substrate

All K-glass substrates (glass coated with FTO, Pilkington, $17 \Omega_{\square}$) were cleaned in a Miele Professional IR6001 washing machine using a program for intensive glass washing. Then the substrate were transferred to an oven and heated at $450 \text{ }^{\circ}\text{C}$ for half an hour in order to remove the adsorbed water, various hydrocarbon molecules and organic materials.

4.1.2 Tungsten trioxide

Stable coating sols for WO_3 were prepared according to an INM receipt [69]. It employs a modified synthesis, based on the reaction of tungsten metal powder with an excess of hydrogen peroxide solution (30 % solution) in the presence of ethanol and glacial acetic acid, to give the peroxotungstic acid. The reaction is conducted, with appropriate cooling, to keep the temperature at $0 \text{ }^{\circ}\text{C}$. The clear yellow sol which is formed is then dried and the powder is then redispersed up to 25 wt.% in ethanol as required. The coating sol thus produced can be stored for several weeks at $6 \text{ }^{\circ}\text{C}$ without any detrimental effect on the coating properties [69].

K-glass were coated by dip coating (withdrawal rate 4 mm/s) under controlled temperature ($20 \text{ }^{\circ}\text{C}$) and humidity ($\text{RH} = 30 \sim 40 \%$). The coated substrates then underwent a heat treatment of 1 hour at $240 \text{ }^{\circ}\text{C}$. Thin crack-free films with a thickness of about 200 nm were prepared in a single dip coating step with an excellent optical quality.

4.1.3 Molybdenum doped Niobium oxide

$\text{Nb}_2\text{O}_5:\text{Mo}$ sol were prepared according to an INM receipt [100, 104]. 27.04 g NbCl_5 (0.4 mol/l Nb) and 4.56 g $\text{H}_3[\text{P}(\text{Mo}_3\text{O}_{10})_4] \cdot x \text{H}_2\text{O}$ (0.12 mol/l Mo) were weighted in a glove box under nitrogen atmosphere. The $\text{H}_3[\text{P}(\text{Mo}_3\text{O}_{10})_4]$ was dissolved in 125 ml anhydrous ethanol in the glove box. After moving them out of the glove box, 125 ml anhydrous ethanol was dropped into the NbCl_5 with pressure equalization under the hood. 30 g acetic acid (99-100 %) (2 mol/l) and the molybdenum solution were then added into the niobium chloroethoxide solution during stirring for 5 minutes. The mixture was put into an ice bath and subjected to ultrasonic treatment (550 W, 20 KHz) during 4 minutes. (Processing time: 4min; 1 second pulsar on/ 1 second pulsar off) [104, 179]. The solution was kept at $20 \text{ }^{\circ}\text{C}$ temperature-constant room in a closed glass recipient for two days before dip-coating.

The layers were coated on pretreated glass coated with FTO (K-glass) by the dip coating procedure.

Conditions for the 1st layer: dipping in the solution for 30 seconds, withdrawal rate 4 mm/s, and heating at 100°C for 30 minutes.

Conditions for the 2nd layer: dipping in the solution for 30 seconds, withdrawal rate 2 mm/s, and heating at 100°C for 30 minutes.

After that, the two layers were put directly into a hot oven preheated to 500°C for 30 minutes, then cooled down the oven to 30°C. The double layers are transparent and homogeneous and their thickness was ~ 120 nm.

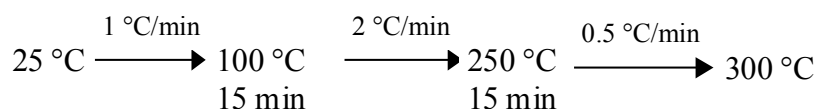
4.1.4 Cerium-titanium oxide

The $(\text{CeO}_2)_x(\text{TiO}_2)_{1-x}$ sol was prepared according to a receipt developed at INM [69, 71]. 24.43 g $\text{Ce}(\text{NO}_3)_3 \cdot 6\text{H}_2\text{O}$ were dissolved in 125 ml anhydrous ethanol (0.45 mol/l Ce), and 19.54 g $\text{Ti}(\text{i-OPr})_4$ were dissolved in 125 ml anhydrous ethanol (0.55 mol/l Ti) and added to the cerium nitrate ethanol solution in a glove box with nitrogen atmosphere. Apart from this composition other mole ratios such as 0.5:1 and 1:1 were also studied. A series of solution with a total concentration of 0.5 mol/l were prepared to obtain various ratios of Ce/Ti. These “coating solutions” were aged at 30°C during several days under mechanical stirring in closed glass vessels to prevent rapid precipitation of the alkoxide due to hydrolysis. Layers with various thickness were obtained depending on the aging time.

The $\text{CeO}_2\text{-TiO}_2$ layers were deposited on pretreated K-glass by the dip-coating technique with a withdrawal rate of 4 mm/s at 20 °C with 30-40 % air humidity. The layers were heated from room temperature up to a temperature between 150 °C to 550 °C with a heating rate of 2.5 K/min maintained at the constant temperature for 1 hour and then cooled to room temperature. For the double layers, the first layers were heat treated at 150 °C or 200 °C for half an hour before making the second layers.

4.1.5 Nickel oxide

The precursors for nickel oxide sol were titanium(IV) n-propoxide $\text{Ti}(\text{n-PrO})_4$ and nickel acetate tetrahydrate $\text{Ni}(\text{CH}_3\text{COO})_2 \cdot 4\text{H}_2\text{O}$. The total concentration of nickel and titanium was 0.5 mol/l and the ratio of Ni/Ti is 3/1. The sol was prepared by dissolving the chemicals in anhydrous ethanol in a glove box. The layers were coated on pretreated K-glass by dip coating with a withdrawal rate of 3 mm/s. The first layer was heated at 80 °C for 15 minutes, and after the second dip coating, the layers were heat treated using the following procedure [154].



4.1.6 Electrolyte

Battery like EC-devices were constructed with an organic-inorganic hybrid electrolyte developed at INM [69, 180] which has an ionic conductivity of 10^{-4} - 10^{-5} S·cm⁻¹. The solid ionic conductor is based on glycidylxypropyltrimethoxysilane (GPTS), tetraethylene glycol (TEG), lithium perchlorate (LiClO₄), and zirconium(IV) n-propoxide Zr(n-OPr)₄ [69,180]. GPTS serves as network former, whereas TEG acts as a plasticizer. LiClO₄ is the conducting salt and Zr(n-OPr)₄ is added as a starter for thermal curing. Dried LiClO₄ was dissolved in TEG, then the mixture was added to prehydrolyzed GPTS. At last Zr(n-OPr)₄ was added to the solvent. Volatiles are removed by rotary evaporation immediately prior to the application to the EC devices.

4.1.7 Mounting of EC-devices

The preparation of the EC devices was performed by mounting a spacer band (thickness 1 mm) at the edges of one of the functional coatings and then assembling the two coatings. The mounted cells were filled with the electrolyte and heated up to 105 °C for 12 hours. For EC devices with water in the electrolyte, the amount of water (1 to 3 wt%) was first dissolved into the electrolyte before filling the EC devices. After the heat treatment the EC devices were sealed.

4.2 Structure and composition analysis

4.2.1 Thermal analysis

Thermal analysis are methods by which the physical and chemical properties of a substance, a mixture and/or reaction mixtures are analyzed as a function of temperature or time, while the sample is subjected to a controlled temperature program. The program may involve heating or cooling (dynamic), or holding the temperature constant (isothermal), or may combination of these [34].

The thermal behavior of the sols were examined simultaneously by differential thermal analysis (DTA) and thermogravimetry (TG) using equipment STA 449C/3G Jupiter (from Netzsch) combined with a mass spectrometer (QMS 403C Aeolos, from Netzsch) and a FTIR (Tensor 27-FTIR, from Brucker). For this purpose the xerogels were obtained by drying the sols and preheated at 50 °C. Then the powder were poured into Al₂O₃ crucibles and heated up to 1000°C at a heating rate of 2 K/min under synthetic air atmosphere.

4.2.2 Profilometry

The thickness of the films was measured by a Tencor P-10 surface profiler. The layers of CeO₂-TiO₂ and Nb₂O₅:Mo were scratched before heat treatment. The WO₃ layers were partial etched with 1 M KOH solution in order to measure the thickness. The surface of the sample was scanned by a diamond stylus through the scratches from one edge to another. The stylus registers the vertical

motion at the edges and thereby allows to determine the thickness of the coatings. Several measurements per sample were performed to average the values.

4.2.3 X-ray diffraction

X-ray diffraction (XRD) can be used to identify a material and give information about the phase, lattice stress, texture orientation and grain size (181). It is based on the constructive interference between x-rays reflected at different atomic planes. By varying the angle between the incident and diffracted beam and recording the diffracted radiation, a chart with material and phase specific peaks is achieved. In this work the method has been used to determine the morphology. In case of crystalline material, the grain size was calculated according to Sherrer's formula. The used X ray Diffractometer was a SIEMENS type D 500 equipment with CuK_α radiation of 1.54 Å.

4.2.4 High Resolution-Transmission Electron Microscopy

High-resolution transmission electron microscopy (HR-TEM) gives information about the crystallinity, structure and the texture of coatings. TEM cross sections were prepared by thinning the specimens using Ar^+ ion-milling. Quantitative chemical compositions of the coatings were obtained using Energy X-ray spectrophotometry (EDX).

The characterization were made using a HRTEM-CM200 FEG, Philips equipped with an energy dispersive X-ray spectrometer (DX-4 system, EDX).

4.2.5 X ray Photoelectron Spectroscopy

X-ray Photoelectron Spectroscopy (XPS) is used in research, development and manufacturing to obtain the chemical composition of various material surfaces up to 3~5 nm depth. Most of the elements can be detected except H, He. Our main interest was to find out the composition i.e. the atomic percentage of each of the components and the valence of the atom.

The equipment was a M-Probe XPS from SSI Surface Science Instruments with $\text{Al-K}\alpha$ monochromatic radiation of 1486.6 eV. The total instrumental resolution is 0.8 eV.

4.3 Electrochemical and optical measurements

4.3.1 Electrochemical characterization of the layers

Electrochemical measurements of the films were performed in an electrochemical three electrode cell containing a working electrode, a counter electrode, and a reference electrode (Fig. 4.1). The layers to be characterized are the working electrode; a platinum foil with a area of 4.2 cm^2 is used as counter electrode and Ag/AgClO_4 is the reference electrode. The active electrode area contacting the electrolyte is 7 cm^2 . 1 M LiClO_4 in propylene carbonate was used as electrolyte. A current may flow between the working and counter electrodes, while the potential of the working electrode is

measured against the reference electrode. This setup was used to investigate the kinetics and mechanism of the electrode reaction occurring on the working electrode surface.

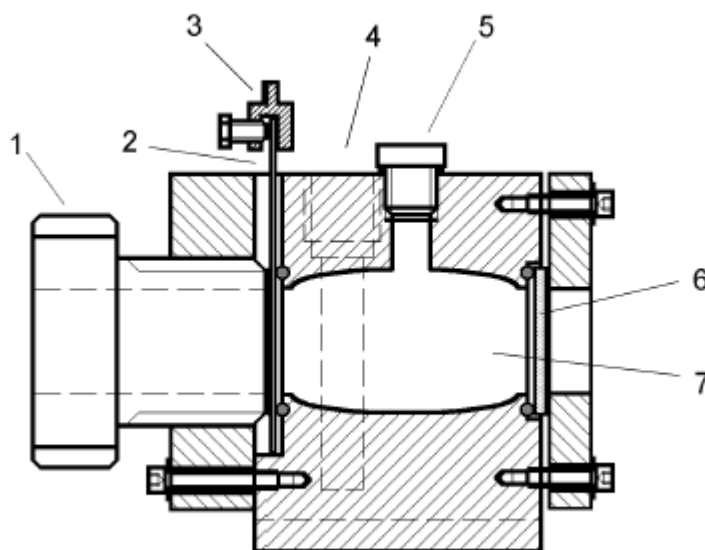


Fig. 4.1. Scheme of the single compartment three-electrode cell for electrochemical measurements [182].
(1) swiveling stopper, (2) working electrode, (3) electrical contact, (4) inlet for reference and counter electrodes, (5) filling, (6) Fused quartz glass disk and (7) electrolyte.

The electrochemical characterization was controlled using a Potentiostat/ Galvanostat (Princeton Applied Research Model 273A). Cyclic voltammetry (CV), chronoamperometry (CA) and chronopotentiometry (CP) were used.

CV, one of the most commonly used electroanalytical techniques, is an excellent method for qualitative analysis. Typically, the potentiostat applies a linear ramp of the potential to the working electrode, and then reverses the scan, returning to the initial potential (Fig.4.2).

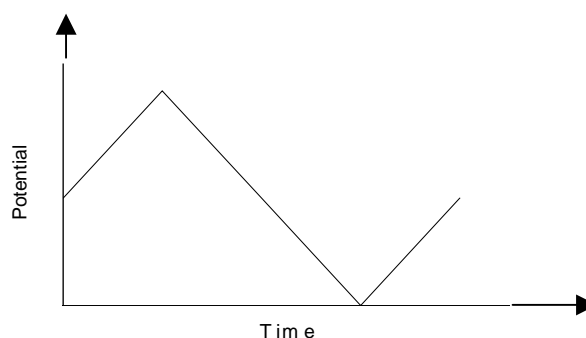


Fig. 4.2. Scheme of principle of one CV cycle.

During the potential sweep, the potentiostat measures the current resulting from the applied potential and the values of the current versus the applied potential are then plotted. The potential limits were $-2\text{ V}/+1\text{ V}$ vs. Ag/AgClO_4 for $\text{CeO}_2\text{-TiO}_2$ layer, $-1.5\text{ V}/+2\text{ V}$ for WO_3 layer,

-2.2 V/ +1.0 V for Nb₂O₅:Mo layer. Higher voltages are not recommended, as the liquid electrolyte may decompose and gas bubbles may develop and isolate the electrochemically active layer from the liquid electrolyte [175].

In CP, the potentiostat applies a constant current I_1 for a specified time t_1 , and monitors the resulting potential. The resulting curve is a sigmoid plot of potential vs. time (E vs. t) showing various plateaus. Each plateau corresponds to the redox potential of an electroactive species. The current applied in this work was $\pm 5 \mu\text{A}/\text{cm}^2$ if not specially mentioned.

In CA, the potentiostat steps the potential from an initial potential (open circuit potential, E_0) to a value (E_1) during a certain length of time (t_1) and then steps to another value (E_2) during a certain length of time (t_2). The resulting faradic currents are recorded as a function of time. There are no inherent limits on the time scale of a CA experiment. At each potential step the response curve looks like a current spike that decays with time. Except for special cases, the time step for coloring and bleaching of EC layers and windows was 120 s. E_0 is the open circuit potential, E_1 and E_2 was -2 V and +1 V, -1.5 V and +2 V, -2.2 V and +1 V vs. Ag/AgClO₄ for CeO₂-TiO₂ layer, WO₃ layer and Nb₂O₅:Mo layer respectively.

4.3.2 Optical characterization

In situ transmittance measurements were carried out with a CARY 5E UV/VIS/NIR spectrophotometer. The transmittance of the layers in the three-electrode electrochemical cell was measured in the range from 200 nm to 1200 nm against a reference cell having a quartz glass and a float glass. The transmittance of the EC devices were measured in the range from 200 nm to 3000 nm against air as a reference.

The coloration efficiency (C.E.) is determined by the slope of the straight line obtained in the plot of the optical density change ΔOD versus the charge consumed per unit area, Q_{in}

$$\text{C.E.} = \Delta\text{OD} / Q_{\text{in}} = \log(T_b/T_c) / Q_{\text{in}} \quad (4.1)$$

where T_b is the transmittance at the bleached state and T_c is the transmittance at the colored state.

Because $30 \times 40 \text{ cm}^2$ EC devices can not be put into the CARY 5E UV/VIS/NIR spectrophotometer, their transmittance of them was measured using the BYK haze-gard plus employing a CIE Source C according to ASTM.

4.4 Microbalance

The Quartz Crystal Microbalance (QCM) is an extremely sensitive mass sensor, capable of measuring mass changes in the nanogram range. QCMs are piezoelectric devices consisting of a thin plate of crystalline quartz with electrodes affixed to each side of the plate.

For many years, QCMs were just regarded as gas-phase mass detectors. However, recently, their application has been extended since scientists realized that they can be also operated in contact with liquids and viscoelastic deposits.

Sauerbrey [183] was the first to recognize the potential usefulness of the QCM technology and demonstrates the extreme sensitive nature of these devices towards mass changes at the surface of QCM electrodes. His results are embodied in the so-called Sauerbrey equation, which relates the mass change per unit area of the QCM electrode surface to the observed change in the oscillation frequency of the crystal:

$$\Delta f = - C_f \cdot \Delta m \quad (4.2)$$

where Δf is the observed frequency change in Hz, Δm is the change in mass per unit area in $\mu\text{g}/\text{cm}^2$, C_f is the sensitivity factor for the crystal ($56.6 \text{ Hz} \cdot \mu\text{g}^{-1} \cdot \text{cm}^2$ for a 5 MHz AT-cut quartz crystal at room temperature). The negative sign indicates that the resonant frequency decreases when the electrode mass increases.

The Sauerbrey equation relates the change of frequency to change in mass for thin, lossless deposited films, whereas Faraday's law relates change passed in an electrochemical experiment to the number of moles of material electrolyzed. Therefore, frequency changes can be related to the total charge passed. The relation is shown in equation 4.3.

$$\Delta f = \frac{10^6 M_w C_f Q}{nF} \text{ (Hz)} \quad (4.3)$$

where: M_w is the apparent molar mass of the depositing species in grams/mole

Q is the integrated charge during the reduction in Coulombs

n is the number of electrons transferred to induce deposition

F is the Faraday's constant = 9.648×10^4 Coulomb/mole

In this work, the CeO_2 - TiO_2 coated quartz was connected to an Electrochemical Quartz Crystal Microbalance (EQCM, Maxtek, Inc) and a Potentionstat/ Galvanostat in order to control the potential and current applied to the quartz. The recording data from EQCM was sent to a computer with a software to record the frequency of the quartz. The crystals were 5 MHz AT-cut quartz from the same company. The exposed area of the front electrode is 137 mm^2 , the thickness of the quartz is $333 \mu\text{m}$. The minimum detectable mass change is typically a few ng/cm^2 and is limited by the noise specification of the crystal oscillator and the resolution of the equipment used to measure the frequency shifts.

The electrochemical cell for EQCMs is different from the three electrode cell used for normal electrochemical measurement. It is a 100 ml double wall glass flask with a cap having holes for three electrodes. Temperature was controlled by circulating water from a thermostat through tubes.

The precision of the EQCM was evaluated by analyzing the electrodepositing of Ag from a 1 mM AgNO_3 / 0.2 M HClO_4 solution. (see Annex A).

5 Results and discussion

5.1 Cerium-titanium oxide sols and layers

Although the use of CeO₂-TiO₂ sol-gel layers as counter electrode in EC devices has been successful, several parameters that either influence or limit the properties of these devices directly linked to this particular electrode have been identified.

The most important property is the Li⁺ charge exchange ability and capacity of the layers. A good counter electrode should have an ion-storage ability high enough to store the ions coming out of the EC layers. The EC layers used in this work have a typical Li⁺ charge exchange capacity of 18 mC/cm² (WO₃ layer) and 45 mC/cm² (Nb₂O₅:Mo double layers) (Table 3.2). Comparing these values, the Li⁺ charge capacity of the CeO₂-TiO₂ sol-gel layers, 7 mC/cm² (-2 V/ 2 min) is too small. There is also a large decrease of the Li⁺ charge exchange in the CeO₂-TiO₂ sol-gel layers observed during the initial electrochemical cycles and for a 200 nm thick layer the stable value only was 7 mC/cm² after about 50 cycles.

This section presents the results of the developments that have been made in order to determine the influence of several processing parameters on the charge capacity and exchange ability of the CeO₂-TiO₂ sol-gel layers. Two of them have been found crucial: one is the water content of the electrolyte, and the other is the sintering temperature of the layers.

Less important ones have been found by optimizing

- a) the pretreatment of the conducting substrate
- b) the lapse of time during which the substrate remains in the sol before drawing out of the solution during dip coating.

However, in comparison with the former results (see section 3.4), no improvement could be obtained by optimizing the sol composition either by changing the Ce/Ti ratio or by adding additives.

5.1.1 Influence of the sol composition on coating thickness and Li⁺ charge exchanged

The best results at INM have been obtained using cerium nitrate Ce(NO₃)₃·6(H₂O) as cerium precursor, a readily commercially available salt soluble in water up to 65 wt.% as well as in a wide range of polar organic solvents such as ketones, alcohols and ethers [69, 71]. Following the receipt given in section 4.1.4, three sols with different Ce:Ti ratios have been prepared: sol I: Ce:Ti = 0.5:1, sol II: Ce:Ti = 0.81:1 and sol III: Ce:Ti = 1:1. The total concentration of Ce and Ti was always 0.5 M. They have been used to prepare coatings by the dip-coating process with different withdrawal rate, all heat treated in air at 450 °C (see section 3.4) and then

electrochemically characterized in a dry liquid electrolyte (1 M LiClO₄ in PC with molecular sieve, water content ≤ 0.03 wt.%). All sols were yellowish and transparent at the beginning, but they gelled and became opaque after heating at 30 °C.

The relationship between aging time of the different sols and the thickness for two withdrawal rates is shown in Fig.5.1. The films obtained after densification are transparent and slightly yellowish for thickness higher than 250 nm and cracks appear in the coatings for thickness higher than 350 nm. There is almost no change of the thickness of the layers with aging time for sol I, but the thickness of the layers increases with the withdrawal rate. An aging effect on the thickness is observed when the Ce:Ti ratio of the sol increases (sol II, III). The thickness of the layers obtained with sol III (Ce/Ti = 1:1) increases too fast with the aging time to well control the property of the sol and the thickness. This sol was therefore not further used.

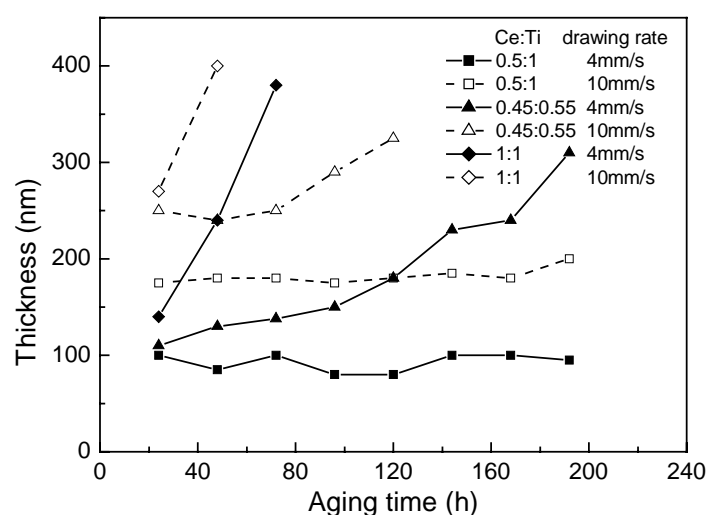


Fig.5.1. Plot of thickness versus aging time for layers obtained with different Ce/Ti ratios and two different withdrawal rates.

Typical CV profiles of the layer coated with sol II with a withdrawal rate of 4 mm/s are shown in Fig. 5.2. The shape of the CV curves are changing with cycle number especially during the initial cycles. The cathodic peak shifts from -1.75 V (the 1st cycle) to -1 V (the 10th cycle) then shifts back to negative values continuously. In the initial cycles, two anodic peaks are observed. After 10 cycles only one peak is observed. This means that the properties of the layer drastically change during the first CV cycles and this maybe due to the not fully reversible Li⁺ intercalation. The intercalated charge Q_{in} is bigger than the deintercalated charge Q_{out} (Q_{out}/Q_{in} is 0.82 for the first cycle and 0.92 since the 50th cycle) and Q_{in} decreases from 13.4 mC/cm² to 4.1 mC/cm² in the first 10 CV cycles (Fig. 5.3). These results show that the Li⁺ intercalation and deintercalation is not fully reversible. The change of the anodic and cathodic current could be also due to the surface change of the layer (see section 5.2).

The shape of the CV curves of the other layers is similar. This indicates that the structure of the films from the different sols is similar and that the charge intercalation mechanism is the same. There is always a sharp decrease of the current density and consequently of the charge intercalated during the first 10 cycles (Fig. 5.3) and then the behavior becomes stable for the following cycles. Sol II leads however to a slightly higher charge intercalation.

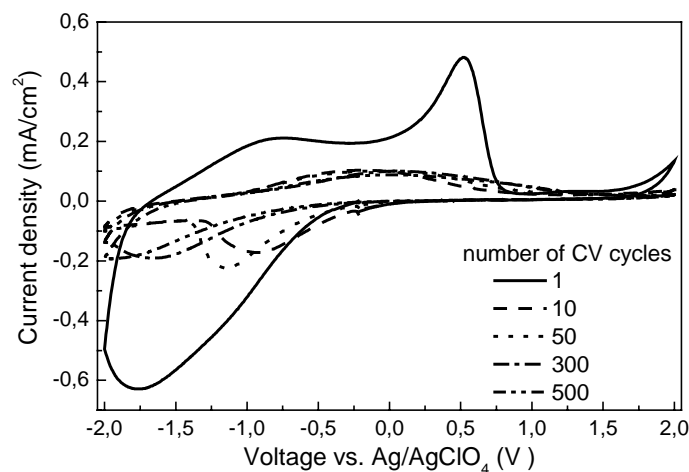


Fig. 5.2. CV profile of the layer coated from sol II ($d = 180$ nm; withdrawal rate: 4 mm/s). Scan rate: 50 mV/s; Electrolyte: dry 1 M LiClO_4 in PC

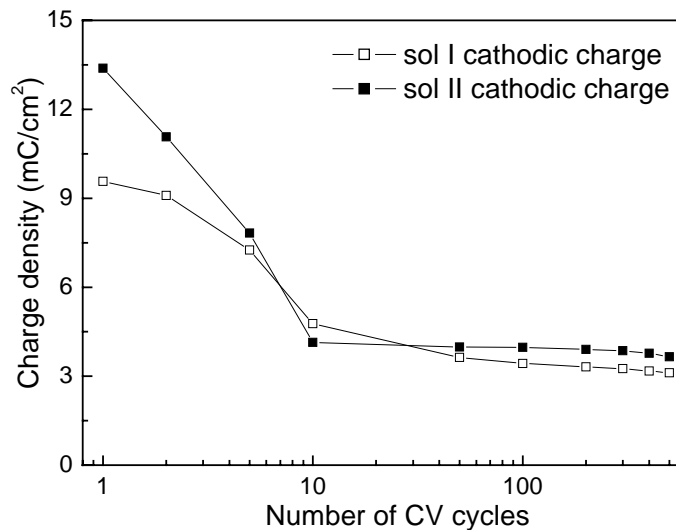


Fig. 5.3. Charge density vs. number of CV cycles for layers dip-coated from sol I (withdrawal rate: 10 mm/s) and sol II (withdrawal rate 4 mm/s). Thickness of all layers: 180 nm. Aging time of all layers: 120 hrs. CV: scan range -2 V/+1 V, scan rate 50mV/s. Electrolyte: 1 M LiClO_4 in PC (dry). $T_s = 450$ °C/ 1 h.

The value of the peak current density, i_p , is however different for the different layers (Fig. 5.4). This has a first pronounced effect on the Li^+ diffusion coefficient, D , that is proportional to i_p^2 according to the Randles-Sevcik equation (5.1):

$$i_p = 0.4463nF\left(\frac{nF}{RT}\right)^{1/2} CD^{1/2}v^{1/2} \quad (5.1)$$

where i_p is the peak current density in A/cm^2 , n is the number of electrons involved in the redox reaction, F is the Faraday constant, R is the gas constant, T is the temperature, C is the concentration of Li^+ in the liquid electrolyte in mol/cm^3 , v is the potential scan rate in V/s , and D is the diffusion coefficient in cm^2/s [184].

The values of D got from the cathodic peak current density in Fig. 5.4 are listed in Table 5.1 for 3 different layers having all a thickness of 180 nm and obtained with sol I and II with the data obtained during the 300th CV cycle. The results show that sol II with Ce:Ti molar ratio 0.81:1 aged 120 h leads to a faster Li^+ diffusion coefficient.

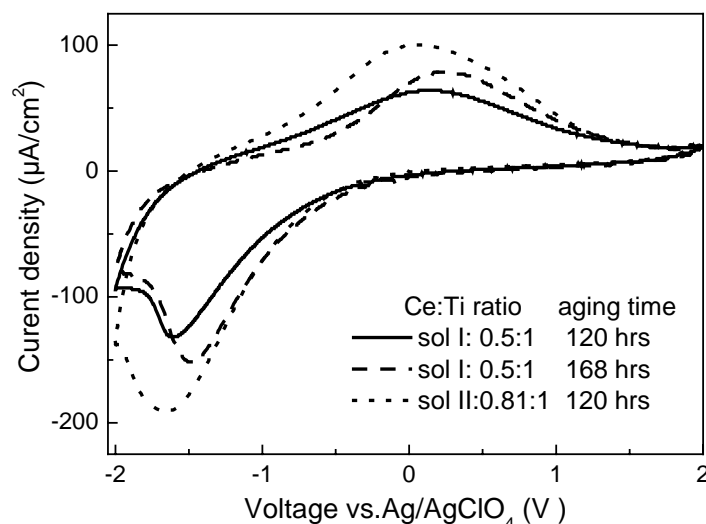


Fig. 5.4. CV profile (300th cycle) of the layers ($d = 180$ nm) coated from different sols. Scan rate: 50 mV/s. Electrolyte: 1 M $LiClO_4$ in PC

Table 5.1. Li^+ ion diffusion coefficient in $(CeO_2)_x(TiO_2)_1$ layers in dry 1 M $LiClO_4$ in PC during the 300th CV cycle obtained with equation (5.1)

Condition of the layer	Ce:Ti = 0.5:1; aging time: 120 h	Ce:Ti = 0.5:1; aging time: 168 h	Ce:Ti = 0.81:1; aging time: 120 h
D ($\times 10^{-12}$ cm^2/s)	4.7	6.2	11

The Li^+ charge exchanged of the different layers obtained with sol I and II during the 300th CV cycle in 1 M $LiClO_4$ in PC is shown in Fig. 5.5 as a function of the aging time. It shows that Sol II with a withdrawal rate of 4 mm/s leads to higher values almost independent of the aging time.

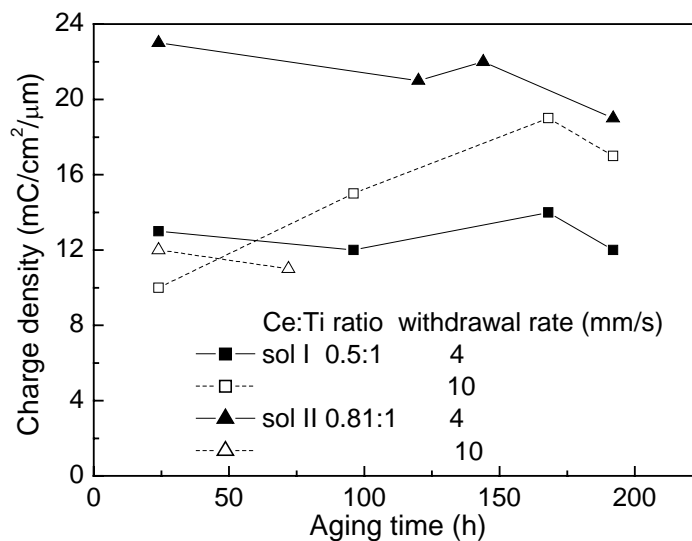


Fig.5.5. Charge intercalation during cathodic sweep of $(\text{CeO}_2)_x(\text{TiO}_2)_1$ sol-gel layers obtained with sol I and II and measured during the 300th CV cycle in 1M LiClO_4 in PC (scan range -2 V/ $+2$ V, scan rate 50 mV/s)

Typical optical spectrum of cerium-titanium oxide layers obtained from sol II sintered at 450 °C for 1 hour are shown in Fig. 5.6. The optical spectrum during the first cycle and the following cycles are similar. The layer is rather transparent in the visible light range in both intercalated and deintercalated states. This is suitable for the counter electrode in EC devices.

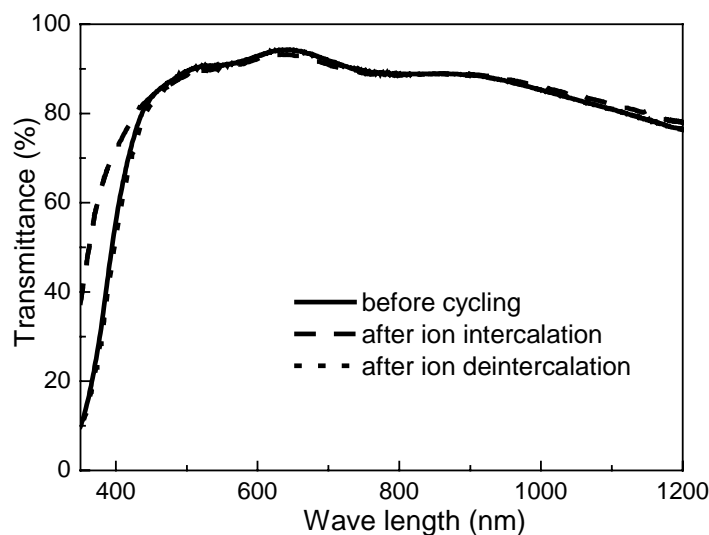


Fig. 5.6. Typical transmittance spectrum of a $(\text{CeO}_2)_{0.81}(\text{TiO}_2)_1$ sol-gel layer sintered at 450 °C (200 nm thick) (-2 V, 2 min/ $+1$ V, 2 min) in 1 M LiClO_4 in PC.

In conclusion, sol II is easier to control, it allows to have coatings with the highest charge exchange and have also a faster Li^+ diffusion coefficient. Moreover this sol can be stored for more than one year in refrigerator at -18 °C and leads to reproducible coating data. This sol was therefore selected

for further experiments. However the electrochemical results obtained for the layers made with sol II are similar to those summarized in section 3.4 and therefore no improvement has been achieved.

5.1.2 Influence of the water content of the electrolyte on Li^+ storage

It is well known that the used electrolyte, propylene carbonate with LiClO_4 , is a highly hygroscopic liquid [175]. In order to characterize the impact of absorbed water on the electrochemical behavior of the ion-storage sample, the charge density was determined using such electrolytes containing different amounts of water measured by Karl-Fisher titration.

The absorption of water by the electrolyte (1 M LiClO_4 in PC) was first determined by laying the electrolyte in a chamber with 70 % humidity, 30 °C. The result is shown in Fig. 5.7.

Water is easily and fast absorbed by propylene carbonate up to an amount 3.2 wt.%. If this compound is used as electrolyte, we have to pay attention to control its water content during its preparation and handling since as already reported in the literature the water content affects the properties of WO_3 layers and sputtered $\text{CeO}_{2-x}\text{TiO}_2$ layers [172, 173, 175, 176, 185].

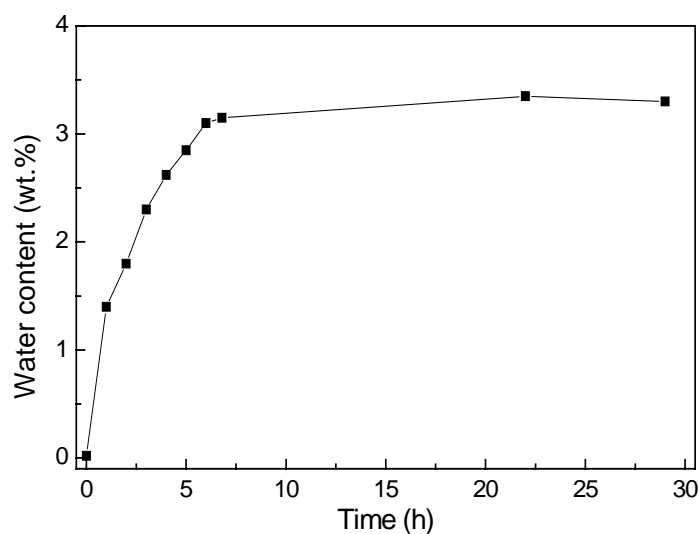


Fig. 5.7. Amount of water absorbed by 1 M LiClO_4 in PC in a chamber with 70 % humidity at 30°C.

The electrolyte resistance, measured by impedance spectroscopy, decreased only slightly by addition of water from 70 Ω (dry electrolyte) to 50 Ω (3 wt.% water). Therefore the IR-drop, 2.5 mV for dry and 1.75 mV for wet electrolyte, can be neglected for the CP, CV and CA measurements.

The cyclic voltammetry (CV) curves of $(\text{CeO}_2)_{0.81}(\text{TiO}_2)_1$ sol-gel single layers (sintered at 450 °C in air, thickness 200 nm) were measured up to 500 cycles in liquid electrolyte without and with addition of water (Fig. 5.8). As already shown, the shape of the CV spectra measured in dry electrolyte alters considerably, especially in the first 10 cycles, and the cathodic and anodic current

densities decrease strongly. The cathodic current peak position changes also drastically. It is at about -1.3 V during the 10th cycle and shift to values smaller than -2 V during the 300th cycle. However the position of the anodic current peak changes only slightly to the positive direction. When 3 wt.% water was added to the electrolyte, the CV-cycles become more reversible and the current density waves decrease only slightly and reach practically stable values after about 100 cycles. The cathodic peak position changes however from -1.75 V during the 1st cycle to -1.3 V after 300 cycles but there is almost no change with the position of the anodic peak up to 500 cycles.

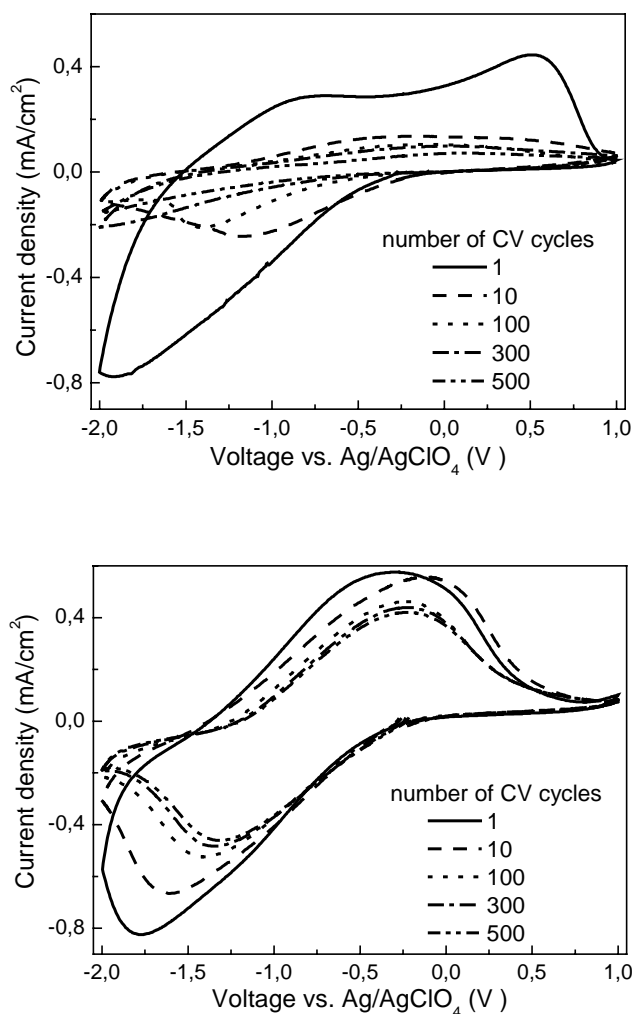


Fig. 5.8. Cyclic voltammetry of $(\text{CeO}_2)_{0.81}(\text{TiO}_2)_1$ sol-gel single layers (200 nm thick, $T_s = 450$ °C/ 1 h) in 1 M LiClO_4 in PC (scan rate 50 mV/s). Top: dry electrolyte (0.03 wt.% water); bottom: wet electrolyte with 3 wt.% water.

The charge intercalated during the CV cycles is shown as a function of the water content in Fig. 5.9. It decreases strongly in the dry electrolyte from 17 mC/cm^2 (first cycle) down to 3.5 mC/cm^2 (500th cycle). The addition of 1 wt.% water to the electrolyte already improves the amount of intercalated charge density, but the effect is more drastic by adding 2 to 3 wt.% water. The decreases of charge

observed during the initial cycles is much smaller and the intercalated charge decreases only down to 11 mC/cm² after 500 cycles i.e. the value is 3 times higher than that measured in dry electrolyte.

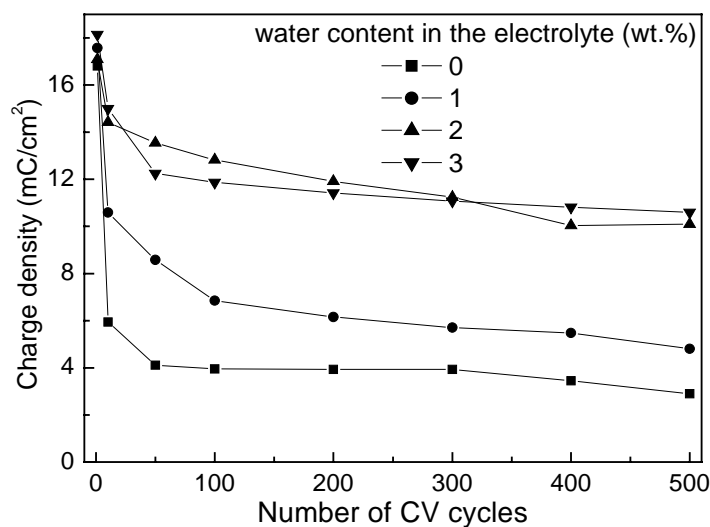


Fig. 5.9. Intercalated charge density (Q_{in}) in $(\text{CeO}_2)_{0.81}(\text{TiO}_2)_1$ sol-gel single layers (200 nm thick, $T_s = 450^\circ\text{C}/1\text{ h}$) in 1 M LiClO_4 in PC with different water content as a function of the number of CV cycles (scan range: $-2\text{ V}/+1\text{ V}$; scan rate: 50 mV/s).

Fig. 5.10 shows that the ratio Q_{out}/Q_{in} of the deintercalated (Q_{out}) to the intercalated charge (Q_{in}) increases with the water content of the electrolyte from 0.90 (without water) up to 0.99 (3 wt.% water) after 500 CV-cycles. This indicates a better reversibility of the Li^+ charge exchange in the wet electrolyte.

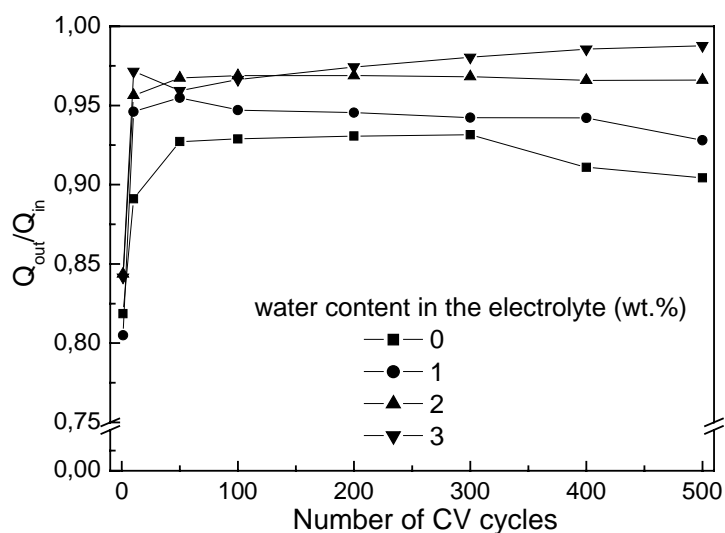


Fig. 5.10. Ratio of deintercalated (Q_{out}) to intercalated charge density (Q_{in}) during CV-cycling of $(\text{CeO}_2)_{0.81}(\text{TiO}_2)_1$ sol-gel single layers (200 nm thick, $T_s = 450^\circ\text{C}/1\text{ h}$) in 1 M LiClO_4 in PC with different water content as a function of the number of CV-cycles (scan range: $-2\text{ V}/+1\text{ V}$; scan rate: 50 mV/s).

The properties of the $(\text{CeO}_2)_{0.81}(\text{TiO}_2)_1$ sol-gel single layers have been further tested in 1 M LiClO_4 in PC with water content up to 10 wt.% (limit of miscibility of these two solvents). As an example, the charge intercalated and deintercalated during the 300th CV cycle is shown in Fig. 5.11.

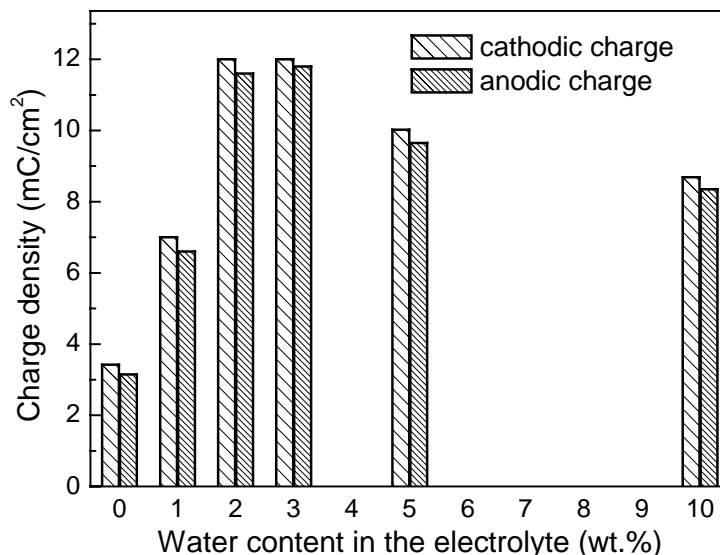


Fig. 5.11. Charge intercalated for a $(\text{CeO}_2)_{0.81}(\text{TiO}_2)_1$ sol-gel single layers (200 nm thick, $T_s = 450\text{ }^\circ\text{C}/1\text{ h}$) during the 300th CV cycle in 1 M LiClO_4 in PC with water content up to 10 wt.%.

The results show that an amount of 2 to 3 wt.% water in the electrolyte leads to the highest charge capacity. However the best reversibility is obtained in the electrolyte containing 3 wt.% water.

The maximum of the cathodic current densities i_{pc} are plotted in Fig. 5.12 as a function of the square root of the scan rate, $v^{1/2}$. In the dry electrolyte, with the scan rate between 10 to 100 mV/s, the cathodic current density of the layer varies linearly with $v^{1/2}$ indicating a diffusion controlled ion transfer. In the electrolyte with 3 wt.% water, the cathodic current density varied also linearly with $v^{1/2}$ with the scan rate between 10 to 200 mV/s, showing that this process is also a diffusion controlled process, but with a higher slope and up to higher scan rates. Therefore it is used to calculate the diffusion coefficient of Li^+ by equation 5.1 which gives $1.1 \times 10^{-11}\text{ cm}^2/\text{s}$ and $1.0 \times 10^{-10}\text{ cm}^2/\text{s}$ in the dry and wet electrolyte (with 3 wt.% water) respectively. The value shows that water addition to the electrolyte improves the diffusion coefficient of the Li^+ ion in the layer by a factor of 10.

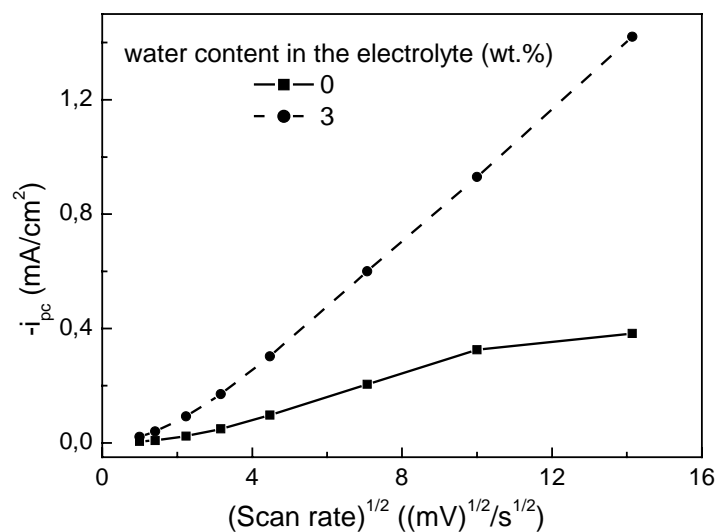


Fig. 5.12. Cathodic peak current density versus $v^{1/2}$ ((scan rate)^{1/2}) of $(\text{CeO}_2)_{0.81}(\text{TiO}_2)_1$ sol-gel single layers (200 nm thick, $T_s = 450^\circ\text{C}/1\text{ h}$) with different amounts of water in the electrolyte (1 M LiClO_4 in PC).

The kinetics of the ion intercalation procedure has been determined by CA measurement. Fig. 5.13 shows typical results obtained during the 50th CA cycle for various amounts of water added to the electrolyte. The results also confirm that the amount of charge intercalated during 2 minutes in wet electrolyte is higher and that the charge insertion kinetics is faster. Both parameters are important for an ion storage layer and are drastically improved. Fig. 5.13 also shows that a lapse of time of 2 minutes for the Li^+ insertion is not enough for a full insertion (at all level of the water content of the electrolyte). The same hold for the deintercalation measured in electrolyte containing 2 and 3 wt.% water.

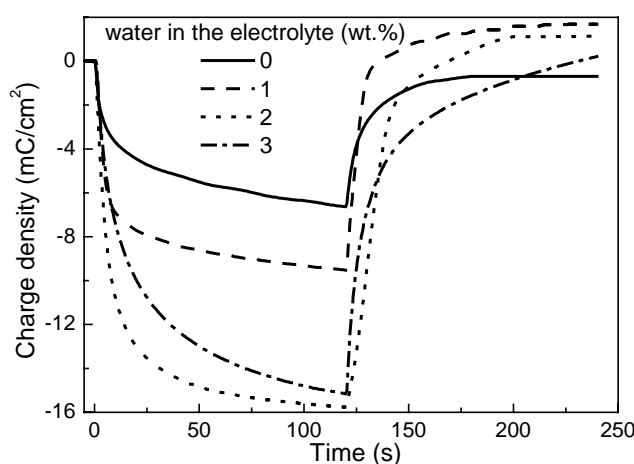


Fig. 5.13. Evolution of the charge density of $(\text{CeO}_2)_{0.81}(\text{TiO}_2)_1$ sol-gel single layers (200 nm thick, $T_s = 450^\circ\text{C}/1\text{ h}$) during the 50th CA cycle (-2 V, 2 min/+1 V, 2 min) with different water content in 1 M LiClO_4 in PC. (-2 V, 2 min/+1 V; 2 min)

Our results are however in contradiction to those obtained by Janke et al. for sputtered $\text{CeO}_{2-x}\text{-TiO}_2$ [175]. They obtained a charge capacity degradation with an increase of the water content in the electrolyte. The CV shape of these sputtered layers was also different from ours. So the properties of sputtered $\text{CeO}_{2-x}\text{-TiO}_2$ appear different.

Because the cathodic and anodic peak positions are different in dry and wet electrolyte (Fig. 5.8), a small amount of water in the electrolyte not only affects the transfer of Li^+ into the coating, but also affects the property of the layer. The coordination of water with Li^+ may increase the mobility of the Li^+ in the electrolyte and in the layer. This causes the faster ion intercalation kinetics of the layer. This improvement in the kinetics and in the charge capacity will be further discussed in detail in section 5.2 where these processes have been studied by using electrochemical quartz crystal microbalance (EQCM).

The water content of the electrolyte has also drastic effects on chronopotentiometric (CP) results. Fig. 5.14 shows the 1st, 5th and 10th CP measurement performed with a $(\text{CeO}_2)_{0.81}(\text{TiO}_2)_1$ sol-gel single layer with electrolytes containing 0 and 3 wt.% water. The shape of the potential-time curve during the intercalation process is strongly altered with the amount of water in the electrolyte. This indicates that the amount of charge which could be inserted without exceeding the safe voltage of -2 V increases with increasing water content of the electrolyte. The intercalated charge nevertheless decreases with the cycle number from 34 mC/cm^2 (first CP cycle) to 32 mC/cm^2 (10th CP cycle) for the wet electrolyte (3 wt.% water) and from 22 mC/cm^2 (first cycle) to 17 mC/cm^2 (10th cycle) for the dry electrolyte in agreement with the long-term cycling behavior of the CV and CA measurements. In wet electrolyte there is a plateau of the potential observed (at -1.9 V) for the 5th and 10th CP cycle.

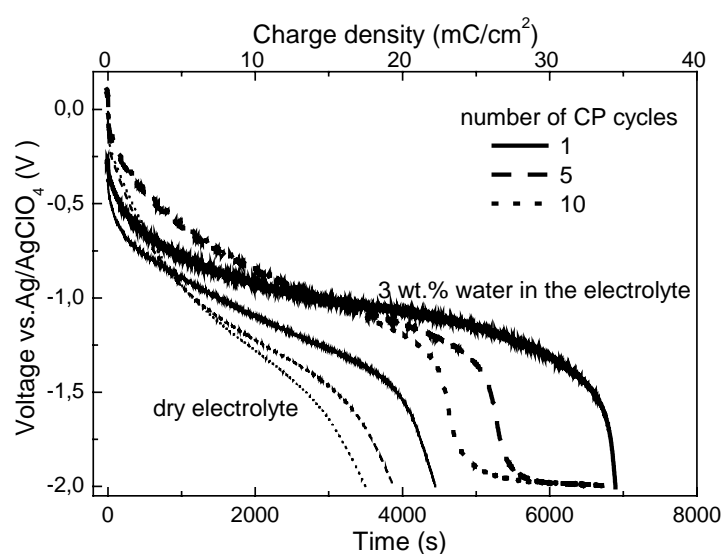


Fig. 5.14. 1st, 5th and 10th chronopotentiometric switching with constant current of $-5 \mu\text{A/cm}^2$ of $(\text{CeO}_2)_{0.81}(\text{TiO}_2)_1$ sol-gel single layers (200 nm thick, $T_s = 450 \text{ }^\circ\text{C}/1 \text{ h}$) with 0 and 3 wt.% water in the electrolyte (1 M LiClO_4 in PC) measured with fresh layers (limiting voltages: -2 V, $+1$ V).

Fig. 5.15 also shows CP measurements for Li^+ intercalation and deintercalation in electrolyte containing different amounts of water but performed after 500 CV cycles. The difference between the slopes of the potential-time behavior with and without water is more pronounced than those presented in Fig. 5.14. The potential-time slope is always higher in the dry electrolyte than that in the wet electrolyte, therefore the safe voltage is reached earlier in the dry electrolyte, so less charge can be intercalated into the layer. In the dry electrolyte, Q_{in} is reduced from 17 mC/cm^2 (10^{th} CP cycle, Fig. 5.14) down to 12 mC/cm^2 (after 500 CV cycles) and is found to further decrease continuously with further CP cycles. On the contrary, the property of the layer in the wet electrolyte remains rather good after 500 CV cycles. The amount of charge intercalated after 500 CV cycles with 3 wt.% water in the electrolyte, $Q_{\text{in}} \approx 20 \text{ mC/cm}^2$ (safe voltage -1.4 V), is similar with that obtained after 10 CP cycles (24 mC/cm^2 , -1.4 V , Fig. 5.14) and is found to remain constant with further CP cycles. So the degradation of the layer in dry electrolyte is more pronounced than that in the wet electrolyte. The potential-time slope for deintercalation until the kink is larger than that for intercalation and decreases with water content. The $Q_{\text{out}}/Q_{\text{in}}$ value is 0.92 in wet electrolyte and only 0.84 in dry electrolyte. This shows again that the reversibility of the intercalation reaction is improved by addition of water to the electrolyte.

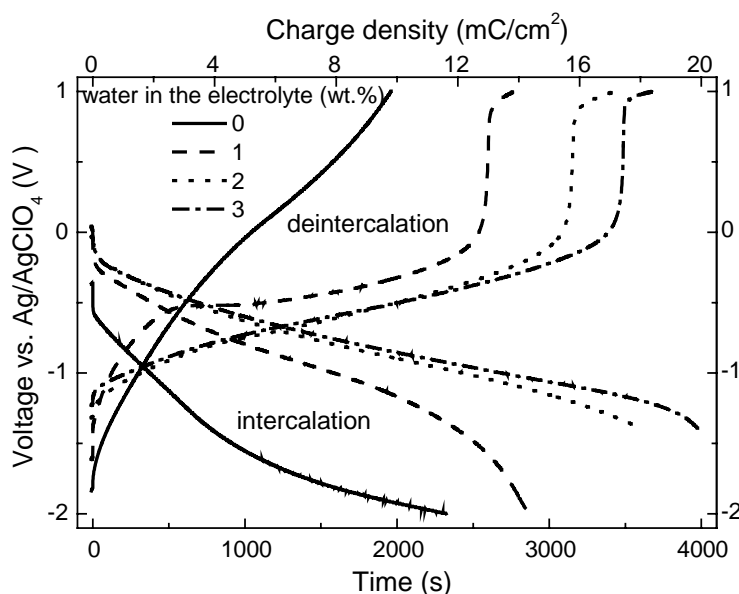


Fig. 5.15. Chronopotentiometric switching with constant current of $\pm 5 \mu\text{A/cm}^2$ of $(\text{CeO}_2)_{0.81}(\text{TiO}_2)_1$ sol-gel single layers (200 nm thick, $T_s = 450 \text{ }^\circ\text{C}/1 \text{ h}$) with different amounts of water in the electrolyte (1 M LiClO_4 in PC) measured after 500 CV cycles (limiting voltages: -2 V , $+1 \text{ V}$ and limiting time: 4000s).

Such results have never been reported for $\text{CeO}_2\text{-TiO}_2$ layers but now allow to understand why the different amount of charge inserted and deinserted reported by the different research groups. For instance, Avellaneda et al. reported a constant value of Q_{in} (16 mC/cm^2) and $Q_{\text{in}}/Q_{\text{out}}$ ratio (0.99) with 2 cm^2 layers cycled in the same Li-PC electrolyte during 4500 cycles [123]. The water content

of their “dry” electrolyte measured at INM was about 1.4 wt.% and was obviously obtained because the electrolyte was prepared and stored in the warm and humid Brazilian atmosphere (see also Fig. 5.7). Therefore all the results reported till now without specifying the water content of the electrolyte have to be taken with caution. This may also be true for other type of layers measured in the same electrolyte.

Three other minor parameters have been identified and tested with coatings prepared using the same sol II and heat treated at 450 °C/ 1 h. The results are described in the next paragraphs.

a) *Pretreatment of the substrate*

Fig. 5.16 shows the intercalated charge density Q_{in} measured during CV cycles for 200 nm thick single layers coated on substrate with and without a previous heat treatment at 450 °C in air for 30 minutes. The large decrease of Q_{in} observed during the first 10 CV cycles is similar for both conditions but the layer coated on the substrate preheated at 450°C leads to a slightly higher charge capacity (about 20 %) and a better long time stability. Heating the conducting glass surface causes a strong desorption of adsorbed water and various hydrocarbon molecules [15]. All the FTO-coated substrates used later have been therefore pretreated in air at 450 °C for 30 minutes.

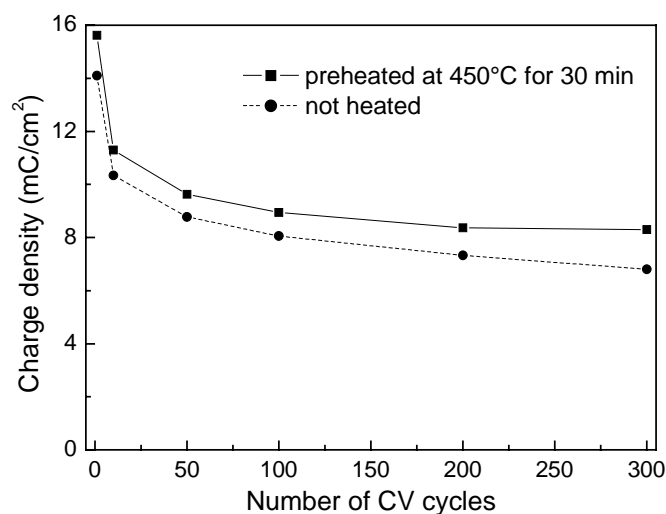


fig. 5.16. Charge density of $(\text{CeO}_2)_{0.81}(\text{TiO}_2)_1$ sol-gel single layer (200 nm) deposited on K-glass without and with heat treatment versus the number of CV cycles in 1 M LiClO_4 in PC with 1.4 wt.% water. (scan range: -2V/ +1V; scan rate: 50 mV/ s)

b) *Optimization of dip-coating soaking time*

The effects of the composition of the sols and the drawing rates during dip coating on the electrochemical property of the layers have been discussed. The lapse of time during which the substrate remains in the sol before its withdrawal was tested from 10 to 600 seconds. Except for time <30 seconds the thickness of the layers did not vary. The ion storage capacity of the layers as a function of the CV cycle number is shown in Fig. 5.17. The initial decrease of Q_{in} is observed for

all coatings. Nevertheless the samples prepared by soaking the substrates in the sol between 30 and 60 seconds give a slightly higher ion storage capacity than the others. In the following results, the $(\text{CeO}_2)_{0.81}(\text{TiO}_2)_1$ sol-gel layers were obtained by fixing the dip-coating soaking time to 30 seconds.

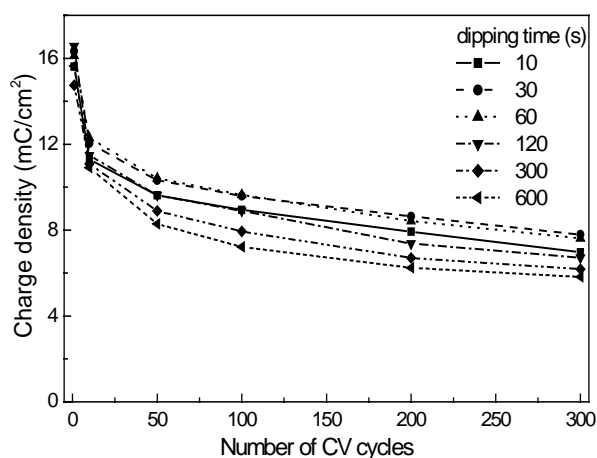


Fig. 5.17. Charge density versus number of CV cycles of $(\text{CeO}_2)_{0.81}(\text{TiO}_2)_1$ sol-gel single layers with different dipping time. Electrolyte: 1 M LiClO_4 in PC with 1.4 wt.% water; Scan range: -2 V/ +1 V; Scan rate: 50 mV/s

c) *Effect of acetyl acetone additive to the sol*

It is well known that acetyl acetone (acac) can reduce and even suppress the hydrolysis and condensation of metal alkoxides in solutions due to chelation of the metal atom. It is often used to reduce the hydrolysis speed [186]. To test if acetyl acetone could act as a stabilizer, 6 sols with different composition were prepared, keeping the concentration of $\text{Ce}(\text{NO}_3)_3 \cdot 6\text{H}_2\text{O}$ fixed to 0.226 mol/l. The total concentration of cerium and titanium was 0.5 mol/l. $(\text{NH}_4)_2\text{Ce}(\text{NO}_3)_6$ was added to the sol to change the Ce/Ti ratio and control the water content in the sol. The details about the sol compositions are listed in Table 5.2. The layers were deposited on an preheated K-glass with a soaking time of 30 seconds and a withdrawal rate of 4 mm/s. The layers were then sintered at 450 °C for 1 hour.

The layers made from sol 5 and 6 were not transparent and did not have a homogeneous surface. The layers from sol 1 gave a maximum charge intercalation and maximum charge density per micrometer during the 10th CA cycle (Fig. 5.18). The sols with acetyl acetone and $(\text{NH}_4)_2\text{Ce}(\text{NO}_3)_6$ added at the same time could not produce a layer with high charge density either calculated in $\text{mC}\cdot\text{cm}^{-2}$ or $\text{mC}\cdot\text{cm}^{-2}\cdot\mu\text{m}^{-1}$. By comparison, the sol without acetyl acetone and Ce:Ti = 0.81 :1 is once again certificated as the best one to produce layers with better ion storage capacity.

Table 5.2. Description of the sols and thickness of the layers made from the sols

Sol No.	Ce:Ti	Concentration of Ti (mol/l)	acac:Ce	Thickness of the layer (nm)
1	0.81:1	0.275	0	190
2	1:1	0.25	0	370
3	2:1	0.167	0	220
4	0.81:1	0.275	1	130
5	1:1	0.25	1	300
6	2:1	0.167	1	400

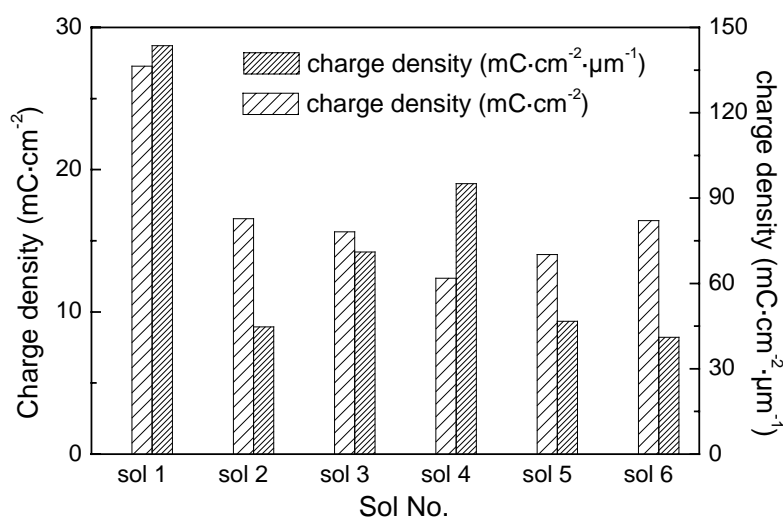


Fig. 5.18. Ion storage capacity of the layers coated from different sols, measured during the 10th CA cycle in 1 M LiClO₄ in PC with 1.4 wt.% water (-2 V/ 2 min, +1 V/ 2 min)

5.1.3 Influence of the sintering temperature

The sintering temperature was already reported in the literature as one of the most important parameters to obtain high Li⁺ charge exchange with sol-gel CeO₂-TiO₂ electrodes [2, 35]. It is therefore needed to carefully reconsider its effect for layers tested in dry and wet electrolyte. (CeO₂)_{0.81}(TiO₂)₁ sol-gel single layers produced from sol II aged for about 120 hours have been investigated with sintering in air for 1 hour at different temperatures from 150°C to 550°C. The conditions for preparing the layers are: preheated K-glass, soaking in the sol for 30 s and withdrawal rate 4 mm/s.

a) $(\text{CeO}_2)_{0.81}(\text{TiO}_2)_1$ powder characterized by TG/DTA technique

The thermal behavior of $(\text{CeO}_2)_{0.81}(\text{TiO}_2)_1$ powder is shown in Fig. 5.19. The Gram Schmidt graph, which is the integration of the FTIR signal from the chemicals evaporated from $(\text{CeO}_2)_{0.81}(\text{TiO}_2)_1$ powder is shown at the same time. By checking the FTIR response and mass spectroscopy, it is found that the mass loss at 100 °C is corresponding to H_2O . The mass loss at 200 °C is mainly due to a mixture of H_2O , CO_2 and NO_2 . The mass loss at 300 °C is due to the evolution of NO_2 and a small amount of CO_2 . The mass loss between 200 to 300 °C is probably due to the oxidation of the organic parts of the dried sol and the product NO_2 is due to the reduction of NO_3^- . There is no phase change and big mass loss during 350°C to 600°C according to the mass change and DTA profile. The small endothermic peak at 650 °C may correspond to a phase change while no substance is released.

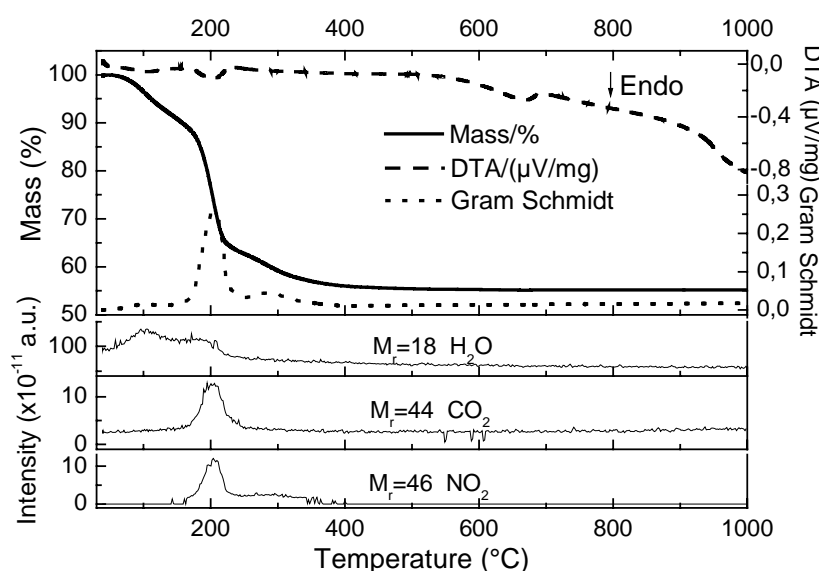


Fig. 5.19. TG-DTA-MS curves and Gram Schmidt curve of the powder dried from $(\text{CeO}_2)_{0.81}(\text{TiO}_2)_1$ sol at 50 °C for 24 hours, detected H_2O , CO_2 and NO_2 are depicted in MS curve.

b) *Thickness of the layers sintered at different temperature*

The thickness of $(\text{CeO}_2)_{0.81}(\text{TiO}_2)_1$ sol-gel layers sintered in air at different temperature decreases with the increase of temperature (Fig. 5.20). A large decrease occurs for heating temperature up to 350 °C and it levels down for $T \geq 500$ °C. As shown in Fig 5.19 this is due to the removal of the solvents (80–150°C), the combustion of the organic materials (150–300°C) and the reduction of the porosity ($T > 300^\circ\text{C}$).

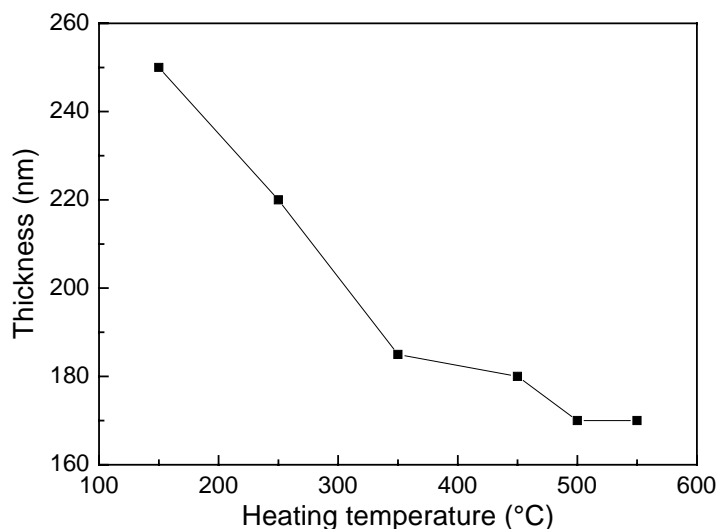


Fig. 5.20. Relationship of thickness vs. sintering temperature of $(\text{CeO}_2)_{0.81}(\text{TiO}_2)_1$ sol-gel single layers sintered for 1 hour.

c) *Crystalline structure of the layers determined by XRD*

The crystalline structure of the layers sintered at different temperatures was determined by XRD and is featured in Fig. 5.21. The layers are amorphous whatever is the sintering temperature. All the XRD peaks come from the FTO layer of K-glass. The only common feature to all samples is a weak and broad hump in the low 2θ region between 25° and 35° , characteristic of short-range order or amorphism. Therefore the structure difference between the $(\text{CeO}_2)_{0.81}(\text{TiO}_2)_1$ sol-gel single layers heated at different temperature is only the density and the thickness. TEM measurements of layers sintered at 450°C and 550°C indicate however that very small crystallites start to appear in the layer sintered at 550°C (see annex B).

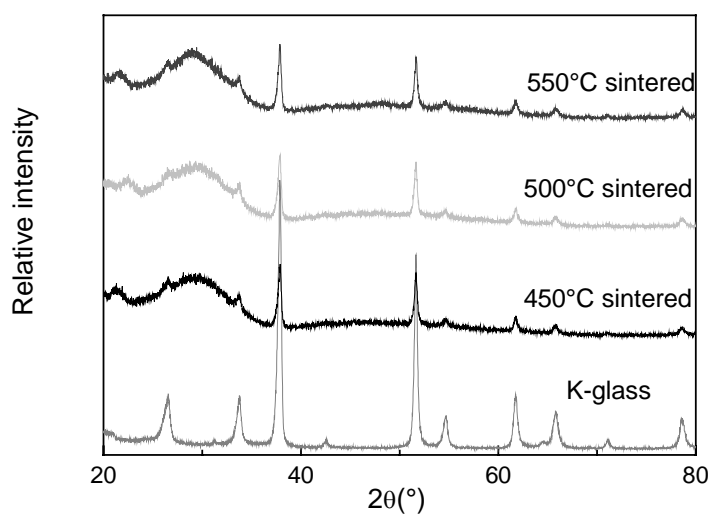


Fig. 5.21. XRD patterns of K-glass and $(\text{CeO}_2)_{0.45}(\text{TiO}_2)_{0.55}$ sol-gel single layers sintered at different temperatures.

d) *Electrochemical properties of the layers*

Cyclic voltammetry of the layers sintered at various temperatures and measured in a dry and wet (3 wt.% water) electrolyte are shown in Fig. 5.22. The CV shape of the layer heated at 150°C is different and both the cathodic and anodic peak are very small.

In the dry electrolyte, the cathodic and anodic peaks increase with the sintering temperature. The cathodic peak position moves to more positive potential and the anodic one moves to negative. The Li^+ mobility in the layers sintered at higher temperature is faster. The highest Li^+ ion insertion process occurs for $T_s = 550^\circ\text{C}$.

With 3 wt.% water added to the electrolyte, the CV profile of all layers sintered at $T \geq 350^\circ\text{C}$ is quite similar and present also higher ion storage ability.

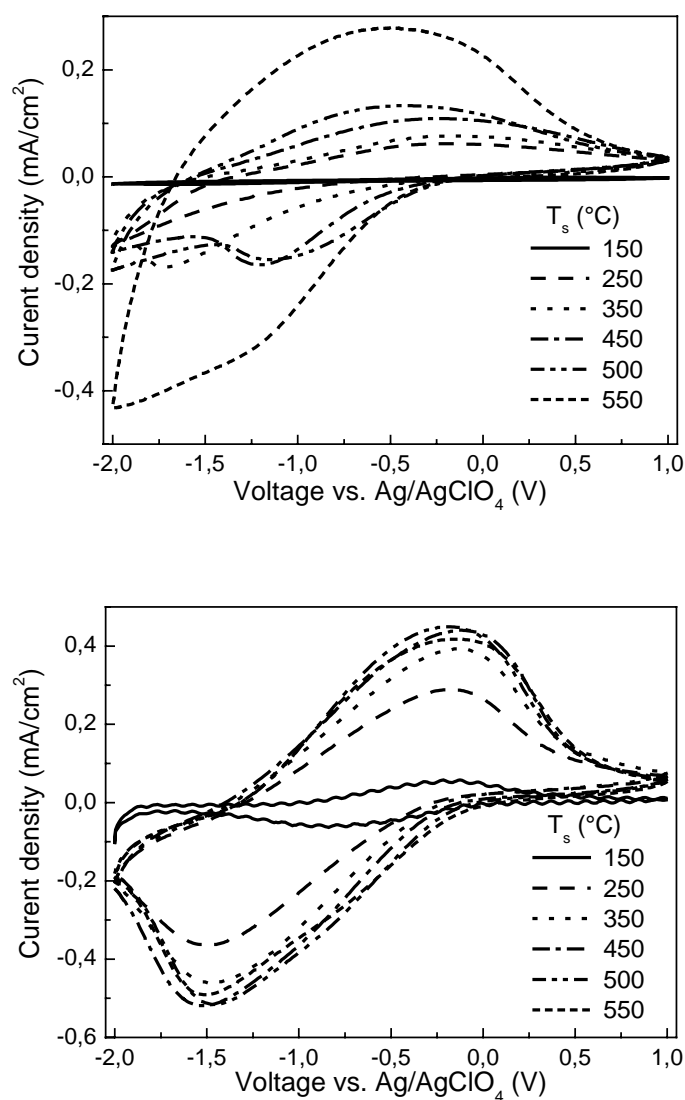


Fig. 5.22. CV profile of $(\text{CeO}_2)_{0.81}(\text{TiO}_2)_1$ sol-gel single layers (300th cycle) sintered at different temperature in 1 M LiClO_4 in PC (scan rate 50 mV/s). Top: dry electrolyte; bottom: wet electrolyte with 3 wt.% water.

During the initial cycles, the values of the intercalated charge decrease very fast in the dry electrolyte (Fig. 5.23). But the values of the long-term behavior (after 10 cycles) increase with the sintering temperature. For layers sintered at 450 °C, the value is 4.2 mC/cm² and similar to that shown in the state of the art (Table 3.2). The best result is observed for layers sintered at 550 °C ($Q_{in} \approx 10$ mC/cm²), a factor 2.5 higher of that shown in Table 3.2.

The intercalated charge is higher with the wet electrolyte and the initial decrease is much smaller. Layers sintered between 450 °C and 550 °C present similar results and the initial loss of the ion storage ability is only 3.5 mC/cm² from 16.5 down to 13 mC/cm². The long-term behavior remains higher (about 13 mC/cm²) than that in the dry electrolyte.

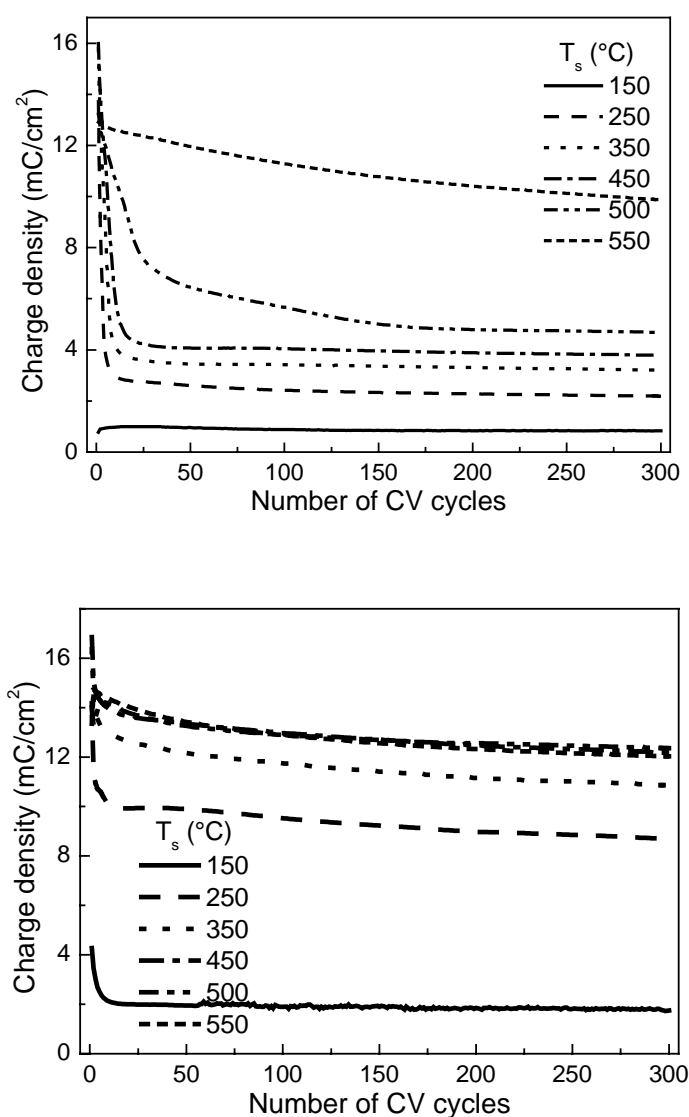


Fig. 5.23. Intercalated charge density (Q_{in}) in $(\text{CeO}_2)_{0.81}(\text{TiO}_2)_1$ sol-gel single layers sintered at different temperature in 1 M LiClO_4 in PC as a function of the CV cycle number (scan range -2 V/ $+1$ V, scan rate 50 mV/s). Top: dry electrolyte; bottom: wet electrolyte with 3 wt.% water.

The charge intercalated into the layers sintered at different temperature measured during the 3rd CA cycle after 300 CV cycles is shown in Fig. 5.24. The charge intercalated into the layer heated at 150°C is again very small and this layer is not a good candidate whatever is the electrolyte. The results show that water added in the electrolyte plays an important role in the ion storage ability and the kinetics of the layers sintered from 250°C to 500°C, as the intercalated charge is one to two times higher in the wet electrolyte than in the dry electrolyte. The bleaching kinetics is faster for the layer sintered at 450°C in the wet electrolyte. However the difference between dry and wet electrolyte for the layers sintered at 550 °C is not significant. This result is in agreement with that observed for the CV cycles.

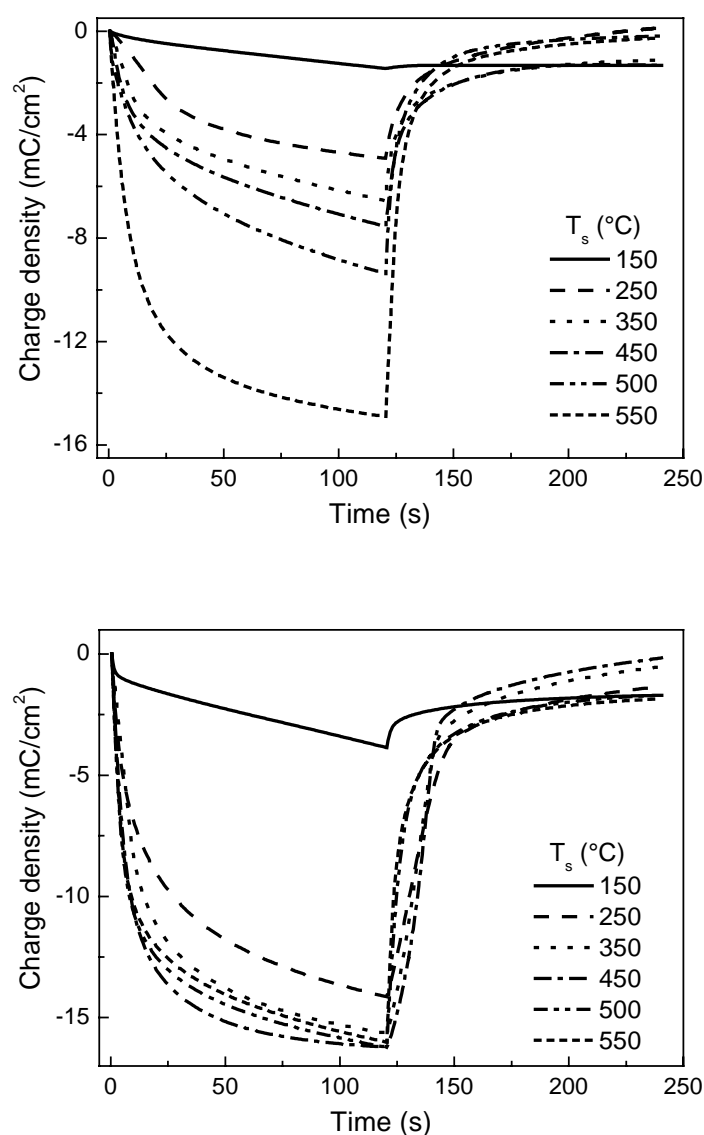


Fig. 5.24. Charge density of $(\text{CeO}_2)_{0.81}(\text{TiO}_2)_1$ sol-gel single layers sintered at different temperature during the 3rd CA cycle (-2 V, 2 min/ +1 V; 2 min) after 300 CV cycles in 1 M LiClO_4 in PC. Top: dry electrolyte; bottom: wet electrolyte with 3 wt.% water

The ion storage ability of the layers measured by chronopotentiometry (CP) is shown in Fig. 5.25. Once again whatever is the electrolyte, the layers heated at 150 °C are not suitable as Li^+ storage layer. In the dry electrolyte, the potential variation that accompanying the charge intercalated decreases continuously and fast and the slope becomes smaller when T_s increases. The charge intercalated up to the potential limit of -2 V increases with the sintering temperature, the largest value being for the layer sintered at 550 °C. The same behavior is observed for the deintercalation, fast increase of the potential with a slope that nevertheless decreases with the sintering temperature up to the value of the charge that has been intercalated. At the end of the curves a kink is observed which is followed by a fast increase of the potential. This is particularly seen for the layer sintered at 550 °C. This corresponds to the exhaustion of Ce^{4+} and electron accumulated at the surface of the electrode. $(\text{CeO}_2)_{0.81}(\text{TiO}_2)_1$ sintered at 550 °C for one hour is a good candidate for ion storage layers used in dry electrolyte within the potential limit -2 V ; $+1\text{ V}$.

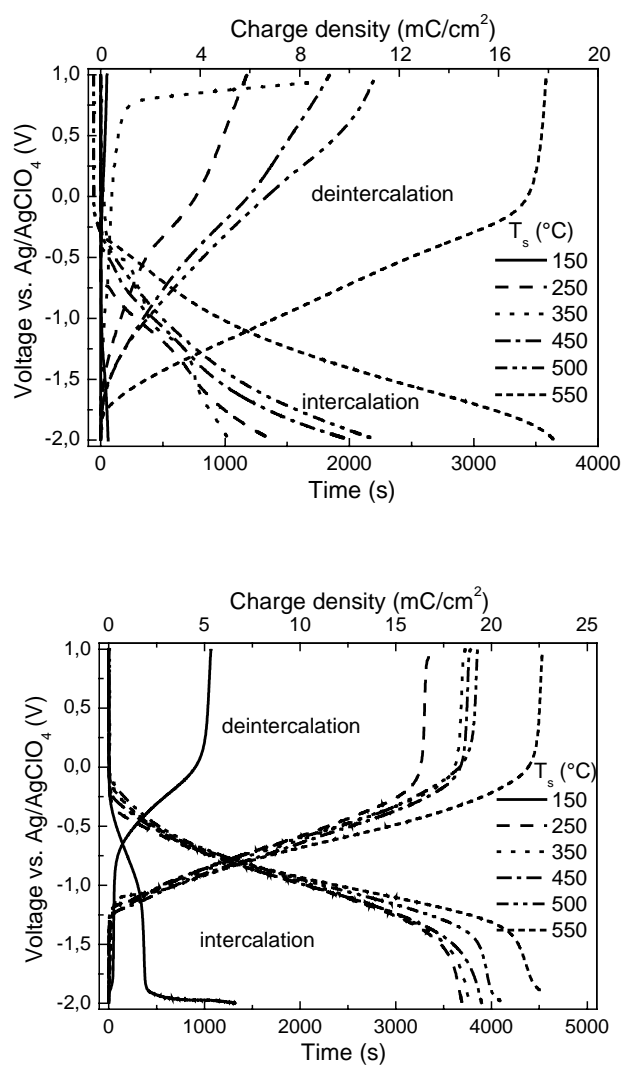


Fig. 5.25. Chronopotentiometric switching in 1 M LiClO_4 in PC with constant current of $\pm 5\ \mu\text{A}/\text{cm}^2$ of $(\text{CeO}_2)_{0.81}(\text{TiO}_2)_1$ sol-gel single layers sintered at different temperature measured immediately after 300 CV cycles (limiting voltages: -2 V , $+1\text{ V}$). Top: dry electrolyte; bottom: wet electrolyte with 3 wt.% water

In the wet electrolyte, the potential-charge slopes are smaller than that in dry electrolyte and decrease when T_s increases. The charge intercalated up to the potential limit of -2 V increases with the sintering temperature and is much larger than that in the dry electrolyte. The intercalated charge is nearly doubled for the layers sintered below 500°C (include 500°C) compared with the result measured in the dry electrolyte. The largest value is for the layer sintered at 550°C and improved from 18 (in dry electrolyte) to 22.5 mC/cm^2 (in wet electrolyte). The same behavior is observed for the deintercalation, the potential-charge slopes are smaller than that in dry electrolyte and decreases with the sintering temperature.

e) *Influence of the sintering atmosphere*

It is known that the sintering atmosphere plays a decisive factor on the physical and chemical properties of the deposited films [111], as electrical and optical properties of coatings have been enhanced in some cases when the sintering process is performed in vacuum or other synthetic gases. The influence of the sintering atmosphere on the ion storage capacity of the layers has been tested for a layer sintered in air or $60\% \text{ N}_2/40\% \text{ O}_2$ for 1 hour (Fig. 5.26). The difference of the ion storage ability of the layers obtained using both processes is not remarkable. The influence of the atmosphere is therefore not important to improve the ion storage ability of $(\text{CeO}_2)_{0.81}(\text{TiO}_2)_1$ sol-gel layers. Layers heated in vacuum turned opaque and are therefore not suitable for using as transparent ion storage layer.

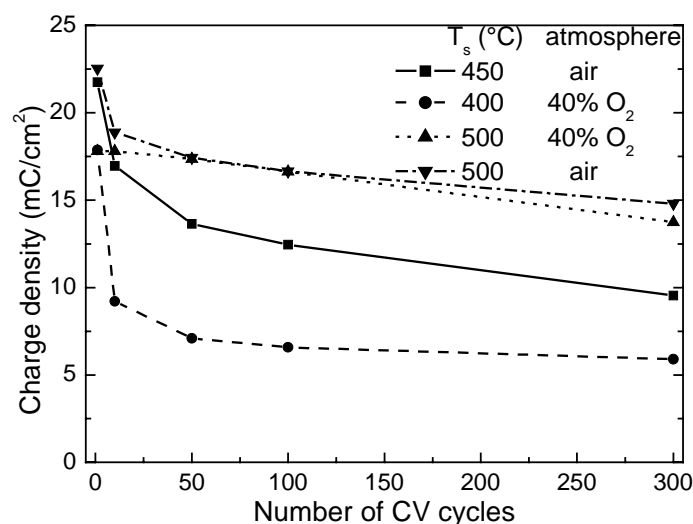


Fig. 5.26. Charge density versus number of CV cycles of $(\text{CeO}_2)_{0.81}(\text{TiO}_2)_1$ sol-gel single layers with different heating condition. Electrolyte: wet 1 M LiClO_4 in PC with 1.4 wt.% water; Scan range: -2 V/+1 V; Scan rate: 50 mV/s

f) *Double layers*

The properties of double $(\text{CeO}_2)_{0.81}(\text{TiO}_2)_1$ layers sintered at different temperatures were also tested. The first layers have been heated at 150 °C or 200 °C for half an hour, and then the two layers stack has been sintered at 450 °C, 500 °C and 550 °C respectively. If the first layers are heated at 100 °C, the layers are opaque.

The CV profiles for the single and double layers sintered at 550 °C are shown in Fig. 5.27. In the dry electrolyte, the current density of the double layers is smaller than that of the single layer. The cathodic and anodic current peaks of the first layer heated at 200 °C are slightly higher than those obtained when the first layer is heated at 150 °C.

In the wet electrolyte, on the contrary, the cathodic and anodic peaks of the double layers are higher than that of single layers. The higher is the heating temperature for the first layer, the higher are the cathodic and anodic current peaks.

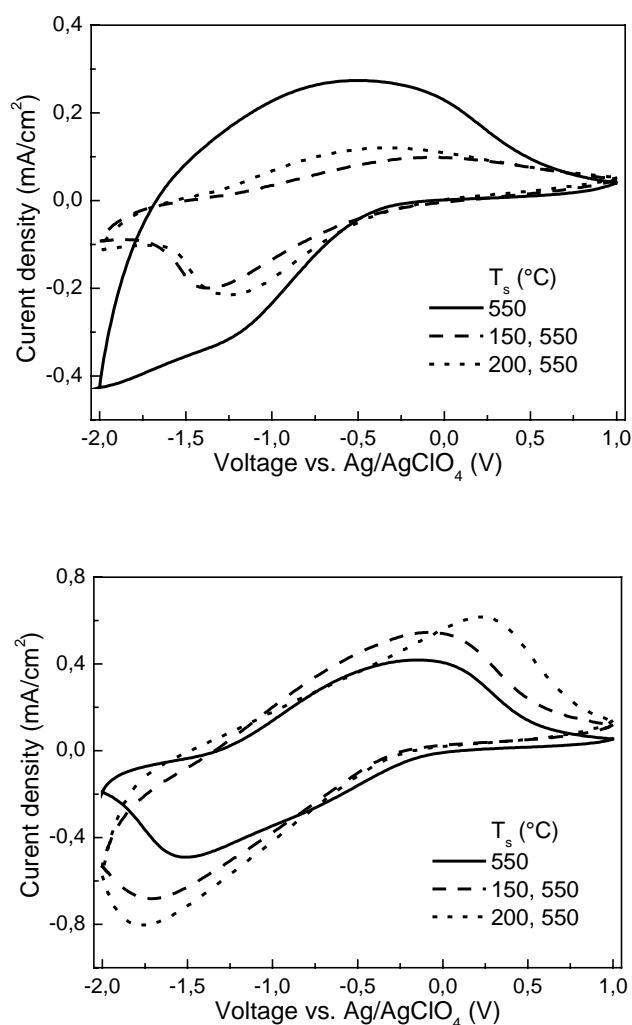


Fig. 5.27. Cyclic voltammetry of $(\text{CeO}_2)_{0.81}(\text{TiO}_2)_1$ sol-gel single and double layers sintered at 550 °C in 1 M LiClO_4 in PC (300th CV cycle) (scan rate 50 mV/s). Top: dry electrolyte; bottom: wet electrolyte with 3 wt.% water

In the dry electrolyte, the charge intercalated with the double layers during CA cycles is also smaller than that of single layers (Fig. 5.28).

In the wet electrolyte, the ion storage capacity of the double layers is higher than that of the single layers except for layers heated at 450 °C. For a final sintering temperature of 550 °C, the charge intercalated during 2 minutes (-2 V) is improved from about 15 mC/cm² (single layer) to 26 mC/cm² (200°C and 550°C heat treated double layer), but is not proportional to the thickness of the stack. This value is now larger than that of a WO₃ layer (CA: 18 mC/cm²; Table 3.2) but smaller than that of a Nb₂O₅:Mo (Mo:Nb = 0.3) layer (CA: 45 mC/cm²; Table 3.2).

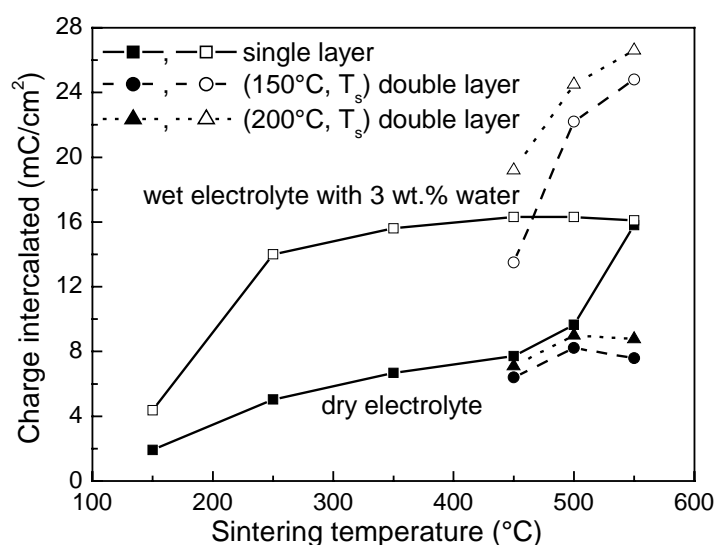


Fig. 5.28. The ion storage ability of (CeO₂)_{0.81}(TiO₂)₁ sol-gel layers sintered at different temperature during the 3rd CA cycle (-2 V, 2 min/+1 V, 2 min) after 300 CV cycles in 1 M LiClO₄ in PC, RE: Ag/AgClO₄)

The charge intercalation behavior measured by CP (-/+5 μA/cm²) of single and double layers sintered at 550 °C in dry and wet electrolyte are shown in Fig. 5.29. Once again in dry electrolyte the charge intercalated into the double layer is only 17.5 mC/cm² and smaller than that of a single layer (22 mC/cm²) and the slope of the potential in the deintercalation is higher.

In the wet electrolyte, the charge intercalated into the double layer reaches safe values as high as 36 mC/cm² at -1.5 V with a high reversibility as Q_{out}/Q_{in} = 0.97. The reversible charge capacity of the double layers in the wet electrolyte is 1.6 times higher than that obtained with the single layer 22.5 mC/cm². It is interesting to note that for such layers the kinks at the end of the scan are not observed and that the slope of the potential variation is even smaller.

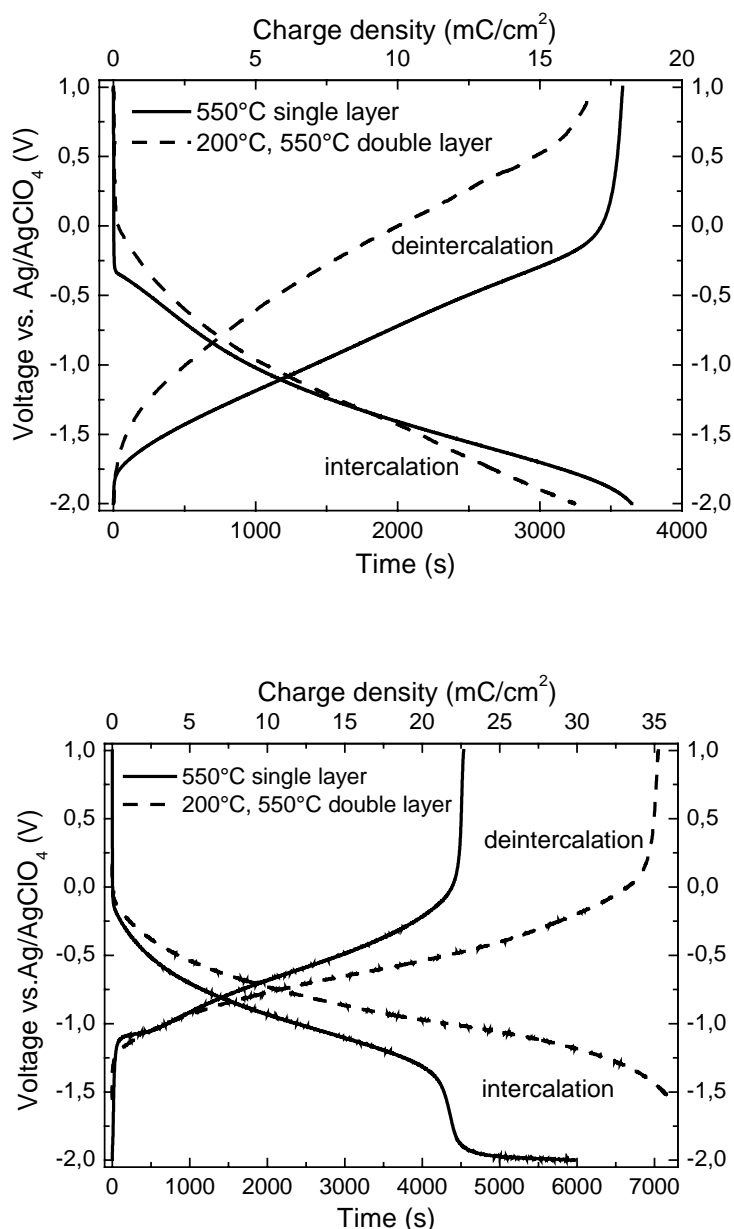


Fig. 5.29. Chronopotentiometric switching with constant current of $\pm 5 \mu\text{A}/\text{cm}^2$ of $(\text{CeO}_2)_{0.81}(\text{TiO}_2)_1$ sol-gel single and double layers sintered at 550°C in 1 M LiClO_4 in PC measured after 300 CV cycles (limiting voltages: -2 V , $+1 \text{ V}$). Top: dry electrolyte; Bottom: wet electrolyte with 3 wt.% water

The double layers with the first layer and the stacks both sintered at $T_s \geq 450^\circ\text{C}$ were also tested. The charge intercalation is similar to that of the first layer heated at 200°C . The charge capacity is not improved in dry electrolyte, but it is drastically improved in wet electrolyte.

By making double layers to increase the thickness of $(\text{CeO}_2)_{0.81}(\text{TiO}_2)_1$ sol-gel layers, the electrochemical properties of the layers is not improved in the dry electrolyte, as the Li^+ ion intercalation seems to only occur in the outer layer and the presence of a blocking interface between the two layers is not overcome. But in the wet electrolyte, this interface does not impede

the Li⁺ ion intercalation into the inner layer and the electrochemical properties of the layers are drastically improved.

In conclusion the water content of the liquid electrolyte 1 M LiClO₄ in PC causes drastic differences in the ion storage capacity of (CeO₂)_{0.81}(TiO₂)₁ sol-gel single and double layers. It improves the ion storage ability of single and double layers, the reversibility and the kinetics. Using a 550 °C heated double layers in wet electrolyte with 3 wt.% water, the ion storage capacity of (CeO₂)_{0.81}(TiO₂)₁ sol-gel layers during CA cycle (-2 V/ 2 min, +1 V/ 2 min) can be increased to 26 mC/cm².

5.2 Li⁺ insertion and deinsertion mechanisms studied in dry and wet liquid electrolyte by EQCM

The electrochemical quartz crystal microbalance (EQCM) is uniquely qualified to address the mechanism of ion insertion into electrode layers. It can detect in situ nanogram mass change of an EC layer deposited on a quartz crystal by recording the resonance frequency during CV, CP or other electrochemical techniques. The high mass sensitivity of the EQCM technique should therefore allow a precise evaluation of the reversibility of ion and solvent flow and of the film degradation processes. However just a few works have been reported on the properties of EC layers such as WO₃ and Nb₂O₅ films (187, 188).

This technique was therefore used to get a better insight on the intercalation and deintercalation of Li⁺ in CeO₂-TiO₂ layers in dry and wet liquid electrolytes and to propose a mechanism for these processes.

For this purpose (CeO₂)_{0.81}(TiO₂)₁ sol-gel double layers (370 nm thick, sintered at 450 °C for 1 hour) were coated on unpolished quartz crystal with gold as conducting layer. The mass change of the layer was tested in 1 M LiClO₄ in PC without water (dry electrolyte) and with 3 wt.% water (wet electrolyte) during CV cycles. The ion insertion and deinsertion mechanism of the (CeO₂)_{0.81}(TiO₂)₁ sol-gel layer was analyzed from the mass change curves obtained simultaneously with CV curves.

Assuming that the charge and mass changes measured are linked to cations and anions and not to other effects, e.g. side reactions, neutral molecular adsorption etc., the molar amount of anion and cation transport determined by the charge and mass changes during the electrochemical measurements are both given at any scan rate by the Faraday's law (Eq. 5.2).

$$n = \frac{Q}{zFA} \quad (5.2)$$

where Q is the total charge recorded during the processes, F is the Faraday constant, A is the area of the electrode, z is the charge of the transferred ion and n is the amount of all transferred ions in mol/cm². To describe the processes occurring with our electrolyte system, z is assumed to be 1.

The inserted charge and the mass change are related by Eq. 5.3,

$$\Delta m = nM_a = \frac{Q}{FA} M_a \quad (5.3)$$

where Δm is the total mass change of the layer in $\mu\text{g}/\text{cm}^2$ and M_a is the apparent molar mass during charge intercalation or deintercalation. The fraction of intercalated cations, x_+ and anions, x_- , can be calculated from equations 5.4 to 5.6.

$$x_+ = \frac{Q_+}{Q}; x_- = \frac{Q_-}{Q} \quad (5.4)$$

$$x_+ + x_- = 1 \quad (5.5)$$

$$|x_+ M_+ - x_- M_-| = M_a \quad (5.6)$$

where Q_- is the charge caused by anion transfer to the electrode, x_- is the fraction of anion species, M_- is the molar weight of anion species, Q_+ is the charge caused by cation transfer to the electrode, x_+ is the fraction of cation species and M_+ is the molar weight of cation species.

5.2.1 Overview of the mass changes during 100 CV cycles

In order to reduce artifacts related to temperature change and to minimize random fluctuations caused by the vibration of the sensor, the crystal was first immersed into the electrolyte for at least 30 minutes before starting the cyclic voltammetry measurement. Then the frequency of the crystal was measured without applied potential. When the response was stable (usually within about five minutes), the cyclic voltammetry measurement was then performed.

The total mass change of the layers Δm recorded during 100 CV cycles (scan rate: 50 mV/s; scan range: -2 V/ +1 V) in dry and wet electrolyte is shown in figure 5.30 for the 1st, 5th, 10th, 50th and 100th cycle. In the dry electrolyte, the overall shape of Δm vs. potential changes drastically during the initial 10 cycles, and then remains identical. In the wet electrolyte, the overall shape of the mass change versus potential remains similar up to 100 cycles.

In both cases the total mass of the crystal increases irreversibly after each cycle as shown in Fig. 5.31.

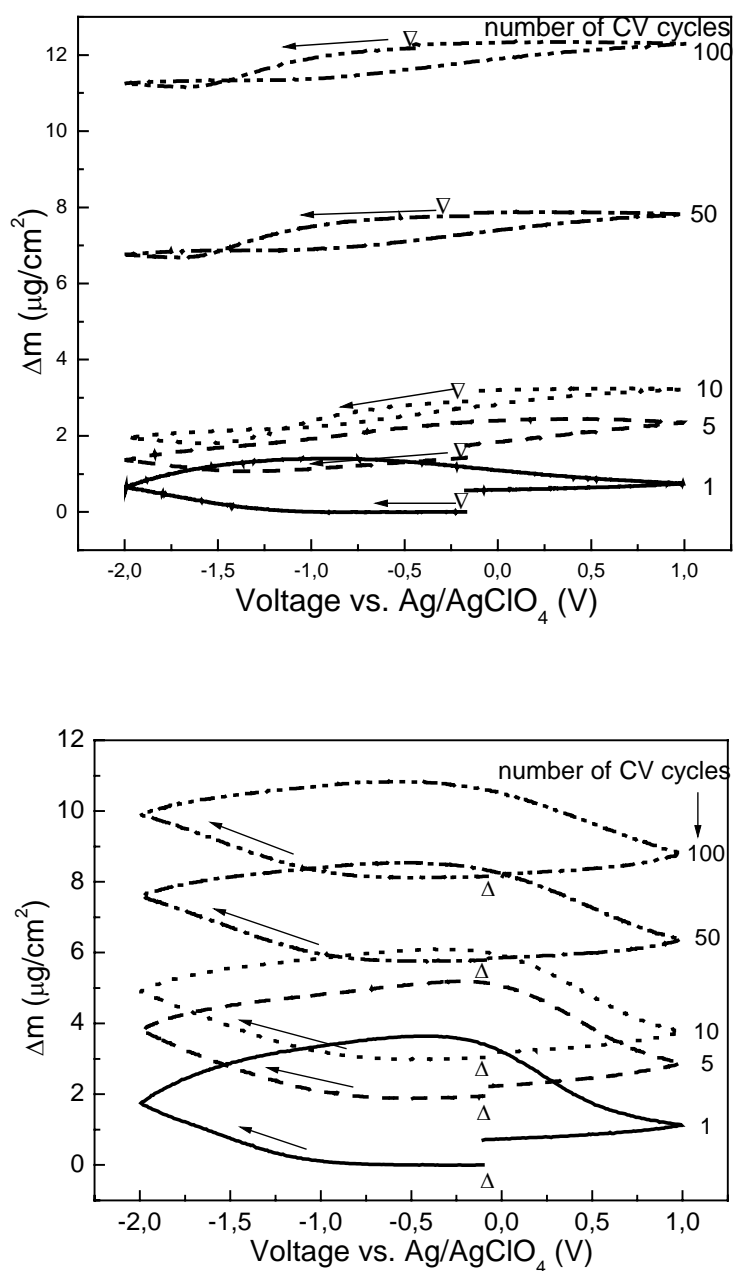


Fig. 5.30. Mass change of $(\text{CeO}_2)_{0.81}(\text{TiO}_2)_1$ sol-gel double layers in 1 M LiClO_4 in PC recorded during the first 100 CV cycles (scan rate: 50 mV/s). Top: dry electrolyte; bottom: wet electrolyte with 3 wt.% water. Δ : start of the cycle; \rightarrow : direction of the initial potential sweep.

The irreversible mass increase per cycle is initially high but shows from the 25th cycle a linear variation with the number of CV cycles. In the dry electrolyte the value of Δm is about $0.6 \mu\text{g}/(\text{cm}^2 \cdot \text{cycle})$ (initial cycles) and then decreases to about $0.1 \mu\text{g}/(\text{cm}^2 \cdot \text{cycle})$ (25th to 100th cycle). In the wet electrolyte the values are $0.7 \mu\text{g}/(\text{cm}^2 \cdot \text{cycle})$ and $0.04 \mu\text{g}/(\text{cm}^2 \cdot \text{cycle})$ respectively. The evolution of the curves suggests that this irreversible mass change can be divided into two processes. One corresponds to a fast mass increase occurring during the initial 25 cycles,

which then levels up without any more variation of Δm (Fig. 5.31). A second process leads to an irreversible linear increase of the mass from the first up to the 100th cycle. Fig. 5.31 shows a decomposition of the measured curves (dry and wet) following this suggestion.

It is interesting to observe that the first process seems to be common to both dry and wet electrolyte/ IS layer system, as the shapes and values obtained are practically the same. This part may be caused by irreversible lithium intercalation. Secondary Neutral Mass Spectroscopy (SNMS) measurements of $(\text{CeO}_2)_{0.81}(\text{TiO}_2)_1$ sol-gel layers of the intercalated and deintercalated state of the 1st and 300th CA cycle in dry electrolyte show that lithium can not be totally deintercalated (Fig. 5.32). Li^+ is found throughout the layer both in intercalated state and deintercalated state [189]. The concentration of Li is higher in the intercalated state than in the deintercalated state, but the deintercalation of Li is not complete. After 300 CA cycles there is a certain amount of Li left in the layer.

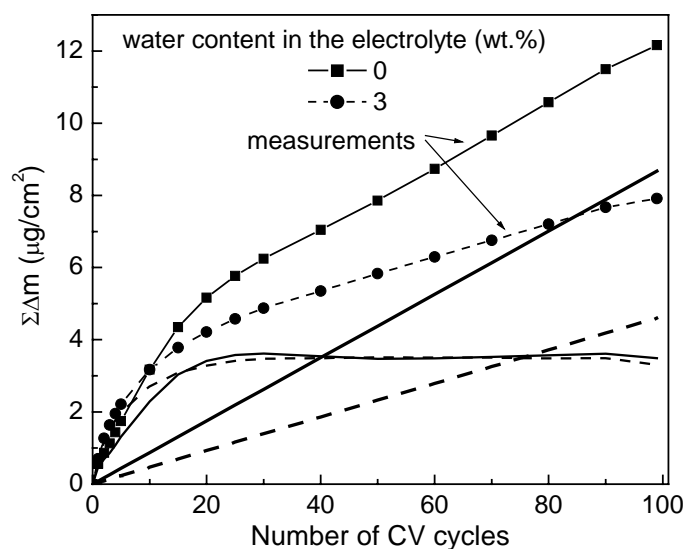


Fig. 5.31. Accumulated mass increase of $(\text{CeO}_2)_{0.81}(\text{TiO}_2)_1$ sol-gel double layers in 1 M LiClO_4 in PC without and with 3 wt% water during 100 CV cycles (scan rate: 50 mV/s, scan range: -2 V/ +1 V). A mathematical decomposition of the results into two processes is also shown.

The linear increase (2nd process) is however more important in the dry electrolyte. In both electrolytes it is proposed that this linear irreversible mass increase is caused by ClO_4^- ions adsorbed at the surface of the layer and may be also due to coordinated solvent molecules e.g. propylene carbonate (PC) in dry electrolyte and PC or water in wet electrolyte. The density of the layer is 4.2 g/cm^3 (calculated from the mass change of the quartz, the geometric area and the thickness of the layer), whereby the theoretical density of the $(\text{CeO}_2)_{0.81}(\text{TiO}_2)_1$ layer calculated from the theoretical density of CeO_2 and TiO_2 is 5.6 g/cm^3 . Thus the porosity of the layer is about 25 % [190, 191]. With such a porous layer it is also possible that neutral molecules e.g. propylene

carbonate come to the surface or into the pores of the layer. The lower mass increase in wet electrolyte may be due to hydration of ClO_4^- .

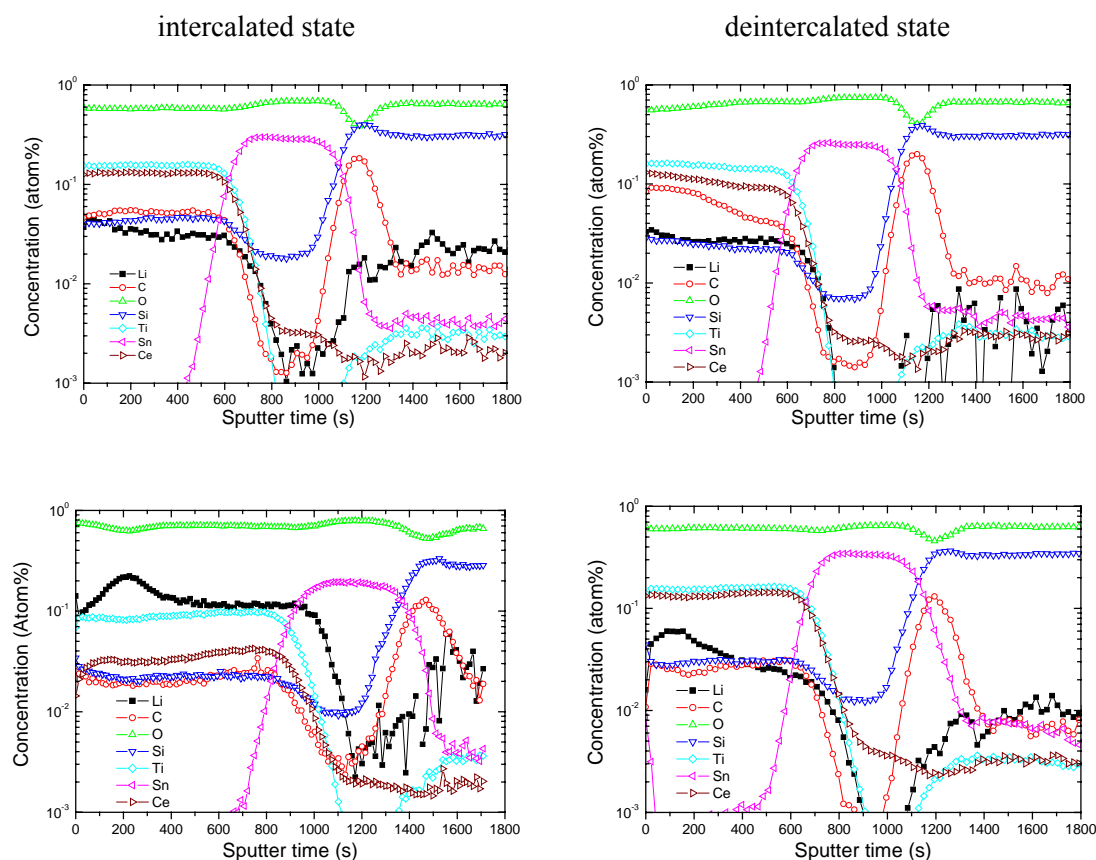


Fig. 5.32 Atom concentration of $(\text{CeO}_2)_{0.81}(\text{TiO}_2)_1$ sol-gel single layer for the intercalated and deintercalated state of the 1st CA cycle (top) and 300th CA cycle (bottom) determined via SNMS measurement. Electrolyte: 1 M LiClO_4 in PC without water. CA: -2 V (2 min)/ +1 V (2 min) [189].

An irreversible increase of the mass mainly during the initial cycles has also been observed in Nb_2O_5 film during Li^+ intercalation (same type of electrolyte, but the water content was not stated) [188]. As the films were allowed to equilibrate prior voltammetric measurement, this irreversible mass increase was interpreted as a filling of the pores of the film by the electrolyte involving a solvophilic effect induced by the applied potential.

5.2.2 Mass change analysis during cycling

a) dry liquid electrolyte

The evolution of the mass, charge density, current density and potential sweep vs. time recorded during the 1st, 5th, 30th and 100th CV cycle is shown in Fig. 5.33. The values of Δm , charge density and current density have been normalized to zero at the beginning of each cathodic cycle ($t = 0$).

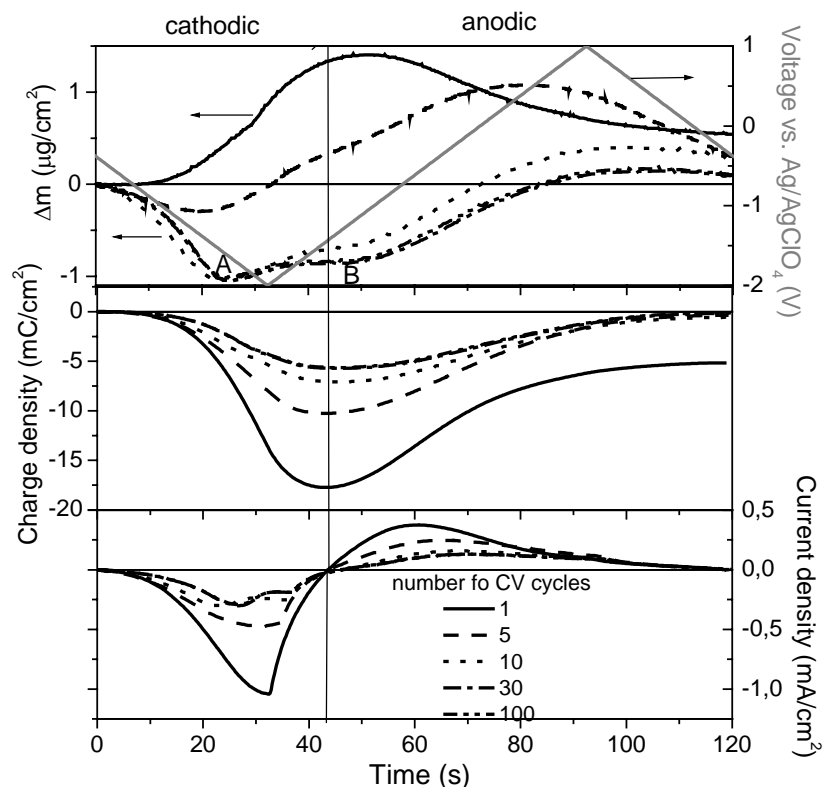


Fig. 5.33 Mass change, charge density and current density of $(\text{CeO}_2)_{0.81}(\text{TiO}_2)_1$ sol-gel double layers in dry 1 M LiClO_4 in PC during the 1st, 10th, 30th, 100th CV cycle (scan rate: 50 mV/s, scan range: -2V/+1V).

During the first cycle, the mass initially increases in the cathodic range and then decreases with the anodic current, but does not return to zero. A rather high mass increase of about $0.6 \mu\text{g}/\text{cm}^2$ is observed at the end of the anodic range. As discussed above, part of this mass increase is due to an irreversible Li^+ intercalation. However another phenomenon occurs, as observed already during the second cycle: the variation of the mass in the cathodic range is first negative and then becomes positive. The effect becomes more pronounced after further cycling up to about the 30th cycle and then no further changes are seen. This negative variation of the mass at the beginning of the cathodic cycles can be explained by a mass release of anions. The most probable process can be due to ClO_4^- adsorbed on the layer during the anodic sweeps, which form an interface on top of the $(\text{CeO}_2)_{0.81}(\text{TiO}_2)_1$ layer. This effect initiates already during the first cycle but more and more ClO_4^- ions can be adsorbed at the surface during the next cycles.

Because the ClO_4^- ions are rather large, they cannot be intercalated into the layer but can only be adsorbed at the surface. This was confirmed by the results of XPS (see annex D) as no Cl atom was detected in the $(\text{CeO}_2)_{0.81}(\text{TiO}_2)_1$ layer after 100 CV cycles whatever the electrolyte is.

In the stationary state, two peaks of mass change are observed: one is in the cathodic current range (labeled A) and is caused by the simultaneous ClO_4^- desorption and Li^+ intercalation. The other one

(labeled B) is in the anodic range and is caused by the simultaneous ClO_4^- adsorption and Li^+ deintercalation. The suggested ion exchange processes occurring in the cathodic and anodic current range are explained in Fig. 5.34.

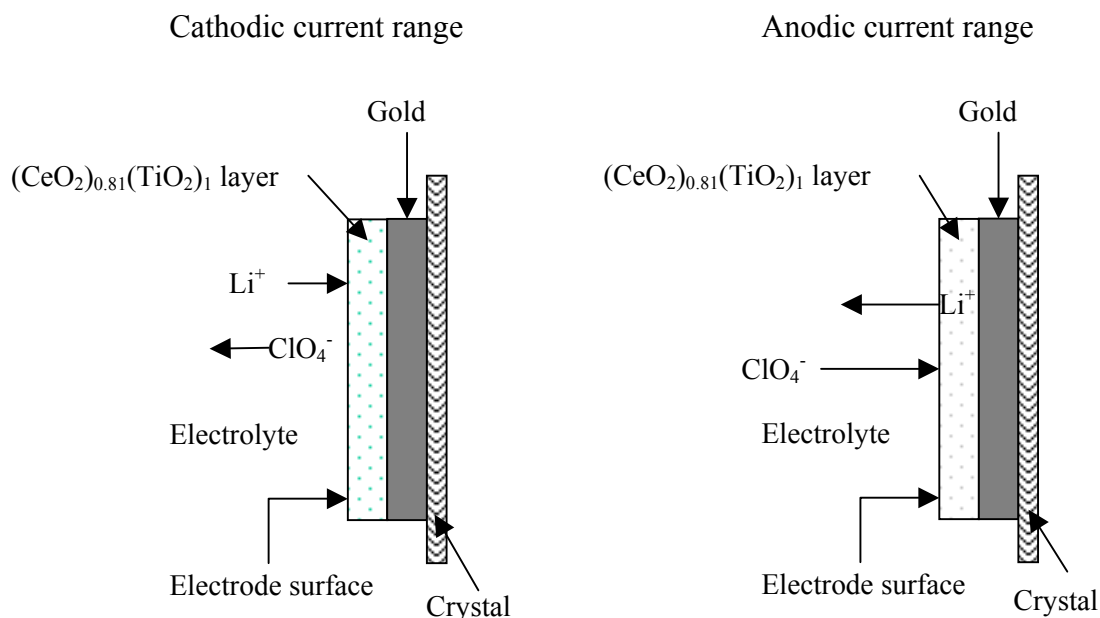


Fig. 5.34 Scheme of ion moving direction at the electrode surface (the arrows show the ion moving direction)

The model has been tested using equation 5.2 to 5.6, where the fraction of Li^+ (x_{Li}) and the fraction of ClO_4^- ($x_{\text{ClO}_4} = 1 - x_{\text{Li}}$) was calculated for each cycle as:

$$x_{\text{Li}^+}(t) = \frac{M_{\text{ClO}_4^-}}{M_{\text{Li}^+} + M_{\text{ClO}_4^-}} - \frac{\Delta m(t)F}{\Delta q(t)(M_{\text{Li}^+} + M_{\text{ClO}_4^-})} \quad (5.7)$$

where $M_{\text{ClO}_4^-}$ is the molar weight of ClO_4^- , M_{Li^+} is the molar weight of Li^+ , $\Delta m(t)$ and $\Delta q(t)$ are the observed mass change and the charge density change of the electrode. Therefore the charge density and the corresponding mass change caused by Li^+ intercalation are now given by

$$Q_{\text{Li}^+} = \int \frac{dq(t)x_{\text{Li}^+}(t)}{dt} dt \quad (5.8)$$

$$\Delta M_{\text{Li}^+} = \frac{M_{\text{Li}}}{F} \int \frac{dq(t)x_{\text{Li}^+}(t)}{dt} dt \quad (5.9)$$

The result for the 50th CV cycle (where a stationary state has been reached in the dry electrolyte) is shown in Fig. 5.35. The total variation of the charge density and mass change for Li^+ intercalation and ClO_4^- adsorption fit well the recorded results. The ion transfer process seems therefore not to be

due only to Li^+ intercalation/ deintercalation as reported in the literature, but also involve a ClO_4^- adsorption/ desorption process. Considering the charge evolution during the cycles, the ion transfer process is mainly due to Li^+ intercalation that is responsible for 60-80 % of the total charge involved. However the mass change behavior is mainly due to ClO_4^- desorption during cathodic current and ClO_4^- adsorption during anodic current, because ClO_4^- is 14 times heavier than the Li^+ atom. Fig. 5.35 shows that at the end of the anodic range the total mass remaining in the layer is about $0.1 \mu\text{g}/\text{cm}^2$ and mainly due to ClO_4^- . This is coherent with our assumption (see Fig. 5.31).

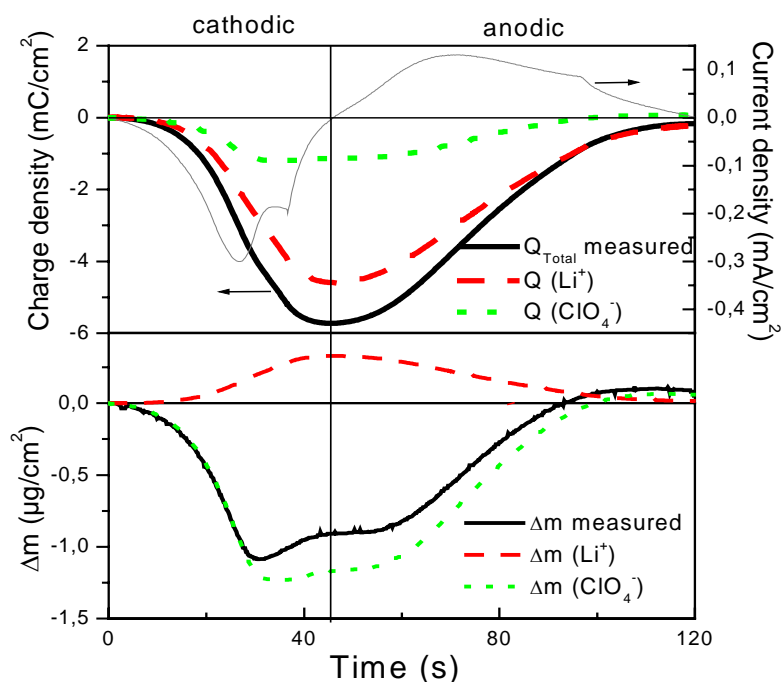


Fig. 5.35 Calculated charge density and mass changes due to Li^+ intercalation and ClO_4^- adsorption of the $(\text{CeO}_2)_{0.81}(\text{TiO}_2)_1$ sol-gel double layers during the 50th CV cycle in dry 1 M LiClO_4 in PC (scan rate: 50 mV/s; scan range: -2 V/ +1 V). Top: charge density change; bottom: mass change. The current density is also shown.

The degradation of the electrochemical properties of the $(\text{CeO}_2)_{0.81}(\text{TiO}_2)_1$ sol-gel layer (Fig. 5.8 to 5.10) occurring during the initial cycles — the charge capacity is reduced from $14 \text{ mC}/\text{cm}^2$ to $4 \text{ mC}/\text{cm}^2$ and the ion intercalation reversibility is only 0.9 in dry electrolyte — may therefore be due either to the formation of a ClO_4^- layer adsorbed on the surface or to the irreversible Li^+ intercalation that change the composition of the layer from $(\text{CeO}_2)_{0.81}(\text{TiO}_2)_1$ to $\text{Li}_x(\text{CeO}_2)_{0.81}(\text{TiO}_2)_1$ or to both processes.

b) *wet liquid electrolyte*

During the first cycle, the overall behavior of the mass change vs. time is at a first sight similar to those observed in dry electrolyte with however a value of 2.5 times higher (Fig. 5.36). The mass of the crystal increases with the cathodic current, but continues to increase until a maximum with the anodic current and finally starts to decrease. As before the value of Δm does not return to zero. The overall shape of the curves for the following cycles however do not change drastically, but the total mass change and charge density measured at the end of the cathodic range slightly decrease with the cycle number. The mass of the electrode always increases with cathodic current and always continues to increase a little in the beginning of the anodic part of the CV cycle. The system reaches a stationary state after typically 25 cycles.

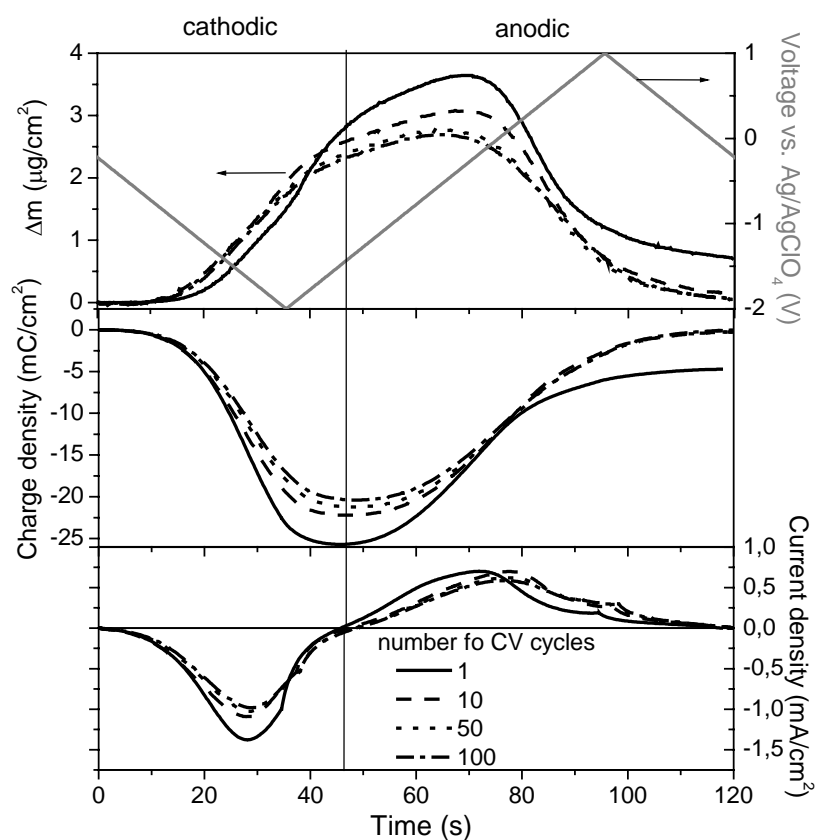


Fig. 5.36 Mass, charge density and current density of $(\text{CeO}_2)_{0.81}(\text{TiO}_2)_1$ sol-gel double layer in 1 M LiClO_4 in PC with 3 wt.% water during the 1st, 10th, 50th, 100th cycle (scan rate: 50 mV/s, scan range: -2V/+1V).

If we apply the same idea and the same model proposed to explain the results of the layer in the dry electrolyte (Fig. 5.37), the charge caused by Li^+ intercalation is found to be bigger than the total charge and there is now a ClO_4^- adsorption in the cathodic part and a desorption in the anodic part. This is physically unrealistic! So, in the wet electrolyte system, it is believed that the intercalation does not involve pure Li^+ ions. As Li^+ ions are likely to become tetrahydrated in aqueous solution

[192], it is reasonable to suppose that the intercalation process involves $\text{Li}(\text{H}_2\text{O})_4^+$ ions. Fig. 5.38 shows the fit of the mass change and charge density of the 50th cycle with the simultaneous $\text{Li}(\text{H}_2\text{O})_4^+$ intercalation and ClO_4^- adsorption. The mass change graph shows that the peak observed in the anodic current range (Fig. 5.36) is caused by the different rates of the cation and anion mass change (Fig. 5.38). Because water can be coordinated with the Li^+ and ClO_4^- ions and increase the mobility of these ions, the amount of cations and anions arriving at the electrode increases. In wet electrolyte the maximum amount of intercalated naked Li is higher than that in dry electrolyte. The corresponding values are $0.94 \mu\text{g}/\text{cm}^2$ in wet electrolyte and $0.32 \mu\text{g}/\text{cm}^2$ in dry electrolyte (Fig. 5.35). A small amount of water in the electrolyte therefore improves the Li^+ intercalation into the layer. This is probably due to the higher mobility of the hydrated lithium ions in the electrolyte, as the diffusion coefficient in the wet electrolyte system is 10 times faster than that in the dry electrolyte system (Fig. 5.12).

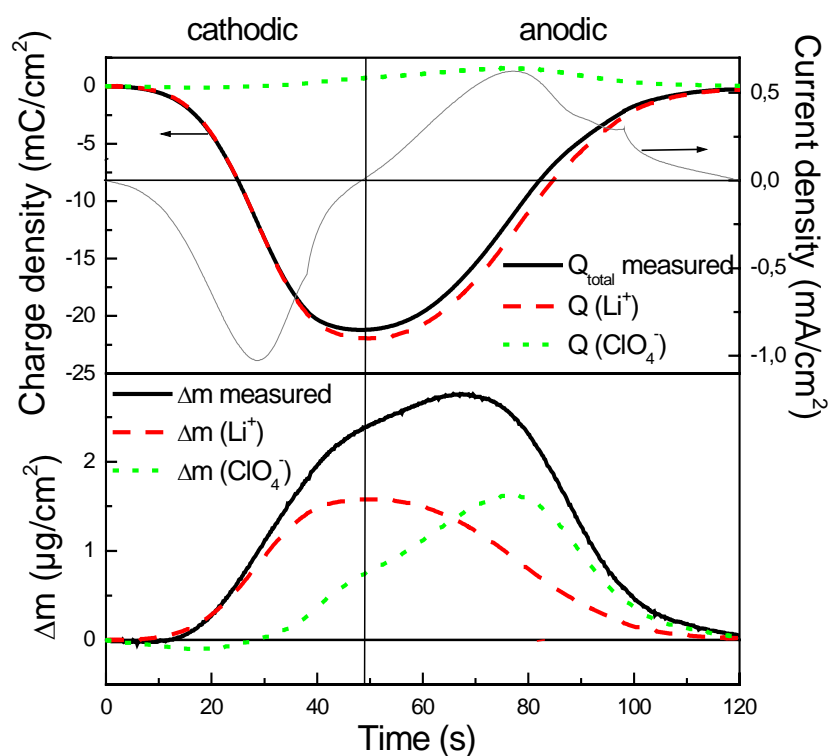


Fig. 5.37 Calculated charge density and mass change by Li^+ intercalation and ClO_4^- adsorption of the $(\text{CeO}_2)_{0.81}(\text{TiO}_2)_1$ sol-gel double layers during the 50th CV cycle in wet (3 wt.% H_2O) 1 M LiClO_4 in PC (scan rate: 50 mV/s; scan range: -2 V/+1 V). Top: charge density change; bottom: mass change. Current density is also shown.

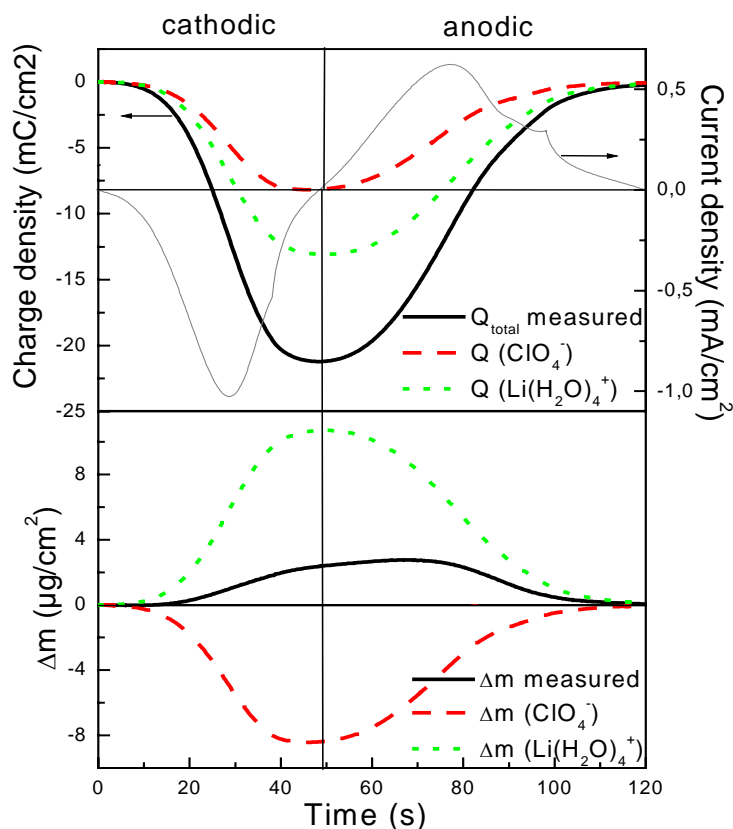


Fig. 5.38 Calculated charge density and mass change by $\text{Li}(\text{H}_2\text{O})_4^+$ intercalation and ClO_4^- adsorption of the $(\text{CeO}_2)_{0.81}(\text{TiO}_2)_1$ sol-gel double layers during the 50th CV cycle in wet (3 wt.% H_2O) 1 M LiClO_4 in PC (scan rate: 50 mV/s; scan range: -2 V/ +1 V). Top: charge density change; bottom: mass change. Current density is also shown.

It was shown that the reversibility in the wet electrolyte system is improved (section 5.1.2). As water is a protonic solvent, PC has a weak basic character. So Li^+ ions will be preferentially solvated by water molecules rather than by PC molecules. The primary hydration shell for Li^+ in aqueous solution is doubtless tetrahedral [192]. So we can suppose that $\text{Li}(\text{H}_2\text{O})_4^+$ is intercalated into the $(\text{CeO}_2)_{0.81}(\text{TiO}_2)_1$ layer in wet electrolyte. But the ClO_4^- may come to the electrode surface as ClO_4^- , hydrated ClO_4^- or propylene carbonate coordinated ClO_4^- . The degradation of the ion storage capacity of the layer (Fig. 5.9) is reduced in wet electrolyte. One possibility is less ClO_4^- is irreversibly adsorbed to the surface (see Fig. 5.31). The reversibility of ClO_4^- adsorption is increased. Another possibility is that the mobility of ions are faster in wet electrolyte, the kinetics of ion intercalation is also improved.

On the other hand, the transient state of $\text{Ce}^{4+} + e \leftrightarrow \text{Ce}^{3+}$ in $(\text{CeO}_2)_{0.81}(\text{TiO}_2)_1$ layer may also be stabilized by water and causes Ce^{4+} to be easily reduced to Ce^{3+} . Therefore the cathodic peak in wet electrolyte occurs at a relatively higher potential than that in dry electrolyte and is continuously increased with the number of CV cycles (Fig. 5.8) and also the current density is higher than that in dry electrolyte.

The ion storage properties of $(\text{CeO}_2)_{0.81}(\text{TiO}_2)_1$ layers are governed largely by the insertion/extraction of electrons. The ion transport, with all its complexity, serves for charge balancing only. The improvement of charge capacity in wet electrolyte should be mainly due to the water effect to the $(\text{CeO}_2)_{0.81}(\text{TiO}_2)_1$ layer. However, the ionic transport is also important. Indeed it usually determines the speed by which the optical properties can be modulated, and interactions between the mobile ions and the immobile oxide layer are important for cycling durability.

Bohnke et al. [173] also observed an increase of the optical and electrochemical properties of a WO_3 layer with a certain amount of water in 1 M LiClO_4 in PC. They also suggest the formation of a double layer but of adsorbed water molecules at the interface WO_3 -electrolyte able to decrease the energy barrier at this interface and to enhance the ionic diffusion. At the same time they suppose that the introduction of water to the organic solvent can facilitate the ion insertion process. But because they do not have the information about the mass change of the electrode, they suggest the improvement is also caused by a coinsertion of hydrogen and lithium into WO_3 during coloration to form a mixed hydrogen-lithium tungsten bronze.

From the above description, it is clear that whatever the electrolyte is the charge intercalation and deintercalation is not pure Li^+ . In the solution Li^+ , ClO_4^- and also hydrated lithium in the wet electrolyte may cooperate at the same time. The ion exchange behavior is a mixture of two or more of these ions. The ion intercalation ability is related to the property of the electrolyte and also to the cycle number and charge density of the layer.

The composition of the $(\text{CeO}_2)_{0.81}(\text{TiO}_2)_1$ layer is changing during the first 25 cycles because of irreversible lithium intercalation. A certain amount of water in the electrolyte can form $\text{Li}(\text{H}_2\text{O})_4^+$ and improves the mobility of Li^+ ions and maybe also of ClO_4^- . The reversibility and kinetics of ion insertion/ extraction of the layer are improved.

It can also be supposed that the $(\text{CeO}_2)_{0.81}(\text{TiO}_2)_1$ layer become hydrated so that the energy barrier for the reaction $\text{Ce}^{4+} + e \leftrightarrow \text{Ce}^{3+}$ is decreased and therefore the charge capacity of the layer is increased.

The case of a liquid electrolyte was discussed above. A similar principle may be applied to the solid electrolyte. Because a certain amount of water increases the mobility of conducting ions and increases the stability of metastable state of the cerium and/ or tungsten electrochemical redox reactions, the ion storage capacity of the $(\text{CeO}_2)_{0.81}(\text{TiO}_2)_1$ sol-gel layer and/ or WO_3 sol-gel layer could be increased with wet electrolyte. The switch in behavior of the window could be reduced and the coloring and bleaching kinetics could be improved.

These results have therefore a considerable importance, not only for this work, but probably for all results that have been reported on the intercalation/ deintercalation of H^+ or Li^+ ions into EC layers. The charge calculated by integrating the current during electrochemical process is usually thought

to be the charge of H^+ or Li^+ only those are the ions of interest to explain the EC properties. Consequently a true understanding of the EC processes needs a more detailed knowledge of all ions transports that is a considerable task to be done as well as a theoretical model that is not obvious to propose.

5.3 Water effect on the electrochromic properties of WO_3 and $Nb_2O_5:Mo$ (Mo:Nb = 0.3) sol-gel layers

Battery type EC devices built at INM also include a coloring EC layer such as WO_3 and $Nb_2O_5:Mo$. If water introduced in the electrolyte drastically improves the behavior of the CeO_2-TiO_2 counter electrode, it is also necessary to determine its effect on the used EC layers.

5.3.1 WO_3 sol-gel layer

Fig. 5.39 illustrates the influence of water content in the electrolyte on the CV shape of WO_3 sol-gel single layers. With 1 wt.% water in the electrolyte, the position of the cathodic and anodic current peaks does not change, so the mechanism of Li^+ intercalation is not changed. But the current densities are drastically increased. Therefore the charge intercalated is increased from 8 mC/cm^2 to 20 mC/cm^2 .

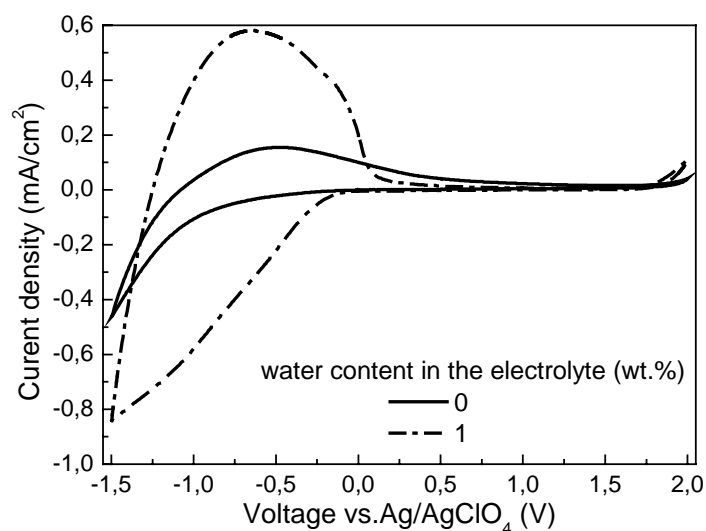


Fig. 5.39 CV profile (800th CV cycle) of WO_3 sol-gel single layer (200 nm) in dry and wet (1 wt.% water) 1 M $LiClO_4$ in PC (scan rate: 50 mV/s)

The amount of Li^+ charge intercalation calculated from CA measurement is shown in Fig. 5.40. It sharply decreases during the initial cycles and then slightly decreases continuously up to 7000 cycles. The value is always higher in the wet electrolyte (about 29 mC/cm^2) than in the dry electrolyte (about 17 mC/cm^2). Moreover in the wet electrolyte, the ion insertion process is practically fully reversible as the Q_{out}/Q_{in} ratio is 0.97.

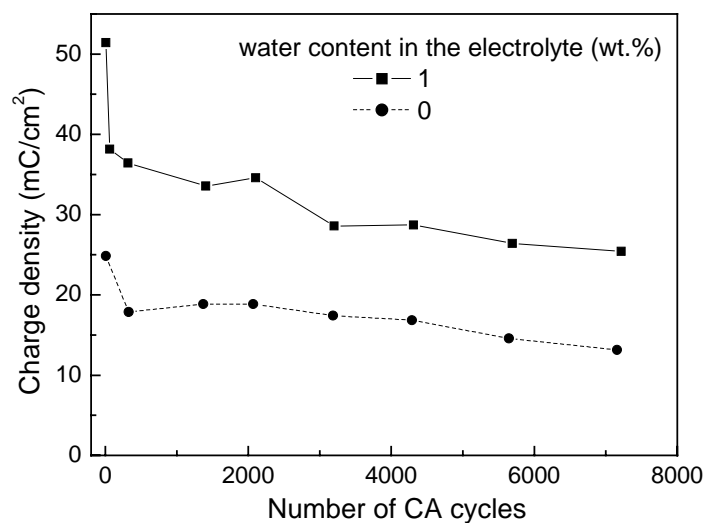


Fig. 5.40 Charge intercalated into the WO₃ sol-gel layer (200 nm thick) during CA cycles (-1.5 V/2 min) versus the cycle number in dry and wet (1 wt.% water) 1 M LiClO₄ in PC

The transmittance spectrum from 320 nm to 1300 nm is shown in Fig. 5.41. The bleached state of the layer in the dry electrolyte is worse in the whole spectrum range. For the colored state, the transmittance of the layer in the dry electrolyte is slightly smaller for wavelength <450 nm, but become higher for $\lambda > 450$ nm.

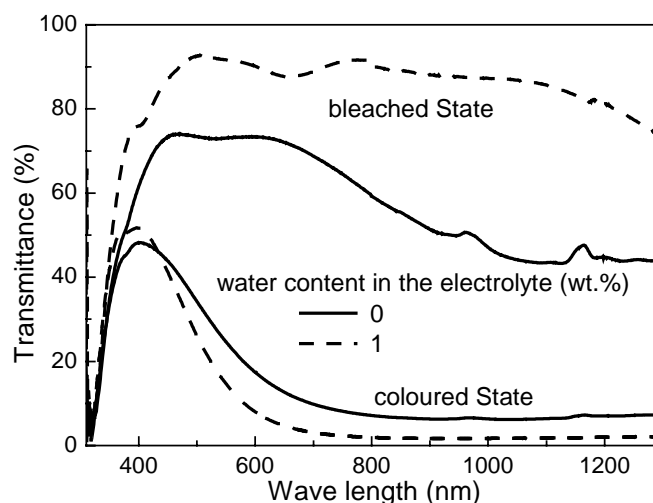


Fig. 5.41 Transmittance spectrum of WO₃ sol-gel layers (200 nm thick) at the 4000th CA cycle (-1.5 V, 2 min/ +2 V, 2 min) in dry and wet (1 wt.% water) 1 M LiClO₄ in PC

The transmittance of a 200 nm thick WO₃ sol-gel single layer measured at the wavelength of 550 nm after potentiostatic switching (-1.5 V, 2 min/ +2 V, 2 min) in dry and wet (1 wt.% water) electrolyte is shown in Fig. 5.42 as a function of the CA cycle number. The transmittance change between the bleached and colored state in the wet electrolyte remains constant ($\Delta T = 74\%$ with

Tb \approx 90 % and Tc \approx 16 %) from the first cycle up to more than 7000 CA cycles and is higher than that in the dry electrolyte. In the dry electrolyte, the transmittance change decreases continuously down to 40 % (4000th CA cycle) because the transmittance of the bleached state becomes worse and the colored state is not as deep colored as initially. The degradation in the bleached state of WO₃ layer is caused by irreversible Li⁺ trapping [185] related to the presence of water in the layer. In their research, e-gun evaporated layer has less water in the layer and has no degradation effect. In our research, because the water is in the electrolyte, its role is different.

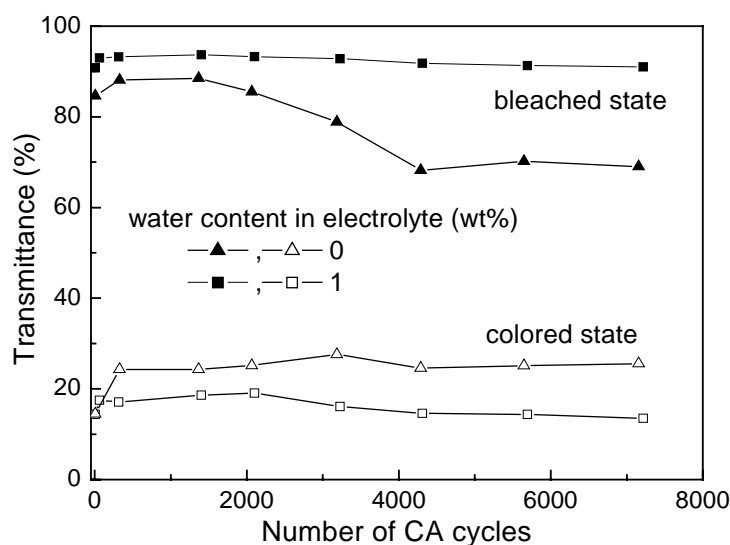


Fig. 5.42 Transmittance of WO₃ sol-gel layers (200 nm thick) at $\lambda = 550$ nm as a function of the CA cycle number (-1.5 V, 2 min/ +2 V, 2 min) in dry and wet (1 wt.% water) 1 M LiClO₄ in PC

The coloration efficiency C.E. has been calculated at 550 nm, using the results of the -1.5 V/ 2 min CA cycles. The average value is practically the same for both electrolytes i.e. about 35 cm²/C (Fig. 5.43). These results are in agreement with those of Bohnke et al. [173] and show that the coloring process of the WO₃ layer in dry and wet electrolyte is basically the same and that the deeper coloration obtained during the application of -1.5 V, 2 min in the wet electrolyte is only due to a faster kinetics that cause a higher charge intercalation (Fig. 5.40).

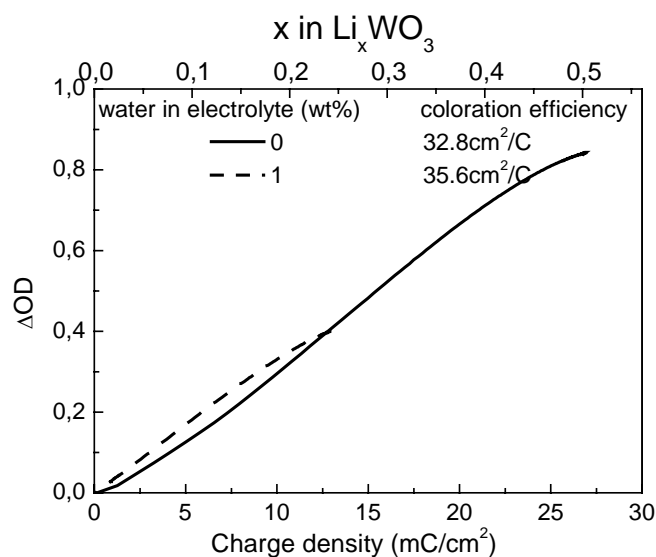


Fig. 5.43 Change of the optical density ($\Delta OD = \log(T_b/T_c)$ at $\lambda = 550$ nm of WO_3 sol-gel single layers (200 nm thick) as a function of the intercalated charge density (Q_{in}) in dry and wet (1 wt.% water) 1 M $LiClO_4$ in PC. The coloration efficiency C.E. is given by the slope of the graph.

The time variation of the normalized ratio T/T_b of WO_3 sol-gel layers measured at 550 nm during the 7000th CA cycle is shown in Fig. 5.44. The coloring and bleaching kinetics are faster with 1 wt.% in the electrolyte so that a 2-min lapse of time is sufficient to color and bleach WO_3 in the wet electrolyte. As already postulated for the $(CeO_2)_{0.81}(TiO_2)_1$ sol-gel layer, the faster kinetics observed with increasing water content might also be due to a faster intercalation of Li^+ ion into the WO_3 layer.

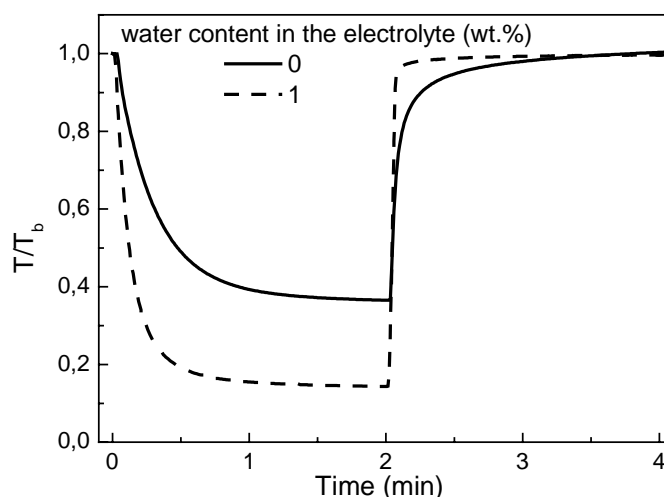


Fig. 5.44 Time evolution of the normalized transmittance T/T_b of WO_3 sol-gel single layers (200 nm thick) at $\lambda = 550$ nm during the 7000th CA cycle (-1.5 V, 2 min) in dry and wet (1 wt.% water) 1 M $LiClO_4$ in PC

In conclusion, a 1 wt.% amount of water added to the electrolyte improves the electrochemical properties of WO_3 sol-gel layers. The charge capacity and the reversibility of the layers are increased as with CeO_2 - TiO_2 sol-gel layer. Therefore the electrochromic properties of the layers are also improved by higher transmittance change and better long-term stability. The use of wet electrolyte in devices is therefore quite positive (see section 5.5.1).

5.3.2 Nb_2O_5 :Mo (Mo:Nb = 0.3) sol-gel double layers

X-ray diffraction spectra indicated that the Nb_2O_5 :Mo (Mo:Nb = 0.3) sol-gel double layers are crystalline. The structure did not correspond to the hexagonal form of pure Nb_2O_5 obtained after heat treatment at $500\text{ }^\circ\text{C}$ (JCPDS file 28-317) [104], but most of the diffraction peaks could be indexed either as a monoclinic Nb_2O_5 (JCPDS 37-1468) or an orthorhombic $\text{Nb}_{12}\text{O}_{29}$ (JCPDS 34-1169). The size of the crystallites could not be determined with precision.

Fig. 5.45 illustrates the influence of water content in the electrolyte on the CV shape of Nb_2O_5 :Mo (Mo:Nb = 0.3) sol-gel double layers. The effect of water content is contrary to that observed with $(\text{CeO}_2)_{0.81}(\text{TiO}_2)_1$ and WO_3 sol-gel layers. In the dry electrolyte, the CV profile does not change significantly with the cycle number and the peak position does not change either. But in the wet electrolyte (3 wt.% water), the current density decreases drastically with the cycle number. The anodic current peak e.g. decreases from 1.2 mA/cm^2 (1st cycle) to 0.2 mA/cm^2 (2000th cycle).

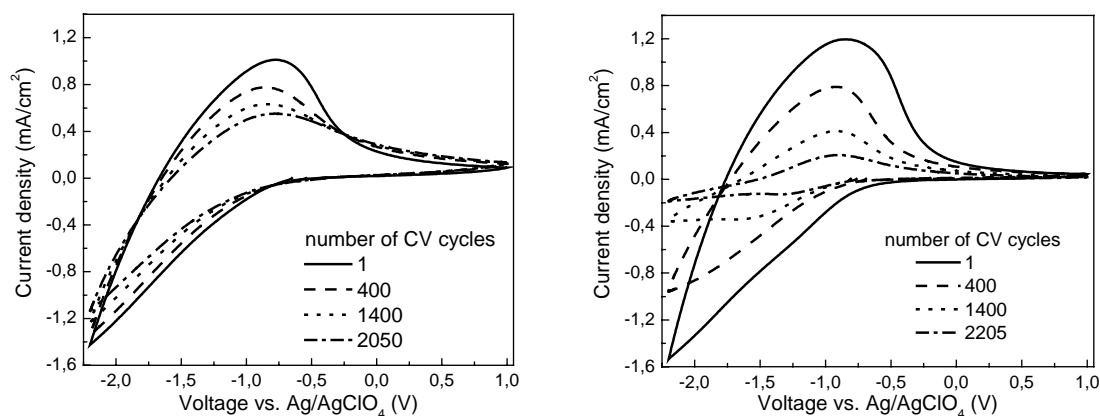


Fig. 5.45 Cyclic voltammetry of Nb_2O_5 :Mo (Mo:Nb = 0.3) sol-gel double layers sintered at $500\text{ }^\circ\text{C}$ in 1 M LiClO_4 in PC. Left: dry electrolyte; right: wet electrolyte with 3 wt.% water.

The charge density intercalated during CA cycles ($-2.2\text{V}/2\text{ min}$, $+1\text{ V}/2\text{ min}$) of Nb_2O_5 :Mo (Mo:Nb = 0.3) sol-gel double layers in the dry and wet electrolytes is shown in Fig. 5.46. In the dry electrolyte, the charge density decreases during the initial cycles and remains stable from the 400th cycle at 45 mC/cm^2 . It however decreases continuously and rather fast in the wet electrolyte from 65 mC/cm^2 (1st cycle) down to 8 mC/cm^2 (3500th cycle).

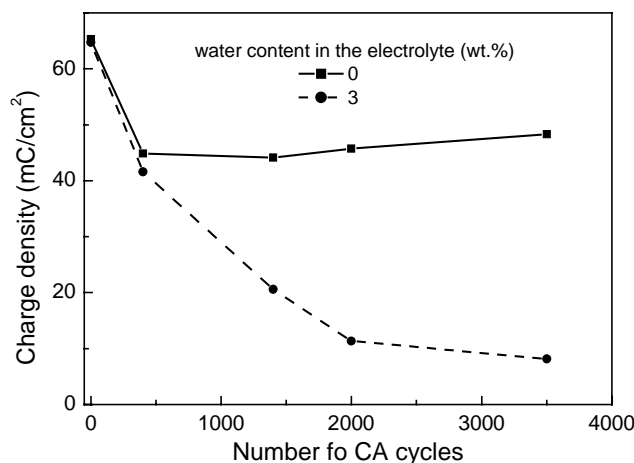


Fig. 5.46 Charge intercalated into the $\text{Nb}_2\text{O}_5:\text{Mo}$ ($\text{Mo}:\text{Nb} = 0.3$) sol-gel double layers (120 nm) during CA ($-2.2 \text{ V}/2 \text{ min}$) versus the cycle number in dry and wet (3 wt.% water) 1 M LiClO_4 in PC

The transmittance change of $\text{Nb}_2\text{O}_5:\text{Mo}$ ($\text{Mo}:\text{Nb} = 0.3$) sol-gel double layers (120 nm) after potentiostatic switching (-2.2 V , 2 min/ $+1.0 \text{ V}$, 2 min) in dry and wet electrolytes are shown in Fig. 5.47.

As shown by Schmitt et al. [104, 179], the transmittance spectrum of the layer in the dry electrolyte does not change very much with the cycle number. In the visible range the bleached state even slightly improves to $T_b \approx 70\%$ and a dark grey color with $T_c \approx 8\%$ is observed. ΔOD in the dry electrolyte decreases only slightly from 1.0 (1st cycle) to 0.85 (3500th CA cycle) (Fig. 5.48). On the contrary, in the wet electrolyte, the colored state becomes brighter and the bleached state becomes darker with the number of cycles and this causes a drastic decrease of ΔOD (Fig. 5.48) from 0.92 to 0.25.

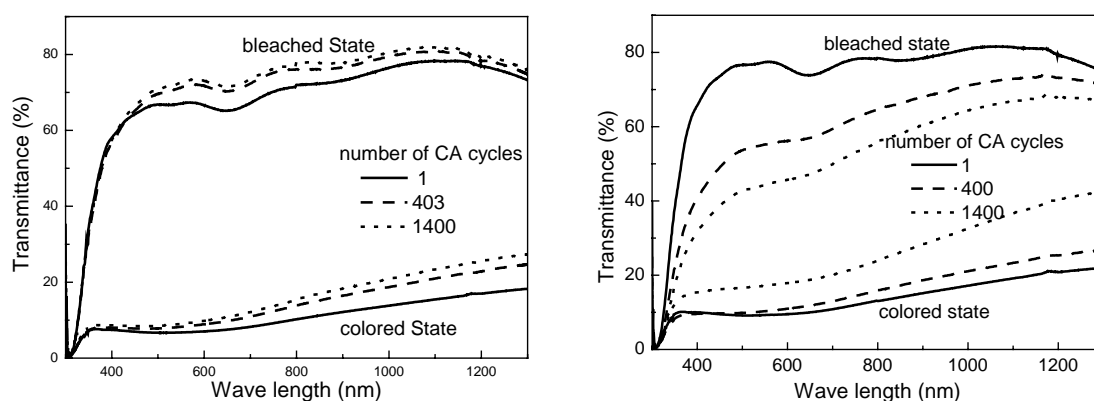


Fig. 5.47 Transmittance spectrum of $\text{Nb}_2\text{O}_5:\text{Mo}$ ($\text{Mo}:\text{Nb} = 0.3$) sol-gel double layers (120 nm) after potentiostatic switching (CA: -2.2 V , 2 min/ $+1.0 \text{ V}$, 2 min) in 1 M LiClO_4 in PC.
Left: dry electrolyte; right: wet electrolyte with 3 wt.% water

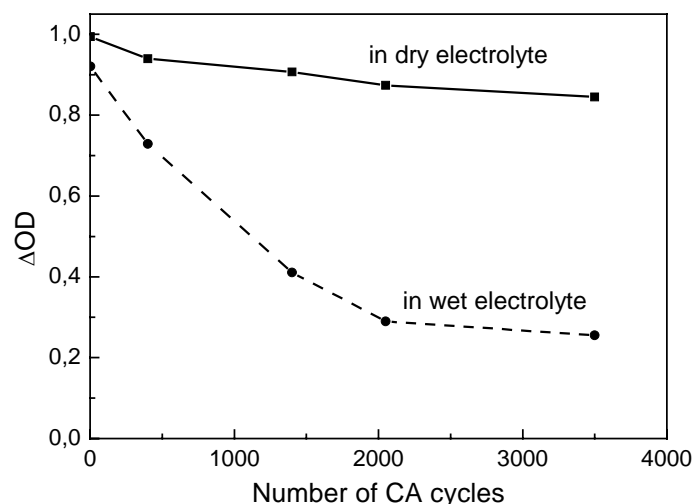


Fig. 5.48 Change of the optical density ΔOD of $Nb_2O_5:Mo$ ($Mo:Nb = 0.3$) sol-gel layers (120nm) at $\lambda = 550$ nm as a function of the CA cycle number (-2.2 V, 2 min/ +1.0 V, 2 min) in dry and wet (3 wt.% water) 1 M $LiClO_4$ in PC.

The coloration efficiency $C.E. = \Delta OD/Q_{in}$, has been calculated at $\lambda = 550$ nm as a function of the number of CA cycles. The initial values obtained in both electrolytes are the same, about $15 \text{ cm}^2/C$. In the dry electrolyte it then increases to $21 \text{ cm}^2/C$ and then slowly decreases, while in the wet electrolyte it continuously increases to values as high as $30 \text{ cm}^2/C$ (Fig. 5.49). Although the C.E. is higher in wet electrolyte, the amount of charge intercalated decreases steadily, contrary to what was obtained in WO_3 . The reason is not known presently.

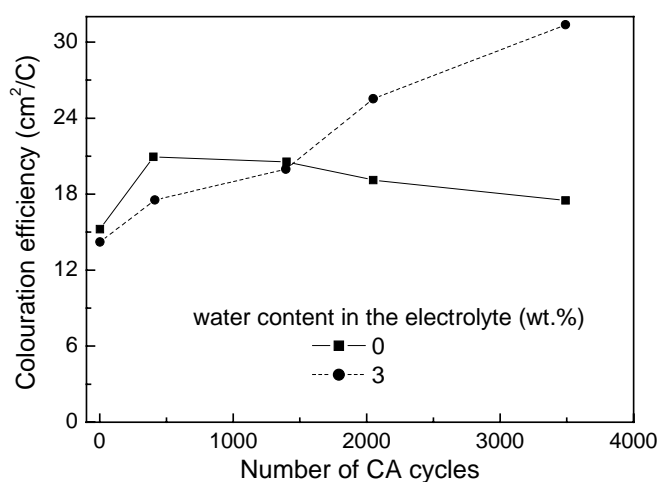


Fig. 5.49 Coloration efficiency of $Nb_2O_5:Mo$ ($Mo:Nb=0.3$) sol-gel double layer (120 nm) after potentiostatic switching (CA: -2.2 V, 2 min) in dry and wet (3 wt.% water) 1 M $LiClO_4$ in PC (calculated from $\Delta OD/Q_{in}$).

The time evolution of the normalized ratio T/T_b of $Nb_2O_5:Mo$ ($Mo:Nb = 0.3$) layers measured at $\lambda = 550$ nm during the 2000th CA cycle are shown in Fig. 5.50. The coloring and bleaching kinetics are faster in the dry electrolyte and a 2 minutes lapse of time is sufficient to color and bleach

$\text{Nb}_2\text{O}_5:\text{Mo}$ (Mo:Nb = 0.3) sol-gel double layers. The coloring kinetics in the wet electrolyte (3 wt.% water) is drastically reduced and two minutes is not enough for reaching a saturated state.

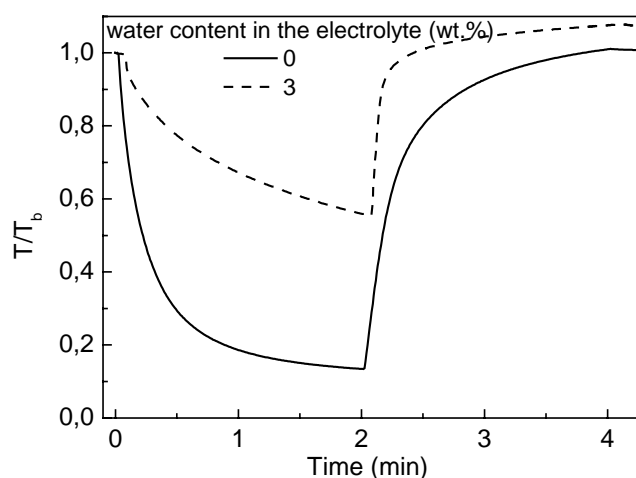


Fig. 5.50 Time evolution of the normalized transmittance T/T_b of $\text{Nb}_2\text{O}_5:\text{Mo}$ (Mo:Nb = 0.3) sol-gel double layers (120 nm) at $\lambda = 550$ nm during the 2000th CA cycle (-2.2 V, 2 min/ +1.0 V, 2 min) in dry and wet (3 wt.% water) 1 M LiClO_4 in PC

The chronopotentiometry (CP) of $\text{Nb}_2\text{O}_5:\text{Mo}$ (Mo:Nb = 0.3) sol-gel double layers (120 nm) after 3500 CA cycles in the dry and wet electrolytes was also tested. The results are shown in Fig. 5.51. While the potential–time slope in dry electrolyte is much smaller than that in the wet electrolyte, the charge that can be intercalated until a safe potential in the dry electrolyte is about 2.7 times higher than that can be intercalated in the wet electrolyte. It reaches values as high as 50 mC/cm^2 and is totally reversible, but because of the lower C.E., ΔOD reached via CP measurement is 0.78 in the dry electrolyte and only 0.47 in the wet electrolyte. The potential transition time of deintercalation is shorter than that of intercalation in the wet electrolyte and $Q_{\text{out}}/Q_{\text{in}}$ is 0.9.

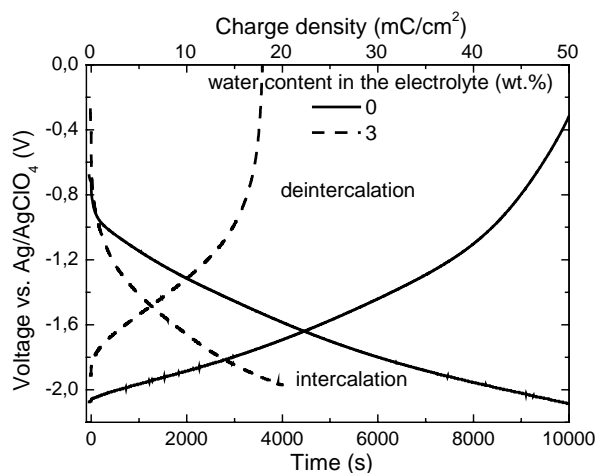


Fig. 5.51 Chronopotentiometric (CP) switching with constant current of $\pm 5 \mu\text{A/cm}^2$ of $\text{Nb}_2\text{O}_5:\text{Mo}$ (Mo:Nb = 0.5) sol-gel double layers (120nm) in dry and wet (3 wt.% water) 1 M LiClO_4 in PC measured after 3500 CA cycles (limiting voltages: -2.2 V, +1 V).

The results obtained for Nb₂O₅:Mo (Mo:Nb = 0.3) sol-gel double layers in wet electrolyte are not encouraging and the addition of water appears deleterious to this EC coatings. In the wet electrolyte, both the electrochemical and the electrochromic properties of the layer become worse.

5.4 Conclusion on the behavior of sol-gel EC layers in liquid electrolyte

The effect of water content in 1 M LiClO₄ in PC to (CeO₂)_{0.81}(TiO₂)₁, WO₃ and Nb₂O₅:Mo (Mo:Nb = 0.3) sol-gel layers are summarised in Table 5.3.

The electrochemical and electrochromic properties of WO₃ and (CeO₂)_{0.81}(TiO₂)₁ sol-gel layers can be drastically improved by adding a small amount of water to 1 M LiClO₄ in PC. The EQCM results show that ClO₄⁻ ions are adsorbed to the (CeO₂)_{0.81}(TiO₂)₁ surface in the dry electrolyte, while in the wet electrolyte ClO₄⁻ adsorption to the (CeO₂)_{0.81}(TiO₂)₁ surface is partly prevented hence the Li⁺ intercalation and deintercalation are improved. The results observed for the Nb₂O₅:Mo (Mo:Nb = 0.3) sol-gel double layers are opposite. The electrochromic behavior and the long-term stability of the Nb₂O₅:Mo (Mo:Nb = 0.3) layers could not be improved by addition of water to this liquid electrolyte and are even worse than those measured in a dry electrolyte. The reason is not yet known.

Table 5.3 Properties of $(\text{CeO}_2)_{0.81}(\text{TiO}_2)_1$, WO_3 and $\text{Nb}_2\text{O}_5:\text{Mo}$ ($\text{Mo}:\text{Nb} = 0.3$) sol-gel layers in 1 M LiClO_4 in PC without or with 1 to 3 wt.% water measured during the 300th CA cycle. The optical values are measured at 550 nm.

Heating temperature and thickness of the layers	electrolyte: 1 M ClO_4 in PC	Q_{in} (CV) (mC/cm^2)	Q_{in} (CA) (mC/cm^2)	$Q_{\text{out}}/Q_{\text{in}}$ (CA)	T_{b} (%)	T_{c} (%)	ΔT (%)	ΔOD	cycle number at which the values are taken	Tested up to (cycles)	Comments																																																							
$(\text{CeO}_2)_{0.81}(\text{TiO}_2)_1$ 450°C, 200 nm	Dry	3	7	0.90	-	-	-	-	500	500	The electrochemical properties are improved in wet electrolyte																																																							
	Wet (3 wt.% water)	11	15	0.99	-	-	-	-				$(\text{CeO}_2)_{0.81}(\text{TiO}_2)_1$ 200°C, 550°C, 340 nm	Dry	11	15	0.94	-	-	-	-	300	300	Wet (3 wt.% water)	13	26	0.97	-	-	-	-	WO_3 240°C, 200 nm	Dry	8	18	0.83	88	24	64	0.6	1400	7000	Wet (1 wt.% water)	20	34	0.93	94	19	75	0.7	$\text{Nb}_2\text{O}_5:\text{Mo}$ 100°C, 500°C, 120 nm	Dry	23	44	1	73	10	63	0.85	1400	3500	The EC properties become worse in wet electrolyte	Wet (3 wt.% water)	9	21	0.78	44
$(\text{CeO}_2)_{0.81}(\text{TiO}_2)_1$ 200°C, 550°C, 340 nm	Dry	11	15	0.94	-	-	-	-	300	300																																																								
	Wet (3 wt.% water)	13	26	0.97	-	-	-	-				WO_3 240°C, 200 nm	Dry	8	18	0.83	88	24	64	0.6	1400	7000	Wet (1 wt.% water)	20	34	0.93	94	19	75	0.7	$\text{Nb}_2\text{O}_5:\text{Mo}$ 100°C, 500°C, 120 nm	Dry	23	44	1	73	10	63	0.85	1400	3500	The EC properties become worse in wet electrolyte	Wet (3 wt.% water)	9	21	0.78	44	17	27	0.4																
WO_3 240°C, 200 nm	Dry	8	18	0.83	88	24	64	0.6	1400	7000																																																								
	Wet (1 wt.% water)	20	34	0.93	94	19	75	0.7			$\text{Nb}_2\text{O}_5:\text{Mo}$ 100°C, 500°C, 120 nm	Dry	23	44	1	73	10	63	0.85	1400	3500	The EC properties become worse in wet electrolyte	Wet (3 wt.% water)	9	21	0.78	44	17	27	0.4																																				
$\text{Nb}_2\text{O}_5:\text{Mo}$ 100°C, 500°C, 120 nm	Dry	23	44	1	73	10	63	0.85	1400	3500		The EC properties become worse in wet electrolyte																																																						
	Wet (3 wt.% water)	9	21	0.78	44	17	27	0.4																																																										

5.5 EC-devices

The results discussed in the previous sections have shown that the Li^+ ion storage capacity of $(\text{CeO}_2)_x(\text{TiO}_2)_{1-x}$ layers could be improved from 6.6 mC/cm^2 to 26 mC/cm^2 (CA: $-2 \text{ V}/2 \text{ min}$; $+1 \text{ V}/2 \text{ min}$) by increasing the sintering temperature, by increasing the thickness of the layer and by adding a few percent of water into the liquid electrolyte. The use of wet electrolyte also improves the reversibility of Li^+ intercalation. The blue coloring WO_3 EC layers and the gray coloring $\text{Nb}_2\text{O}_5:\text{Mo}$ ($\text{Mo}:\text{Nb} = 0.3$) EC layers were also tested with dry and wet liquid electrolyte. The next and crucial step is now to check what will happen when these layers are used to realize battery type EC devices using a composite solid electrolyte. This section describes and discusses the research on such devices having the configuration K-glass/ EC layer [WO_3 or $\text{Nb}_2\text{O}_5:\text{Mo}$ ($\text{Mo}:\text{Nb} = 0.3$) sol-gel layers]/ inorganic-organic composite electrolyte (dry or wet)/ $(\text{CeO}_2)_{0.81}(\text{TiO}_2)_1$ / K-glass.

5.5.1 EC-devices made with WO_3 sol-gel EC layers

$5 \times 10 \text{ cm}^2$ devices with configuration K-glass/ WO_3 (200 nm)/ inorganic-organic composite electrolyte/ $(\text{CeO}_2)_{0.81}(\text{TiO}_2)_1$ (240 nm)/ K-glass have been mounted with water content from 0 to 3 wt.% in the solid composite electrolyte. The WO_3 layer was a 200 nm thick single sol-gel layer sintered at $240 \text{ }^\circ\text{C}$ for 1 hour. The $(\text{CeO}_2)_{0.81}(\text{TiO}_2)_1$ layer was a 240 nm thick single sol-gel layer made from sol II and sintered at $450 \text{ }^\circ\text{C}$ for 1 hour. The substrates were dipped in the sol for 30 seconds and withdrawn at a speed of 4 mm/s .

The CV profiles of the EC devices without and with 3 wt.% water in the solid electrolyte are shown in Fig. 5.52. The overall current densities with the wet electrolyte are almost twice of those obtained with a dry electrolyte. There are no cathodic current peak and no well defined anodic peak in the “dry” device. The anodic peak is not as obvious as the one of the device with 3 wt.% water. The shape of the CV curves of the 5th cycle looks different from that of the 2000th and the followings. The current density increases from the 5th cycle to the 2000th cycle and then does not change drastically after 2000 cycles. With 3 wt.% water in the electrolyte a cathodic and an anodic peak are clearly observed and their positions do not shift during the cycling. The shape of the initial CV cycles looks also different from that of the following cycles. The overall current densities increase up to 2000 cycles and then slowly decrease.

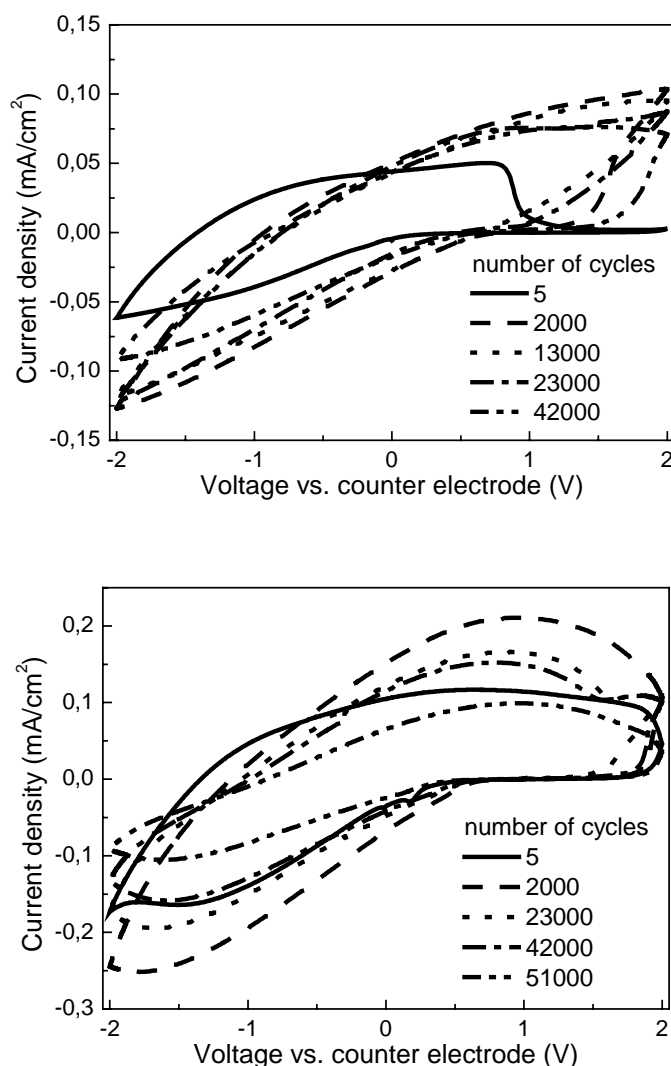


Fig. 5.52 CV profile of EC devices with configuration K-glass/ WO_3 (200 nm)/ inorganic-organic composite electrolyte/ $(\text{CeO}_2)_{0.81}(\text{TiO}_2)_1$ (240 nm)/ K-glass (scan rate: 50 mV/s). Top: dry electrolyte; bottom: with 3 wt.% water in the electrolyte;

The charge intercalated during 2 minutes CA cycles is shown in Fig. 5.53. In the “dry” device, the charge density increases from 4.1 mC/cm^2 (1st cycle) up to 8 mC/cm^2 (2000th cycle), remains rather constant up to the 25000th cycle and then decreases quickly back to 4.4 mC/cm^2 till the 42000th cycle. The device could not be operated further. The maximum charge intercalated is compatible with the ion storage capacity of the $(\text{CeO}_2)_{0.81}(\text{TiO}_2)_1$ layer measured in the dry liquid electrolyte but much smaller than that of the WO_3 layer (about 18 mC/cm^2). In the “wet” device (3 wt.% water), the charge intercalated during the initial cycles is about 11 mC/cm^2 and slowly decreases to about 7.5 mC/cm^2 up to more than 50000 cycles. This behavior is due to slower kinetics as 13 mC/cm^2 can be intercalated after applying -2 V for 15 minutes after 50000 cycles. If the potential is applied for a longer time, even more charge can be intercalated (e.g. 21 mC/cm^2 for 60 min).

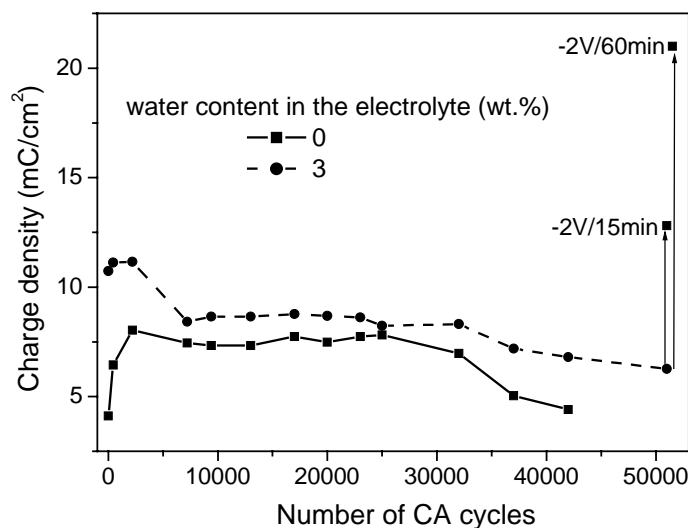


Fig. 5.53 Intercalated Charge density of EC devices with configuration K-glass/ WO_3 (200 nm)/ inorganic-organic composite electrolyte/ $(\text{CeO}_2)_{0.81}(\text{TiO}_2)_1$ (240 nm)/ K-glass as a function of the CA cycle number. (CA: -2 V/ 2min; +2 V/ 2 min)

The transmittance spectra of the EC devices with different water content in the solid electrolyte measured during the 50th CA cycle are shown in Fig. 5.54. By increasing the water content in the solid electrolyte, the transmittance of the bleached state slightly decreases by about 5% but a larger decrease of the transmittance is observed in the colored state, increasing considerably the change of the optical density.

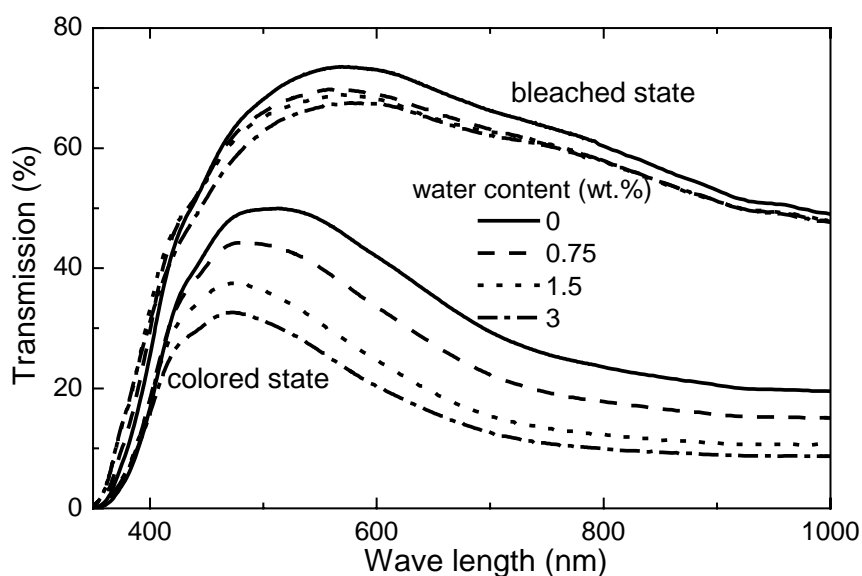


Fig. 5.54 Transmittance spectra of EC devices with configuration K-glass/ WO_3 (200 nm)/ inorganic-organic composite electrolyte/ $(\text{CeO}_2)_{0.45}(\text{TiO}_2)_{0.55}$ (200 nm)/ K-glass with different water content in the electrolyte measured during the 50th CA cycle (-2 V, 2 min/ 2 V, 2 min).

The long-term behavior of the transmittance and ΔOD measured at $\lambda = 550$ nm are shown in Fig. 5.55 and 5.56, respectively. Drastic variations are observed in devices made with the dry electrolyte. Initially ΔOD is small (about 0.15) and increases continuously to about 0.3 up to 2000 cycles, then slightly decreases and finally the device starts to strongly degrade from the 25000th cycle. The variations of T_b , T_c and ΔOD starting around the 25000th cycle are clearly seen in Fig. 5.55 and 5.56 respectively.

Adding water into the electrolyte increases the initial ΔOD and reduces the initial variation of the transmittance. When 3 wt.% water was added into the electrolyte, ΔOD reaches a value of 0.4 and remains practically constant from the 1st up to 2000 cycles and then decreases slowly. The variation is however due to a kinetic effect, as the same value of the optical density ($\Delta OD = 0.4$) and transmittance $T_c = 26\%$ are obtained by applying -2 V for 15 minutes. Therefore the device remains working in fact for more than 50000 cycles.

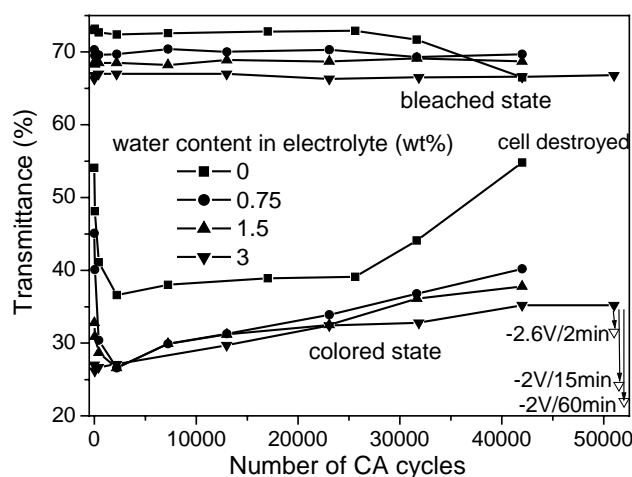


Fig. 5.55 Change of transmittance at $\lambda = 550$ nm of EC-devices containing different amounts of water in the composite electrolyte as a function of the number of CA cycles (-2 V, 120 s / $+2$ V, 120 s).

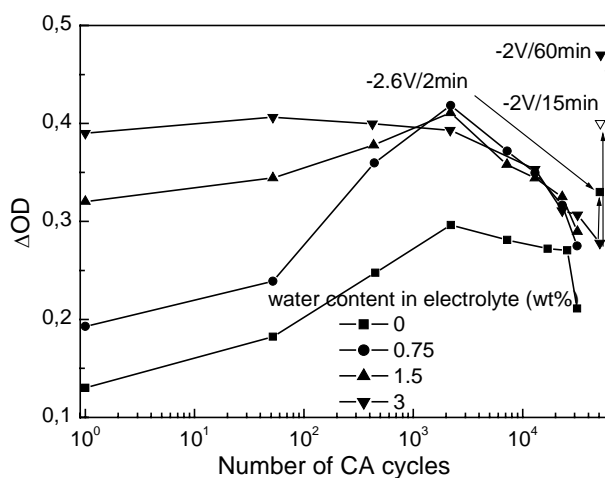


Fig. 5.56 Change of the optical density ΔOD at $\lambda = 550$ nm of EC-devices containing different amounts of water in the composite electrolyte as a function of the number of CA cycles (-2 V, 120 s / $+2$ V, 120 s).

The coloration efficiency C.E. is also determined using the results of the CA cycles (Fig. 5.57). For windows made with a “dry” composite electrolyte the value remains practically constant up to 25000 cycles (ca. $33 \text{ cm}^2/\text{C}$), but then strongly decreases. This is also in agreement with the change of transmittance and absorbance and indicates that after 25000 cycles drastic change occurs in the exchange of the charge due to a destruction (delamination) of the cell. Therefore the changes observed in the transmittance and ΔOD in “dry” devices after 25000 cycles are not due to a kinetic effect, but to a decrease of the coloration efficiency.

The C.E. values of the EC-devices with water remain constant up to 50000 cycles ($\text{CE} \approx 35 \text{ cm}^2/\text{C}$). This indicates that no change occurred in the mechanism of the charge exchange and that the variation in T and ΔOD are essentially due to a kinetic effect.

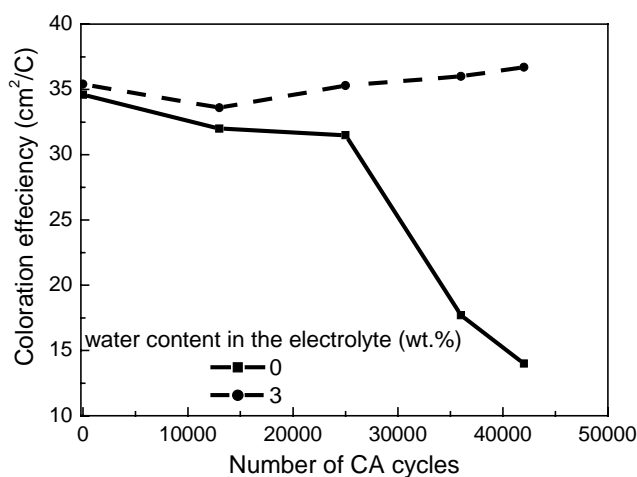


Fig. 5.57 Coloration efficiency C.E. of EC devices ($\lambda = 550 \text{ nm}$) with configuration K-glass/ WO_3 (200 nm)/ inorganic-organic composite electrolyte/ $(\text{CeO}_2)_{0.45}(\text{TiO}_2)_{0.55}$ (200 nm)/ K-glass as a function of the CA cycle number.

The time evolution of the normalized transmittance T/T_b of the EC devices measured at 550 nm during the 450th CA cycle (-2 V, 2 min/ +2 V, 2 min) is shown in Fig. 5.58 for different water contents in the inorganic-organic composite electrolyte. Similar results were obtained up to 7000 CA cycles. The coloration and bleaching kinetics are faster with water in the electrolyte. Although the overall behavior of the transmittance spectra are not changed, an EC device with water colored deeper than that built without water after a 2 min switching time. The lapse of time of 2 minutes is not enough for a full coloration, but this time was used in order to switch the devices in a reasonable time up to 50000 cycles. 2 minutes bleaching time is however enough for all devices whatever the water content in the composite electrolyte.

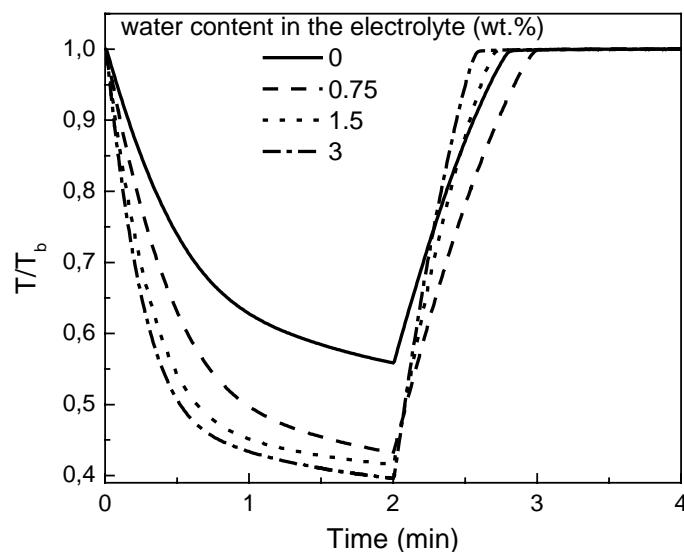


Fig. 5.58 Normalized transmission, T/T_b , versus time of EC devices containing different amounts of water in the inorganic-organic composite electrolyte measured at $\lambda = 550$ nm during the 450th CA cycle (-2 V, 2 min/ +2 V, 2 min)

The time evolution of the normalized transmittance T/T_b of the EC devices with dry and wet (3 wt.% water) inorganic-organic composite electrolyte measured at 550 nm as a function of time at different CA cycles (-2 V, 2 min/ +2 V, 2 min) are shown in Fig 5.59. In the case of the EC device with dry electrolyte, the transmittance of the colored state continuously decreases during the first 2000 CA cycles, then increases slowly up to about 9000 cycles and finally remains stable up to 25000 cycles, where the destruction of the device starts. The bleaching step is slower than that of the devices with wet electrolyte.

The EC device with wet electrolyte reaches the same colored state for the first 2000 CA cycles. For higher number of cycles, the transmittance of the colored state increases slowly up to 50000 cycles. This is essentially due to a slowing of the coloring kinetics and the initial value could be reached again by increasing the time duration of the coloring step (see also Fig. 5.55). The bleaching step is always very fast whatever the cycle number is. As Fig. 5.59 shows, 1 minute is enough for the cell to recover the bleached state at all cycle number. By using a wet electrolyte, the bleaching kinetics is drastically improved.

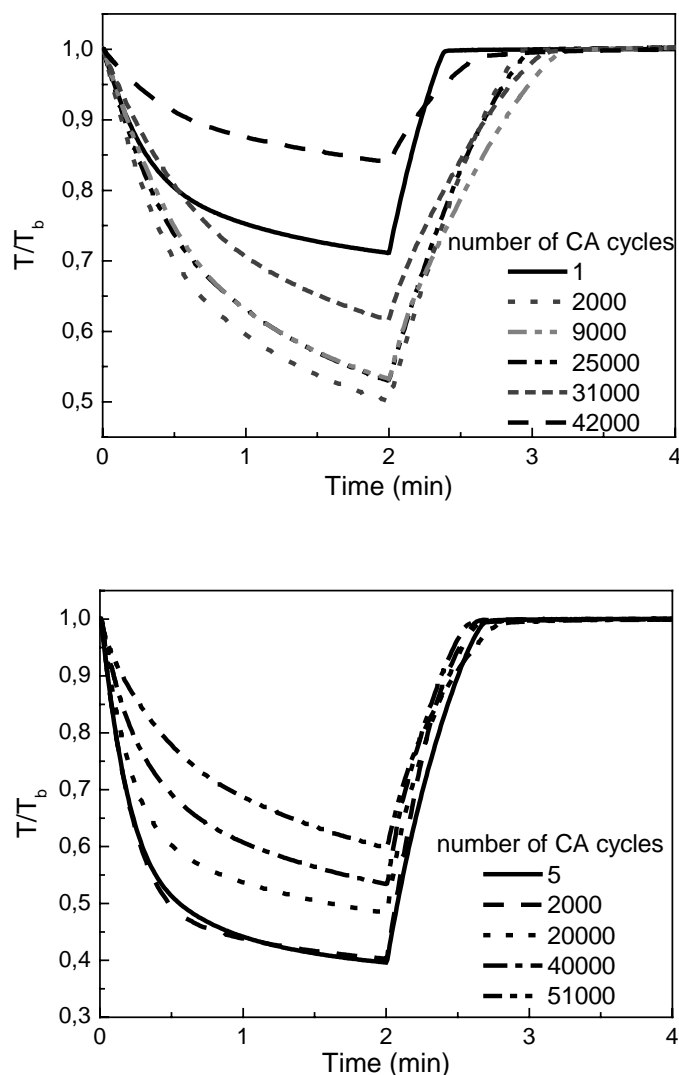


Fig. 5.59 Normalized transmission, T/T_b , versus time of EC-devices with dry and wet inorganic-organic composite electrolyte measured at $\lambda = 550$ nm during different CA cycles (-2 V, 2min/ +2 V, 2 min).
Top: dry electrolyte; bottom: wet electrolyte, with 3 wt.% water;

The EC device with 3 wt.% water in the electrolyte is not destroyed even after 52000 cycles. Its contrast (ΔOD) can still be improved either by applying a higher voltage for the same time (Fig. 5.60) and/ or by applying the same voltage (-2 V) for a longer time (Fig. 5.55 and 5.56). In the first case the improvement is due to the higher charge that can be inserted by increasing the voltage but is not due to a better kinetics as practically the same laps of time (60-70s) is necessary to reach 80% of the transmittance change ΔT . In the second case the same initial ΔOD is reached ($\Delta OD = 0.4$) by applying -2 V for 15 minutes and even a value as high as 0.47 can be reached for 60 minutes (Fig. 5.56). This corresponds to a transmittance change from 66% to 22%. The addition of 3 wt.% of water in the electrolyte has therefore improved the kinetics of the coloration and bleaching process of the EC devices, but the coloring kinetics still need to be improved for higher cycle numbers.

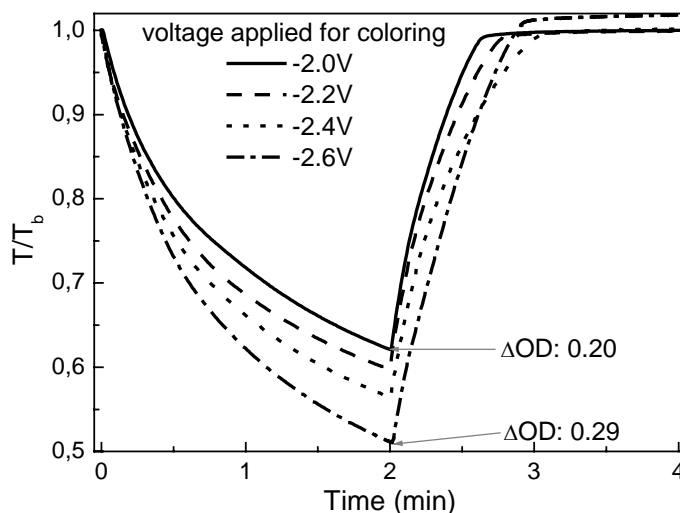
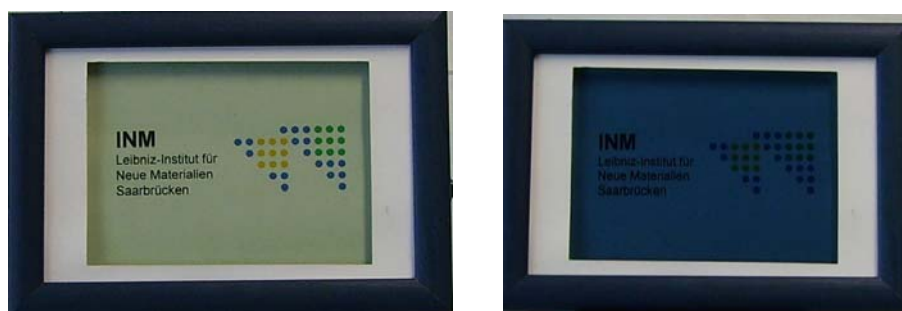


Fig. 5.60 Normalized transmission, T/T_b , versus time of EC device with configuration K-glass/ WO_3 (200 nm)/ inorganic-organic composite electrolyte (3 wt.% water)/ $(\text{CeO}_2)_{0.81}(\text{TiO}_2)_1$ (240 nm)/ K-glass measured at $\lambda = 550$ nm by applying different voltage after 51000 CA cycles.

In conclusion, EC devices with configuration K-glass/ WO_3 (200 nm)/ inorganic-organic composite electrolyte (0 to 3 wt.% water)/ $(\text{CeO}_2)_{0.81}(\text{TiO}_2)_1$ (240 nm)/ K-glass have been successfully tested. The lifetime of the EC device is prolonged up to more than 52000 cycles with rather stable coloration efficiency, optical density and without delamination when 3 wt.% water is added to the electrolyte. Adding water to the electrolyte also has improved the absorbance of the devices and even a ΔOD value as high as 0.47 could be obtained if however a long switching time is used.

Several $10 \times 15 \text{ cm}^2$ size EC devices with the configuration K-glass/ WO_3 (200 nm)/ inorganic-organic composite electrolyte (3 wt.% water)/ $(\text{CeO}_2)_{0.81}(\text{TiO}_2)_1$ / K-glass have been assembled and tested.

In Fig. 5.61 a device is shown in the colored and bleached state after galvanostatic coloring and bleaching with a current density of $-/+100 \mu\text{A}/\text{cm}^2$ for 3 min using a safety voltage limit of $-/+2.5$ V. The transmittance at 550 nm changed from 70% to 25% and the ΔOD at 550 nm was 0.45.



A: bleached state: transmittance 70 % ($\lambda = 550$ nm) B: coloured state: transmittance 25 % ($\lambda = 550$ nm)

Fig. 5.61 Picture of $10 \times 15 \text{ cm}^2$ blue-colored EC devices after galvanostatic coloring and bleaching for 3 minutes.

5.5.2 EC devices made with Nb₂O₅:Mo (Mo:Nb = 0.3) EC layer

EC devices with the configuration K-glass/ Nb₂O₅:Mo (Mo:Nb = 0.3) (120 nm)/ inorganic-organic composite electrolyte/ (CeO₂)_{0.81}(TiO₂)₁/ K-glass were mounted with a water content from 0 to 3 wt.% in the composite electrolyte. The Nb₂O₅:Mo (Mo:Nb = 0.3) sol-gel layers were double layers of about 120 nm thickness, which were sintered at 100 °C for the first layer and then 500 °C for the stacks. Several (CeO₂)_{0.81}(TiO₂)₁ sol-gel layers with different thickness have been used. They all have been prepared with sol II. The substrates were dipped in the sol for 30 seconds and withdrawn at a speed of 4 mm/s. The layers then were sintered at different temperature.

a) Influence of the water content in the electrolyte

The CV profiles of the devices mounted with a single (CeO₂)_{0.81}(TiO₂)₁ layer (200 nm, sintered at 450°C) and a composite electrolyte with different water content are shown in Fig. 5.62. The current densities increase with increasing water content, whereas the shape of the graphs does not change significantly with increasing water content. The charge exchange mechanisms are basically the same. However the anodic and cathodic peak positions are shifted when different amount of water was added to the composite electrolyte. The reversibility of ion transfer in the devices is different. In “wet” devices, the reversibility is improved, while the ratio of Q_{out}/Q_{in} increases with water conditions from 0.88 of a “dry” device to 0.95 of a “wet” device with 3 wt.% water in the electrolyte at 240th CA cycle.

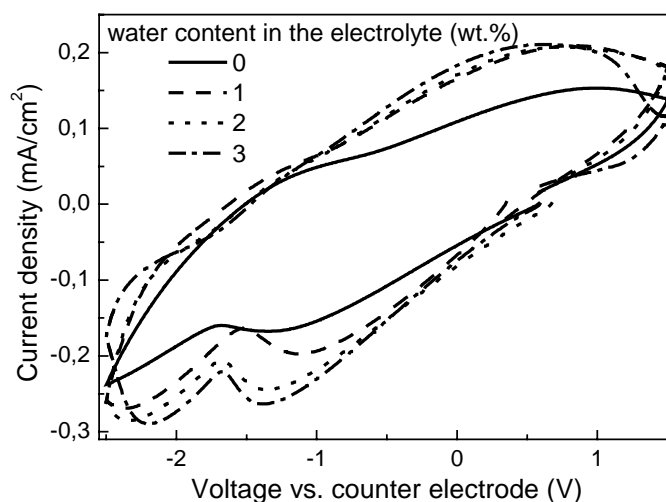


Fig. 5.62 CV profile of EC devices with configuration K-glass/ Nb₂O₅:Mo (Mo:Nb = 0.3) (120 nm)/ inorganic-organic composite electrolyte/ (CeO₂)_{0.81}(TiO₂)₁ (200 nm)/ K-glass after 240 CA cycles (–2.5 V, 2 min/ 2.5 V, 2 min). (scan rate: 50 mV/s).

The transmittance spectra of the devices are shown in Fig. 5.63. With Nb₂O₅:Mo (Mo:Nb = 0.3) EC layers, a flat absorption band is observed in the visible range of the transmittance spectra so that the colored state of the devices is gray. With 2 to 3 wt.% water added to the composite electrolyte, the

transmittance of the colored state is slightly lower and that of the bleached state is slightly higher than those obtained without water added to the electrolyte. Thus the transmittance change (ΔT) is increased using the wet electrolyte.

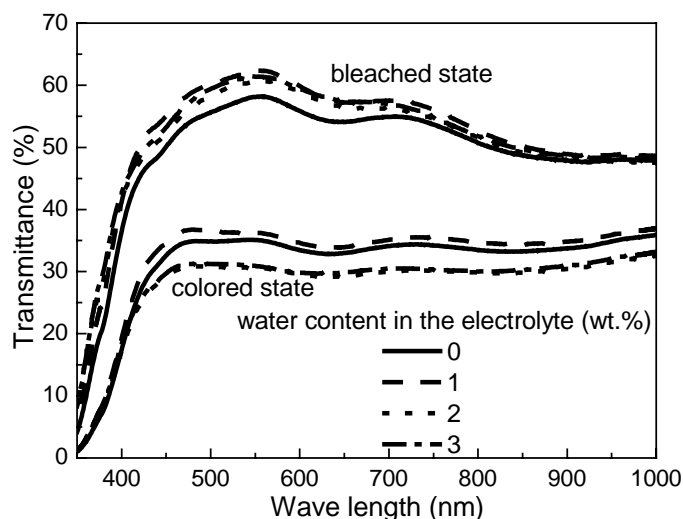


Fig. 5.63 Transmittance spectra of EC devices with configuration K-glass/ $\text{Nb}_2\text{O}_5:\text{Mo}$ ($\text{Mo}:\text{Nb} = 0.3$) (120 nm)/ inorganic-organic composite electrolyte/ $(\text{CeO}_2)_{0.81}(\text{TiO}_2)_1$ (200 nm)/ K-glass in the colored (-2.5 V, 2 min) and bleached state (2.5 V, 2 min) of the 240th CA cycle.

This interesting result is better seen in Fig. 5.64 that shows the relative transmittance change T/T_b during the 240th CA cycle of devices with different amount of water added to the electrolyte. First the coloring kinetics becomes faster with increasing water content while the bleaching kinetics is not disturbed. More important is the fact that the values of T/T_b clearly show an increase of the transmittance change with increasing water content (lower plateau), whereby for 2 and 3 wt.% water content the behavior of the devices is similar.

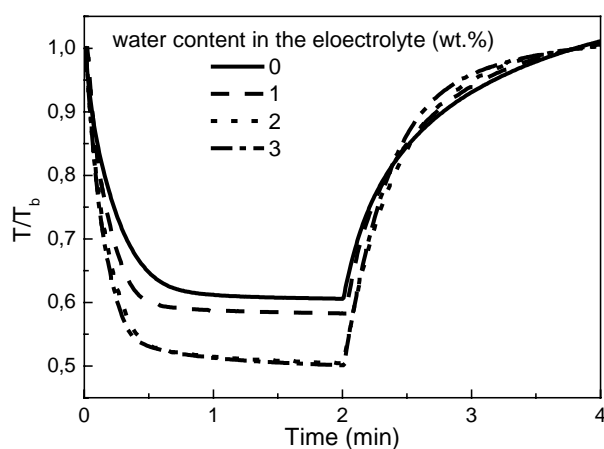


Fig. 5.64 Normalized transmittance, T/T_b , ($\lambda = 550\text{nm}$), versus time of EC devices with configuration K-glass/ $\text{Nb}_2\text{O}_5:\text{Mo}$ ($\text{Mo}:\text{Nb} = 0.3$) (120 nm)/ inorganic-organic composite electrolyte/ $(\text{CeO}_2)_{0.81}(\text{TiO}_2)_1$ (200 nm)/ K-glass at the 240th CA cycle (-2.5 V, 2 min/ 2.5 V, 2 min).

A still more intriguing but promising result was obtained by studying the evolution of the optical properties up to 60000 CA cycles. Although $\text{Nb}_2\text{O}_5:\text{Mo}$ ($\text{Mo}:\text{Nb} = 0.3$) layers studied in wet liquid electrolyte showed a deterioration of the transmittance spectra of the bleached and colored state up to 3500 cycles (strong decrease of ΔOD), complete cells made with the same layers using a wet solid state electrolyte show exactly an opposite behavior (Fig. 5.65, 5.66). Neglecting the changes occurring during the initial cycles, T_b , T_c and ΔOD remain practically constant up to 60000 cycles and as already shown by Schmitt [104, 179] these values are drastically altered and worsen in a dry composite electrolyte where the cells are destroyed after 15000 CA cycles.

Without water, ΔOD is small (about 0.1) during the initial cycling and increased continuously to about 0.33 up to 700 cycles and then decreased down to 0.1 after about 14000 cycles where the cell is destroyed. With 3 wt.% water, ΔOD is higher during the first cycle (about 0.2), increases up to 0.31 (700th – 2000th CA cycle) and then only slightly decreased up to 58000 cycles. This slight variation is again due to a kinetic effect, because, after applying -2.5 V for 4 minutes (instead of 2 minutes), the same high value of the optical density ($\Delta\text{OD} = 0.31$) is reached. The ΔOD variation of the device with dry electrolyte is caused by the change of both colored and bleached state, but in the case of the device with wet electrolyte, the variation is only caused by the colored state. Higher and stable transmittance change is reached when water is added to the electrolyte no matter the EC layer is WO_3 or $\text{Nb}_2\text{O}_5:\text{Mo}$ ($\text{Mo}:\text{Nb} = 0.3$). This improvement is however certainly due to the improvement discussed earlier for the $(\text{CeO}_2)_{0.81}(\text{TiO}_2)_1$ sol-gel layers, because the ion storage capacity of $(\text{CeO}_2)_{0.81}(\text{TiO}_2)_1$ layers could be drastically improved by using a wet electrolyte.

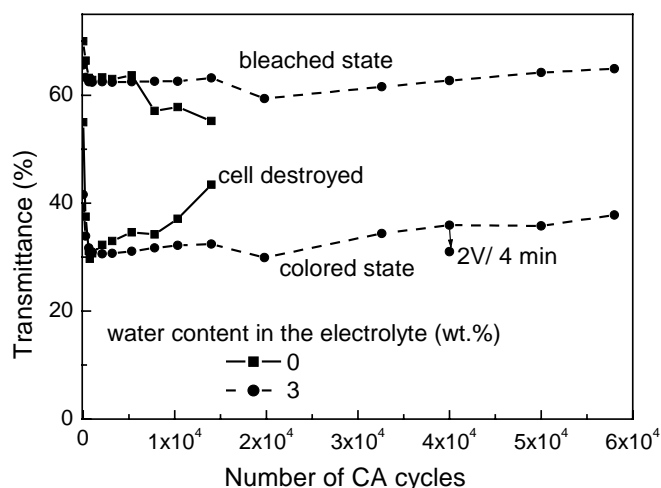


Fig. 5.65 Evolution of the transmittance change at $\lambda = 550$ nm of EC devices with configuration K-glass/ $\text{Nb}_2\text{O}_5:\text{Mo}$ (120 nm)/ inorganic-organic composite electrolyte/ $(\text{CeO}_2)_{0.81}(\text{TiO}_2)_1$ (200 nm)/ K-glass without and with addition of 3 wt.% water in the composite electrolyte as a function of the number of CA cycles (-2.5 V, 120 s/ $+2.5$ V, 120 s).

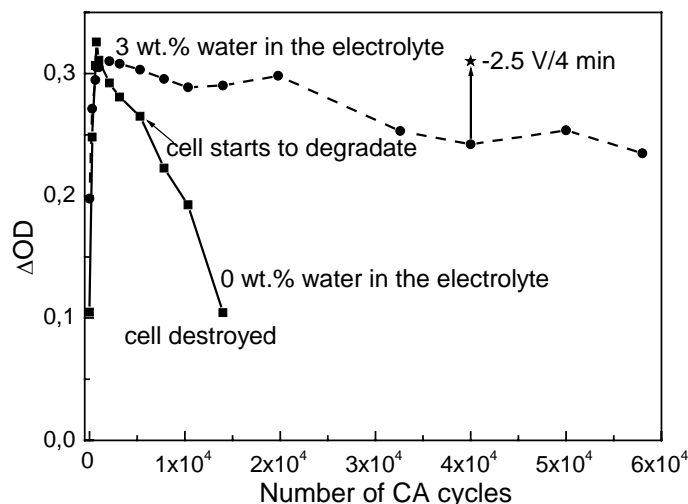


Fig. 5.66 Change of the optical density ΔOD at $\lambda = 550$ nm of EC devices with configuration K-glass/ $Nb_2O_5:Mo$ (120 nm)/ inorganic-organic composite electrolyte/ $(CeO_2)_{0.81}(TiO_2)_1$ (200 nm)/ K-glass without and with addition of 3 wt.% water in the composite electrolyte as a function of the number of CA cycles (-2.5 V, 120 s/ $+2.5$ V, 120 s).

The coloration efficiency (C.E.) of the devices with dry and wet (3 wt.% water) composite electrolyte is shown in Fig. 5.67. The value decreases rapidly during the first thousand CA cycles whatever is the water content of the composite electrolyte. The C.E. value of the EC device made with a dry electrolyte is $35 \text{ cm}^2/\text{C}$ after 700 cycles and stable up to 5000^{th} CA cycle, but then strongly decreases. With a wet electrolyte the C.E. values remain then practically constant after 700 cycles up to 40000 cycles ($CE \approx 27.5 \text{ cm}^2/\text{C}$, like the C.E. values measured for the layer in the wet liquid electrolyte at 2000^{th} CA cycle). They are however smaller than those of EC devices made with the WO_3 sol-gel layer ($35 \text{ cm}^2/\text{C}$).

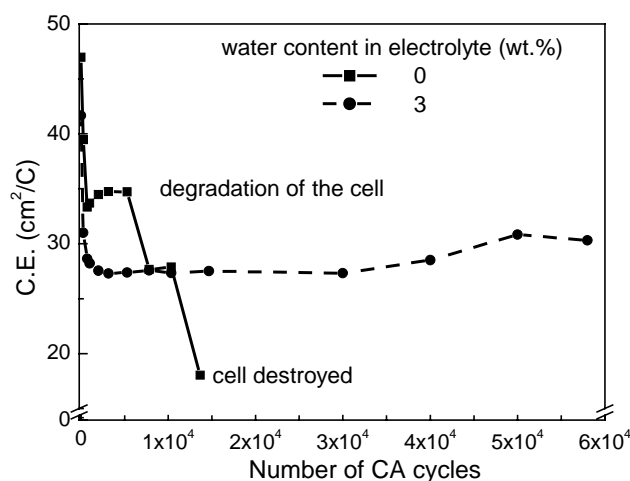


Fig. 5.67 Coloration efficiency, C.E., calculated from 2 minutes CA cycle of EC devices with configuration K-glass/ $Nb_2O_5:Mo$ ($Mo:Nb = 0.3$) (120 nm)/ inorganic-organic composite electrolyte/ $(CeO_2)_{0.81}(TiO_2)_1$ (200 nm)/ K-glass without and with addition of 3 wt.% water in the composite electrolyte as a function of the CA cycles (-2.5 V, 120 s/ $+2.5$ V, 120 s).

These results confirm that in the case of the devices with wet electrolyte the slight decrease of the change of the optical density observed during CA cycling shown in Fig. 5.66 is only due to a kinetic effect. For the dry system, the higher C.E. value (about $35 \text{ cm}^2/\text{C}$) is quite different from that observed for the layer measured in the dry liquid electrolyte ($16.5 \text{ cm}^2/\text{C}$, 2000th CA cycle). The sharp decrease of C.E. shows that the sharp decrease of ΔOD observed in Fig. 5.66 from the 6000th cycle is not due to a kinetic effect, but to a still unknown effect that degraded the coloration efficiency of the device, which led finally to its breakdown.

The positive influence of water in the solid electrolyte is mainly caused by the positive effect of wet electrolyte to the $(\text{CeO}_2)_{0.81}(\text{TiO}_2)_1$ sol-gel layers because the EC properties of $\text{Nb}_2\text{O}_5:\text{Mo}$ ($\text{Mo}:\text{Nb} = 0.3$) EC layer is not improved by adding water to the electrolyte. It is found that the maximum charge exchange capacity of the devices is $9.8 \text{ mC}/\text{cm}^2$ in “dry” devices and $11.3 \text{ mC}/\text{cm}^2$ in “wet” devices (3 wt.% water). The values are much smaller than that can be intercalated in the $\text{Nb}_2\text{O}_5:\text{Mo}$ ($\text{Mo}:\text{Nb} = 0.3$) EC layer in wet electrolyte ($21 \text{ mC}/\text{cm}^2$). The negative effect of water to the EC layer observed in liquid electrolyte does not exist with wet composite electrolyte.

The destroyed cells were investigated by optical microscopy. This will be discussed in chapter 5.5.4.

b) Influence of the $(\text{CeO}_2)_{0.81}(\text{TiO}_2)_1$ sintering temperature

In order to optimize the performance of $\text{Nb}_2\text{O}_5:\text{Mo}$ ($\text{Mo}:\text{Nb} = 0.3$) based EC devices, and remembering that the ion storage ability of the $(\text{CeO}_2)_{0.81}(\text{TiO}_2)_1$ could be improved by increasing the sintering temperature and its thickness, $\text{Nb}_2\text{O}_5:\text{Mo}$ ($\text{Mo}:\text{Nb} = 0.3$) based EC devices have been investigated using $(\text{CeO}_2)_{0.81}(\text{TiO}_2)_1$ counter electrode prepared under different conditions. In this section, EC devices with $(\text{CeO}_2)_{0.81}(\text{TiO}_2)_1$ sol-gel single layers sintered at different temperatures are investigated. The EC devices with $(\text{CeO}_2)_{0.81}(\text{TiO}_2)_1$ sol-gel double layers with different thickness will be discussed in the next section.

The name and configuration of the devices made with $(\text{CeO}_2)_{0.81}(\text{TiO}_2)_1$ sol-gel single layers sintered at different temperatures are listed in Table 5.4.

Table 5.4 EC devices with the configuration K-glass/ Nb₂O₅:Mo (Mo:Nb = 0.3) (120 nm)/ inorganic-organic composite electrolyte/ (CeO₂)_{0.81}(TiO₂)₁/ K-glass made to test the influence of the sintering temperature of the counter electrode (single layer).

EC device	(CeO ₂) _{0.45} (TiO ₂) _{0.55} sol-gel layer		Water content in the inorganic-organic composite electrolyte (wt.%)
	Sintering temperature (°C)	Thickness (nm)	
D_S_250	250	220	0
W_S_250	250	220	3
D_S_350	350	185	0
W_S_350	350	185	3
D_S_450	450	180	0
W_S_450	450	180	3
D_S_500	500	170	0
W_S_500	500	170	3
D_S_550	550	170	0
W_S_550	550	170	3

Fig. 5.68 shows the respective CV profiles. The EC devices with (CeO₂)_{0.81}(TiO₂)₁ layers heated at 250 °C and 350 °C show similar CV shape and similar current density. There is only one cathodic and one anodic peak whatever the electrolyte is. The CV shape of that with CE layers sintered between 450 °C and 550 °C is similar, and the current density is higher than that heated at 250 °C and 350 °C. The second cathodic peak of the “dry” devices is observed, whereas the CV shape of the “wet” devices has two cathodic peaks and two anodic peaks. With wet electrolyte, the current density is higher whatever the sintering temperature of the CE layers is.

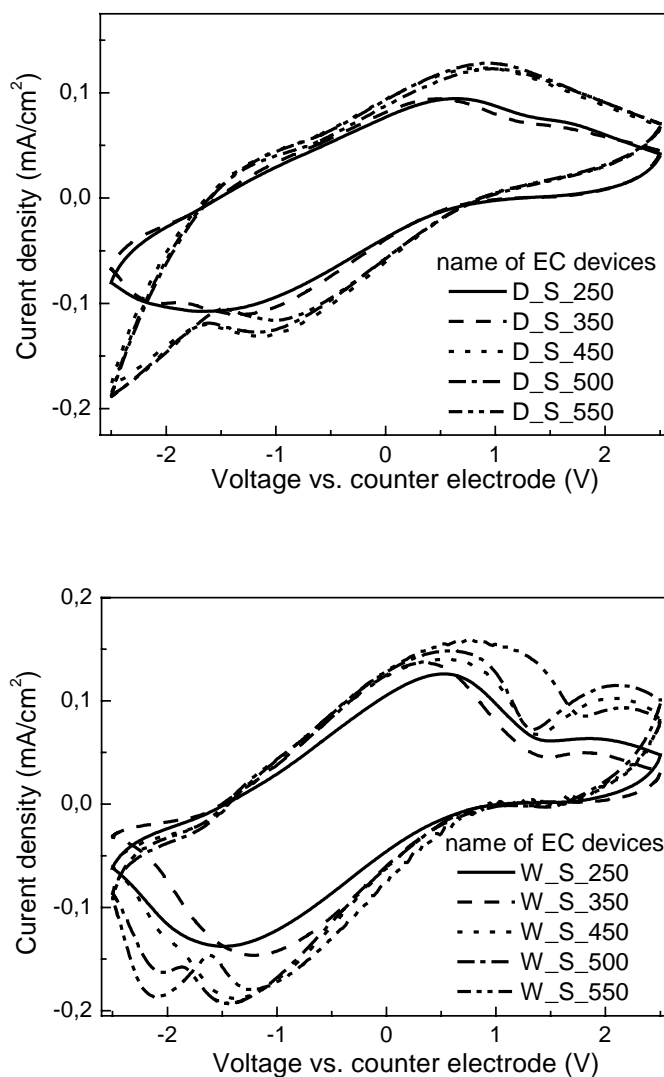


Fig. 5.68 CV profile of the EC devices with configuration K-glass/ Nb₂O₅:Mo (120 nm)/ inorganic-organic composite electrolyte/ (CeO₂)_{0.81}(TiO₂)₁/ K-glass. Top: devices with dry electrolyte after 1000 CA cycles; bottom: devices with wet electrolyte (3 wt.% water) after 2000 CA cycles. (Scan rate: 50 mV/s)

The transmittance change of these EC devices are shown in Fig. 5.69. With the dry electrolyte, the devices made with (CeO₂)_{0.81}(TiO₂)₁ layers sintered at 250 °C and 350 °C could only be cycled for about 1000 cycles, and for $T_s \geq 450$ the devices could be cycled for about 5000 cycles. After that all cells present delamination and black dots and were destroyed.

With the wet electrolyte, the long-term stability is improved to different extend for all cells. With (CeO₂)_{0.81}(TiO₂)₁ single layers sintered at 250 and 350 °C, the long-term stability is improved up to 15000 and 30000 cycles respectively, but with layers sintered at higher temperature the long-term stability can be extended to more than 50000 cycles. The best result is observed for a single (CeO₂)_{0.81}(TiO₂)₁ layer sintered at 550 °C. The transmittance in the colored state is however higher

than that shown in Fig. 5.65 because of the smaller thickness of the counter electrode (180 nm instead of 200 nm).

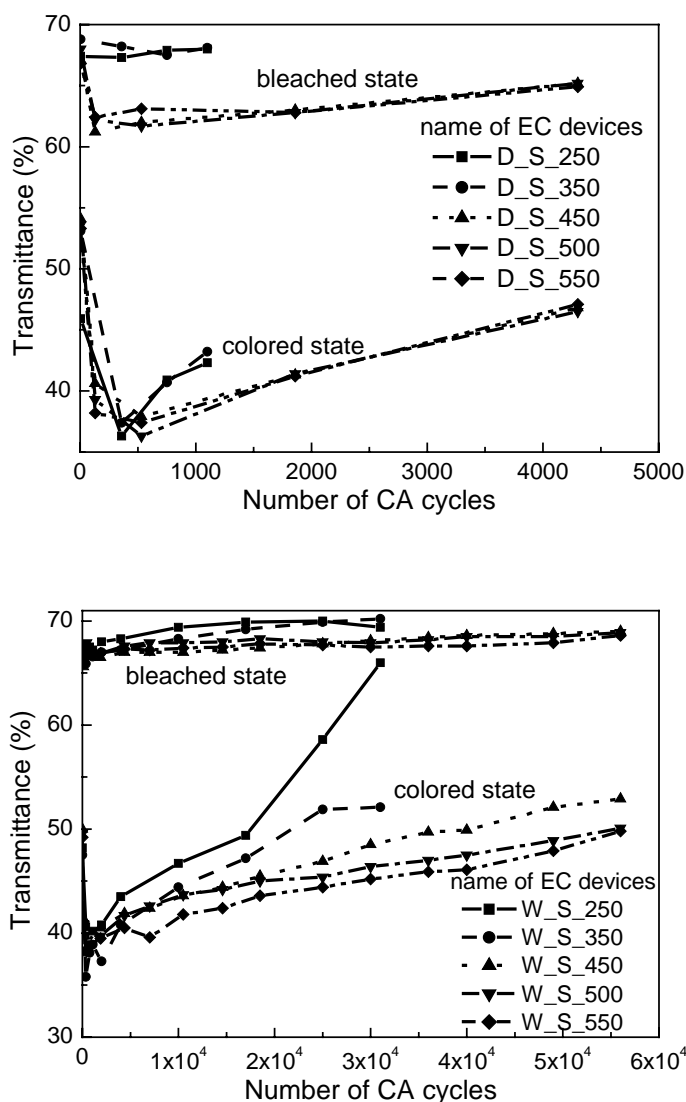


Fig. 5.69 Evolution of the transmittance change at $\lambda = 550$ nm of EC devices with configuration K-glass/ $\text{Nb}_2\text{O}_5\text{:Mo}$ (120 nm)/ inorganic-organic composite electrolyte/ $(\text{CeO}_2)_{0.81}(\text{TiO}_2)_1$ / K-glass as a function of the number of CA cycles (-2.5 V, 120 s/ +2.5 V, 120 s). Top: devices with dry electrolyte; bottom: devices with wet electrolyte (3 wt.% water).

The coloration efficiency of the EC devices made with these $(\text{CeO}_2)_{0.81}(\text{TiO}_2)_1$ counter electrodes are shown in Fig. 5.70. It is interesting to note that for single layers with wet electrolyte the value is the highest for layers sintered at 350 °C and then decreases continuously as a function of the sintering temperature. This confirms that the opposite trend observed for the transmittance change (increase of ΔT with the sintering temperature) is due to a kinetic effect.

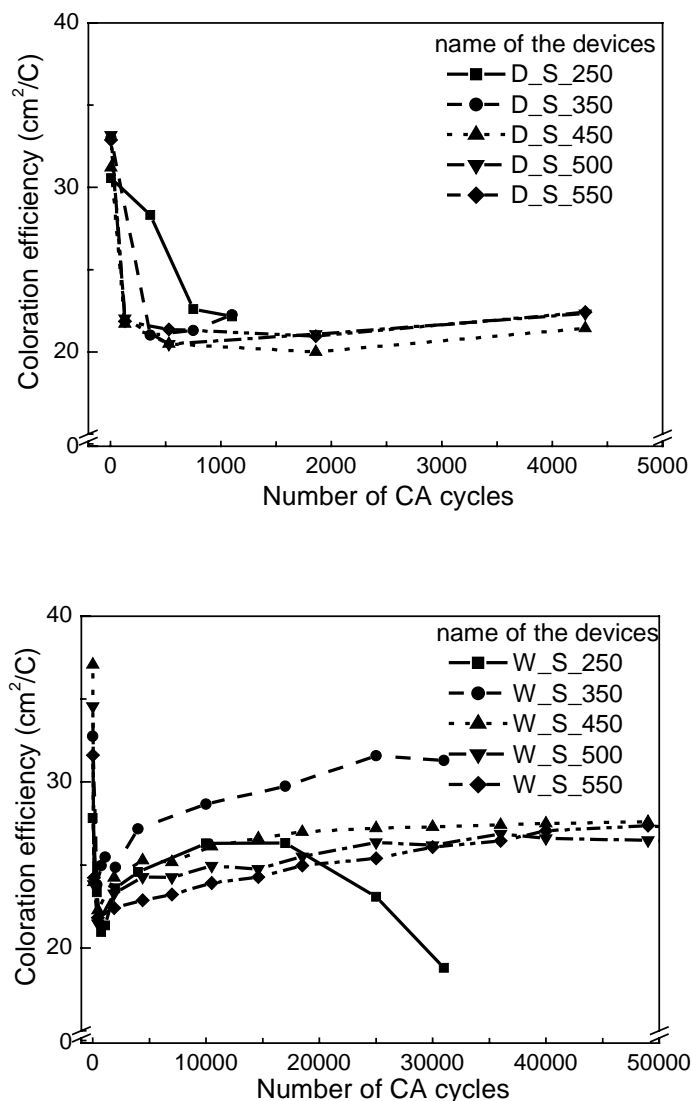


Fig. 5.70 Coloration efficiency, C.E. of EC devices with configuration K-glass/ $\text{Nb}_2\text{O}_5:\text{Mo}$ (120 nm)/ inorganic-organic composite electrolyte/ $(\text{CeO}_2)_{0.81}(\text{TiO}_2)_1$ / K-glass as a function of the CA cycles (-2.5 V, 120 s/ +2.5 V, 120 s). Top: with dry electrolyte; bottom: with wet electrolyte (3 wt.% water).

c) *Influence of the $(\text{CeO}_2)_{0.81}(\text{TiO}_2)_1$ thickness*

EC devices can also reach a lower transmittance in the colored state by applying -2.5 V for 2 minutes if thicker $(\text{CeO}_2)_{0.81}(\text{TiO}_2)_1$ layer are used as e.g. by making double layers, using single layers prepared with an aged sol or double layers prepared with an aged sol.

The counter electrode layers have been differently processed: single layers sintered at 450, 500 or 550 °C, double layers with the first layers sintered at 150 or 200 °C and then the final stacks sintered at 450, 500 or 550 °C. The results obtained for EC devices with the double layers are practically the same when the thickness of the layers is similar. So only the results of those devices obtained for layers sintered at 150 °C for the first layer and 500 °C for the stacks are presented and

discussed here. The other results are shown in annex E. The list of devices tested is given in Table 5.5.

Table 5.5 List of EC devices with the configuration K-glass/ $Nb_2O_5:Mo$ ($Mo:Nb = 0.3$) (120 nm)/ inorganic-organic composite electrolyte/ $(CeO_2)_{0.81}(TiO_2)_1$ / K-glass to test the influence of the thickness of the counter electrode.

EC device	$(CeO_2)_{0.81}(TiO_2)_1$ sol-gel layer			Water content in the inorganic-organic composite electrolyte (wt.%)
	Sintering temperature		Thickness (nm)	
	1 st layer	Final sintering temperature (°C)		
D_S_500		500	170	0
W_S_500		500	170	3
D_D_500a	150	500	340	0
W_D_500a	150	500	340	3
D_D_500c	150	500	500	0
W_D_500c	150	500	500	3

The change of the optical density of EC devices made with $(CeO_2)_{0.81}(TiO_2)_1$ layers of 170, 340 and 500 nm thickness as a function of the number of CA cycles is shown in Fig. 5.71.

ΔOD increases with the thickness of the counter electrodes for all devices with dry and wet electrolyte. The results obtained in dry electrolyte show again that this choice is not adequate: ΔOD first increase to a maximum value up to ca. 700 CA cycles and then strongly decreases and all the windows fail near 8000 CA cycles. The windows tested with a wet electrolyte show an overall behavior similar to that already discussed: an increase of ΔOD to a maximum value (0.25 for a 170 nm thick $(CeO_2)_{0.81}(TiO_2)_1$ layer, 0.3 for the 340 nm thick layer and 0.43 for the 500 nm thick layer) and then slowly decrease with the cycling number. This slow decrease is again due to a kinetic problem as the maximum contrast can be observed by applying the coloring potential for a longer time of 10 minutes (Fig. 5.71). The windows made with 170 and 340 nm thick counter electrode have been safely cycled up to 55000 CA cycles. But that made with a 500 nm thick layer failed after 42000 cycles (the reason is unknown).

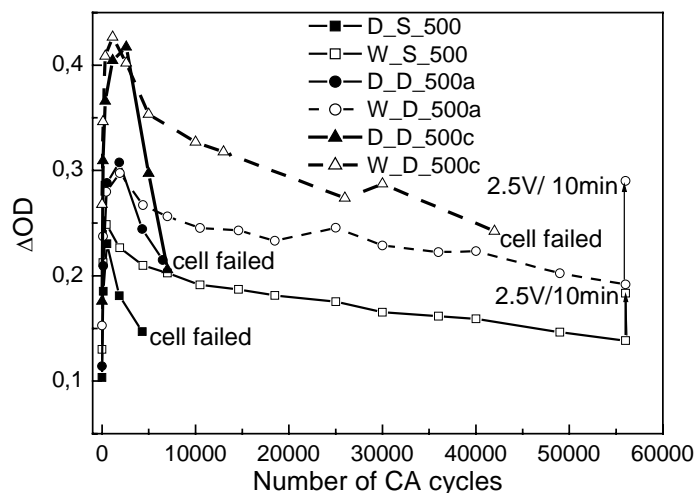


Fig. 5.71 Change of the optical density ΔOD at $\lambda = 550$ nm of EC-devices with configuration K-glass/ $Nb_2O_5:Mo$ ($Mo:Nb = 0.3$) (120 nm)/ inorganic-organic composite electrolyte/ $(CeO_2)_{0.81}(TiO_2)_1$ / K-glass without and with addition of 3 wt.% water in the composite electrolyte as a function of the number of CA cycles (-2.5 V, 120 s/ +2.5 V, 120 s).

In Fig. 5.72 ΔOD / thickness (μm) is plotted against the number of CA cycles for several windows made with a single or double $(CeO_2)_{0.81}(TiO_2)_1$ layers. Two groups of results are obtained: one for single layers and the other for double layers. In each group ΔOD scales with the thickness with a coefficient of proportionality of $1.4 \pm 0.1 \mu m^{-1}$ for single layers and $0.86 \pm 0.05 \mu m^{-1}$ for double layers (measured at 2000th cycle). Although more charge can be inserted in the devices made with a $(CeO_2)_{0.81}(TiO_2)_1$ double layer, the total charge that is effectively inserted does not scale with the thickness (see discussion below and Table 5.6) and this explains the above results. The reason is still unknown but it seems that when 2 layers are deposited, a discontinuity is created at the interface between the 2 layers, which impede the Li^+ ions to fully use the capacity of the second deposited layer.

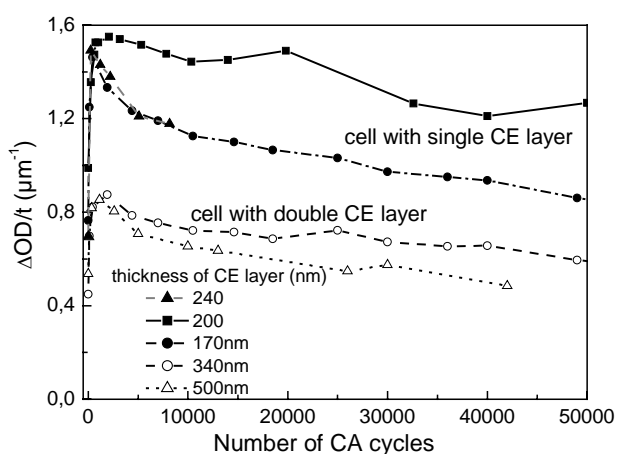


Fig. 5.72 Change of the optical density ΔOD per μm of CE layer at $\lambda = 550$ nm of EC-devices with configuration K-glass/ $Nb_2O_5:Mo$ (120 nm)/ inorganic-organic composite electrolyte (3 wt.% water)/ $(CeO_2)_{0.81}(TiO_2)_1$ / K-glass as a function of the number of CA cycle (-2.5 V, 120 s/ +2.5 V, 120 s).

Some characteristic parameters measured during the 1500~2000 CA cycles (maximum value of ΔOD) are given in Table 5.6. The charge inserted increases linearly with the thickness of the counter electrode, but the proportionality factor is different for single and double layers ($68 \text{ mC}\cdot\text{cm}^{-2}\cdot\mu\text{m}^{-1}$ and $45 \text{ mC}\cdot\text{cm}^{-2}\cdot\mu\text{m}^{-1}$, respectively). The coloration efficiency is however practically identical for all windows, C.E. $\approx 20 \text{ cm}^2/\text{C}$. It is higher than what was reported by Schmitt et al. [179].

Table 5.6 Parameters measured for EC devices with configuration K-glass/ $\text{Nb}_2\text{O}_5:\text{Mo}$ (120 nm)/ inorganic-organic composite electrolyte (3 wt.% water)/ $(\text{CeO}_2)_{0.81}(\text{TiO}_2)_1$ / K-glass

EC device	Number of EC layer	Thickness of CE layer (nm)	$\Delta T(\text{max})^*$	ΔOD	Q_{in} (mC/cm^2)	C.E. (cm^2/C)
W_S_500	1	170	0.29	0.25	11.6	21.5
W_D_500a	2	340	0.311	0.30	16.0	18.6
W_D_500c	2	500	0.406	0.43	21.6	19.8

$\Delta T(\text{max})^*$: the maximum transmittance change at $\lambda = 550 \text{ nm}$ of the EC devices by -2.5V , 120s/ $+2.5\text{V}$, 120s.

Recalling the results discussed in section 5.3.2, a 120 nm thick $\text{Nb}_2\text{O}_5:\text{Mo}$ ($\text{Mo}:\text{Nb} = 0.3$) layer could easily withstand a charge of $42 \text{ mC}/\text{cm}^2$ showing an optical density change of 0.9 (10 % transmittance of the colored state). A double $(\text{CeO}_2)_{0.81}(\text{TiO}_2)_1$ layers in wet liquid electrolyte exhibits an inserted charge of about $26 \text{ mC}/\text{cm}^2$. This means that the contrast of the niobia windows is probably still limited by the charge storage capacity of the $(\text{CeO}_2)_{0.81}(\text{TiO}_2)_1$ counter electrode. Therefore it is not discarded that by eliminating the probable discontinuity at the interface of the two counter electrode layers and/ or by using thicker counter electrode, contrast higher than $\Delta OD = 0.43$ can be obtained by CA cycling with a $-2.5 \text{ V}/+2.5 \text{ V}$ applied voltage.

The normalized transmittance of the EC devices at the 4000th CA cycle is shown in Fig. 5.73. The results are compatible with the above discussion and clearly show that a colouring time longer than 2 minutes is needed to reach minimum of T/T_b . However 2 minutes at $+2.5 \text{ V}$ is sufficient to completely bleach the devices.

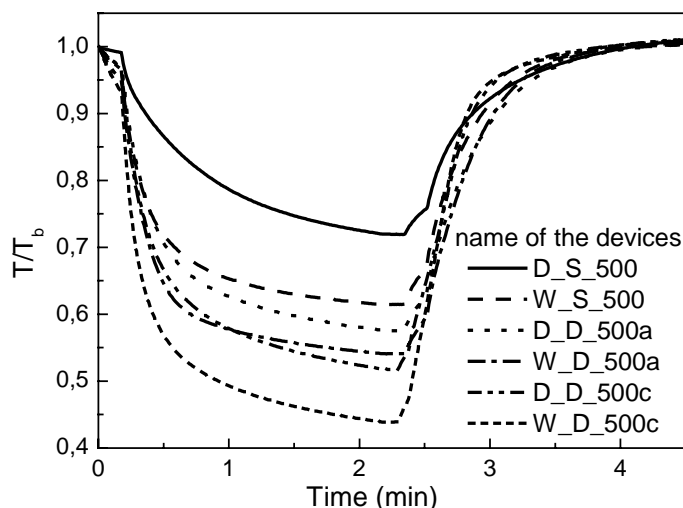


Fig. 5.73 Normalized transmittance, T/T_b , ($\lambda = 550\text{nm}$), versus time of EC devices with configuration K-glass/ $\text{Nb}_2\text{O}_5:\text{Mo}$ (120 nm)/ inorganic-organic composite electrolyte/ $(\text{CeO}_2)_{0.45}(\text{TiO}_2)_{0.55}$ / K-glass with different water content in the electrolyte and different thickness of $(\text{CeO}_2)_{0.45}(\text{TiO}_2)_{0.55}$ layer at the 4000th CA (-2.5 V , 2 min/ 2.5 V , 2 min) cycle.

From the above discussion, it is concluded:

- Gray coloring EC devices with the configuration K-glass/ $\text{Nb}_2\text{O}_5:\text{Mo}$ ($\text{Mo}:\text{Nb} = 0.3$) (120 nm)/ inorganic-organic composite electrolyte/ $(\text{CeO}_2)_{0.81}(\text{TiO}_2)_1$ / K-glass which can be cycled up to more than 60000 CA cycles have been realized and tested using the following conditions:
 - a) Potential: -2.5 V / 2 min coloring and $+2.5\text{ V}$ / 2 min bleaching.
 - b) sintering temperature of $(\text{CeO}_2)_{0.81}(\text{TiO}_2)_1$ layers should lie between $450\text{ }^\circ\text{C}$ and $550\text{ }^\circ\text{C}$.
 - c) the inorganic-organic composite electrolyte should contain 2 to 3 wt.% water.
- The EC properties are dependant on the thickness of the $(\text{CeO}_2)_{0.81}(\text{TiO}_2)_1$ sol-gel layer. Thick $(\text{CeO}_2)_{0.81}(\text{TiO}_2)_1$ layer leads to an improved ion storage capacity and consequently the ΔOD of the device is higher. The maximum variation of the optical density $\Delta\text{OD} = 0.43$ was obtained with a 500 nm $(\text{CeO}_2)_{0.81}(\text{TiO}_2)_1$ sol-gel double layer as counter electrode.
- The coloring kinetics of the devices with wet electrolyte is faster than that with dry electrolyte and decreases with cycle number; therefore -2.5 V / 2 min is not enough to get a full color after 40000 cycles.
- The bleaching kinetics is fast and $+2.5\text{ V}$ / 2 min is enough to completely bleach the devices.

d) $30 \times 40 \text{ cm}^2$ prototype EC devices

Gray coloring EC devices with a $30 \times 40 \text{ cm}^2$ size with the configuration K-glass/ $\text{Nb}_2\text{O}_5:\text{Mo}$ ($\text{Mo}:\text{Nb} = 0.3$)/ inorganic-organic composite electrolyte (3 wt.% water)/ $(\text{CeO}_2)_{0.81}(\text{TiO}_2)_1$ / K-glass were assembled and tested.

The devices have been colored and bleached by a galvanostatic process, $-240 \mu\text{A}/\text{cm}^2$ for 3 min until -3.3 V and $240 \mu\text{A}/\text{cm}^2$ for 3 min until $+2.5 \text{ V}$ respectively. Pictures of the devices are shown in Fig. 5.74. The transmittance changed from 60% to 25% at 550 nm and ΔOD was 0.38 at 550 nm. The results are better than those of the best windows with a $5 \times 10 \text{ cm}^2$ size due to the galvanostatic switching for a longer time (3 min).



A: bleached state: transmittance 60 % ($\lambda = 550 \text{ nm}$)

B: coloured state: transmittance 25 % ($\lambda = 550 \text{ nm}$)

Fig. 5.74 Picture of $30 \times 40 \text{ cm}^2$ EC devices after galvanostatic coloring and bleaching for 3 minutes.

5.5.3 Memory effect of the EC devices

Memory effect, the ability to keep at the colored or bleached state without voltage, is one property of the battery type EC devices. The memory effect of EC devices with the configuration K-glass/ $\text{Nb}_2\text{O}_5:\text{Mo}$ (120 nm) or WO_3 (200 nm)/ inorganic-organic composite electrolyte/ $(\text{CeO}_2)_{0.81}(\text{TiO}_2)_1$ (200nm)/ K-glass has been studied with devices made without and with addition of 3 wt.% water to the composite electrolyte. The change of the transmittance in the colored state has been recorded without applying a voltage after coloring with a voltage of $-2 \text{ V}/ 2\text{min}$ (WO_3 EC device) and $-2.5 \text{ V}/ 2 \text{ min}$ ($\text{Nb}_2\text{O}_5:\text{Mo}$ EC device). In order to compare the behavior of the four studied EC devices, the transmittance has been normalized as $(T-T_b)/(T_c-T_b)$ where T_b and T_c are the transmittance of the bleached and colored state respectively and T is the transmittance at anytime (Fig. 5.75).

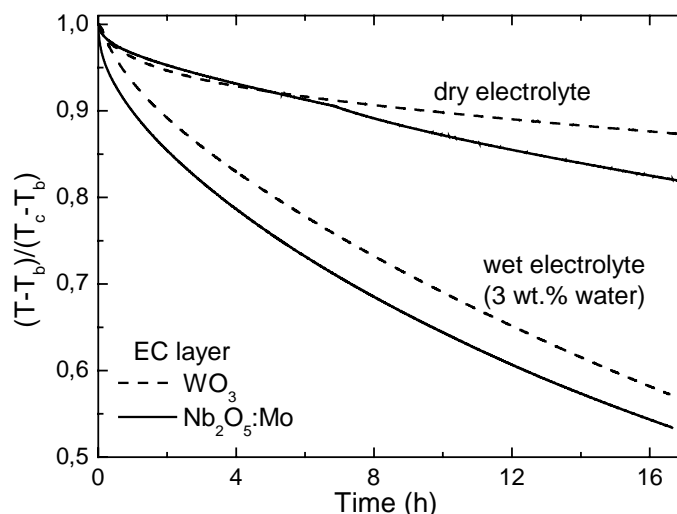
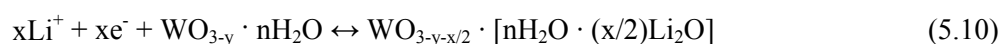


Fig. 5.75 Recovery of the normalized transmittance (memory effect) of EC devices with the configuration K-glass/ Nb₂O₅:Mo (120 nm) or WO₃ (200 nm)/ inorganic-organic composite electrolyte/ (CeO₂)_{0.81}(TiO₂)₁ (200 nm)/ K-glass (after 50 CA cycles)

For a given electrolyte (dry or wet) the memory effect is rather similar for EC devices built with Nb₂O₅:Mo or WO₃ sol-gel layer. The devices made with a wet composite electrolyte return faster to their bleached state than those made with a dry composite electrolyte. The result for WO₃ as EC layer in dry electrolyte is in agreement with that reported by Heusing et al. [72]. The behavior is nevertheless still adequate for windows as only a 40 % relative variation is observed after about 17 hours.

A possible mechanism was presented by Leftheriotis et al [185]. The following reaction is proposed for the coloration of hydrous tungsten oxide films:



The above reaction is reversible. As Li₂O cannot escape easily from the film to the surrounding environment, it is accumulated into the WO₃ matrix. With reversal of the electric field polarity, the lithium oxide breaks up, Li⁺ is released and WO₃ is bleached.

In order to study the memory effect, the normalized transmittance $(T-T_b)/(T_c-T_b)$, measured at different cycle numbers of the devices made with Nb₂O₅:Mo as EC layer 17 hours after switching off the voltage is shown in Fig.5.76 as a function of the cycle number. The values for the devices made with dry composite electrolyte are higher than that with wet electrolyte. The addition of 1 to 3 wt.% water to the composite electrolyte causes a decrease of the memory effect of the devices. The values increase during the initial cycles until the 2000th cycle and slowly decrease, but remain adequate for windows even after 8000 CA cycles.

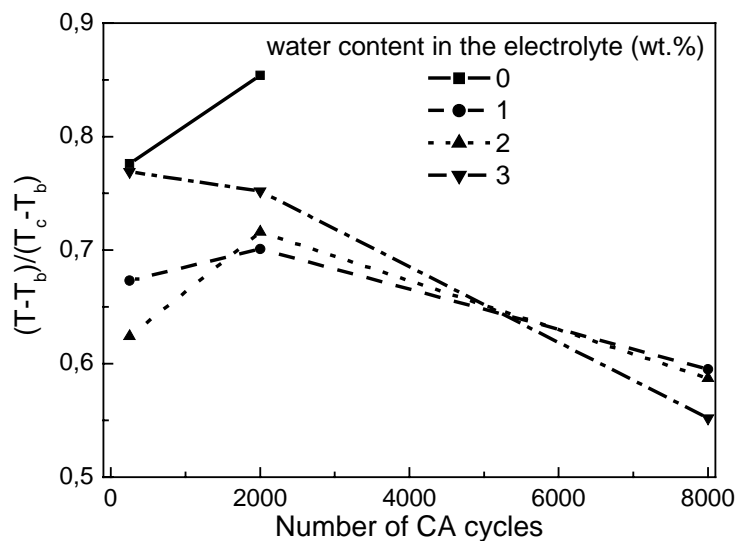


Fig. 5.76 Normalized transmittance of the EC devices with the configuration K-glass/ $\text{Nb}_2\text{O}_5:\text{Mo}$ (120 nm)/ inorganic-organic composite electrolyte/ $(\text{CeO}_2)_{0.81}(\text{TiO}_2)_1$ (200 nm)/ K-glass, 17 hours after switching off the voltage for coloration (-2.5 V/ 2 min) as a function of the CA cycle number.

5.5.4 Optical microscopy analysis of WO_3 or $\text{Nb}_2\text{O}_5:\text{Mo}$ (Mo:Nb = 0.3) based EC devices

The EC devices made with either WO_3 or $\text{Nb}_2\text{O}_5:\text{Mo}$ (Mo:Nb = 0.3) sol-gel EC layer and dry composite electrolyte began to crack and delaminate after about 10000 CA cycles. EC devices with wet electrolyte did not show any crack or delamination even after 50000 to 60000 cycles. The $5 \times 10 \text{ cm}^2$ gray coloring EC device with wet electrolyte that was still working after 58000 CA cycles and the “dry” one that was destroyed after 14000 CA cycles are shown in Fig 5.77. The blue coloring EC devices are not shown here but presented similar results.

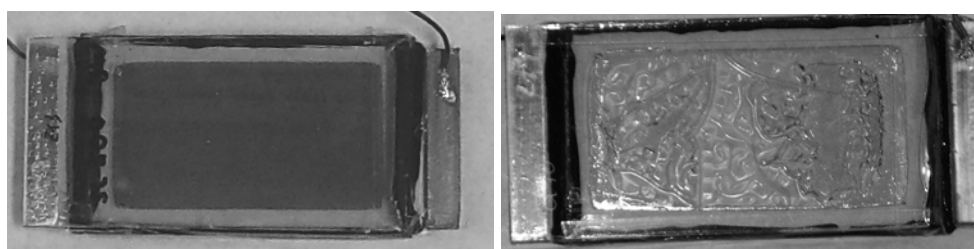


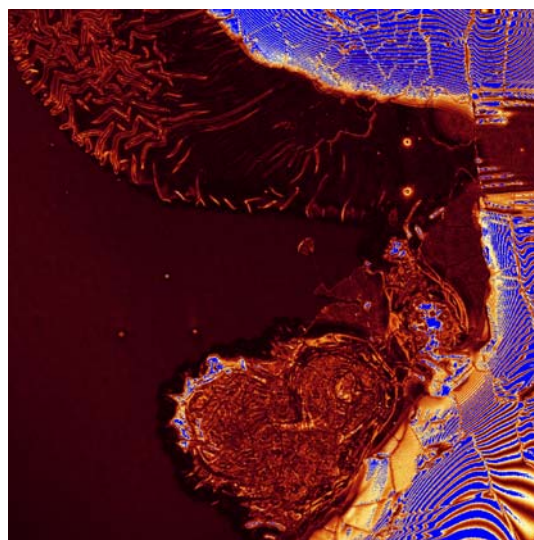
Fig. 5.77. $5 \times 10 \text{ cm}^2$ EC devices with configuration K-glass/ $\text{Nb}_2\text{O}_5:\text{Mo}$ (Mo:Nb = 0.3) (120 nm)/ inorganic-organic composite electrolyte/ $(\text{CeO}_2)_{0.81}(\text{TiO}_2)_1$ (200 nm)/ K-glass. Left: with wet electrolyte after 60000 CA cycles at colored state; right: with dry electrolyte after 14000 CA cycles.

These devices have been further studied using a Confocal Laser Scanning Microscope (CLSM) (Leica). The analyzed area of CLSM is $1.5 \times 1.5 \text{ mm}^2$ and is taken in the middle of the EC devices. The pictures are shown in Fig. 5.78 and 5.79.

Fig. 5.78a and b show pictures of the $(\text{CeO}_2)_{0.81}(\text{TiO}_2)_1$ layer in the EC device with configuration K-glass/ WO_3 (200 nm)/ inorganic-organic composite electrolyte/ $(\text{CeO}_2)_{0.81}(\text{TiO}_2)_1$ (200 nm)/ K-glass with wet and dry electrolyte separately. Fig. 5.78c and d show pictures of the WO_3 layer in the same EC devices with wet and dry electrolyte. The WO_3 layer is still intact, but its roughness seems to be higher in the destroyed device. Delamination clearly appear at the interface of $(\text{CeO}_2)_{0.81}(\text{TiO}_2)_1$ layer and the composite electrolyte and not at the interface of WO_3 and the composite electrolyte.



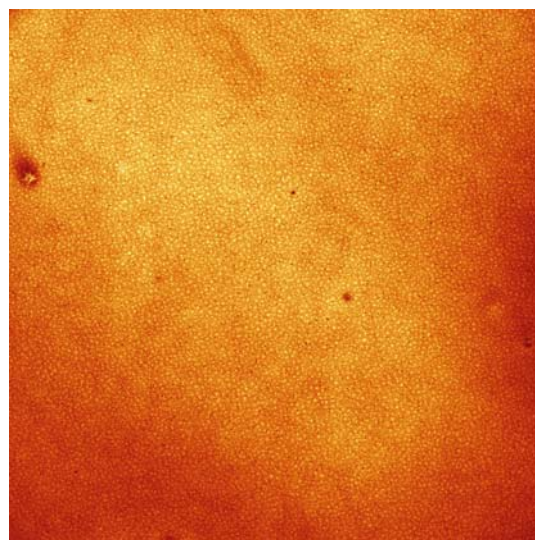
a) $(\text{CeO}_2)_{0.81}(\text{TiO}_2)_1$ layer in the EC device with wet electrolyte (after 52000 CA cycles).



b) $(\text{CeO}_2)_{0.81}(\text{TiO}_2)_1$ layer in the EC device with dry electrolyte (after 42000 CA cycles).



c) WO_3 layer in the EC device with wet electrolyte (after 52000 CA cycles).

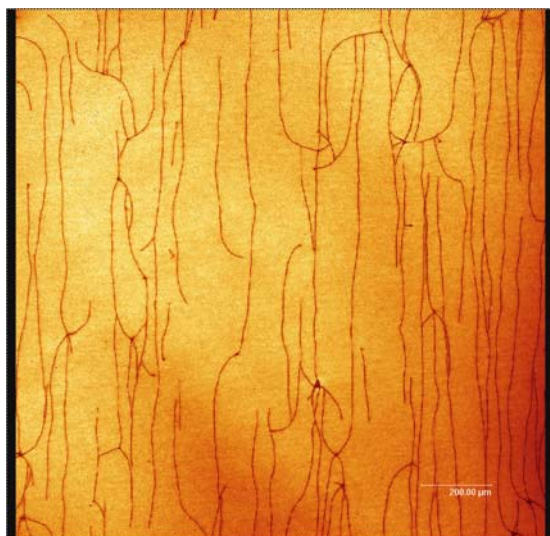


d) WO_3 layer in the EC device with dry electrolyte (after 42000 CA cycles).

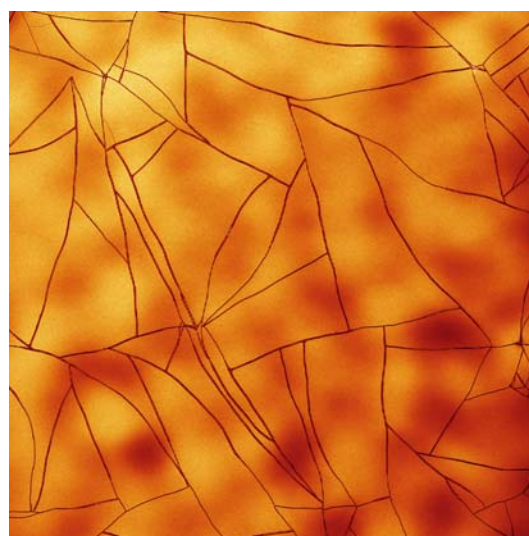
Fig.5.78 Microscopy of the CE and EC layer in EC devices with the configuration K-glass/ WO_3 (200 nm)/ inorganic-organic composite electrolyte/ $(\text{CeO}_2)_{0.81}(\text{TiO}_2)_1$ (200 nm)/ K-glass by CLSM. Measured area: $1.5 \times 1.5 \text{ mm}^2$

Similar results have been obtained for the EC device with the configuration K-glass/ $\text{Nb}_2\text{O}_5:\text{Mo}$ (120 nm)/ inorganic-organic composite electrolyte/ $(\text{CeO}_2)_{0.81}(\text{TiO}_2)_1$ (200 nm)/ K-glass (Fig. 5.79).

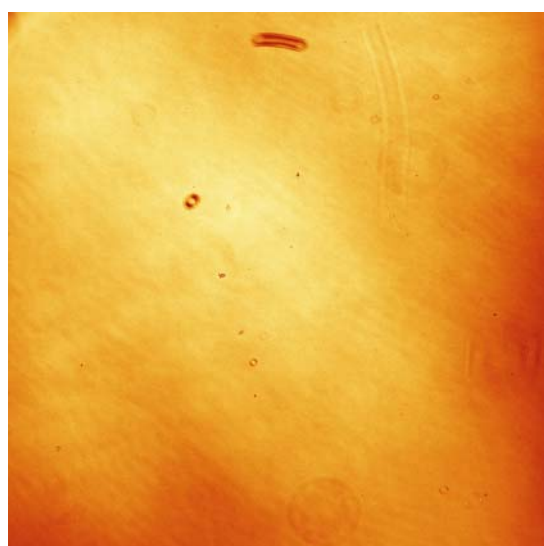
Different pattern of cracks are observed with the $\text{Nb}_2\text{O}_5:\text{Mo}$ ($\text{Mo}:\text{Nb} = 0.3$) layer. The cracks on the layer in contact with the wet electrolyte seem to be caused by uniaxial tension as most of them are stretching in one direction. On the other hand, the cracks on the layer in contact with the dry electrolyte seem to be caused by biaxial tension. Many intersections of cracks formed an angle of near 90 degree. But the difference between the $(\text{CeO}_2)_{0.81}(\text{TiO}_2)_1$ layers with wet and dry electrolyte is more obvious. The delamination is clearly observed at the $(\text{CeO}_2)_{0.81}(\text{TiO}_2)_1$ layer of the EC device with dry electrolyte. The roughness of the $(\text{CeO}_2)_{0.81}(\text{TiO}_2)_1$ layer also increased (Fig. 5.79 c and d).



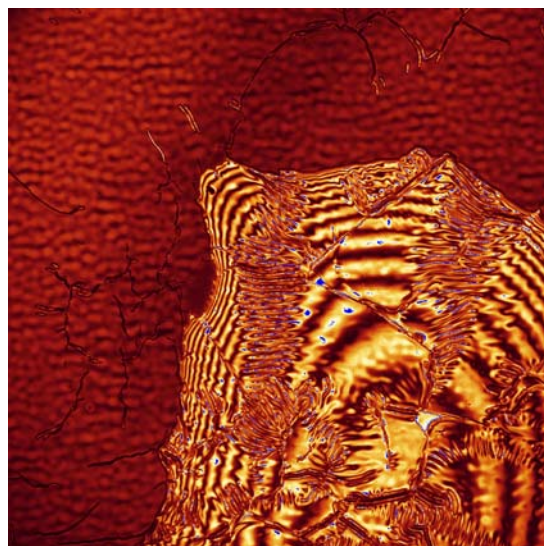
a) $\text{Nb}_2\text{O}_5:\text{Mo}$ layer in the EC device with wet electrolyte (after 56000 CA cycles).



b) $\text{Nb}_2\text{O}_5:\text{Mo}$ layer in the EC device with dry electrolyte (after 14000 CA cycles).



c) $(\text{CeO}_2)_{0.81}(\text{TiO}_2)_1$ layer in the EC device with wet electrolyte (after 56000 CA cycles).



d) $(\text{CeO}_2)_{0.81}(\text{TiO}_2)_1$ layer in the EC device with dry electrolyte (after 14000 CA cycles).

Fig.5.79 Microscopy of the CE and EC layer in EC devices with the configuration K-glass/ $\text{Nb}_2\text{O}_5:\text{Mo}$ (120 nm)/ inorganic-organic composite electrolyte/ $(\text{CeO}_2)_{0.81}(\text{TiO}_2)_1$ (200 nm)/ K-glass by CLSM. Measured area: $1.5 \times 1.5 \text{ mm}^2$

The following conclusions can be drawn: comparing the pictures taken from the EC devices with wet and dry electrolyte, drastic differences occur in the $(\text{CeO}_2)_{0.81}(\text{TiO}_2)_1$ layers either in the WO_3

or Nb₂O₅:Mo device. With water added to the electrolyte, the destruction of the EC devices is impeded and the stability of the device could be improved.

5.5.5 Devices made with NiO_x-TiO₂ as ion storage layer

There are three kinds of battery type EC devices: one is made by a cathodic EC layer and a transparent ion storage layer like those described in this work, another one is made by an anodic EC layer and a transparent ion storage layer and the third one is made by a cathodic EC layer and an anodic EC layer that works as an ion storage layer. In the last device, as both layers color and bleach simultaneously, an increase of the transmittance change can be expected.

An anodic electrochromic layer NiO_x-(TiO₂) was developed at INM by Santos Lopez [189]. The layer was prepared with a sol with a molar ratio Ni/Ti = 3. A 225 nm thick transparent triple layer was obtained by dip coating followed by a thermal treatment at 300 °C. The Li⁺ ion storage capacity of the layer reached 22 mC/cm² causing an anodic transmittance change from 89% to 48% (brown color).

Battery type EC devices with the configuration K-glass/ Nb₂O₅:Mo (120 nm) or WO₃ (200 nm)/ inorganic-organic composite electrolyte/ (NiO_x-(TiO₂) (225 nm)/ K-glass were therefore tested under the following conditions: -2.5 V/ 2 min; +1.5 V/ 2 min. The largest optical density change ΔOD was 0.4 when 17 mC/cm² was intercalated during the 5th CA cycle with the device composed of a WO₃ layer and a wet electrolyte. The ΔOD of the same device with dry composite electrolyte was only 0.18 during the 5th CA cycle.

Battery type EC devices using 1 M LiClO₄ in PC (dry or with 3 wt.% water) as electrolyte were also tested. The cells were cycled with CA: -2 V/ 2 min; +2 V/ 2 min. The largest change in optical density was ΔOD = 0.69 and was obtained during the 9th CA cycle with the device composed of a WO₃ layer and a wet electrolyte while the value was ΔOD = 0.42 with the device with dry liquid electrolyte.

The properties of EC devices made with NiO_x-(TiO₂) sol-gel layer appear to be also improved by adding water to the electrolyte. Compared to devices using (CeO₂)_{0.81}(TiO₂)₁, a higher ΔOD can be obtained because of the simultaneous coloring of both EC layers. However the lifetime of these devices was smaller than 100 cycles whatever the electrolyte was. The details are shown in annex F.

6 Summary

➤ Cerium-titanium oxide layers

Cerium-titanium oxide layers acting as ion storage layer in electrochromic devices have been prepared via the sol-gel method. The electrochemical properties of the layers were tested in 1 M LiClO₄ in propylene carbonate.

- Various molar ratios of (CeO₂) to (TiO₂) were tested. The coatings obtained with the composition (CeO₂)_{0.81}(TiO₂)₁ gave the best ion storage capacity. The sol can be stored for more than one year in a refrigerator at -18 °C.
- (CeO₂)_{0.81}(TiO₂)₁ sol-gel single layers coated on preheated K-glass show a slightly higher ion storage capacity than those without pre heat treatment (about 1 mC/cm² higher).
- Sintering in air or a mixture of 40% oxygen with 60% nitrogen gives layers with similar ion-storage ability. Vacuum is not suitable as it leads to opaque layers.
- Acetyl acetone as a sol stabilizer is not recommendable as it reduces the thickness of the layer and hence the ion storage capacity of the layer is reduced.
- (CeO₂)_{0.81}(TiO₂)₁ sol-gel single layers sintered between 150 °C to 550 °C are all X-ray amorphous. When the sintering temperature increases, the Li⁺ storage capacity tested in the dry electrolyte increases with the temperature. During CA cycle (-2 V, 2 min) in 1 M LiClO₄ in PC, a value as high as 14.5 mC/cm² has been obtained for layers sintered at 550 °C, 1 hour (185 nm thick).
- The ion storage capacity of (CeO₂)_{0.81}(TiO₂)₁ sol-gel double layers sintered at 450°C to 550°C is not improved in dry liquid electrolyte. Values are similar or even smaller than that of single layers sintered at the same temperature.

➤ Effect of water content of the liquid electrolyte on the properties of (CeO₂)_{0.81}(TiO₂)₁, WO₃ and Nb₂O₅:Mo (Mo:Nb = 0.3) sol-gel layers

The addition of small amounts of water (up to 3 wt.%) to the 1 M LiClO₄ in PC electrolyte has an important effect on the electrochemical and optical properties of (CeO₂)_{0.81}(TiO₂)₁, WO₃ and Nb₂O₅:Mo (Mo:Nb = 0.3) sol-gel layers.

- A large increase in the ion storage capacity is observed for the sol-gel (CeO₂)_{0.81}(TiO₂)₁ counter electrode in contrast to Janke et al. [175], who observed an opposite behavior with sputtered (CeO₂)-(TiO₂) layers. The ion storage capacity of a 200 nm (CeO₂)_{0.81}(TiO₂)₁ sol-gel layer sintered at 450 °C measured during a CA process (-2 V, 2 min) is improved from 6.6 mC/cm² (0 wt.% water) to 15 mC/cm² (3 wt.% water). By making a (CeO₂)_{0.81}(TiO₂)₁

double layer with a total thickness of 340 nm, the first layer being heated to 150-200 °C before the deposition of second layer and the whole stack finally sintered at 550 °C, the ion storage capacity in wet electrolyte is increased to 26 mC/cm² during a CA process (-2 V, 2 min).

- The study of the ion insertion mechanism of (CeO₂)_{0.81}(TiO₂)₁ layer in dry and wet electrolyte by EQCM show that the ion intercalation process is not a pure Li⁺ intercalation. It is the cooperation of cations and anions of the electrolyte. The composition of the (CeO₂)_{0.81}(TiO₂)₁ layer is changing with the cycle number because of irreversible Li⁺ intercalation. A certain amount of water in the electrolyte may hydrate the Li⁺ ions and improves the mobility of the Li⁺ ions. It may also improve the mobility of other ions.
- For WO₃ sol-gel layers, 1 wt.% of water in the electrolyte leads to a higher transmittance change ($\Delta T = 75\%$ and $\Delta OD = 0.7$) compared to a single layer tested in a dry electrolyte ($\Delta T = 64\%$ and $\Delta OD = 0.6$). The coloration efficiency however remains practically similar, about 35 cm²/C in both electrolytes, in agreement with Bohnke et al. [175].
- A faster kinetics is observed for both (CeO₂)_{0.81}(TiO₂)₁ and WO₃ sol-gel layers in wet electrolyte. The reversibility of the intercalation and deintercalation processes is also considerably improved.
- Opposite results are obtained for Nb₂O₅:Mo (Mo:Nb = 0.3) sol-gel layers. ΔOD decreases only slightly from 1.0 (1st cycle) to 0.85 (3500th cycle) in dry electrolyte, but strongly decreases from 0.92 to 0.25 after addition of 3 wt.% water to the liquid electrolyte. The coloring kinetics is slower with the wet electrolyte. The charge intercalated into the layer in the dry electrolyte in a CP process ($-5 \mu\text{A}/\text{cm}^2$ until -2.2 V) is 50 mC/cm² and ΔOD is 0.78 due to a low coloration efficiency (16 cm²/C).

➤ **Effect of the water content in a solid inorganic-organic composite electrolyte in the performance of EC devices made with WO₃ as EC layer**

- With 3 wt.% water added into the inorganic-organic composite electrolyte, ΔOD of EC devices with the configuration K-glass/ WO₃ (200 nm)/ inorganic-organic composite electrolyte/ (CeO₂)_{0.81}(TiO₂)₁ (200 nm)/ K-glass tested under CA (-2 V, 2 min/ +2 V, 2 min) process have been increased to 0.41 in comparison to $\Delta OD = 0.3$ for a dry electrolyte.
- Contrary to devices made with a dry electrolyte, no switch-in behavior during the initial cycles is observed.
- The long-term stability of EC devices is greatly improved up to 50000 CA cycles (14000 cycles with dry electrolyte).

- The coloration efficiency (C.E.) of devices made with water in the composite electrolyte is $C.E. = 35 \text{ cm}^2/\text{C}$ and slightly higher than that obtained with a dry composite electrolyte ($C.E. = 32 \text{ cm}^2/\text{C}$).

➤ **Electrochemical and optical density of EC devices made with Nb₂O₅:Mo (Mo:Nb = 0.3) as EC layer**

Grey coloring EC devices can be fabricated using molybdenum doped niobium oxide as EC electrode. The configuration of the EC devices was K-glass/ Nb₂O₅:Mo (Mo:Nb = 0.3)/ inorganic-organic composite electrolyte/ (CeO₂)_{0.81}(TiO₂)₁/ K-glass. The effect of the water content in the electrolyte and the effect of the thickness of (CeO₂)_{0.81}(TiO₂)₁ coatings on the performance of the EC devices have been tested.

- The maximum ΔOD of the devices is proportional to the thickness of (CeO₂)_{0.81}(TiO₂)₁ layer. The value is similar for identical thickness of (CeO₂)_{0.81}(TiO₂)₁ whatever is the water content of the electrolyte (about 0.3 for the device with 200 nm thick (CeO₂)_{0.81}(TiO₂)₁ and 0.4 for that with 500 nm thick (CeO₂)_{0.81}(TiO₂)₁).
- The switch-in behavior of the EC devices with wet composite electrolyte (3 wt.% water) is reduced compared to that observed with devices with dry composite electrolyte.
- The long-term stability is drastically improved from 14000 cycles for devices with dry electrolyte to more than 50000 cycles for devices with wet electrolyte
- The C.E. of devices with (CeO₂)_{0.81}(TiO₂)₁ single layers made with wet composite electrolyte is smaller than that obtained with dry composite electrolyte. For example with a 200 nm thick (CeO₂)_{0.81}(TiO₂)₁, the value with wet electrolyte is $C.E. = 27 \text{ cm}^2/\text{C}$ while it is $C.E. = 35 \text{ cm}^2/\text{C}$ with dry electrolyte. But the C.E. of devices with (CeO₂)_{0.81}(TiO₂)₁ doubles are similar with dry and wet composite electrolyte.
- Large area (30 x 40) EC-devices with the configuration K-glass/ Nb₂O₅:Mo (Mo:Nb = 0.3)/ inorganic-organic composite electrolyte/ (CeO₂)_{0.81}(TiO₂)₁ (200 nm)/ K-glass are also prepared. The transmittance change varies from 60% to 25% using galvanostatic switching (coloring with $-240 \mu\text{A}/\text{cm}^2$ for 3 min until -3.3 V and bleaching with $240 \mu\text{A}/\text{cm}^2$ for 3 min until $+2.5 \text{ V}$).

➤ **Memory effect of EC devices with WO₃ or Nb₂O₅:Mo (Mo:Nb = 0.3) as EC layer**

The memory effect of EC devices with the configuration K-glass/ Nb₂O₅:Mo (Mo:Nb = 0.3)/ inorganic-organic composite electrolyte/ (CeO₂)_{0.81}(TiO₂)₁/ K-glass and K-glass/ WO₃/ inorganic-organic composite electrolyte/ (CeO₂)_{0.81}(TiO₂)₁/ K-glass have been tested. Without applied potential, the colored state of the devices made with a wet composite electrolyte bleaches faster than those made with a dry electrolyte. The behavior is nevertheless still

adequate for architectural windows as only a 40% relative variation of the transmittance change is observed after about 17 h.

➤ **Optical microscopy analysis of WO_3 or $\text{Nb}_2\text{O}_5:\text{Mo}$ (Mo:Nb = 0.3) based EC devices**

The delamination of the “dry” EC devices starts from the interface of $(\text{CeO}_2)_{0.81}(\text{TiO}_2)_1$ layer and composite electrolyte.

A summary of the properties of the EC devices tested in this work is finally listed in Table 5.7.

Table 5.7 Comparison of Sol-Gel EC devices studied in this dissertation to what was achieved at INM (state of the art 2001): Materials and configurations, device size, maximum variation of transmittance ΔT and ΔOD at $\lambda = 550$ nm, number of CA cycles and switching time (t_{sw}).

Device configuration	Size (cm ²)	T _b (%)	T _c (%)	T (%)	ΔOD	Number of CA cycles	t _{sw} (s)	C.E. (cm ² /C)	Reference
K-glass/ WO ₃ / inorganic-organic composite electrolyte/ (CeO ₂) _{0.81} (TiO ₂) ₁ / K-glass	4000	70	25	45	0.45	10000	180		73, 164
K-glass/ WO ₃ / dry inorganic-organic composite electrolyte/ (CeO ₂) _{0.81} (TiO ₂) ₁ / K-glass	5 x 10	71	36	35	0.3	10000*	120	32	73,164
K-glass/ WO ₃ / inorganic-organic composite electrolyte (3 wt.% water)/ (CeO ₂) _{0.81} (TiO ₂) ₁ / K-glass	5 x 10	66	26	40	0.41	>50000	120	35	This work
K-glass/ WO ₃ / inorganic-organic composite electrolyte (3 wt.% water)/ (CeO ₂) _{0.81} (TiO ₂) ₁ / K-glass	10 x 15	70	25	45	0.45		180	35	This work
K-glass / Nb ₂ O ₅ :Mo/ 1 M LiClO ₄ in PC/ (CeO ₂) _{0.81} (TiO ₂) ₁ (480 nm)/ K-glass	6 x 8			28		15000*	120	16	104, 179
K-glass / Nb ₂ O ₅ :Mo (Mo:Nb = 0.3)/ dry inorganic-organic composite electrolyte/ (CeO ₂) _{0.81} (TiO ₂) ₁ (200 nm)/ K-glass	5 x 10	65	31	34	0.33	14000*	120	35	This work
K-glass/ Nb ₂ O ₅ :Mo (Mo:Nb = 0.3)/ dry inorganic-organic composite electrolyte/ (CeO ₂) _{0.81} (TiO ₂) ₁ (500 nm)/ K-glass	5 x 10	66	25	41	0.42	7000*	120s	~20	This work
K-glass/ Nb ₂ O ₅ :Mo (Mo:Nb = 0.3)/ inorganic-organic composite electrolyte (3 wt.% water)/ (CeO ₂) _{0.45} (TiO ₂) _{0.55} (200 nm)/ K-glass	5 x 10	63	31	32	0.31	>50000	120	27.5	This work
K-glass/ Nb ₂ O ₅ :Mo (Mo:Nb = 0.3)/ inorganic-organic composite electrolyte (3 wt.% water)/ (CeO ₂) _{0.81} (TiO ₂) ₁ (500 nm)/ K-glass	5 x 10	63	23	40	0.43	>40000	120s	20~25	This work
K-glass/ Nb ₂ O ₅ :Mo (Mo:Nb = 0.3)/ inorganic-organic composite electrolyte (3 wt.% water)/ (CeO ₂) _{0.45} (TiO ₂) _{0.55} (200 nm)/ K-glass	30 x 40	60	25	35	0.38		180	27.5	This work

* failure of the device

Annex

In the annex several results and discussions can be found. They are either not fundamental for the understanding of the thesis, or give more specific indications, or complement results shown earlier (memory of the work), or show results that have not been successful but are still interesting. Also it can be found the list of chemicals and equipments used during the work.

- A. Calibration of the electrochemical quartz crystal microbalance (EQCM)
- B. TEM results of the $(\text{CeO}_2)_{0.81}(\text{TiO}_2)_1$ sol-gel layers.
- C. CV profile of sol-gel $(\text{CeO}_2)_{0.81}(\text{TiO}_2)_1$ layer with different scan rate
- D. XPS spectrum
- E. Results on EC devices with single and double sol-gel $(\text{CeO}_2)_{0.81}(\text{TiO}_2)_1$ layers as counter electrode
- F. Devices made with $\text{NiO}_x\text{-TiO}_2$ as ion storage layer
- G. List of chemicals used in this work
- H. List of equipments used in this work

A) Calibration of the microbalance (EQCM)

The calibration was done by performing a silver deposition in 1×10^{-3} M AgNO_3 in 0.2 M perchloric acid as recommended by the manufacturer [193] during a cyclic voltammetry (Fig. A-1). The value of the sensitivity factor of the crystal $C_f' = 51.9 \text{ Hz} \cdot \mu\text{g}^{-1} \cdot \text{cm}^2$ (CV process) calculated by the following relation differs slightly from the theoretical value $C_f = 56.6 \text{ Hz} \cdot \mu\text{g}^{-1} \cdot \text{cm}^2$ by less than 10% (Fig. A-1).

$$\Delta f = \frac{QW_{\text{Ag}}}{FA} C_f' \quad (\text{A-1})$$

where Δf = frequency change, Q = charge deposited, W_{Ag} = molar weight of Ag, F = Faraday constant, A = area of gold coated quartz, C_f = sensitivity factor of the crystal, C_f' = calculated sensitivity factor of the crystal by calibration.

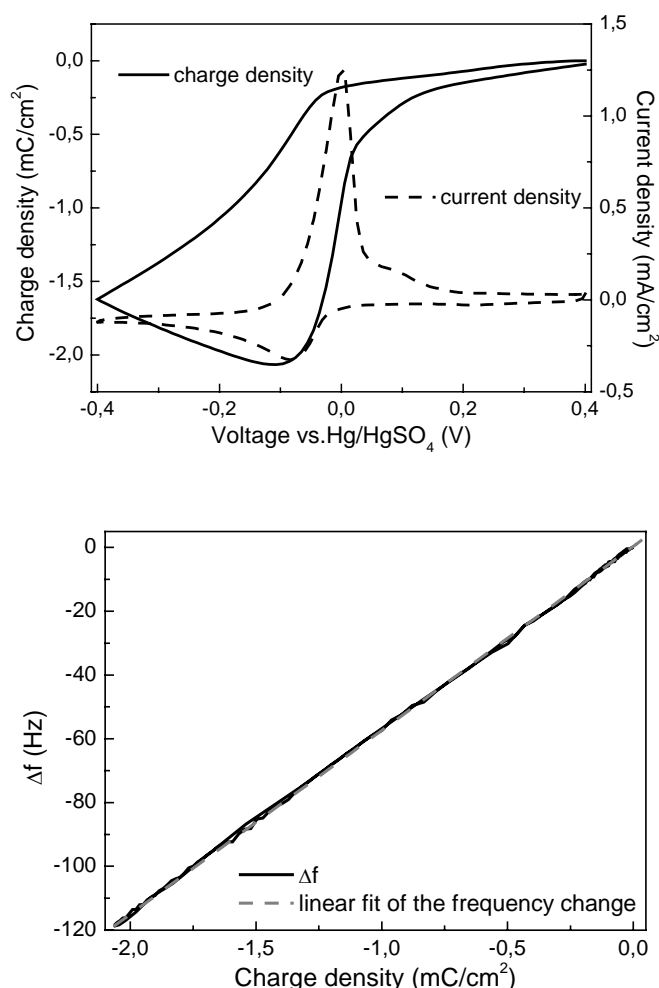


Fig. A-1. CV profile (top) and frequency change vs. charge density (bottom) of silver deposited on an unpolished quartz crystal in 1 mM AgNO_3 in 0.2 M HClO_4 (scan rate: 50 mV/s).

Surface analysis of the quartz with coated $(\text{CeO}_2)_{0.81}(\text{TiO}_2)_1$ sol-gel single layer was also analyzed by AFM (Fig. A-2). The roughness of the surface is about 200 nm. The ratio of real area to

geometrical area is about 1.1:1. This means the 10 % deviation of the value of the sensitivity factor of the crystal is caused by the area of the electrode.

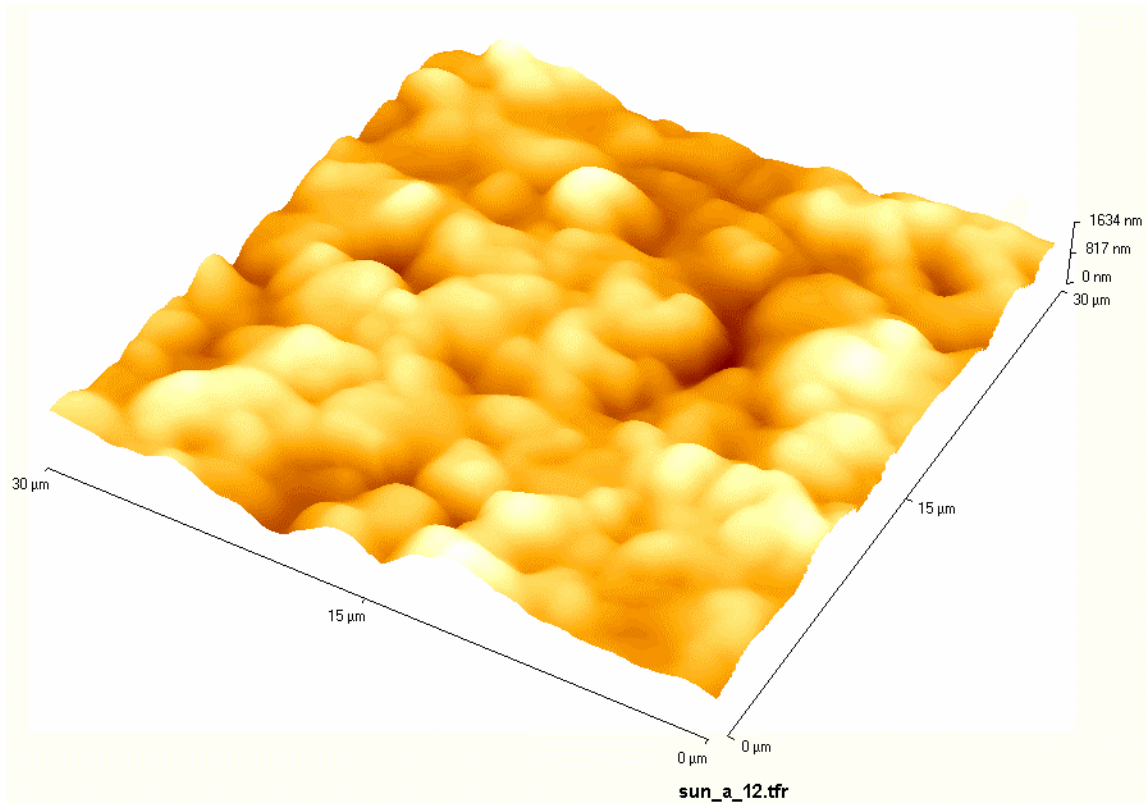


Fig. A-2. AFM picture of $(\text{CeO}_2)_{0.81}(\text{TiO}_2)_1$ sol-gel single layer on Quartz heated at $450\text{ }^\circ\text{C}$

B) TEM results of the $(\text{CeO}_2)_{0.81}(\text{TiO}_2)_1$ sol-gel layers.

The layer/ substrate system to obtain TEM cross-section was handled as follows:

- bonding face to face by epoxy resin, forming sandwiches,
- cutting into slices perpendicular to the interface, and mechanical thinning,
- drilled by an ultrasonic cutter into discs, typical 3 mm in diameter,
- after moulding/ polishing procedure (\Rightarrow dimpling) the specimens are thinned by Ar ion milling up to perforation.

After the complex preparation procedure the TEM specimens are thin enough (≈ 100 nm) near the perforation, and can be used for a TEM characterization.

The typical morphological structure of the layer heated at 450°C is shown in Fig. B-1a. No crystalline structure can be identified in the CeO_2 - TiO_2 layer. According to the electron diffraction experiment this layer is starting to get a crystalline state (*in statu nascendi*). Thus, the dark / bright contrasts (cf. Fig. B-1b) refer to etch pits caused by Ar ion milling. The contrasts do not define particle sizes; the coherent ordered structures are small, namely in the range < 1 nm.

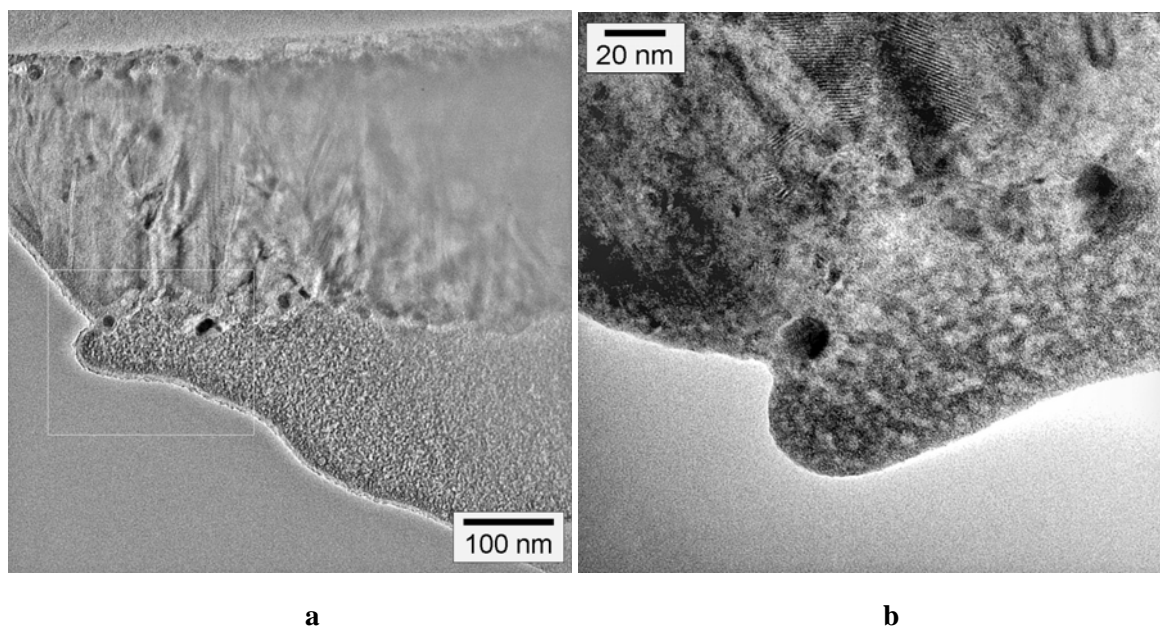
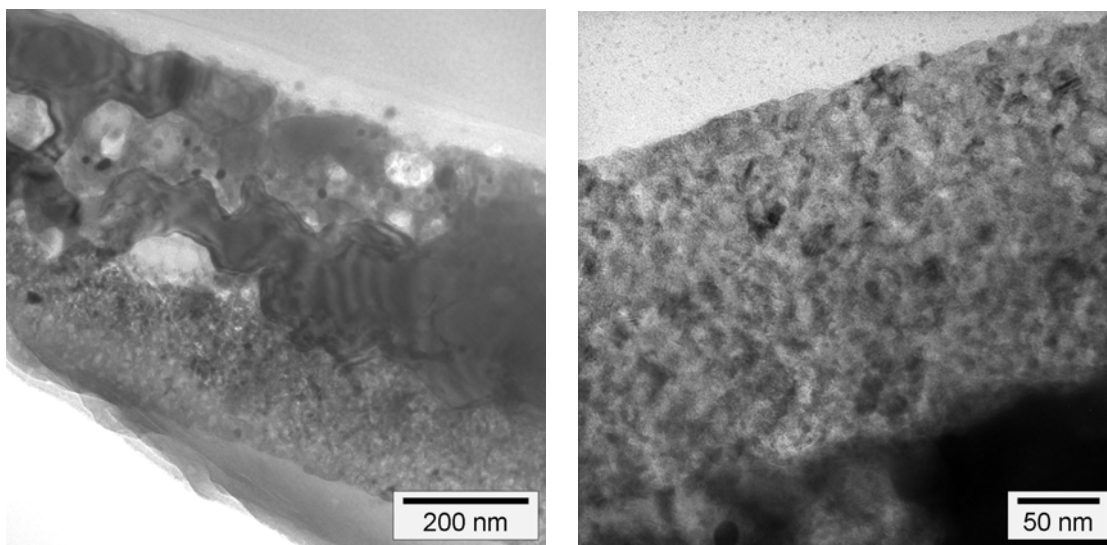


Fig. B-1 HR-TEM microscopy of $(\text{CeO}_2)_{0.81}(\text{TiO}_2)_1$ sol-gel layers heated at 450°C / 1 h.
a - cross-section of the material system: substrate (top) / FTO / $(\text{CeO}_2)_{0.81}(\text{TiO}_2)_1$ layer.
b - enlargement of the marked cross-section.

In Fig. B-2a an overview of the layer heated at 550°C is shown. The CeO_2 - TiO_2 layer (Fig. B-2b) is crystalline with particle sizes ≤ 5 nm but some particles with 10 nm to 15 nm size are also identified (compare with the sample heated at 450°C). Crystal growth was therefore intensified. The particle shapes are somewhat foggy. This is due to the amorphous (carbon) surroundings of the oxides and to the possible presence of residual non-crystalline cerium and titanium oxides. A

structure imaging of the crystalline phase could not be performed because of the too strong amorphous background disturbing the interference contrast.



a **b**
Fig. B-2 HR-TEM microscopy of $(\text{CeO}_2)_{0.81}(\text{TiO}_2)_1$ sol-gel layers heated at 550°C .
a - cross-section of the material system: substrate (top) / FTO / TiO_2 - CeO_2 layers.
b - detailed cross-section view at the TiO_2 - CeO_2 layer.

C) CV profile of sol-gel $(\text{CeO}_2)_{0.81}(\text{TiO}_2)_1$ layer with different scan rate

The cyclic voltammetry of the sol-gel $(\text{CeO}_2)_{0.81}(\text{TiO}_2)_1$ layer (sintered at $450\text{ }^\circ\text{C}/1\text{ h}$) measured with different scan rates (1 mV/s to 200 mV/s) in 1 M LiClO_4 in PC without and with 3 wt.% water (corresponding to the curves shown in Fig. 5.11) are shown in Fig. C-1.

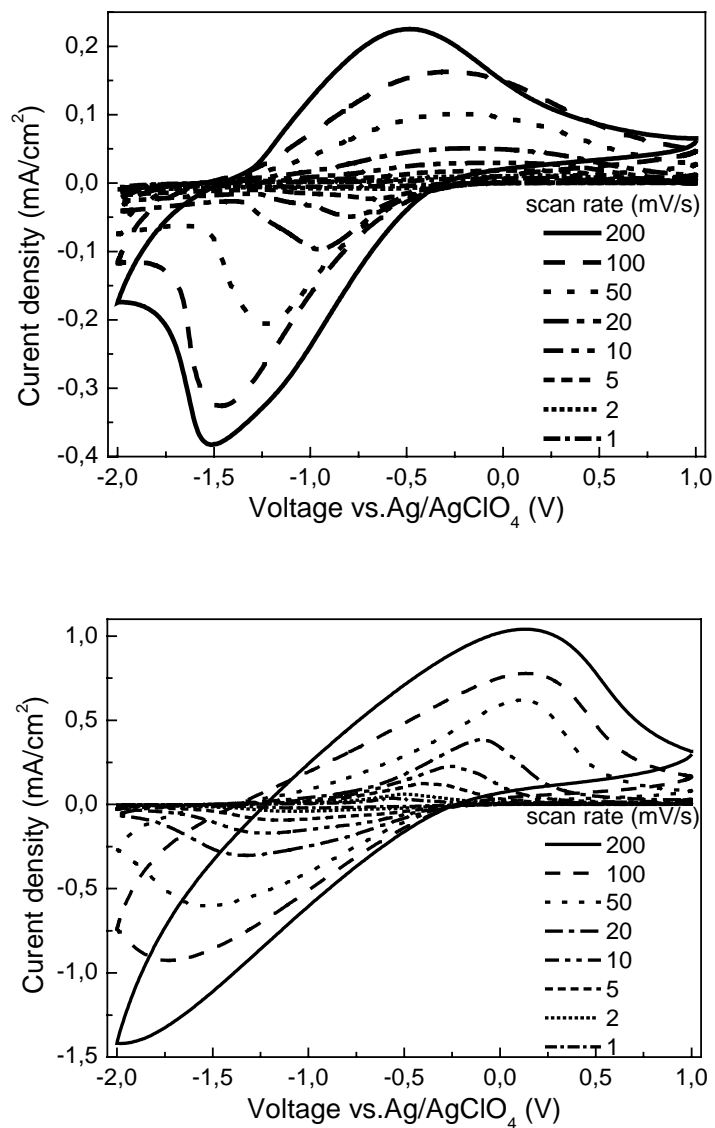


Fig. C-1 CV profile of sol-gel $(\text{CeO}_2)_{0.81}(\text{TiO}_2)_1$ layer measured with different scan rates in dry and wet (3 wt.% water) 1 M LiClO_4 in PC. Top: dry electrolyte; bottom: wet electrolyte with 3 wt.% water

D) XPS spectrum

The homogeneity of the $(\text{CeO}_2)_{0.81}(\text{TiO}_2)_1$ layer was tested by measuring 5 different probing points on a $2 \times 2 \text{ cm}^2$ as-deposited sample by XPS. The 5 points were taken at the 4 corners (1 to 4) and the center (5). The atom content of the layer is listed in Table D-1. From the mean value and the deviation, it can be seen that the layer is rather homogeneous. The ratio of Ce:Ti is 0.67 instead of 0.81 in the solution. It is possible that an enrichment of Ti on the surface is found due to diffusion induced by heat treatment. Therefore a depth-profile of Ce:Ti should be useful to check the homogeneity along the z direction [194].

Table D-1. Average atom content (atom%) of as-deposited $(\text{CeO}_2)_{0.81}(\text{TiO}_2)_1$ layer via XPS measurement

Position	O (1s)	Ti (2p)	C (1s)	Ce (3d)	Ce:Ti
1	51.72	9.97	32.29	6.02	0.60
2	51.60	9.16	33.31	5.94	0.65
3	50.67	8.40	34.86	6.08	0.72
4	49.75	9.21	34.45	6.59	0.71
5	50.07	9.25	34.42	6.26	0.68
mean	50.8 ± 0.9	9.2 ± 0.6	33.9 ± 1.1	6.2 ± 0.3	0.67 ± 0.05

The samples after 100 CV cycles in dry and wet 1 M LiClO_4 in PC in the deintercalated state have been also measured (Fig. D-1 and D-2). It was found that 14 atom% Li ions was left in the layer after cycling in the dry electrolyte whereas only 6 atom% Li ions remained in the layer when cycled in the wet electrolyte (Table D-2). The ratio of Ce(IV):Ce(III) after cycling in the dry electrolyte is 1.7, quite similar to that of the as-deposited layer (Ce(IV):Ce(III) = 1.8). On the contrary the ratio of Ce(IV):Ce(III) increases to 2.2 after 100 CV cycles in wet electrolyte. This maybe due to the stability increase of hydrated Ce(IV) [107].

Table D-2. Atom content of $(\text{CeO}_2)_{0.81}(\text{TiO}_2)_1$ layers after 100 CV cycles (-2 V/+1 V, 50 mV/s) in 1 M LiClO_4 in PC via XPS measurement.

Elements	O (1s)	Ti (2p)	C (1s)	Ce (3d)	Li (1s)	Ce(IV):Ce(II) I)
Sample 1*	44.8	1.8	38.1	1.6	13.7	1.7
Sample 2*	44.0	6.1	39.5	4.7	5.8	2.2

Sample 1: without water in the electrolyte.

Sample 2: with 3 wt.% water in the electrolyte

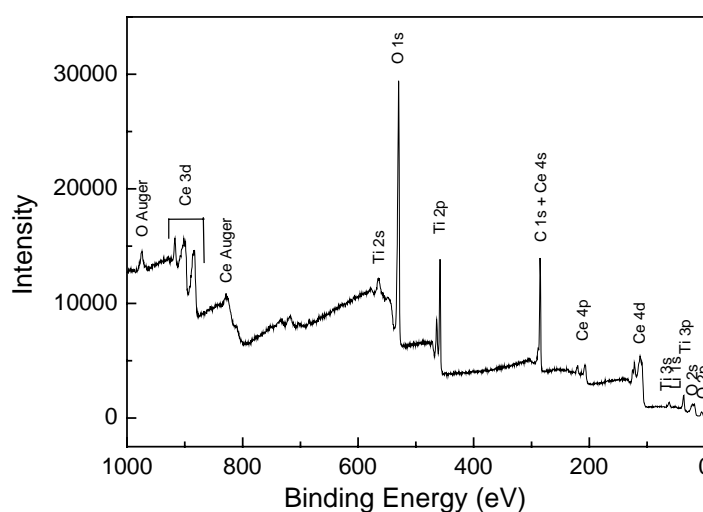
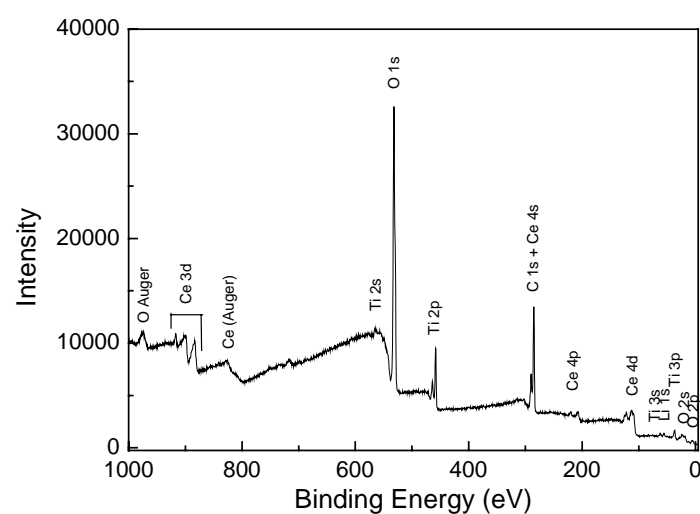


Fig. D-1 Overview of $(\text{CeO}_2)_{0.81}(\text{TiO}_2)_1$ layer after 100 CV cycles (-2 V/+1 V, 50 mV/s) in 1 M LiClO_4 in PC. Top: in dry electrolyte; bottom: in wet electrolyte with 3 wt.% water.

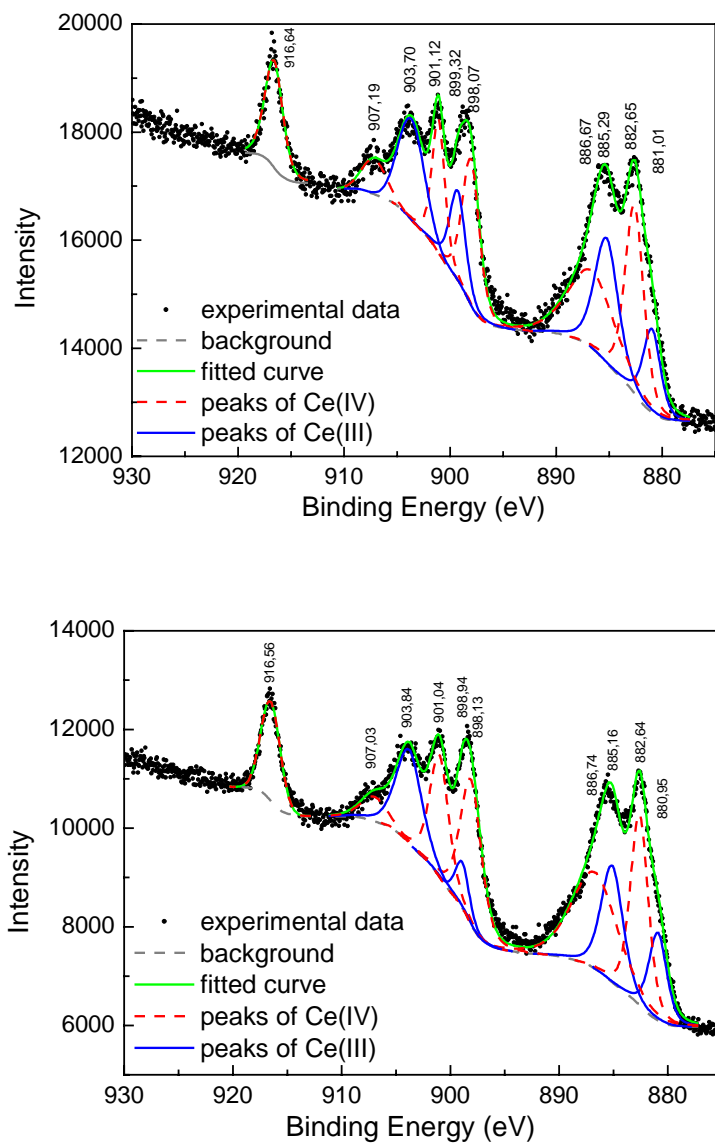


Fig. D-2 XPS Ce 3d spectra of the $(\text{CeO}_2)_{0.81}(\text{TiO}_2)_1$ layers after 100 CV cycles (-2 V/+1 V, 50 mV/s) in 1 M LiClO_4 in PC. Top: cycled in dry electrolyte (the ratio of Ce(IV):Ce(III) = 1.7); bottom: cycled in wet electrolyte with 3 wt.% water (the ratio of Ce(IV):Ce(III) = 2.2)

E) Results on EC devices with single and double sol-gel $(\text{CeO}_2)_{0.81}(\text{TiO}_2)_1$ layers as counter electrode.

The configuration of these devices was K-glass/ $\text{Nb}_2\text{O}_5:\text{Mo}$ ($\text{Mo}:\text{Nb} = 0.3$) (120 nm)/ inorganic-organic composite electrolyte/ $(\text{CeO}_2)_{0.81}(\text{TiO}_2)_1$ / K-glass. The list of devices tested is given in Table E-1.

Table E-1 List of EC devices with configuration K-glass/ $\text{Nb}_2\text{O}_5:\text{Mo}$ ($\text{Mo}:\text{Nb} = 0.3$) (120 nm)/ inorganic-organic composite electrolyte/ $(\text{CeO}_2)_{0.81}(\text{TiO}_2)_1$ / K-glass.

Nomenclature of EC device	$(\text{CeO}_2)_{0.81}(\text{TiO}_2)_1$ sol-gel layer			Water content in the inorganic-organic composite electrolyte (wt.%)
	Sintering temperature		Thickness (nm)	
	1 st layer	Final sintering temperature (°C)		
D(dry)_S(single)_450		450	180	0
W(wet)_S_450		450	180	3
D_D(double)_450a	150	450	360	0
W_D_450a	150	450	360	3
D_D_450b	200	450	360	0
W_D_450b	200	450	360	3
D_S_500		500	170	0
W_S_500		500	170	3
D_D_500a	150	500	340	0
W_D_500a	150	500	340	3
D_D_500b	200	500	340	0
W_D_500b	200	500	340	3
D_S_550		550	170	0
W_S_550		550	170	3
D_D_550a	150	550	340	0
W_D_550a	150	550	340	3
D_D_550b	200	550	340	0
W_D_550b	200	550	340	3

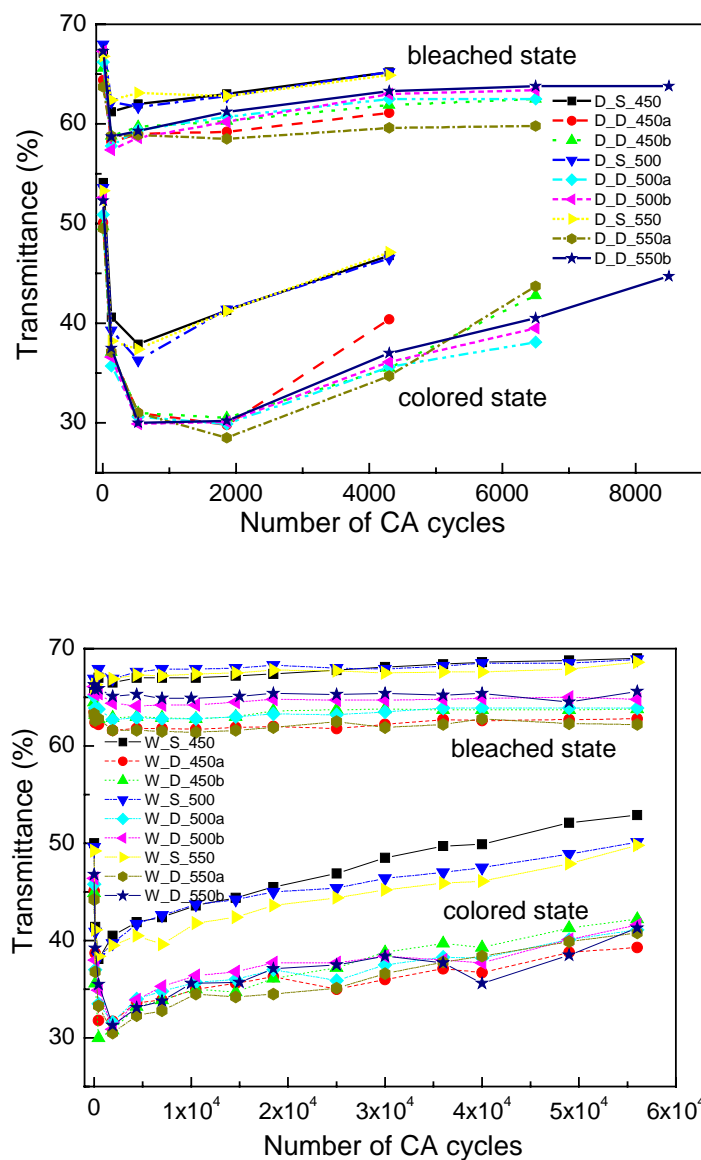


Fig. E-1 Change of transmittance at $\lambda = 550$ nm of EC-devices listed in Table E-1 with configuration K-glass/ $\text{Nb}_2\text{O}_5:\text{Mo}$ (120 nm)/ inorganic-organic composite electrolyte/ $(\text{CeO}_2)_{0.81}(\text{TiO}_2)_1$ / K-glass as a function of the number of CA cycles (-2.5 V, 120 s/ +2.5 V, 120 s). Top: with dry electrolyte; bottom: with wet electrolyte (3 wt.% water)

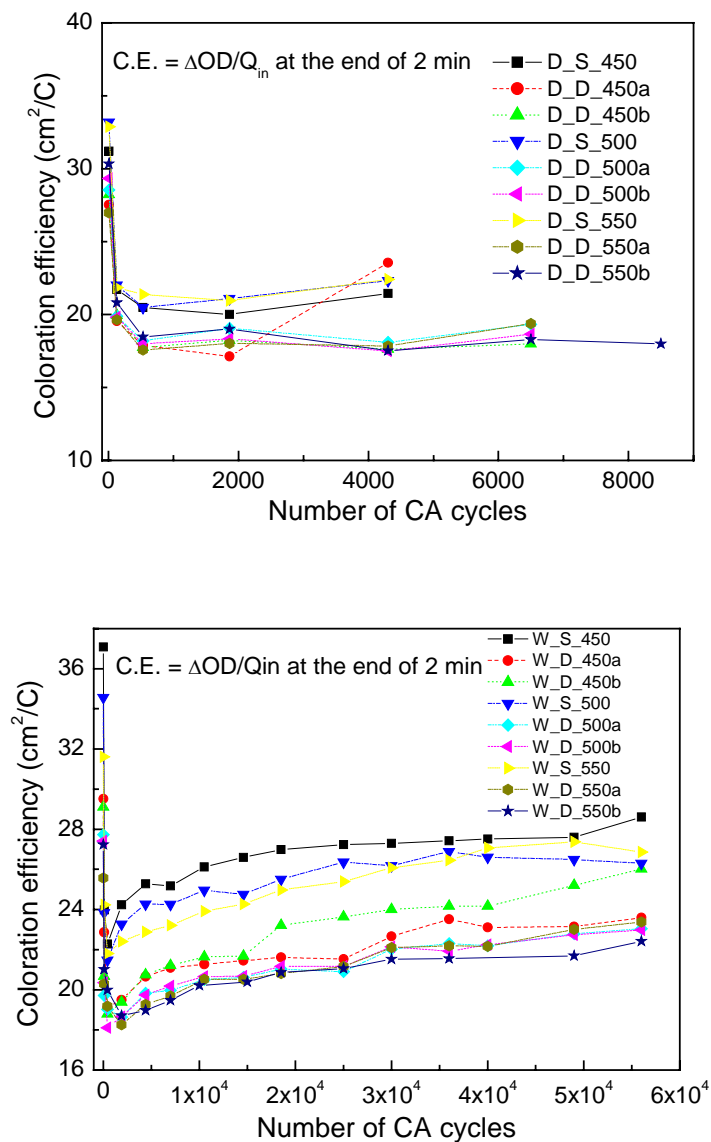


Fig. E-2 Coloration efficiency C.E. of EC-devices listed in Table E-1 with configuration K-glass/ $\text{Nb}_2\text{O}_5:\text{Mo}$ (120 nm)/ inorganic-organic composite electrolyte/ $(\text{CeO}_2)_{0.81}(\text{TiO}_2)_1$ / K-glass as a function of the CA-cycle number. ($\lambda = 550 \text{ nm}$; -2.5 V , 120 s). Top: with dry electrolyte; bottom: with wet electrolyte (3 wt.% water)

F) Devices made with NiO_x-TiO₂ as ion storage layer

i) Devices made with composite electrolyte

A small amount of water added to the inorganic-organic composite electrolyte has a favorable effect on the electrochromic properties of the devices made with (CeO₂)_{0.81}(TiO₂)₁ as ion storage layers and cathodic electrochromic colored layers. In order to check this effect on anodic electrochromic materials, NiO_x-TiO₂ made by the sol-gel process was selected and used to make electrochromic devices built with a cathodic EC material (WO₃ or Nb₂O₅).

Four cells with the configuration glass/ FTO/ Nb₂O₅:Mo (Mo:Nb = 0.3)(120 nm)/ inorganic-organic composite electrolyte/ NiO_x-TiO₂ (Ni:Ti = 3) (225 nm)/ FTO/ glass were prepared and tested. The details about these devices are listed in Table F-1.

Table F-1 EC devices with configuration glass/ FTO/ Nb₂O₅:Mo (Mo:Nb = 0.3)/ inorganic-organic composite electrolyte/ NiO_x(TiO₂)(Ni:Ti = 3)/ FTO/ glass

Sample nomenclature	Li ⁺ preloading condition of Ni layer	Water content in composite electrolyte (wt.%)
Cm0	No preloading	3
Cy0	No preloading	0
Cm1	Preloading in 1 M LiClO ₄ in PC with 3 wt.% water with -2.6 V vs. Ag/AgClO ₄ for 300 s, charge intercalated was 24 mC/cm ²	3
Cy1	Same treatment as Cm1. The charge intercalated was 25.3 mC/cm ²	0

According to the work of Decker et al. [195], a preloading of the NiO_x-TiO₂ layer with lithium ions is supposed to “activate” the host structure for a subsequent fast and reversible insertion and deinsertion process of lithium ions. The process is expressed according to the following electrochemical reaction



The first CV profiles of these devices are shown in Fig. F-1. The CV profile of the devices with NiO_x-TiO₂ sol-gel layer without preloading has a cathodic peak and an anodic peak, but the current density is very small. With NiO_x-TiO₂ sol-gel layer preloaded with Li⁺, there are one cathodic peak and two anodic peaks in the scan range from -2.5 V to +1.5 V and the current peaks are higher. The CV shapes of the devices with wet and dry composite electrolyte are similar and hence the mechanism of Li⁺ intercalation is not changed by adding water to the electrolyte.

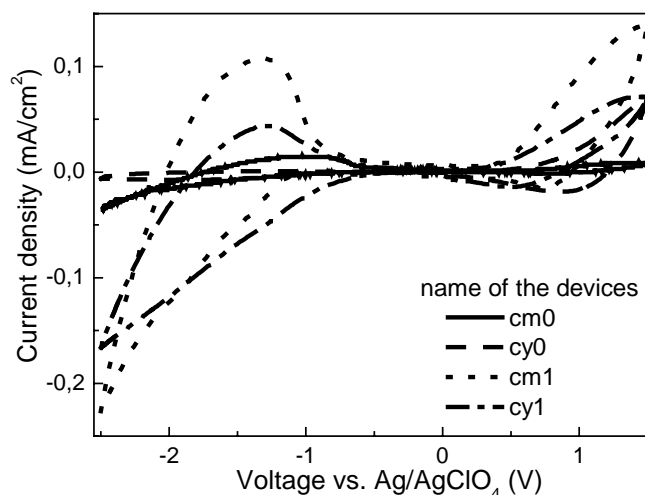


Fig.F-1 The 1st CV cycle of EC devices with configuration glass/ FTO/ Nb₂O₅:Mo (Mo:Nb = 0.3)/ inorganic-organic composite electrolyte/ NiO_x(TiO₂) (Ni:Ti = 3)/ FTO/ glass. Scan rate: 50 mV/s.

The optical characteristics of these cells during the first CA cycle (-2.5 V, 2 min/ +1.5 V, 2 min) are listed and shown in Table F-2 and Fig. F-2. With dry composite electrolyte, the change of the optical density (ΔOD) of the device with nonpreloaded NiO_x-TiO₂ layer is 0.33, bigger than that of the device with preloaded NiO_x-TiO₂ layer. But the transmittance reversibility is worse. The transmittance of the bleached state changes from 65% to 56% after the 1st CA cycle of the device with unpreloaded NiO_x-TiO₂ layer, whereas it changes only 3% for the device with preloaded NiO_x-TiO₂ layer.

With wet composite electrolyte, the change of the optical density is larger than that with dry electrolyte whatever the NiO_x-TiO₂ layer is. ΔOD is 0.35 for the device with nonpreloaded NiO_x-TiO₂ layer and 0.39 for the device with preloaded NiO_x-TiO₂ layer. The reversibility of the transmittance change is also better. The difference between the bleached states after the first cycle is 4% and 3% for the device with unpreloaded and preloaded NiO_x-TiO₂ layer respectively. With wet composite electrolyte, the optical properties of the devices with NiO_x-TiO₂ layer are improved. Preloading of the NiO_x-TiO₂ layer leads to a better contrast by improving the transmittance of the bleached state.

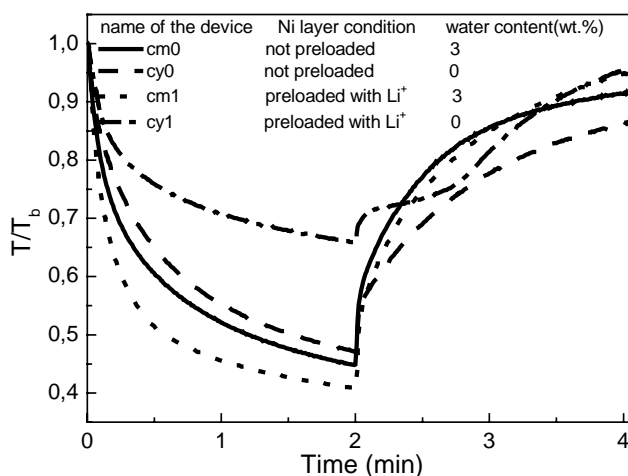


Fig. F-2 Normalized transmittance of EC devices with configuration glass/ FTO/ Nb₂O₅:Mo (Mo:Nb = 0.3)/ inorganic-organic composite electrolyte/ NiO_x(TiO₂) (Ni:Ti = 3)/ FTO/ glass. (the 1st CA: -2.5V, 2min/ +1.5V, 2min)

Table F-2 Optical characteristics of EC devices with configuration glass/ FTO/ Nb₂O₅:Mo (Mo:Nb = 0.3)/ inorganic-organic composite electrolyte/ NiO_x(TiO₂) (Ni:Ti = 3) / FTO/ glass during the 1st CA cycle (-2.5V, 2min/ +1.5V, 2min)

Nomenclature of EC devices	T _{b1} * (%)	T _c * (%)	T _{b2} * (%)	ΔOD*	Q _{in} (mC/cm ²)	C.E. (cm ² /C)
Cm0	46.0	20.7	42.1	0.35	15	23
Cy0	64.6	30.4	55.8	0.33	11	30
Cm1	49.5	20.2	46.9	0.39	17	23
Cy1	52.6	34.5	50.4	0.18	7	26

T_{b1}: transmittance at 550 nm before the CA cycle

T_{b2}: transmittance at 550 nm after the CA cycle

T_c: transmittance at 550 nm after applying -2.5 V for 2 minutes

ΔOD = log(T_{b1}/T_c)

Except for device cy1 (preloaded with Li⁺, with dry composite electrolyte), the coloring behavior of these devices is rather good during the initial cycles. ΔOD reaches 0.4 with the cell cm1 (preloaded with Li⁺, with wet composite electrolyte) and the transmittance in the colored state can be as low as 20% at 550 nm. From the value listed in Table F-2, it is clearly seen that the electrochromic properties, charge intercalated and transmittance change of the devices could be improved if a certain amount of water is added to the composite electrolyte. The reversibility of the devices was improved by preloading the NiO_x-TiO₂ layer with Li⁺. T_{b2} - T_{b1} is about 3% by the

device with pretreatment of NiO_x-TiO₂ layer instead of 10% (cy0) and 4% (cm0) with a NiO_x-TiO₂ sol-gel layer without pretreatment.

No matter how good the devices were during the initial cycling, those with 3 wt.% water added to the electrolyte were destroyed after about 40 cycles, and the two devices without water in the composite electrolyte after about 50 cycles. There were cracks and delamination in the devices. An optical analysis shows that these defects occurred at the interface of the electrolyte and the NiO_x-TiO₂ sol-gel layer, in a way similar to that seen for devices made with (CeO₂)_{0.81}(TiO₂)₁ as counter electrode (Fig. 5.78 and 5.79).

ii) Devices made with liquid electrolyte

In order to test the property of the devices with different electrolytes, liquid electrolyte 1 M LiClO₄ in PC was thought to be a good substitute for the solid electrolyte. EC devices with configuration K-glass/ EC-layer/ 1 M LiClO₄ in propylene carbonate (PC)/ NiO_x-TiO₂/ K-glass have been prepared. The detail for every device is listed in Table F-3.

Table F-3. Condition for EC devices with 1 M LiClO₄ in PC as electrolyte and NiO_x-TiO₂ as counter electrode.

Sample nomenclature	EC-layer	Water content in PC (wt.%)
L1	Nb ₂ O ₅ :Mo (Mo:Nb = 0.3)	0
L2	WO ₃	0
L3	Nb ₂ O ₅ :Mo (Mo:Nb = 0.3)	3
L4	WO ₃	3

For the devices with Nb₂O₅:Mo (Mo:Nb = 0.3) as EC layer, CA cycles (-2.5 V, 2 min/ 2 V, 2 min) have been applied. For the other two the conditions were -2 V, 2 min/ 2 V, 2 min. The devices were only cycled up to about 70 cycles before they were destroyed.

As NiO_x-TiO₂ layer is an anodic electrochromic material, devices made with this layer as counter electrode showed a rather high transmittance change. This is especially observed for the L4 device having the configuration K-glass/ WO₃/ 1 M LiClO₄ in propylene carbonate (3 wt.% water)/ NiO_x-TiO₂/ K-glass. Large ΔOD (~0.7) is observed during the 9th cycle, but this value strongly decreased to 0.3 in the 70th CA cycle (Fig. F-3). The change of the optical density (ΔOD) of the devices with wet electrolyte is generally larger than that with dry electrolyte.

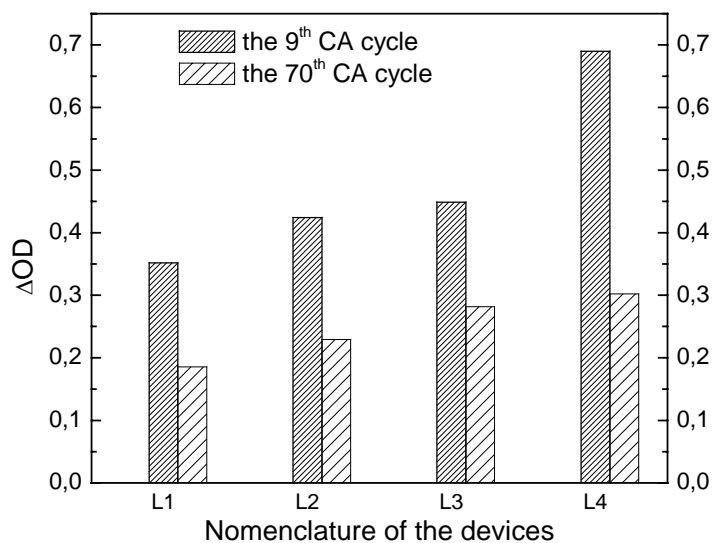


Fig. F-3. ΔOD of different devices measured at the 9th and 70th CA cycle. (L1, L3: -2.5 V, 2 min/ +2 V, 2 min; L2, L4: -2 V, 2 min/ +2 V, 2 min).

The coloration efficiency C.E. of the devices measured during the 9th and 70th CA cycle are shown in Fig. F-4. The device with the dry electrolyte has a higher C.E. than that with the wet electrolyte. The C.E. of L2 at the 9th cycle is 50 cm²/C, higher than that of the WO₃ layer in liquid electrolyte (C.E. \approx 35 mC/cm²). This is caused by the parallel coloration of the anodic electrochromic NiO_x-TiO₂ layer with the cathodic electrochromic WO₃ layer. Except for Device L1, the C.E. of the 70th cycle is smaller than that of the 9th cycle.

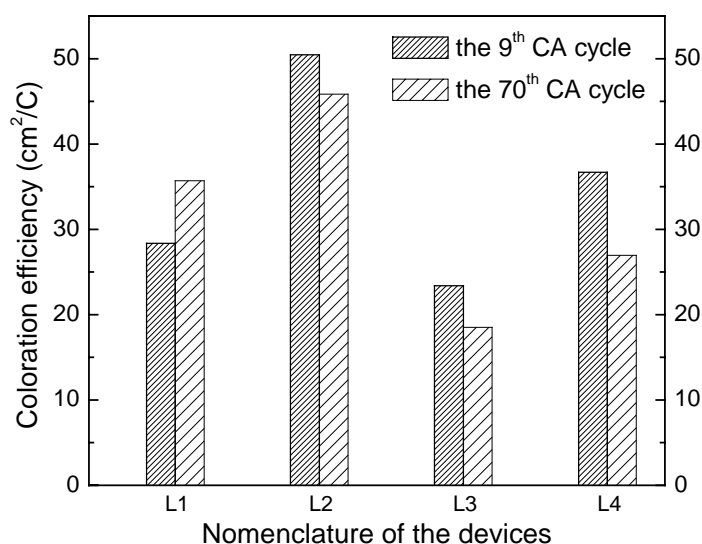


Figure F-4. C.E. of different devices at the 9th and 70th CA cycle. (L1, L3: -2.5 V, 2 min/ +2 V, 2 min; L2, L4: -2 V, 2 min/ +2 V, 2 min).

The electrochemical properties of the devices were also measured by Chronopotentiometry (CP) after their 10th CA cycle. The current density used for the CP was $\pm 10 \mu\text{A}/\text{cm}^2$ and was applied for 2000 s or until the potential reached ± 3 V, respectively (Fig. F-5). The potential vs. the charge density and the time are shown in Fig. F-5. The potential to time slope of the devices with “wet” electrolyte is smaller. By reaching the same charge density, 20 mC/cm^2 , the voltage of the devices with “wet” electrolyte is only about -2 V, the others reach about -2.5 V in the same time. When the charge intercalated reached 20 mC/cm^2 , the ΔOD of the cell with configuration K-glass/ WO_3 / 1 M LiClO_4 in propylene carbonate (PC) (0 wt.% water)/ $\text{NiO}_x\text{-TiO}_2$ / K-glass reaches 0.85 and the C.E. value reaches $42.5\text{cm}^2/\text{C}$, both values being very promising. The devices made with niobium oxide as EC layer could not reach such a high ΔOD because the transmittance of the bleached state was lower (about 60%) and the transmittance of the colored state did not reach values as low as those of the devices with tungsten oxide could reach. The charge deintercalation procedure includes two parts separated by one kink at 500 s for the “dry” devices and 200 s for the “wet” devices, that are corresponding to CV anodic peaks in Fig. F-1. Most charge deintercalation happened during the second deintercalation parts, including 12.5 mC/cm^2 for the “dry” devices and 15 mC/cm^2 for the “wet” devices. The slope of the potential to time before the first kink are similar for all devices, but larger during the second part of the “dry” devices than that of the “wet” devices. This cause the irreversible ion intercalation in the “dry” devices is larger than that of the “wet” devices.

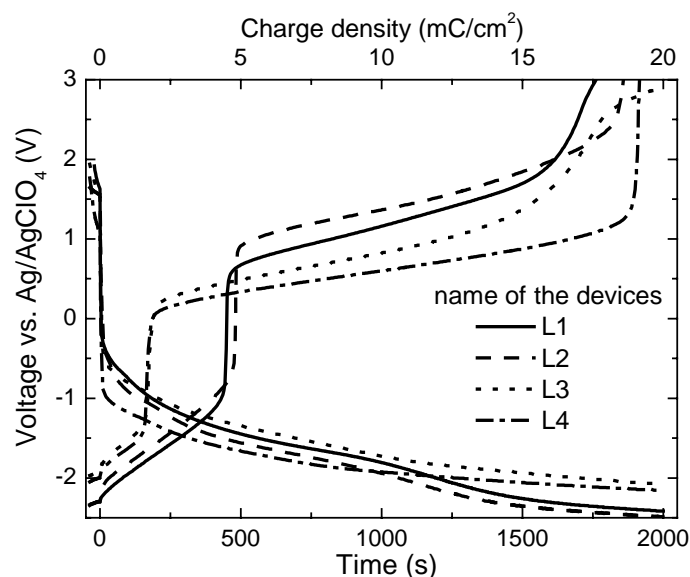


Fig. F-5: Potential vs. time or charge density of EC devices with the configuration K-glass/ EC-layer/ 1 M LiClO_4 in propylene carbonate (PC) / $\text{NiO}_x\text{-TiO}_2$ / K-glass during CP process after 9 CA cycles. ($I_0 = 10 \mu\text{A}/\text{cm}^2$, $\lambda = 550$ nm)

Comparing the transmittance change caused by CA and CP, ΔOD of L2 is drastically improved from 0.42 (9th CA cycle) to 0.85 (CP) (Table F-4) because of the increase of the charge intercalated

and higher voltage (-2.5 V instead of -2 V) are applied. There are no obvious difference between the results obtained with the CA and CP processes for the device L3 and L4. Because the kinetics of these two devices is fast enough so that more charge can be intercalated into the layer in 2 minutes and the voltage during CA was as high as reached during CP. Without water in the liquid electrolyte, the charge intercalated during CA is smaller than that during CP, because for wet electrolyte -2 V is enough whereas in the dry electrolyte it needs -2.5 V. Water in the liquid electrolyte improved the kinetics of Li^+ intercalation process hence improved the electrochromic properties of the EC devices.

Table F-4 EC results of devices L1 to L4

Nomenclature	Results from 9 th CA			Results from CP cycle after 9 th CA cycle		
	ΔOD	Q_{in} (mC/cm ²)	C.E. (cm ² /C)	ΔOD	Q_{in} (mC/cm ²)	C.E. (cm ² /C)
L1	0,35	12,4	28,4	0,48	20	24
L2	0,42	8,4	50,5	0,85	20	42,5
L3	0,45	19,2	23,4	0,42	20	21
L4	0,69	18,8	36,7	0,67	20	33,5

The results obtained with liquid electrolyte are similar to those obtained with the inorganic-organic composite electrolyte. A certain amount of water added to the electrolyte improved the kinetics of the charge intercalation and deintercalation. The devices made with $\text{NiO}_x\text{-TiO}_2$ and WO_3 have a large transmittance change, the maximum ΔOD being 0.85 (by CP: $I_0 = \pm 10 \mu\text{A}/\text{cm}^2$).

Unfortunately the devices worked only during 50 cycles with solid electrolyte and less than 100 cycles with liquid electrolyte.

iii) Devices made with a modified $\text{NiO}_x\text{-TiO}_2$ layer

Because of the strong oxidizing ability of nickel oxide, the electrolytes currently used for cerium-titanium oxide cannot be used as the decomposition of the electrolyte is strongly accelerated. Some trials have been done to circumvent this observation by covering the nickel-titanium oxide layer with a cerium-titanium oxide sol-gel layer.

The $\text{NiO}_x\text{-TiO}_2$ and $(\text{CeO}_2)_{0.81}(\text{TiO}_2)_1$ layers were made as described before. After the deposition of $(\text{CeO}_2)_{0.81}(\text{TiO}_2)_1$, the system was heated at $300\text{ }^\circ\text{C}$ for 15 minutes. The thickness of the $\text{NiO}_x\text{-TiO}_2$ layer was about 225 nm, that of the $(\text{CeO}_2)_{0.81}(\text{TiO}_2)_1$ was 30 nm only.

The configuration of the devices was K-glass/ $\text{Nb}_2\text{O}_5\text{:Mo}$ (Mo:Nb = 0.3)/ inorganic-organic composite electrolyte/ $(\text{CeO}_2)_{0.81}(\text{TiO}_2)_1$ / $\text{NiO}_x\text{-TiO}_2$ / K-glass. Unfortunately, the charge capacity was sharply impaired by the presence of the added layer. After applying -2.5 V for 2 minutes to the devices, the transmittance change of the “dry” device was only 3% and the intercalated charge was only 0.02 mC/cm^2 (for the same device without layer covering, ΔT was 27% and ΔQ was 11 mC/cm^2) (Fig. F-6), and the transmittance change of the “wet” device was less than 10% and the intercalated charge was only 1.6 mC/cm^2 (for the same device without covering, ΔT was 43% and ΔQ was 15 mC/cm^2).

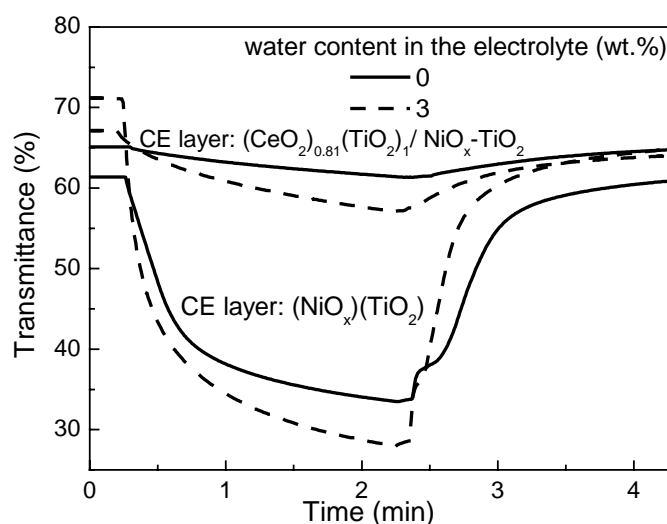


Fig. F-6. Transmittance change during the 1st CA ($-2.5\text{V}/2\text{min}$; $2.5\text{V}/2\text{min}$) cycle for the device with configuration K-glass/ $\text{Nb}_2\text{O}_5\text{:Mo}$ (Mo:Nb = 0.3)/ inorganic-organic composite electrolyte/ CE/ K-glass

The devices were also destroyed after 40 to 50 cycles. Cracks occur and many point defects were found in the nickel-titanium oxide layer but the niobium oxide layer remains smooth (Fig. F-7).

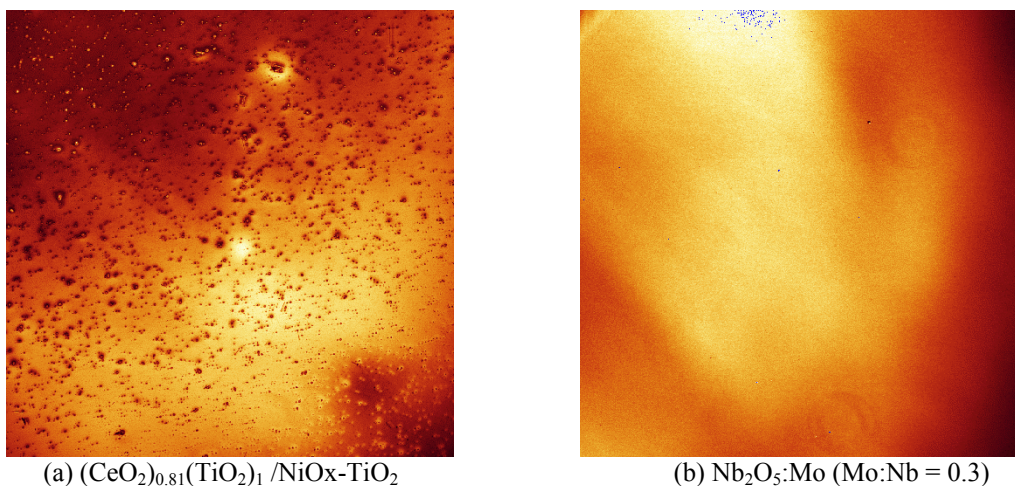


Fig. F-7 Microscopy of the $(\text{CeO}_2)_{0.81}(\text{TiO}_2)_1/\text{NiO}_x\text{-TiO}_2$ sol-gel layer and the $\text{Nb}_2\text{O}_5:\text{Mo}$ (Mo:Nb = 0.3) sol-gel double layer in the electrochromic device with the configuration K-glass/ $\text{Nb}_2\text{O}_5:\text{Mo}$ (Mo:Nb = 0.3)/inorganic-organic composite electrolyte/ $(\text{CeO}_2)_{0.81}(\text{TiO}_2)_1/\text{NiO}_x\text{-TiO}_2$ /K-glass by CLSM. Measured area: $1.5 \times 1.5 \text{ mm}^2$

In conclusion water has a similar effect for $\text{NiO}_x\text{-TiO}_2$ layer as for $(\text{CeO}_2)_{0.81}(\text{TiO}_2)_1$ layer. Using the layer as ion storage layer in an electrochromic device, the devices show a larger transmittance change because the ion intercalating kinetics is improved. But because of the strong oxidizing property of nickel oxide, the devices made with $\text{NiO}_x\text{-TiO}_2$ sol-gel layer as ion storage layer had a lifetime limited to less than 100 cycles. A 30 nm $(\text{CeO}_2)_{0.81}(\text{TiO}_2)_1$ sol-gel layer deposited on top of the $\text{NiO}_x\text{-TiO}_2$ layer totally impaired the ion storage capacity of the $\text{NiO}_x\text{-TiO}_2$ layer, and did not improve the lifetime of the devices.

G) List of chemicals used in this work:

Chemicals	Symbol	Supplier	Purity (%)
niobium(V) chloride	NbCl ₅	Chempur	99+
phosphomolybdic acid hydrate	H ₃ [P(Mo ₃ O ₁₀) ₄] _x H ₂ O	Fluka	≥ 98,5
acetic acid	CH ₃ COOH	RdH	99-100
cerium(III) nitrate hexahydrate	Ce(NO ₃) ₃ ·6H ₂ O	Chempur	99.9
tetraisopropyl orthotitanate	Ti(OCH(CH ₃) ₂) ₄	Fluka	≥ 95
ammonium cerium(IV) nitrate	(NH ₄) ₂ Ce(NO ₃) ₆	Fluka	≥ 99
acetyl acetone	CH ₃ COCH ₂ COCH ₃	Fluka	≥ 98,0
titanium(IV) n-propoxide	Ti(C ₃ H ₇ O) ₄	Heraeus	≥ 90
ammonium cerium(IV) nitrate	Ni(CH ₃ COO) ₂ ·4H ₂ O	Fluka	≥ 99
3-Glycidyloxypropyl-trimethoxysilane (GPTS)	C ₉ H ₂₀ O ₅ Si	ABCR	≥ 98
tetraethylene glycol (TEG),	HO(CH ₂ CH ₂ O) ₃ CH ₂ CH ₂ OH	Acros Organics	≥ 99,5
lithium perchlorate anhydrous	LiClO ₄	Fluka	≥ 98,0
zirconium(IV) n-propoxide	Zr(OC ₃ H ₇) ₄	Chempur	70% solution in propanol
propylene carbonate	C ₄ H ₆ O ₃	Fluka	puriss: ≥ 99,0
silver perchlorate	AgClO ₄	RdH	≥ 98,5
hydrogen peroxide	H ₂ O ₂	Fluka	30% in water
tungsten powder	W	Chempur	99,9

H) List of equipments used in this work

Measurements	Equipment	Supplier
Dip Coater	iselautomation CNC Kontroller C142-1	Rosenberg Elektronik Messtechnik & Datenierabteilung
Film Thickness	Profilometer, P10 surface Profiler	TENCOR
Transmittance	CARY 5E UV-Vis-NIR Spectrophotometer	Varian
Heat treatment up to 300°C	furnace	Heraeus
Heat treatment up to 600°C	furnace	Carbolite
Special atmospheres heat treatment	Protective gas tube furnace (Gero furnace)	GERO GmbH
Electrochemical measurement	VMP2 Multichannel Potentiostat and Potentiostat/ Galvanostat Model 273A	Princeton Applied Research
Microbalance	Research Quartz Crystal microbalance	MAXTEK
High Resolution Transmittance Electron Microscope (HRTEM)	CM200 FEG	Philips
Confocal Laser Scanning Microscopy	TCS SP2 with green 543nm Laser	Leica
X-ray Diffraction	XRD D500	Siemens
Thermal Analysis (DTA/TG) Combined with Mass Spectroscopy and FTIR	STA 449C/ 3G Jupiter QMS403C Aeolos TENSOR27-FTIR	Netzsch Netzsch Brucker
Substrate cleaning	Wash machine, Professional IR 6001	Miele
X ray Photoelectron Spectroscopy	M-Probe with Al-K α 1486,6eV monochromatic radiation	SSI Surface Science Instruments

References

1. Aegerter M.A. "Sol-gel chromogenic materials and devices" In Structure and Bonding, Vol. **85**, Reisfeld R., Jorgensen C.K. eds. Springer-Verlag, Berlin, 1996, p. 149-194
2. Granqvist C.G., Handbook of Inorganic Electrochromic Materials, Elsevier, Amsterdam, 1995.
3. Monk P.M.S., Mortimer R.J., Rosseinsky D.R., Electrochromism-Fundamentals and Applications VCH, Weinheim, 1995
4. Lampert C.M. (1998) "Smart switchable glazing for solar energy and daylight control", *Solar Energy Materials and Solar Cells* **52**: 207 – 221.
5. Lampert C.M., Agrawal A., Baertlien C., Nagai J. (1999) "Durability evaluation of electrochromic devices- an industry perspective", *Solar Energy Materials and Solar Cells* **56**: 449 – 463.
6. Lampert C.M. (2003) "Large-area smart glass and integrated photovoltaics", *Solar Energy Materials and Solar Cells* **76**: 489 – 499.
7. Lee E.S., DiBartolomeo D.L. (2002) "Application issues for large-area electrochromic windows in commercial buildings", *Solar Energy Materials and Solar Cells* **71**:465-491.
8. Elshabini A., Barlow F., Thin Film Technology Handbook, McGraw-Hill, New York, 1998
9. Anderson J., Boudart M., Catalysis: Science and Technology, 1, Springer-Verlag, Berlin, 1981
10. Talbot D., Talbot J., Corrosion Science and Technology, CRC Press, Boca Raton, 1998
11. Madou M., Morison S., Chemical Sensing with Solid State Devices, Academic Press, Inc., Boston, 1989
12. Chopra K., Kaur I., Thin Film Device and Applications, Plenum Press, New York, 1983
13. Nitzsche K., Schichtmeßtechnik, 1, Vogel Buchverlag, Würzburg, 1996
14. Ohring M., The Material Science of Thin Films, Academic Press, INC., San Diego, 1992
15. Pulker H., Coatings on Glass, second revised edition. Elsevier Science, Amsterdam, 1984
16. Szanyi J. (2002), "The origin of haze in CVD tin oxide thin films", *Applied Surface Science* **185**: 161
17. Kozuka H., Kajimur M., Hirano T., Katayama K. (2000) "Crack-free, thick ceramic coating films via non-repetitive dip-coating using polyvinylpyrrolidone as stress-relaxing agent", *Journal of sol-Gel Science and Technology* **19**: 205
18. Brinker C.J., Scherer G.W., Sol-Gel Science: the Physics and Chemistry of Sol-Gel Processing, Academic Press, INC, San Diego, 1990
19. <http://www.chemat.com/html/solgel.html>
20. Livage J., "Basic Principles of sol-gel chemistry", in: Aegerter M.A., Mennig M. eds. "Sol-gel Technologies for Glass producers and Users", Kluwer Academic Publishers, 2004, p1
21. Landau L.D., Levich B.G.(1942) *Acta Physiochem*, **17**: 42
22. Schmidt H., Mennig M., <http://www.solgel.com/articles/Nov00/mennig.htm>, 2000

23. Brinker C.J., Hurd A.J., Ward K.J. in *Ultrastructure Processing of Advanced Ceramics*, Eds. Mackenzie J.D., Ulrich D.R., Wiley, New York (1988) 223
24. Stern Z.O., (1924) "Zur Theorie der elektrolytischen Doppelschicht", *Z. Electrochem.* **30**: 508
25. Brinker C.J., Hurd A.J., Schunk P.R., Frye G.C., Ashley C.S. (1992) "Review of sol-gel thin-film formation", *Journal of Non-Crystalline Solids* **147**: 424-436
26. Wright J.D., Sommerdijk N.A.J.M., *Sol-Gel Materials-Chemistry and Applications*, Gordon and Breach Science Publishers
27. Rauh R.D., (1999) "Electrochromic windows: an overview", *Electrochim.Acta* **44**: 3165.
28. O'Brian N.A., Gordon J., Mathew H., Hichwa B.P. (1999) "Electrochromic coatings-applications and manufacturing issues", *Thin Solid Films* **345**: 312 – 318
29. Dornan C.A., Habibi H., Lynam N.R., McCabe I.A., "Electrochromic Mirrors and Devices", Donnelly Corp. WO Patent 95 30 495 (1994).
30. Bauer F.T., Bechtel J.H., "Automatic rearview mirror for automotive vehicles", Gentex Corp., US Patent 4,443,057 (1984).
31. Bechtel J.H., Byker H.J., "Automatic rearview mirror system for automotive vehicles", Gentex Corp., US Patent 4,917,477 (1990)
32. Byker H.J., "Single-compartment, self-erasing, solution-phase electrochromic devices, solutions for use therein, and uses thereof", Gentex Corp., US Patent 4,902,108 (1990)
33. Byker H.J., "Variable reflectance motor vehicle mirror", Gentex Corp., US Patent 5,128,799 (1992)
34. Al-Dahoudi N., "Wet chemical deposition of transparent conducting coatings made of redispersible crystalline ITO nanoparticles on glass and polymeric substrates" Ph.D Thesis, Institute für Neue Materialien, INM and Universität des Saarlandes, Saarbrücken, Germany, 2003
35. Heusing S., Aegerter M.A., "Sol-gel coatings for electrochromic devices". in Sakka S. Eds. "Handbook of Sol-Gel Science and Technology: Processing Characterization and Applications" Vol. III: Applications of Sol-Gel Technology Kluwer Academic Publishers (2005) 719 - 760
36. Granqvist C.G., "Transparent Conductive Electrodes for Electro chromic Devices: A Review", *Appl.Phys.* 1993; A57:19-24
37. Vaivars G., Furlani M., Mellander B.-E., Granqvist C.G., (2003) "Proton-conducting zirconium phosphate/ poly(vinyl acetate)/ glycerine gel electrolytes", *J. Solid State Electrochem.* **7**: 724 – 728
38. Truong V.V., Giroud F.E., Ashrit P.V., (1990) "Large-Area Chromogenics: Materials and Devices for Transmittance control", eds. Lampert C.M., Granqvist C.G. SPIE, Optical Engineering Press, Bellingham, Washington, p. 386
39. Agrawal A., Cronin J.P., Zhang R., (1993), "Review of solid state electrochromic coatings using sol-gel techniques", *Solar Energy Materials and Solar Cells*; **31**: 9-21.
40. Kraus T (1953) unpublished report (Balzers, Liechtenstein)
41. Deb S.K., (1969) "A novel electrophotographic system" *Applied optics /Supplement*, **3**: 192

42. Deb S.K., (1973) "Optical and photoelectric properties and color centers in thin-films of tungsten oxide", *Phil. Mag.*, **27**: 801
43. Gazotti W. A., Casalbore-Miceli G., Geri A., Berlin A., De Paoli M. A., (1998) "An all-plastic and flexible electrochromic device based on elastomeric blends" *Adv. Mater.*, **10**: 1522.
44. De Paoli M. A., Casalbore-Miceli G., Giroto E. M., Gazotti W. A., (1999) "All polymeric solid state electrochromic devices", *Electrochim. Acta*, **44**: 2983.
45. De Paoli M. A., Nogueira A. F., Machado D. A., Longo C., (2001) "All-polymeric electrochromic and photoelectrochemical devices: new advances", *Electrochim. Acta*, **46**: 4243.
46. Heuer H. W., Wehrmann R., Kirshmeyer S., (2002) "Electrochromic window based on conducting poly (3,4-ethylenedioxythiophene)poly(styrene sulfonate)" *Adv. Funct. Mater.*, **12**: 89.
47. www.ne.se
48. Nagai J., Kamimori T., Mizuhashi M., "Mechanism of long-term Change in electrochromism of Li_2WO_3 films", *Proc. SPIE* 1984; **502**: 59
49. Cogan S.F., Plante T.D., Parker M.A., Rauh R.D., (1986) "Electrochromic solar attenuation in crystalline and amorphous Li_2WO_3 ", *Solar energy Materials and Solar Cells* **14**: 185
50. Svensson J.S.E.M., Granqvist C.G., (1985), "Electrochromic coatings for smart windows-crystalline and amorphous WO_3 films", *Thin Solid Films* **126**(1-2): 31-36
51. Chemseddine A., Morineau R., Livage J., (1983), "Electrochromism of colloidal tungsten oxide", *Solid State Ionics* **9-10**: 357
52. Xu G., Chen L., (1988), "Lithium diffusion in WO_3 films", *Solid State Ionics* **28-30** 1726
53. Judeinstein P., Livage J., (1989), "Role of the water-content on the electrochromic properties of $\text{WO}_3 \cdot n\text{H}_2\text{O}$ thin-films", *Materials Science and Engineering B* **133**: 129
54. Yamanaka K., (1981), "The electrochromic properties of thermally decomposed films of an organic tungsten compound", *Jpn J. Applied Physics* **20** : L307
55. Oi J., Kishimoto A., Kudo T., (1992),"Hexagonal tungsten trioxide obtained from peroxopolytungstate and reversible lithium electro-intercalation into its framework", *J. Solid State Chemistry* **96**: 13
56. Yamanaka K., Ohkawoto H., Kidon H., Kudo T., (1986), "Peroxytungstic acid coated films for electrochromic display devices", *Jpn. J. Applied Physics* **25**: 1420
57. Itoh K., Okamoto T., Wakita S., NiiKura H., Murabayashi M., (1991), "Thin-films of peroxopolytungstic acids – Applications to optical wave-guide components", *Appl. Organometallic Chem.* **5**: 295
58. Cronin J. P., Tarico D. J., Agrawal A., Zhang R. L., "Method for depositing electrochromic layers", United States Patent, 5,252,354, October 12, 1993.
59. Unuma H., Tonooka K., Suzuki Y., Furusaki T., Kodaira K., Matsushita T., (1986), "Preparation of transparent amorphous tungsten trioxide thin-films by a dip-coating method", *Journal of Materials Science Letters.* **5**: 1248

-
60. Takase A., Miyakawa K., (1991), "Raman-study on sol-gel derived tungsten-oxides from tungsten ethoxide", *Jpn. J. Appl. Phys. Part 2* **30**: L1508
 61. Bell J.M., Green D.C., Patterson A., Smith G.B., MacDonald K.A., Lee K., Kirkup L.D., Cullen J.D., Weat B.O., Spiccia L, Kenny M.J., Wielunski L.S., (1991) "Structure and properties of electrochromic WO₃ produced by sol-gel methods" in: *Optical Materials Technology for Energy Efficiency and Solar Energy Conversion X*. SPIE **1536**, 29, SPIE, Bellingham, Washington, USA
 62. Judeinstein P., Livage J., (1991) "Sol-gel synthesis of WO₃ thin-films", *J. Mater. Chem.* **1**: 621
 63. Judeinstein P., Livage J., (1990). "Electrochromic properties of Sol-gel derived WO₃ coatings" In *Sol-Gel Optics – SPIE*, Bellingham, Washington, USA, **1328**,344
 64. Moser F.H., Lynam N.R., "Method for deposition of electrochromic layers", US patent (1989) 4,855,161
 65. Habib M.A., Glueck D., (1989), "The electrochromic properties of chemically deposited tungsten oxide films", *Solar Energy Materials* **18**: 127
 66. Livage J., (1992), "Sol-gel ionics", *Solid State Ionics* **50**: 307
 67. Cronin J. P., Tarico D. J., Agrawal A., Zhang R. L., "Method for depositing high performing electrochromic layers", United States Patent 5,277,986, January 11, 1994
 68. Denesuk M., Cronin J. P., Kennedy S. R., Law K. J., Nielson G. F., Uhlmann D. R., "Coloration behavior of Hybrid Electrochromic Films", *Proceedings of SPIE Optical materials technology for energy efficiency and solar energy conversion XIII*, Bellingham, Washington, USA 1994; SPIE Vol. 2255: 52-61.
 69. Schmidt H., Krug H., Merl N., Moses A., Judeinstein P., Berni A., "Electrochromic thin-film systems and components thereof", Patent WO 95/28663; April 18, 1994.
 70. Munro B., Krämer S., Zapp P., Krug H., (1998), "Characterization of electrochromic WO₃-layers prepared by sol-gel nanotechnology", *J. Sol-gel Science and Technology*, **13**: 673 - 678.
 71. Munro B., Conrad P., Krämer S., Schmidt H., Zapp P., (1998), "Development of electrochromic cells by the sol-gel process", *Solar Energy Materials and Solar Cells*; **54**: 131 – 137
 72. Heusing S., Munro B., Koch T., Zapp P., Mennig M., Schmidt H., „Weiterentwicklung elektrochromer Dünnschichtsysteme auf Glas über basschemische Verfahren“, *Proceedings of the 73. Glastechnische Tagung 1999*; Mai 31 – June 02; Halle (Saale), Germany, p. 40 – 43
 73. Mennig M., Fink-Straube C., Heusing S., Kalleder A., Koch T., Munro B., Zapp P., Schmidt H., (1998) "Large area decorative and functional sol-gel coatings on glass", *Proc. 2nd international Conference on Coatings on Glass (ICCG)*, 1998, Sept. 6-10, Saarbrücken, Germany, pp442.
 74. Vroon Z. A. E. P., Spee C. I. M. A., (1997), "Sol-gel coatings on large area glass sheets for electrochromic devices", *J. Non-Cryst. Solid*; **218**:189 – 195

75. Craigen D., Mackintosh A., Hichman J., Colbow K., (1986), "Spray deposition and properties of electrochromic tungsten-oxide films", *J. Electrochem. Soc.* **133**: 1529
76. Cheng W., Naudrin E., Dunn B., Zink J.I., (2001), "Synthesis and electrochromic properties of mesoporous tungsten oxide", *J. Mater. Chem.*; **11**: 92 – 97
77. Ozkan Zayim E., Lee S.-H., Liu P., Tracy C.E., Tepehan F.Z., Pitts J.R., Deb S.K., (2002), "Electrochromic and optical properties of mesoporous tungsten oxide films", *Solid State Ionics*; **149**: 139 – 146
78. Zayim E.O., Liu P., Lee S.-H., Tracy C.E., Turner J.A., Pitts J.R., Deb S.K., (2003), "Mesoporous sol-gel WO₃ thin films via poly(styrene-co-allyl-alcohol) copolymer templates", *Solid State Ionics*; **165**: 65 – 72
79. Choy J., Kim Y., Kim B., Park N., Campet G., Grenier J., (2000), "New Solution Route to Electrochromic Poly(acrylic acid)/WO₃ Hybrid Film", *Chem. Mater.*, **12(10)**: 2950
80. Aegerter M.A., (2001), "Sol-gel niobium pentoxide: A promising material for electrochromic coatings, batteries, nanocrystalline solar cells and catalysis", *Solar Energy materials & Solar Cells* **68**: 401
81. Gmelin L., Gmelin-Handbuch der Anorganischen Chemie, Niob und Sauerstoff B1 (1970) 49; Verlag Chemie GmbH, Weinheim/Bergstrasse.
82. Eckert J., Niobium and niobium compounds, in: Elvers B., Hawkins S., Schulz G., eds., Ullman's Encyclopedia of Industrial Chemistry, 5th Edition, Vol. A17, 1990, pp. 251 - 264.
83. Alquier C., Vandenborre M.T., Henry M., (1986) "Synthesis of niobium pentoxide gels", *J. Non-Cryst. Solids* **79**: 383.
84. Griesmar P., Papin G., Sanchez C., Livage J., (1991), "Sol-gel route to niobium pentoxide", *Chem. Mater.* **3**: 335.
85. Reichman B., Bard A.J., (1980) "Electrochromism at niobium pentoxide electrodes in aqueous and acetonitrile solutions", *J. Electrochem. Soc.* **127**: 241.
86. Reichman B., Bard A.J., (1981) "The application of Nb₂O₅ as a cathode in non-aqueous lithium cells", *J. Electrochem. Soc.* **128**: 344.
87. Maruyama T., Kanagawa T., (1994) "Electrochromic properties of niobium oxide thin-films prepared by chemical-vapor-deposition", *J. Electrochem. Soc.* **141**: 2868.
88. Yoshimura K., Miki T., Iwama S., Tanemura S., (1995) "Niobium oxide electrochromic thin-films prepared by reactive DC magnetron sputtering", *Jpn. J. Appl. Phys. Part-2 Letters* **34**: L1293.
89. Lee G.R., Crayston J.A., (1996) "Studies on the electrochemical deposition of niobium oxide", *J. Mater. Chem.* **6**: 187.
90. Lee G.R., Crayston J.A., (1994) "Sol-gel processing of niobium chloroalkoxides", *J. Mater. Chem.* **4 (7)**: 1093.
91. Faria R.C., L.-O. de, Bulhoes S., (1994) "A novel synthetic route to Nb₂O₅ thin-films for electrochromic devices", *J. Electrochem. Soc.* **141**: L29.
92. Ohtani B., Iwai K., Nishimoto S.-I., Inui T., (1994) "Electrochromism of niobium oxide thin-films prepared by the sol-gel process", *J. Electrochem. Soc.* **141**: 2439.

93. Özer N., Barreto T., Büyüklimanli T., Lambert C. M., (1995), "Characterization of sol-gel deposited niobium pentoxide films for electrochromic devices", *Solar Energy Materials & Solar Cells* **36**: 433.
94. Özer N., Chen D.-G., Lampert C.M., (1996) "Preparation and properties of spin-coated Nb₂O₅ films by the sol-gel process for electrochromic applications", *Thin Solid Films* **277**: 162.
95. Avellaneda C.O., Macedo M.A., Florentino A.O., Aegerter M.A., in: Wittwer V., Granqvist C.G., Lampert C.M. (Eds.), *Optical Materials Technology for Energy Efficiency and Solar Energy Conversion XIII*, SPIE, Vol. 2255, SPIE, Bellingham, Washington, USA, 1994, pp. 38-51.
96. Avellaneda C.O., Macedo M.A., Florentino A.O., Barros Filho D.A., Aegerter M.A., "Niobia sol-gel: a new material for electrochromic and photoelectric applications" in: Mackenzie J.D. (Eds.), *Sol-Gel Optics III*, SPIE, Vol. 2288, SPIE, Bellingham, Washington, USA, 1994, pp. 422 – 434.
97. Aegerter M.A., Avellaneda C.O., "Sol-gel electrochromic coatings" in: Pope E.J.A., Sakka S., Klein L. (Eds.), *Sol-Gel Science and Technology*, Ceramic Transactions, Vol. 55, The American Ceramic Society, Westerville, OH, USA, 1995, pp.223-234.
98. Pawlicka A., Atik M., Aegerter M.A., (1995) "Synthesis of Nb₂O₅ Thin-films for electrochromic devices", *J. Mater. Sci. Lett.* **14**: 1568
99. Avellaneda C.O., Pawlicka A., Aegerter M.A., (1998), "Two methods of obtaining sol-gel Nb₂O₅ thin films for electrochromic devices", *J. Mater. Sci.* **33**: 2181.
100. Schmitt M., Heusing S., Aegerter M.A., Pawlicka A., Avellaneda C.O., (1998), "Electrochromic properties of Nb₂O₅ sol-gel coatings", *Solar Energy Mater.& Solar Cells* **54**: 9.
101. Schmitt M., Aegerter M.A., in: Lampert C.M. (Ed.), "Switchable Materials and flat displays", SPIE, Vol. 3788, SPIE, Bellingham, Washington, USA, 1999, pp. 93-102.
102. Macek M., Orel B., Opara Krasovec U., (1997) "The effect of lithiation on the electrochromism of sol-gel derived niobium oxide films", *J. Electrochem. Soc.* **144**: 3002.
103. Macek M., Orel B., (1998), "Electrochromism of sol-gel derived niobium oxide films", *Solar Energy Materials & Solar Cells* **54**: 121.
104. Schmitt M., "Entwicklung dotierter und undotierter Nb₂O₅ Sol-Gel-Schichten zur Anwendung als färbende Elektrode in electrochromen Systemen" Ph. D. Thesis, Leibniz-Institute of New Materials, INM and University of Saarlandes, Saarbruecken, Germany, 2000
105. Schmitt M., Aegerter M.A., "Properties of electrochromic devices made with Nb₂O₅ and Nb₂O₅:X (X = Li, Ti or Mo) as coloring electrode" in: Lampert C.M. (Ed.), *Switchable Materials and Flat Displays*, SPIE, Vol. 3788, SPIE, Bellingham, Washington, USA, 1999, pp. 75-83.
106. Heusing S., Sun D.L., Aegerter M. A.. "Grey, brown and blue colouring sol-gel electrochromic devices", *Proceedings of the 5th International Conference on Coatings on Glass*, July 4 - 8, 2004, p. 761 – 769, will also appear in *Thin Solid Films*, in print.

-
107. Kilbourn B.T., "Cerium: a guide to its role in chemical technology",
 108. Atkinson A, Guppy R.M., (1991) "Mechanical stability of sol-gel films", *J. Mater. Sci.* **26**: 3869
 109. Stangar U.L., Orel B., Grabec I., Ogoreve B., Kalcher K., (1993), "Optical and electrochemical properties of CeO₂ and CeO₂-TiO₂ coatings", *Solar Energy Materials and Solar Cells* **31**: 171
 110. Orel Z.C., Orel B., (1994) "Optical-properties of pure CeO₂ and mixed CeO₂/SnO₂ thin-film coatings", *Physica Status Solidi B-Basic Research* **186(1)**: K33
 111. Skofic I.K., Sturm S., Ceh M., Bukovec N., (2002) "CeO₂ thin films obtained by sol-gel deposition and annealed in air or argon", *Thin Solid Films* **422(1-2)**: 170
 112. Porqueras I., Person C., Corbella C., Vives M., Pinyol A., Bertan E., (2003) "Characteristics of e-beam deposited electrochromic CeO₂ thin film", *Solid State Ionics* **165(1-4)**: 131
 113. Flamini C., Ciccioli A., Guidoni A.G., Mele A., (2001) "A thermodynamic study of laser-induced ablation of ZrO₂, CeO₂, V₂O₅, and mixed Ce-V oxides", *J Mater Synthesis and Processing* **9(3)**: 143
 114. El Idrissi B., Addou M., Outyourhit A., Regragui M., Bourgrine A., Kachouane A., (2001) "Sprayed CeO₂ thin films for electrochromic application", *Solar Energy Materials & Solar Cells* **69(1)**: 1
 115. Baudry P, "Etude de vitrages electrochromes a electrolyte polymere", PhD Thesis, l'institut National Polytechnique de Grenoble (Grenoble, France, 1989)
 116. Ottaviani M., Panero S., Morzilli S., Scrosati B., Lazzari M., (1986) "The electrochromic characteristics of titanium-oxide thin-film electrodes", *Solid State Ionics* **20**: 197
 117. Baudry P., Rodrigues A.C.M., Aegerter M.A., Bulhoes L.O. (1990) "Dip-coated TiO₂-CeO₂ films as transparent counterelectrode for transmissive electrochromic devices", *J Non-Crystalline Solids* **121(1-3)**: 319
 118. Macedo M.A., Dall'Antonia L.H., Aegerter M.A., (1992). "Sol-gel coatings for electrochromic devices" In: Sol-Gel Optics II - SPIE 1758, 320, SPIE, Bellingham, Washington, USA
 119. Tonazzi J.C.L., Valla B., Macedo M.A., Baudry P., Aegerter M.A., "Characterization of an all solid state electrochromic window" (1990). In: Sol-Gel Optics, SPIE 1328, 375, SPIE, Bellingham, Washington, USA
 120. Macedo M.A., Dall'Antonia L.H., Valla B., Aegerter M.A., (1992) " Electrochromic smart windows", *J Non-Cryst Solids* **147/148**: 792
 121. Macedo M.A., Aegerter M.A., (1994) "Sol-gel electrochromic devices" *J Sol-Gel Science and Technology* **2**: 667
 122. Valla B., Tonazzi J.C.L., Macero M.A., Dall'Antonia L.H., Aegerter M.A., Leones M.A.B., Bulhoes L.O.S., (1991) "Transparent storage layers for H⁺ and Li⁺ ions prepared by the Sol-Gel technique" in: Optical Materials Technology for Energy Efficiency and Solar Energy Conversion X, SPIE 1536, SPIE, Bellingham, Washington, USA
 123. Avellaneda C.O., Pawlicka A., (1998) "Preparation of transparent CeO₂-TiO₂ coatings for electrochromic devices", *Thin Solid Films* **335(1-2)**: 245

124. Ghodsi F.E., Tepehan F.Z., Tepehan G.G., (1999) "Optical and electrochromic properties of sol-gel made CeO₂-TiO₂ thin films", *Electrochimica Acta* **44**: 3127
125. Keomany D., Petit J.P., Deroo D., (1995) "Electrochemical insertion in sol-gel made CeO₂-TiO₂ from lithium conducting polymer electrolyte – relation with the material structure", *Solar Energy Mater and Solar Cells* **36(4)**: 397
126. Keomany D., Poinsignon C., Deroo D., (1994) "Sol-gel preparation of mixed cerium-titanium oxide thin films", *Solar Energy Materials and Solar Cells* **33**: 429
127. Makishima A., Kubo H., Wada K., Kitami Y., Shimohira T., (1986) "Yellow coatings produced on glasses and aluminum by the sol-gel process", *J Am Ceram Soc* **69**: C127
128. Ozer N., De Souza S., Lampert C.M., (1995) "Optical and electrochemical properties of sol-gel spin coated CeO₂-TiO₂ films" In : Proceedings of SPIE 2531, 143
129. Ottermann C.R., Temmink A, Bange K., (1991). "Comparison of tungsten and nickel-oxide electrochromism in single films and in all-solid-state devices." *Thin Solid Films* **193(1-2)**: 409
130. Cotton F.A., Wilkinson. G. "Advanced Inorganic Chemistry", Chapter 20: "The lanthanides; Also Scandium IIIB(3) and Yttrium IIIB(3)" Wiley, 1988
131. Svensson J.S.E.M., Granqvist. C., (1986). "Electrochromic hydrated nickel-oxide coatings for energy-efficiency windows - Optical-properties and coloration mechanism." *Appl. Phys. Lett.* **49(23)**: 1566.
132. Lampert C.M., Omstead T.R., Yu P.C., (1986) "Chemical and optical-properties of electrochromic nickel-oxide films"; *Solar Energy Materials* **14**: 161
133. Agrawal A, Habibi H. R., Agrawal R.K., Cronin J.P., Roberts D.M., Caron-Popowich R., Lampert C.M., (1992). "Effect of deposition pressure on the microstructure and electrochromic properties of electron-beam-evaporated nickel oxide films." *Thin Solid Films* **221**: 239.
134. Nagai J. (1993). "Characterization of evaporated nickel-oxide and its application to electrochromic glazing." *Solar Energy Materials and Solar Cells* **31(2)**: 291
135. Azens A., Kullmann L., Vaivars G., Nordborg H., Granqvist C.G., (1998). "Sputter-deposited nickel oxide for electrochromic applications." *Solid State Ionics* **115**: 449.
136. Mehrotra R.C. (1989). "Transition-Metal alkoxides", *Advances in Inorganic Chemistry and Radiochemistry* **26**: 269.
137. Moser F.H., Lynam. N. R., "Electrochromic coating and method for making same", US Patent 4,959,247 (1990)
138. Wang L., Zhang Z., Cao Y., (1993). "Preparation of nickel-oxide films by sol-gel process", *Nippon Seramikkusu Kyokai Gakujutsu Ronbunshi-Journal of the Ceramic Society of Japan* **101**: 227.
139. MiKi T., Yushimura K., Tai Y., Tazawa M., Jin P., Tanemura S., "Electrochromic properties of nickel oxide thin films prepared by the sol-gel method". Proceedings of SPIE, 1995; Vol. 2531:135-142

140. Surca A., Orel B., Pihlar B., Bukovec P., (1996). "Optical, spectroelectrochemical and structure properties of sol-gel derived Ni-oxide electrochromic film." *J. Electroanal. Chem.* **408**: 83.
141. Surca A., Orel B. (1997). "Sol-gel derived nickel oxide electrochromic films: Optical, spectroelectrochemical and structure properties." *J. Sol-gel Science and Technology* **8**: 743.
142. Korosec R.C., Bukovec P., Pihlar B., Vuk A.S., Orel B., Drazic G., (2003). "Preparation and structure investigations of electrochromic nanosized NiOx made via the sol-gel route." *Solid State Ionics* **165(1-4)**: 191.
143. Korosec R.C., Bukovec P., Pihlar B., Gomilsek J.P., (2003). "The role of thermal analysis in optimization of the electrochromic effect of nickel oxide thin films, prepared by the sol-gel method. Part I." *Thermochimica Acta* **402(1-2)**: 57.
144. Korosec R.C., Bukovec P. (2004). "The role of thermal analysis in optimization of the electrochromic effect of nickel oxide thin films, prepared by the sol-gel method. Part II." *Thermochimica Acta* **410(1-2)**: 65.
145. Sharma P.K., Fantini M. C. A., Gorenstein A., (1999). "Synthesis characterization and electrochromic properties of NiOxHy thin film prepared by a sol-gel method." *Solid State Ionics* **113-115**: 457.
146. Sharma P.K., Mracia M. C. A., Fischer H., Craievich A.F., Gorenstein A., "Factores influencing the electrochromic properties of nickel oxide thin films derived from sol-gel method by dip-coating", *Mat. Res. Soc. Symp. Proc.* (1999); 547: 351-356
147. Jiao Z., Wu M., Qin Z., Xu H., (2003). "The electrochromic characteristics of sol-gel prepared NiO thin films." *Nanotechnology* **14**: 458.
148. Jimenez-Gonzalez A.E., Cambray J. G. (2000). "Deposition of NiOx thin films by sol-gel technique." *Surf. Eng.* **16(1)**: 73.
149. Williams P.A., Jones A. C., Bickley J.F., Steiner A., Davies H.O., Leedham T.J., Impey S.A., Garcia J., Allen S., Rougier A., Blyr A. (2001). "Synthesis and crystal structures of dimethylaminoethanol adducts of Ni(II) acetate and Ni(II) acetylacetonate. Precursors for the sol-gel deposition of electrochromic nickel oxide thin films." *J. Mater. Chem.* **11(9)**: 2329.
150. Garcia-Miquel J.L., Zhang Q., Allen S.J., Rougier A., Blyr A., Davies H.O., Jones A.C., Leedham T.J., Williams P.A., Impey S.A., (2003). "Nickel oxide sol-gel films from nickel diacetate for electrochromic applications." *Thin Solid Films* **424**: 165.
151. Kim C-Y., Choi J-W., Hwang T-W., Lim T-Y., "Electrochromic NiO thin film synthesis by Sol-gel method and its electrochemical and optical properties", In :6th International Meeting on Electrochromism-I.M.E. –6, 2004, Organizing committee: Vondrak J., Sedlarikova M. Aug. 29th – Sept. 2nd, 2004, Brno/ Czech Republic, pp 68
152. Svegl F., Orel B., Kaucic V., (2000). "Electrochromic Properties of lithiated Co-oxide (Li_xCoO₂) and Ni-oxide (Li_xNiO₂) thin films prepared by the sol-gel route." *Solar Energy* **68(6)**: 523.

153. Martini M., Brito G.E.S., Fantini M.C.A., Craievich A.F., Gorenstein A., (2001) "Electrochromic properties of NiO-based thin films prepared by sol-gel and dip coating", *Electrochimica Acta*, **46 (13-14)**: 2275-2279
154. Santos Lopez D., "Development and Characterization of a Counterelectrode of Nickel and Titanium by Sol-Gel route for an electrochromic window" Diploma Thesis, Leibnitz-Institute of New Materials, INM, Germany, 2003
155. Wigginton M., *Glass in Architecture*, Phaidon, London, UK, 1996
156. Lampert C.M., (2003) "Large-area glass and intergrated photovoltaics", *Solar Energy materials and Solar Cells* **76**: 489
157. Becker H., Wittkopf H., "Variable solar control glazing-an outstanding application for electrochromics", Proceedings of the Third International Meeting on Electrochromics, London, UK, Proc. *Electrochim. Acta.* **44** (1999) 3268
158. Krasovec U.O., Vuk A.S., Orel B., (2002) "Comparative studies of "all sol-gel" electrochromic windows employing various counter electrodes", *Solar Energy Materials and Solar Cells*, **73**: 21-37
159. Granqvist C.G., Avendano E., Atens A., (2003) "Electrochromic coatings and devices: survey of some recent advances" *Thin Solid Films* **442**: 201-211
160. Judeinstein P., Livage J., Zarudiansky A., Rose R., (1988) "An all gel electrochromic device", *Solid State Ionics* **28**: 1722-1725
161. Ozer N., Lampert C.M., (1998) "Electrochemical characterization of sol-gel deposited coatings", *Solar Energy Materials & Solar Cells* **54**: 147-156
162. Orel B., Vuk A.S., Jese R., Lianos P., Stathatos E., Judeinstein P., Colomban P., (2003) "Development of sol-gel redox I³-/I⁻ electrolytes and their application in hybrid electrochromic devices", *Solid State Ionics* **165**: 235-246
163. Heusing S., Niegisch N., Zapp P., Mennig M., Schmidt H., Laackmann P., Krings L.H.M., Arstsen H.J., "Large area electrochromic displays", Proc. International Meeting On Electrochromism, IME-4, 2000, August 21-23, Uppsala, Sweden.
164. Mennig H., Heusing S., Zapp P., Niegisch N., Schmidt H., "Fabrication of large area, curved electrochromic modules for automotive application", Proc. 3rd international Conference on Coatings on Glass (ICCG), 2000, Oct. 29. – Nov. 02, Maastricht, The Netherlands pp787.
165. Avellaneda C.O., Dahmouche K., Bulhoes L.O.S., Pawlicka A., (2000) "Characterisation of an all sol-gel electrochromic device WO₃/ormolyte/ CeO₂-TiO₂", *J. Sol-Gel Science and Technology* **19**: 447-451
166. Dahmouche K., Atik M., Mello N.C., Bonagamba T.J., Panepucci H., Aegerter M.A., Judeinstein P., (1997) "Investigation of new ion-conducting ormolyte: structure and properties", *J. Sol-Gel Science and Technology* **8(1-3)**: 711-715
167. Avellaneda C.O., "Preparation and Characterization of electrochromic devices prepared by the sol-gel process" Ph.D. Thesis, University of São Paulo at São Carlos, Brazil, 1999
168. Orel B., Krasovec U.O., Macek M., Svegl F., Stangar U.L., (1999), "Comparative studies of "all sol-gel" electrochromic devices with optically passive counter-electrode films, ormolyte

- Li⁺ ion-conductor and WO₃ or Nb₂O₅ electrochromic films", *Solar Energy Materials and Solar Cells* **56**: 343
169. Cummins D., Boschloo G., Ryan M., Corr D., Rao S.N., Fitzmaurice D., (2000), "Ultrafast Electrochromic Windows Based on Redox-Chromophore Modified Nanostructured Semiconducting and Conducting Films", *J.Phys.Chem.B*, **104 (48)**: 11449
170. Deb S.K., Lee S.H., Tracy C.E., Pitts J.R., Gregg B.A., Branz H.M., (2001) "Stand-alone photovoltaic-powered electrochromic smart window", *Electrochimica Acta*, **46 (13-14)**: 2125
171. Hauch A., Georg A., Baumgartner S., Krasovec U.O., Orel B., (2001) "New photoelectrochromic device", *Electrochimica Acta*, **46 (13-14)**: 2131
172. Judeinstein P., Morineau R., Livage J., (1992), "Electrochemical degradation of WO₃·nH₂O thin films", *Solid State Ionics* **51**: 239
173. Bohnke O., Bohnke C., Robert G., Carquille B., (1982), "Electrochromism in WO₃ thin-films. 1. LiClO₄-Propylene carbonate-water electrolytes", *Solid State Ionics* **6**: 121
174. Knowles T.J., Hersh H.N., Kramer W., Reported in 19th Electronic Materials Conference of AIME, Cornell, NY, 1977
175. Janke N., Bieberle A., Weissmann R., (2001) "Characterization of sputter-deposited WO₃ and CeO_{2-x}-TiO₂ thin films for electrochromic applications" *Thin Solid Films* **392**: 134
176. Pyper O., Kaschner A., Thomsen C., (2002) "In situ Raman spectroscopy of the electrochemical reduction of WO₃ thin films in various electrolytes", *Solar Energy Materials and Solar Cells* **71**: 511
177. Arnoldussen T.C., (1981) "A model for electrochromic tungstic oxide microstructure and degradation", *J. Electrochem. Soc.* **128(1)**: 117
178. Munro B., Krämer S., Zapp P., Krug H., Schmidt H., (1997), "All sol-gel electrochromic system for plate glass", *J. Non-Cryst. Solids* **218**:185-188
179. Schmitt M., Aegerter M.A., (2001) "Electro chromic properties of pure and doped Nb₂O₅ coatings and devices", *Electrochimica Acta* **46**: 2105
180. Zapp P., „Entwicklung und Charakterisierung lithiumionenleitender Nanokompositelektrolyte für die Anwendung in elektrochromen Bauteilen“, Ph.D. Thesis, Leibniz-Institute of New Materials, INM and University of Saarlandes, Saarbruecken, Germany, 2004
181. Cullity B.D., Elements of x-ray diffraction, Addison-Wesley, Massachusetts, 1956
182. Guo Y.P., "Nanocrystalline sol-gel Nb₂O₅ coatings: Preparation, characterisation and application to photovoltaic cell, lithium battery and electrochromic device" Ph. D. Thesis, Leibniz-Institute of New Materials, INM and University of Saarlandes, Saarbruecken, Germany, 2003
183. Sauerbrey G., (1959) "Verwendung von Schingquarzen zur Wägung dünner Schichten und zur Mikrowägung". *Zeitschrift für Physik* **155**: 206
184. Bard A.J., Faulkner L.R., Electrochemical methods: Fundamentals and Applications, John Wiley & Sons, Inc. 1980

-
185. Leftheriotis G., Papaefthimiou S., Yianoulis P., (2004) "The effect of water on the electrochromic properties of WO₃ films prepared by vacuum and chemical methods", *Solar Energy Materials & Solar Cells* **83**: 115
 186. Livage J., Henry M., Sanchez C., (1988) "Sol-gel chemistry of transition metal oxides", *Progress in Solid State Chemistry*, **18**: 259-341.
 187. Babinee S.J., (1992) "A quartz crystal microbalance analysis of ion insertion into WO₃". *Solar Energy Materials & Solar Cells*, **25**: p. 269-291.
 188. Bueno P.R., F.R.C., Bullhoes L.O.S. (2005) "EQCM study during lithium insertion/deinsertion processes in Nb₂O₅ films prepared by polymeric precursor method". *Solid State Ionics*, **176**: p. 1175-1180.
 189. Heusing S., communication in Leibniz-Institute of new materials, 2005
 190. <http://www.webelements.com/webelements/compounds/text/Ce/Ce1O2-1306383.html>
 191. <http://www.azom.com/details.asp?ArticleID=1179>
 192. Cotton F.A., Wilkinson. G. "Advanced Inorganic Chemistry", Chapter 4: "The group IA(1) elements: Li, Na, K, Rb, Cs, Fr" Wiley, 1988
 193. Gabrielli, C., Keddad, M., Torrei, R., (1991) "Calibration of the Electrochemical Quartz Crystal Microbalance", *Journal of electrochemical Society*, **139**: 2657
 194. Terrier C., Chatelon J.P., Roger J.A., (1997) "Analysis of antimony doping in tin oxide thin films obtained by the sol-gel method", *Journal of Sol-Gel Science and Technology*, **10**: 75
 195. Decker F., Passerini S., Pileggi R., Scrosati B., (1992) "The electrochromic process in non-stoichiometric nickel oxide thin film electrodes", *Electrochimica Acta* **37**: 1033

List of publications:

1. **D. L. Sun**, J. Puetz, S. Heusing, M. A. Aegerter, "Influence of water on the electrochemical properties of $(\text{CeO}_2)_x(\text{TiO}_2)_{1-x}$ sol-gel coatings and electrochromic devices", in: *Proceedings of SPIE Sol-gel Optics VI*, Seattle, 7-11. July 2002, pp17.
2. **D. L. Sun**, S. Heusing, J. Puetz, M. A. Aegerter, "Influence of water on the electrochemical properties of $(\text{CeO}_2)_x(\text{TiO}_2)_{1-x}$ and WO_3 sol-gel coatings and electrochromic devices", *Solid State Ionics* 165/1-4, pp181, 2003.
3. **D. L. Sun**, S. Heusing, M. A. Aegerter, "Electrochromic properties of $\text{Nb}_2\text{O}_5:\text{Mo}$, WO_3 and $(\text{CeO}_2)_x(\text{TiO}_2)_{1-x}$ sol-gel coatings and devices using dry and wet electrolytes", in: *Electrochromic materials and applications : Proceedings of the International Symposium*, Rougier, A.; Rauh, D.; Nazri, G.A.(eds.) Pennington, NJ: ECS, 2003.- (Electrochemical Society Proceedings Volume; 2003-17), pp119
4. **D. L. Sun**, S. Heusing, J. Otero-Anaya, M.A. Aegerter, „Elektrooptische Eigenschaften von grau- und braunfärbenden elektrochromen Fenstern, hergestellt mit der Sol-Gel-Technologie“, *Proceedings of the 78. Glastechnische Tagung*, 7-9. Juni 2004, Nürnberg, pp216.
5. **D. L. Sun**, S. Heusing, M.A. Aegerter, "Influence of some processing parameters on the properties of electrochromic devices", in: *Proceedings of the 6th International Meeting on Electrochromism (IME6)*, Aug. 29th – Sept. 2nd, 2004, Brno/ Czech Republic, pp 204.
6. S. Heusing, **D. L. Sun**, J. Otero-anaya, M. A. Aegerter, "Grey, brown and blue colouring sol-gel electrochromic devices", in: *Proceedings of the 5th ICCG*, July 4 - 8, 2004, Saarbrücken/ Germany, J. Puetz, A. Kurz, M. A. Aegerter (eds.), pp761, will also appear in *Thin Solid Films*, in print.